

FOR REFERENCE ONLY

41 0565960 8



ProQuest Number: 10290277

All rights reserved

INFORMATION TO ALL USERS

The quality of this reproduction is dependent upon the quality of the copy submitted.

In the unlikely event that the author did not send a complete manuscript and there are missing pages, these will be noted. Also, if material had to be removed, a note will indicate the deletion.



ProQuest 10290277

Published by ProQuest LLC (2017). Copyright of the Dissertation is held by the Author.

All rights reserved.

This work is protected against unauthorized copying under Title 17, United States Code
Microform Edition © ProQuest LLC.

ProQuest LLC.
789 East Eisenhower Parkway
P.O. Box 1346
Ann Arbor, MI 48106 – 1346

**Evaluation of Fibres
and Transverse Composites
Using Advanced Acoustic Emission
Signal Processing.**

DIMITRIOS KALOEDES

A thesis submitted in partial fulfilment of the
requirements of the Nottingham Trent University
for the degree of Master of Philosophy.

November 1997

Ref.

M.PHIL | CP | 97

KAL

ACKNOWLEDGEMENT

I would like to thank most gratefully Dr R. Hill and Dr R. Brooks, for their guidance and encouragement. I also wish to thank Prof N. Davies, Dr M. Baxter and Dr C. Beardah, together with Mr P Langly and all the technical staff with the physics laboratories at Nottingham Trent University. Finally, my colleagues Ms Ann-Marie Priston and Mr M. Banerjee for useful discussion during the development of this work and Dr L. Norwood of Scott Bader.Co for providing the materials. I do have to express my gratitude to my family for providing financial and psychological support for so many years in order for me to obtain a Bachelor of Engineering, a Master of Science and hopefully now an Master of Philosophy. The decision to travel and study in England was hard and needed determination, but it proved worthwhile for my academic education but more importantly for my personal maturity and growth.

ABSTRACT

Acoustic Emission (AE) has been established during recent years as a convenient method for determining the fracture characteristics of both **transverse fibre-reinforced composite** materials (TFRC) and **fibre bundles** under tensile testing. Degradation of these materials is by propagation of a range of defects which ultimately control failure. AE events were easily detected and distinguished from each other by either relative Peak amplitude (AMP) or ringdown counts (RDC) using simple piezoelectric transducers as detectors and advanced signal processing. Stress-strain data were also simultaneously recorded and then correlated to AE data.

For the first part of this investigation an AE technique has been employed to deduce information regarding the level of adhesion and the strength of the bond between **glass or Kevlar fibres and polyester resin matrix**. Composites provide a strong, lightweight material suitable for engineering applications. Since composite materials used for engineering applications are manufactured by cross-ply methods, transverse failure is an important damage mechanism in controlling the initiation of damage in a complete composite. Different treatments such as post-curing of the composite material and ultrasound treatment of the Kevlar fibres, with the specimen subjected to transverse tension, showed different characteristics for the interfacial strength and the associated AE events. The pattern of AE indicates the fact that resin toughness has increased due to post-cure. The severity of these AE events was examined although this measure was not conclusive in identifying differences in AE data due to different source mechanisms. Weibull plots derived from the composite tensile test involving AE data, were also employed. This particular application of the statistics does not bear a fundamental relationship to the microscopic damage mechanisms and was applied in an empirical way. The AE related Weibull parameters proved sensitive to material condition, due to cure, post cure and resin-fibre adhesion modification. Pattern Recognition was also considered with regard to quantification and identification of damage.

For the second part of this investigation, AE has been used in order to monitor the strength of glass and carbon fibres bundles under tension. Generally, when testing materials using AE, the relationship between the source excitation and the detected stress

wave is complex. The mode of failure in this case was mainly one kind (fracture transverse to the fibre axis). Bundles of different types have been strained to failure in order to investigate the relationship between AE data and fibre strength. Where appropriate the statistical distribution of mechanical failure was characterised using three different statistical techniques. By using mainly the AE ringdown counts, these methods have been able to predict the behaviour of such bundles under tension and therefore describe their strength distribution. Two parameter Weibull distribution function, two parameter log-normal function and quantile distribution function provided the means for characterising the failure of these bundles. AE has proved useful in monitoring the exact time and load of fibre breaks, since the breaking of each individual fibre is accompanied by an associated AE signal.

Generally the AE data were used to study aspects of material failure. The analysis techniques based on AE, proved effective, bearing in mind the relative uncertainties during manufacturing and testing processes. AE has proved an effective method of monitoring composite failure and fibre fracture. The results allow transverse composite and fibre bundle failure to be characterised using various statistical approaches. The simplicity of the instrumentation establishes AE as a useful technique with broad application to materials characterisation having a number of advantages over both conventional ultrasonic and radiographic methods.

SYMBOLS

E:	Young's Modulus
N:	Number of Events
V:	Voltage
ε:	Strain
σ:	Stress
RDC:	Ringdown Counts
AMP:	Amplitude
COD:	Crack Opening Displacement
AE:	Acoustic Emission
WS:	Weibull Statistics
NDT:	Non Destructive Testing
NDE:	Non Destructive Evaluation
M.E.E:	Mechanical Elastic Energy
T.F.R.C:	Transverse Fibre Reinforced Composite.

CONTENTS

CHAPTER 1

ACOUSTIC EMISSION AND COMPOSITE MATERIALS

1.1.	Introduction.	1
1.2.	Literature Review.	3
1.3.	Structural Applications of composites and Cost Effectiveness.	7
1.4.	Fibres and Fibre Characteristics.	8
	1.4.1. Glass Fibres Characteristics.	8
	1.4.2. Kevlar and Carbon Fibres Characteristics.	10
1.5.	Matrix-Fibre Interfacial Characteristics.	11
1.6.	Polymer Matrices and Thermosetting Resins.	13

CHAPTER 2

AE CHARACTERISTICS AND TESTING PROCEDURES

2.1.	Fundamentals of AE.	14
2.2.	Important AE Parameters.	16
	2.2.1. Ringdown Counts and Count Rate.	17
	2.2.2. Peak Amplitude and Amplitude Distribution.	17
	2.2.3. Event Duration.	18
2.3.	Ultrasound, AE and AE Transducers.	18
2.4.	Transducer Uncertainties and Attenuation.	21
2.5.	Experimental Procedure.	24
	2.5.1. Preparation of the Composite Material.	24
	2.5.2. Tensile Testing Conditions.	25

CHAPTER 3**TESTING E-GLASS AND KEVLAR-49 TRANSVERSE FIBRE COMPOSITE
MATERIALS**

3.1.	Aim of the Testing on Composites.	28
3.2.	Curing and Post Curing Processes.	28
3.3	Micromechanics for Transverse Fibre Reinforced Composites.	30
3.4.	Transverse Cracking in E-Glass Fibre Reinforced Composites.	35
3.4.1.	Stress-Strain Data.	36
3.4.2.	AE System Monitoring Transverse Cracking in Composite Materials.	37
3.5.	Experimental Results for Transverse Fibre Reinforced Testing.	38
3.6.	Experimental Results for Kevlar-49 Transverse Reinforced Composite Materials.	48
3.7.	Conclusions.	65

CHAPTER 4**STATISTICAL TECHNIQUES USED FOR AE CHARACTERISATION OF
TRANSVERSE FIBRE REINFORCED COMPOSITE MATERIALS**

4.1.	Aim of Statistical Analysis.	67
4.2.	Weibull Theory.	68
4.2.1.	Regression Analysis Applied to Weibull Statistics.	70
4.3.	Weibull Statistics Applied to AE data from Transverse Failure of Glass Fibre Reinforced Composites.	71
4.4.	Acoustic Emission Event Severity for the Characterisation of E-Glass Composite Materials.	82
	4.4.1. Aim in Using a Severity Measure.	82
	4.4.2. AE Severity, Results and Discussion.	82
4.5.	Pattern Recognition.	90
	4.5.1. Reasons for AE signal.	91
	4.5.2. Discussion of the Pattern Recognition Philosophy.	91
4.6.	Conclusions on Composite Materials.	101

CHAPTER 5**APPLICATION OF AE TO THE TESTING OF FIBRE BUNDLES**

5.1.	Introduction.	103
5.2.	Physical Dimensions and Defects in Fibres.	105
	5.2.2. Fibre Diameter.	106
	5.2.3. Fracture Energy Models.	106
5.3.	Experimental Testing of Glass and Carbon Fibre Bundles.	107
	5.3.1. Preparation of Materials.	107
	5.3.2. Fibre Bundle Test Conditions.	111
5.4.	Fibre Bundle Testing.	112
	5.4.1. Aim of the Fibre Bundle Testing.	112
	5.4.2. Bundle Fracture Processes.	112
5.5.	Experimental Results and Discussion for the Testing of Fibre Bundles.	114
5.6.	Conclusions on Fibre Bundles.	129

CHAPTER 6**STATISTICAL DISTRIBUTION METHODS APPLIED TO AE**

6.1.	Aim of the Statistical Analysis of Fibre Bundle Failure.	130
6.2.	Distribution of AE Ringdown Counts and Events.	131
6.3.	Statistical Analysis and Fibre Bundles.	141
6.4.	The Weibull Distribution Function and AE Testing.	143
6.5.	Application of Weibull Statistics to Fibre Bundle Failure- Results and Discussion.	145
6.6.	Two Parameter Logarithmic Normal Function.	159
6.7.	The Quantile Distribution Function.	176
	6.7.1. Model Estimation.	178
	6.7.2. Prediction.	181
	6.7.3. Conclusions.	184
6.8.	Conclusions in the Statistical Analysis of Fibre Bundles.	185

CHAPTER 7**OVERALL CONCLUSIONS AND FUTURE WORK**

7.1.	Overall Conclusions and Future Work.	187
7.1.1.	Testing of Transverse E-glass and Kevlar-49 Reinforced Composite Materials Using AE.	187
7.1.2.	Testing of E-glass and carbon fibre bundles using AE.	188
7.1.3.	Future Work.	189
	APPENDIX 1	190
	APPENDIX 2	193
	APPENDIX 3	200
	APPENDIX 4	201
	REFERENCES	203

CHAPTER 1

ACOUSTIC EMISSION AND COMPOSITE MATERIALS

1.1. Introduction

Since the 1940's, when plastic resins and light strong fibres were developed, composites and fibres began to offer real structural benefits. The market for these materials has increased rapidly, since composites offer better performance characteristics in many areas, replacing many traditional materials such as steel and aluminium. Since there has been an increase in demand for lightweight, high strength/stiffness materials in automotive, chemical and sports goods industries, then a thorough program for the testing of these materials is necessary.

One of the limitations of using composite materials is their lack of reliability due to sensitivity to the presence of manufacturing defects. Common defects found are voids, cracks, non uniform resin distribution, incorrect fibre orientation and the challenge of controlling their microstructure and overall performance characteristics has increased. Some current non-destructive (NDT) techniques for proof testing of composites and fibres such as radiography, ultrasonics, thermography and eddy current testing are common but acoustic emission has the advantage of being a real time technique for continuous monitoring of material degradation.

AE is regarded as a passive technique, "passive" referring to the fact that there is no need to inject an ultrasonic signal into the structure. The defects themselves are active, radiating ultrasonic radiation derived from perhaps the stress energy applied to the material under test. When localised damage or failure occurs within the material which is deformed or subjected to some environmental changes during loading, the elastic energy decreases resulting in elastic stress waves (AE) which travel through the material and which can be detected by suitable, sensitive transducers. The AE events recorded have a signature which might be characterised in terms of signal amplitude (AMP) and ringdown counts (RDC) and which might be used to monitor different failure mechanisms.

In this work, two primary types of composite as well as three different types of fibre bundles have been tested under tension using the of AE technique: E-glass and Kevlar-49 transverse fibre reinforced composite materials and E1-glass, E2-glass and carbon fibre bundles. Composites and fibres were tested, using various treatments since one of the main advantages of using composites and fibres instead of metals, is that designers can vary composite specifications such as fibre/matrix type, content and orientation, to meet special applications such as thermal insulation, corrosion resistance and improved strength.

The primary objective during this study has been to monitor the fracture behaviour of composite materials and fibre bundles. However, one of the limitations of using composites and fibres is the variability of mechanical properties and sensitivity to flaws. Common flaws that are found in these materials are voids, cracks, non-uniform matrix distributions, incorrect fibre orientation, delimitation, inclusion and fibre breakage. As the number of composite materials available and their application in the market scene increases, so does the challenge of controlling their performance characteristics by detecting damage propagation, understanding the cause of damage, predicting failure load to strain service life and identifying failure mechanisms and the sequence of failure. In other words AE employed during tensile testing provides the possibility for the “quality control of composites and fibres”.

1.2. Literature Review

Historically, the concept of fibrous reinforcement is very old. There are references to straw-reinforced clay bricks in ancient Egypt. The first fibre glass boat was made in 1942; reinforced plastics were also used in aircraft and electrical components at this time while Kevlar fibres were developed in 1973. Starting in the late 1970s applications of composites expanded widely in the aircraft, automotive, sporting goods and biomedical industries. Now emphasis is being placed on the development of ceramics/matrix components for high temperature applications. Applications abound, including underground pipes and containers, boats, ground vehicles, aircraft and aerospace structures.

Acoustic Emission and microseismic activity are naturally occurring phenomena. The first AE used by an artisan may well have been in making pottery (the oldest variety of hardfired pottery dates back to 6500 BC). In order to access the quality of their products, potters traditionally relied on the audible cracking sounds of clay vessels cooling in the kiln. These acoustic emissions were accurate indications that the ceramics were defective and did indeed structurally fail. The progress of AE was slow until recent decades. It is reasonable to assume that the first observation of AE in metals was when man learn to smelt pure tin and it produced audible emission by mechanical twinning during deformation, this occurring as early as 3700 BC.

If AE could be described by the use of a simple definition then this could be as follows: “transient elastic stress waves generated by the rapid release of energy from localised source within a material”. The first scientific documentation on AE has been reported by Jabin Ibn Hoyyan (known as Geber) [1]. However, the first comprehensive investigation into AE phenomena was carried-out by Kaiser[2]. He observed that by amplifying the signals from materials subjected to tensile testing, noise could be detected from well below the yield point. His most significant contribution was the discovery of the “Kaiser effect” named after him. Kaiser asserted that AE signals are not generating significant amounts during the re-loading of a material unless the stress exceeds the previous minimum value. Kim, Neto and Stephens [3], were among those who first seriously challenged the Kaiser effect. In their work on carbon fibre/epoxy composite, they found a nearly stabilised AE release process after several cycles. The most important point

made by them was perhaps the emphasis of correlating different AE signatures with the type of damage mechanism. Therefore, it was thought that the Kaiser effect applies to most metals, but not generally to other materials.

Observations of AE were rapidly exploited during 19th century and throughout the 20th century mainly in the USA as a part of the space technology requirements. Since then the AE technique has grown from good idea to a useful tool through pure research or applied research and into practical technique in industry, mainly to monitor the performance of a number of structures, including aircraft[4], aerospace structures[5], pressure vessels[6], tanks[7] and rotating mechanical equipments such as turbines [8], pumps[9] and bearings [10].

Since the 1970's, extensive work has been done on the characterisation of composite and fibre structures by the means of the AE. In the case of fibre reinforced composite materials the need to detect the onset and location of the matrix cracking and fibre debonding has led to the development of AE methods. In certain instances optical microscopy of the polishing sections on the edges of the test specimen has been applied, in order to prove the advantages and method of AE.

P.T Mc Gowan [11] showed the importance of AE in detecting early damage and thus estimate the remaining service life of glass fibre reinforced plastics. Simple models, such as a hexagonal arrays of fibres in a matrix suggested that transverse resin cracking is the mode of failure detected by conventional AE tests. However, the failure progression has also been monitored by a microscopic viewpoint in order to relate the microscopic analysis to the AE detector. The relationship between AE and composites has also extensively studied by a number of people over the years. Kanji Ono[12] in 1995 reported an experimental investigation on the mechanical and A.E behaviour of specially designed carbon fibre epoxy composites. Fibre fracture, delamination splitting and friction of delaminated faces contributed to characteristic behaviour. He tried to characterise these failure mechanisms on the basis of peak amplitude and event duration of observed AE signals. This approach referred to as "pattern recognition", has been studied by a number of scientists. Barre and Benzeggagh [13] reported a study of damage fracture mechanisms in short-glass fibre reinforced thermoplastics. The use of AE and scanning electron microscopy (SEM) enable them to identify several damage mechanisms. They also

correlate the AE amplitude ranges to different damage mechanisms. Ono and Huang [14] reviewed various approaches of pattern recognition of AE signals, together with Prosser [15] where he studied the initiation of cracking in cross-ply graphite epoxy composites and by the corresponding microscopic measurements he showed that the same source mechanism can generate a wide range of AE signal amplitudes which can be categorised. Hamstad [19], Harris [20], Lorenzo [21] all found that types of failure in these materials such as ply delamination, matrix cracking, interface debonding, fibre breakage and fibre pull-out produce A.E signals of different characteristics. Finally, Ely [16], Kawamoto [17] and Laws [18] have also during the year contributed to studies on the subject of characterising composite structures.

Together with this kind of more general research some workers have reported exclusively studies on transverse fibre composites and factors influencing AE in composite samples [22-23]. Hill and Okoroafor [24, 25] and Netravali [26] have published a number of papers on the determination of fibre resin interface strength in fibre reinforced plastics using AE techniques. These papers provide the main core of the background information for this investigation, since AE has been employed by them in a new way to deduce information regarding the level of adhesion between fibres and matrix resin. AE has been shown to respond on the different conditions of the materials tested and has proved a useful technique in casting new light on the quality (and reality) of surface adhesion.

For the investigation of fibre bundles Hill and Cowing have published a number of papers [27-30]. In their studies AE was used for the characterisation of fibre bundles of E-glass and Kevlar-49. The Bundles subjected to various treatment have been strained to failure in order to investigate the relationship between A.E and fibre strength. The distribution of mechanical failure was characterised using Weibull statistics applied to the AE signals, which was thoroughly examined with their corresponding Weibull parameters extracted. Studies were made of the distribution of fibre break locations [31], [28], the occurrences of the multiple fibre breaks locations, the occurrences of multiple fibre breaks and the attenuation of the AE signals.

Generally, all this research has been used as a guide and has provided a major driving force and inspiration during this research. At first, this thesis considers further progress in the investigation of glass/Kevlar fibre reinforced transverse composites. For

the second part of the investigation fibre bundles will be examined during tensile testing in order to characterise the failure process by means of AE.

In summary, Chapter 2, deals with experimental system used for the building/manufacturing and testing of composites. Chapter 3 gives the different characteristics of the composites after curing and post-curing treatments and addresses the results for glass and Kevlar fibre composites. It also deals with the interfacial adhesion characteristics between fibre and matrix. Chapter 4 considers statistical analysis of the A.E data mainly by the means of Weibull Statistics. Chapter 5 considers experiments monitoring the AE events during tensile testing of fibre bundles of glass and carbon. Finally, Chapter 6 works on three different statistical approaches on the characterisation and prediction of the AE data and chapter 7 provides an overall view of this research as well as the possibility for applying AE to future work.

1.3. Structural Applications of Composites and Cost Effectiveness

The types of composites and composite design technologies adopted by different sectors of industry can be quite specific to the particular requirements and practice of that particular sector. Since weight reduction is critical, composite elements are used widely for automotive, aerospace, marine and architectural structures in addition to consumer products such as skis, golf clubs and rackets.

Military aircraft designers were among the first to realise the potential of composites with high specific strength, high specific stiffness, and low weight, having smooth surfaces which reduce drag. As for the commercial aircraft industry, composite applications have steadily increased as materials cost came down, as design and manufacturing capability developed and experience increased. Boeing 757 and 767 were among the first commercial airliners to make extensive use of composites, with 30% of the external surface area of the Boeing 767 consisting of composites.

The cost per unit weight is an important factor for the spacecraft industry. This makes composites extremely attractive for such applications. NASA have considered the use of composite components for large space structures such as the proposed space station, where the key properties of the materials are high stiffness-to-weight, low thermal expansion coefficient and good vibration damping characteristics, which composites offer over conventional metallic materials. Structural weight is also very important in automotive vehicles, offering possibilities for fibre reinforced materials. Composites also offer the possibility, of using fewer parts with associated lower assembly and manufacturing costs. As with airliners, the applications of composites in automotive vehicles up to this point have been mainly in secondary structural elements and cosmetic components and the full potential of composite construction remain to be explored and developed.

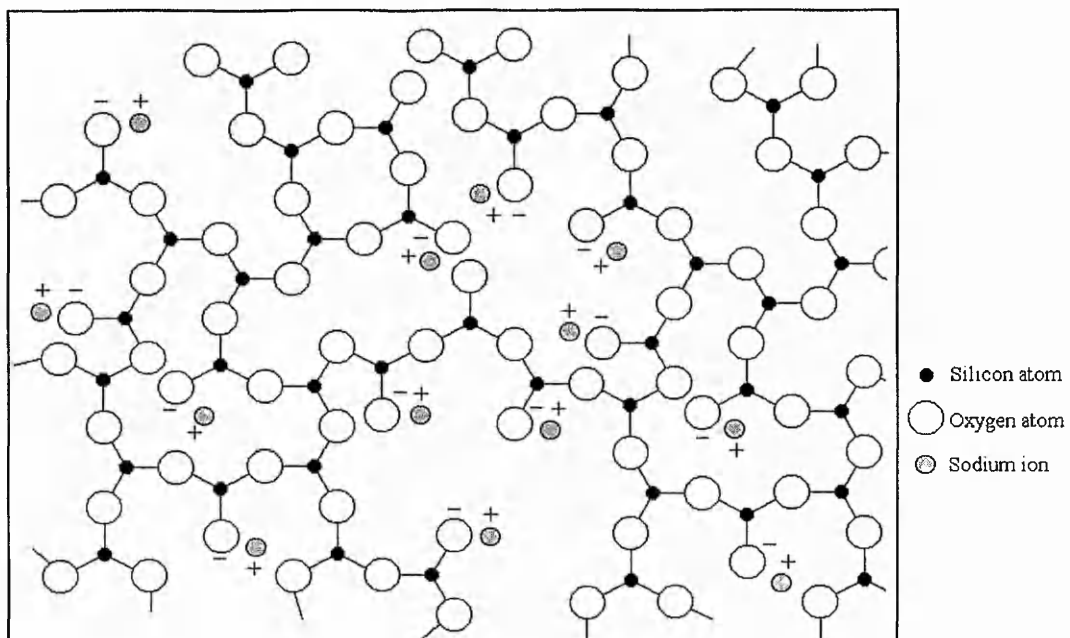
The use of composites in structural applications is also growing since corrosion resistance and electrical and thermal insulation are added advantages in comparison with metals. One of the important advantages of composites is reduction in assembly and / or life cycle costs. This is effected through weight savings, lower tool costs, reduced number

of parts and fewer assembly operations. These observations indicate the need for further development in the quality and application of composite materials.

1.4. Fibres and Fibre Bundles Characteristics

1.4.1 Glass Fibres Characteristics.

Glass fibres are the most convenient reinforcement for polymer matrix composites. Low cost, high tensile and impact strengths and high chemical resistance, stiffness and good electrical and weathering properties are some of the main advantages. However, low modulus, abrasion, low fatigue resistance are some of the disadvantages compared to some of the organic fibres. The strength and modulus of glass is determined primarily by the 3-dimensional structure of the constituent oxides. Figure 1.1 shows a 2-dimensional representation of the 3-dimensional network of linked polyhedron units in a simple sodium silicate glass. Each polyhedron is a combination of oxygen atoms around a silicon atom and they are bonded to each other by strong covalent bonds. In contrast to carbon and Kevlar-49 fibres, the properties of glass fibres are isotropic so that, for example, Young's modulus along the fibre axis is the same as transverse to the axis. The strength is strongly dependent on the processing conditions and testing environment. Since the most important factor determining the ultimate strength of glass is the damage which fibres sustain when they rub against each other during processing operations, the application of size coating at a very early stage in manufacture helps to minimise damage. It is noticeable that in the aerospace industry and military engineering the output of glass reinforced plastics exceeds 50% of the total range of polymeric composite material manufacture.

TYPICAL REPRESENTATION OF THE STRUCTURE OF GLASS FIBRES

◆ **Figure 1.1:** A two dimensional representation of constituent oxides for glass fibres.

1.4.2 Kevlar and Carbon Fibre Characteristics.

Aramid fibres, (such as Kevlar-49) is a generic term used to describe aromatic polyamide fibres. The strong covalent bonds in the fibre axis direction provide high longitudinal strength, whereas the weak hydrogen bonds in the transverse direction result in low transverse strength. The more rigid and complex molecules impart high mechanical and thermal properties to aramid fibres. These fibres, with high specific strength, have great cohesiveness and they absorb much more energy than the brittle fibres, that is why they are widely used in lightweight armour and other impact resistant structures. However, they do have a highly anisotropic structure that leads to low longitudinal shear moduli, for transverse properties and low axial compressive strength. Finally, the thermal stability of Kevlar-49 is inferior to both glass and carbon, while probably adequate for use in most polymer matrix systems.

High strength, high modulus carbon fibres are manufactured by treating organic fibres with heat and tension, leading to highly ordered carbon structure. Carbon fibres are far superior to E-glass fibres in terms of specific modulus with Kevlar-49 fibres significantly better than the E-glass but inferior to carbon. Also another characteristic of these fibres is that in the absence of air and other oxidising atmospheres carbon fibres possess exceptionally good high temperature properties. Carbon and glass fibres are almost completely brittle and fracture without any reduction in cross section area. In contrast Kevlar-49 fibres fracture in ductile manner. Table 1.1 includes information on the basic characteristics that these three types of fibres offer [32].

- ◆ **Table 1.1:** Advantages and Disadvantages of Glass, Kevlar and Carbon Reinforcing Fibres.

<i>Fibre type</i>	<i>Advantages</i>	<i>Disadvantages</i>
E-glass	High Strength/Low Cost	Low Stiffness and Fatigue life High Temperature Sensitivity
Aramid (Kevlar)	High Tensile Strength	Low Compressive Strength
	Low Density	High Moisture Absorption / High Cost
Carbon	High Strength / High Stiffness	Moderately High Cost

1.5. Matrix - Fibre Interfacial Characteristics

The role of the matrix in a fibre reinforced composites is to transfer stresses between the fibres, to provide a barrier against an adverse environment and to protect the surface of the fibres from mechanical abrasion. The matrix plays a minor role in the tensile load-carrying capacity of a composite structure. The processability and defects in a composite material depend strongly on the physical characteristics, such as viscosity, melting point for the plastic composite and curing temperature of the matrix.

The fibre-matrix interface performance has an effect on the mechanical and physical properties of composite materials. Properties affected can include interlaminar shear strength, delamination resistance, fatigue and corrosion resistance. In particular, large differences between the elastic properties of the matrix and the fibres have to be communicated through the interface. In other words, the stresses acting on the matrix are transmitted to the fibres through the interface.

A number of assumptions have to be made about the properties of the interface in order to be able provide any model of mechanical behaviour. These assumptions would include:

- (a) the matrix and the fibre behave as elastic materials.
- (b) the interface is infinitesimally thin.
- (c) the bond between the fibre and matrix is perfect which implies that there is no strain discontinuity across the interface.
- (d) the material close to the fibre has the same strain properties as the material in bulk form and
- (e) the fibres are arranged in a regular or repeating array.

These assumptions are necessary to obtain solutions to the mathematical models and the results obtained are an important guide as to what is likely to happen in real composite systems. Theocaris, [33] has conducted a comprehensive study on the modeling of the composite interface and its role in the prediction of the composite material performance.

Evaluation of the magnitude of fibre adhesion can be achieved in a number of ways including the use of single fibres embedded in a resin and subject to longitudinal fragmentation or the "single fibre pullout" test. [34]. In the work reported here, the experimental procedure follows that previously used by Okoroafor and Hill [24] where a complete fibre bundle is used with the load applied transverse to the resin fibre interface. By using a complete fibre bundle, the system more accurately reflects the situation in an engineering composite. Transverse strength evaluated in this way is of interest, providing a way of evaluating the "quality" of the resin/fibre interface.

Finally, in the case where the load is applied to a composite lamina at an angle of 90° with respect to fibres, it has to be mentioned that the fibres act as hard inclusions in the matrix and enhance the local strain and stress magnitude in the matrix near the fibre-matrix interface. The concept of interfacial adhesion, as defined by this type of transverse test, will be extensively examined for both the E-glass and Kevlar-49 fibre-matrix interface.

1.6. Polymer Matrices and Thermosetting Resins

In thermosetting polymers the liquid resin is converted into a hard solid by chemical cross-linking, which leads to the formation of a tightly bound three-dimensional molecular network. This is usually done while the composite is being formed. The mechanical properties of the resin depend on the molecular units making up the network and on the length and density of cross-links. The former is determined by the initial chemicals used and the latter by control of cross-linking processes in the cure. Curing can be achieved at room temperature, but is usual to use a cure schedule which involves heating at one or more temperatures for predetermined times to achieve optimum cross-linking and hence optimum properties.

Thermosetting resins are usually isotropic and one of their most useful properties is in response to heat since, unlike thermoplastics, they do not melt on heating. They are essentially brittle materials but generally epoxies are stiffer than unsaturated polyesters. In fibre reinforced composite materials the fibres are incorporated into the liquid thermosetting resin to which catalyst and hardener have been added. These cause the resin to polymerise and after curing form a solid polymer reinforced with fibres.

CHAPTER 2

AE CHARACTERISTICS AND TESTING PROCEDURES

2.1 Fundamentals of AE

Formally defined, AE is “the class of phenomena where transient elastic waves are generated by the rapid release of energy from localised sources within a material, or the transient elastic waves so generated” [35]. This is a definition embracing both the process of wave generation and the wave itself. AE differs from most other non-destructive methods in two significant aspects. First, the energy that is detected is released from within the test object (in the case of this work, from debonding of the fiber/matrix interface, from matrix cracking or from fiber fracture) rather being supplied by the non-destructive method, as in the case of ultrasonics or radiography. Second, AE is capable of detecting the dynamic fracture processes in real time, associated with the degradation of structural integrity. Crack growth and plastic deformation (in the case of metals) are major sources of AE. Latent discontinuities that enlarge under load and are active sources of AE by virtue of their size, location or orientation are also the most likely to be significant in terms of structural integrity. These discontinuities are found in large numbers, in systems such as composites, due to different characteristic nature of each of the composites and to manufacturing irregularities.

AE monitoring of fiber reinforced composite material has proven effective when compared to other non-destructive testing methods. When the characteristic AE response has been defined, AE tests can be used to evaluate the structural integrity of the component. However, attenuation of the AE signals in cross-ply transverse fiber reinforced materials presents unique problems. Effective AE monitoring of fiber reinforced components requires much closer sensor spacing and a sensor location nearer the emitted source than would be the case with a metal component. When a crack begins to grow, AE is detected by the sensor/s which (for instance) in the case of transverse composite tests reported here are placed directly on to the fiber/matrix area. The sensor's output is amplified and fed into the electronic processing unit. It is important to note here that because of the Kaiser effect, AE signal may only occur once, so that AE inspections

have a “now-or-never” quality. In this respect, AE is at a disadvantage when compared with NDT techniques that can be applied again by different operators or instruments.

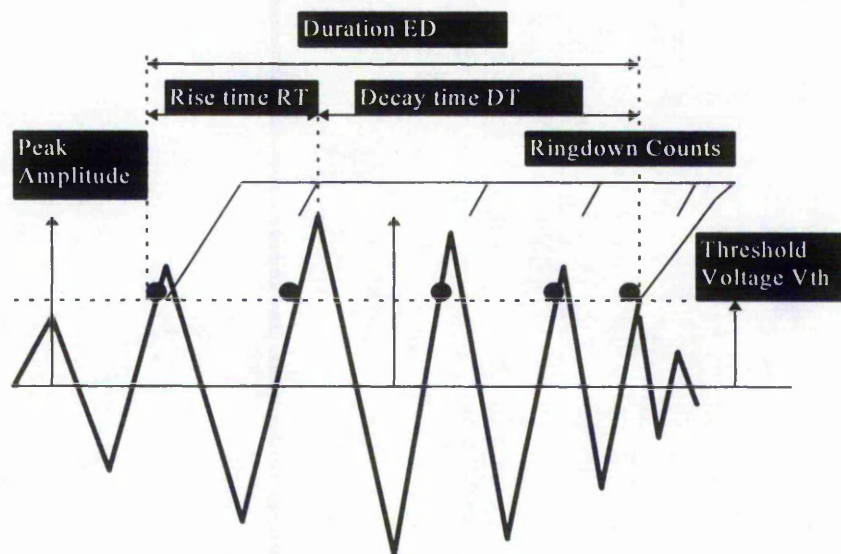
Generally, the field of AE is still growing vigorously and presents many challenges. The mathematical theory of the AE source was developed during the 1970s and the practical application of this theory is still in early stages. Sometimes it seems that the technology lacks universal frameworks for the description of material emissivities and the interpretation of structural test data. There is a constant need to improve instrumentation and testing techniques as AE is pressed into service in tougher environments and more demanding applications.

2.2 Important AE Parameters

Several parameters can be used to characterise the AE source as is been shown in figure 2.1, which schematically represents a resonant transducer AE signal. In the case of fiber glass and Kevlar composite materials as well as the various fiber bundles, the AE is emitted as a short duration transient signal. During emission, acoustic energy builds in the tested system while the source is in operation. This period is defined as the rise time “RT”. Once the transducer signal has reached its maximum the signal begins to decay, mainly controlled by the stress pulse arrivals and the signal decay in the transducer until the decaying signal fall below a pre-set value (threshold) “ V_{th} ”. This period is known as the decay time “DT”. The total event duration (ED) is:

$$ED = RT + DT \quad (2.1)$$

Research work reported in this thesis has involved measurements of AE signal parameters in order to draw as much information as possible from the recorded AE signals. The following three parameters have been mainly used throughout this investigation: (i) ringdown counts, (ii) peak amplitude, (iii) event duration, (iv) number of events.



◆ **Figure 2.1: Acoustic Emission Parameters**

2.2.1 Ringdown Counts and Count Rate

This is a measure of the total number of times a signal crosses a pre-set threshold level versus time. This number of threshold crossing per unit time is generally analogous to the sensor frequency. The ringdown count per event also depends on the damping characteristics of the sensor, damping characteristics of the structure and pre-set threshold level. Ringdown counts are caused by the resonant characteristics of the detecting transducer and the multiple reflections at the specimen boundaries.

A transducer signal can be assumed to have the form:

$$V = V_0 \exp(-Bt) \sin \omega t \quad (2.2)$$

Where: V = Output voltage of sensor.

V_0 = Initial signal amplitude.

B = Decay constant.

ω = Angular frequency.

2.2.2 Peak Amplitude and Amplitude Distribution

Acoustic emission events can also be described by using the peak amplitude and its statistical distribution. It has been suggested that for composite materials and fiber bundles, matrix deformation, matrix cracking, fiber debonding and fracture can be identified by their relatively different amplitude distribution. [36], [37]. The peak amplitude of AE signal is calculated in respect to a reference pre-set voltage (V_{th}), which in this investigation is 0.2 V for 40/60 dB preamplifiers. Although the change in threshold voltage significantly changes the count number, it does not, however, greatly change the amplitude - distribution values.

2.2.3 Event Duration

As shown in figure 2.1 event duration (ED) can be defined as:

$$ED = RT + DT \quad (2.1)$$

However, the use of this parameter was not used extensively in this investigation since the parameter seems to provide little advantage over the use of ringdown counts per AE event.

2.3 Ultrasound, AE and AE Transducers

Ultrasound is acoustic energy above the audio spectrum and in common with all acoustic energies, requires a physical medium to propagate. The nature of the ultrasonic energy propagating, in the case of AE from composites, depends on; the type of fibers, fiber orientation, type of matrix, fiber to resin ratio, resin cure conditions, material conditioning, presence of discontinuities and overall quality. In this experimental work, ultrasound, in the form of AE, is employed to listen to the noise by breaking fibers or propagating cracks and defects. This noise is called Acoustic Emission.

Typically, ultrasound is detected and emitted using piezoelectric transducers. The application of electric field causes the ultrasonic transducer to vibrate at a frequency corresponding to the exciting frequency and transmit. When this transducer is matched properly to the signal sources, and is linked by a suitable transmission medium to the test material, it can both send out and receive ultrasonic energy. Through the display and study of the modifications that such energy undergoes as it is transmitted, refracted or reflected say by different test objects, it is possible to make interpretations about the size, location and character of interior structures.

Any transducer will have a characteristic frequency called a **resonant frequency**. If the transducer is excited by a single pulse, as is the case in most commercial pulsed-

ultrasound systems, the transducer will vibrate and radiate at this resonant frequency. This resonant frequency is excited whether the excitation of the transducer is electrical (transmitting mode) or mechanical (receiving mode).

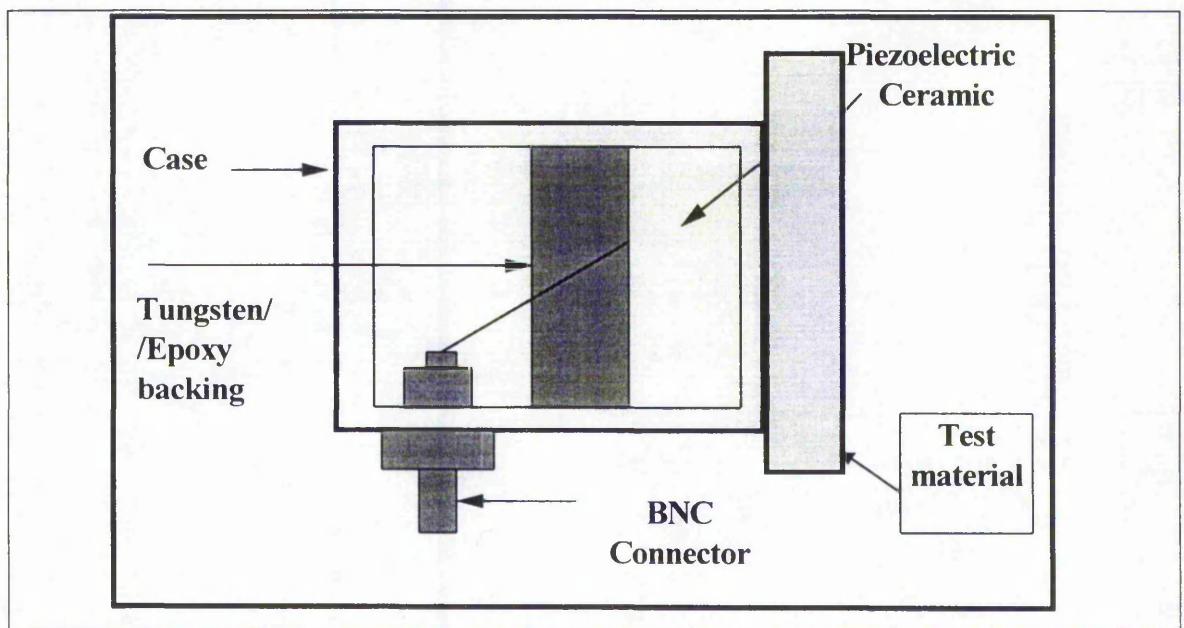
Although the piezoelectric effect has been known for practically 90 years, it is during the last 30 years that practical piezoelectric transducers have become common. Piezoelectricity (discovered by Pierre and Jacques Curie in 1880) is a term meaning pressure electricity. If a particular type of crystals are squeezed along specified directions, an electric charge will be developed by the crystal. Typical example of a transducer is shown in figure 2.2. When a transducer is excited by an electrical spike, (as an ultrasound generator), impulses of opposite sign will be excited at each interface. Each time a stress wave strikes a boundary, the amplitude and phase of the reflected and transmitted waves will be governed by the relative acoustic impedance of the two materials making up the boundary. Maximum energy transfer happens when the acoustic boundary impedances are equal.

Acoustic Emission transducers are typically, of simple design, with single resonant piezoelectric elements being used. Recently more advanced transducers have been manufactured using a piezoelectric of **piezoelectric ceramic rods** embedded in polymer matrix [38-41]. Such structure can resonate at a number of different frequencies depending on the width of the rods and the width to thickness ratio of the rods. It is desirable for any transducer to have high electromechanical coupling coefficient " K_t " which reflects the ability to convert electrical energy into mechanical, low acoustic impedance. Dielectric constant " ϵ_s " should be adjustable over a wide span and electrical and mechanical losses should be kept as low as possible.

Significant advantages in performance characteristics of motion, force and pressure transducers have made in the past decade using new piezoelectric materials. In piezoelectric ceramic materials, the directions of the electrical and mechanical axes depend upon the direction of the original 'DC' polarising field. During the poling process, a ceramic element experiences a permanent increase in dimensions between poling electrodes and a permanent decrease in dimensions parallel to the electrodes.

When a 'DC' voltage of the same polarity as the poling voltage but of smaller magnitude subsequently is applied between the poling electrodes, the element experiences further but temporary expansion in the poling direction and expands parallel to the electrodes. The thickness and transverse effects are not of equal magnitude; accordingly there is a small volume change when voltage is applied to the electrodes.

The main considerations in AE sensor selection are the operating frequency, sensitivity, environmental and physical characteristics. The physical, chemical and piezoelectric characteristics of the piezoelectric material used can be adjusted to specific applications. Piezoelectric materials are chemically inert, and immune to moisture and other atmospheric interferences. Ceramic piezoelectrics have a number of advantages, providing a combination of low cost, high sensitivity, ease of handling, selective frequency responses and can be manufacture in a range of shape or size.

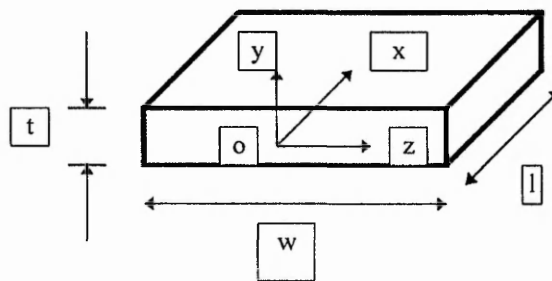


◆ **Figure 2.2: Typical Example of a Transducer design.**

2.4 Transducer Uncertainties and Attenuation

As a closing remark to this chapter it may be helpful to point out potential difficulties which need to be considered when using AE transducers. [42-43]. AE measurements may be carried out under a variety of different experimental conditions, in some cases with the transducer receiving bulk like waves (testing on small structures) and in other cases receiving Lamb waves, on structures such as pressure vessels.

Lamb waves, (also called plate waves), only occur where two parallel surfaces are found as in plates. For a plate separated by thickness t , the remaining parallel surfaces are assumed to be separated by a much larger distances, l and w , that do not affect the wave propagation. This is shown in figure 2.3.



◆ **Figure 2.3: Plate for Lamb waves**

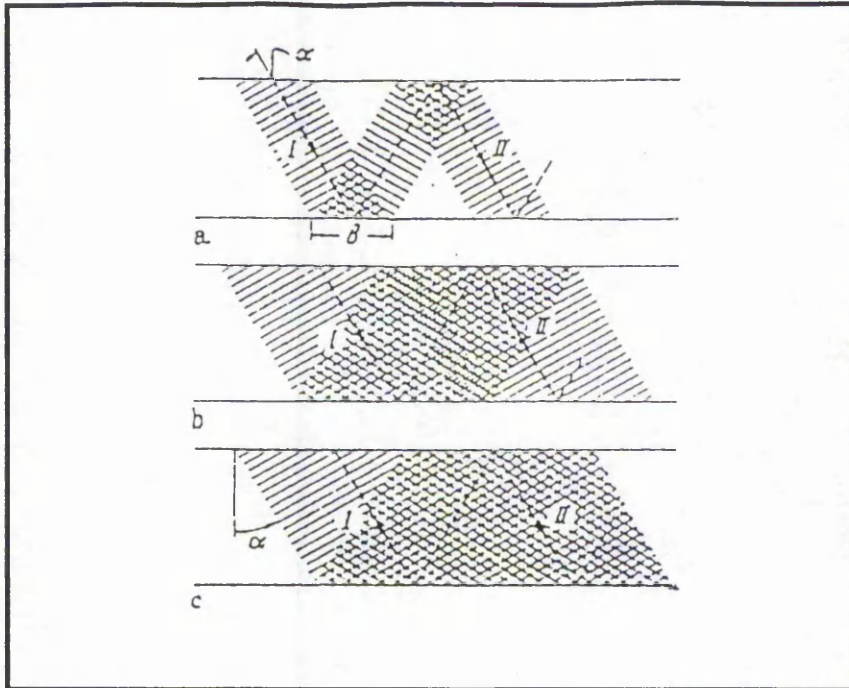
For a certain incident angle of the P and S waves their reflections lead to a constructive interference. After multiple reflections these rays build a waveform called a Lamb wave as is been shown in figure 2.4. Lamb waves posses some characteristics that make them particularly useful for some specialised applications in NDE. As guided waves, or they will travel within flat mildly curved plates, giving a possible path of inspection to an otherwise inaccessible area.

Ultrasonic inspection in most cases is conducted using bulk type waves or quasibulk waves. A pure bulk wave may be excited with point source, as for example an AE source, occurring in an unbounded medium. With this configuration, the propagation

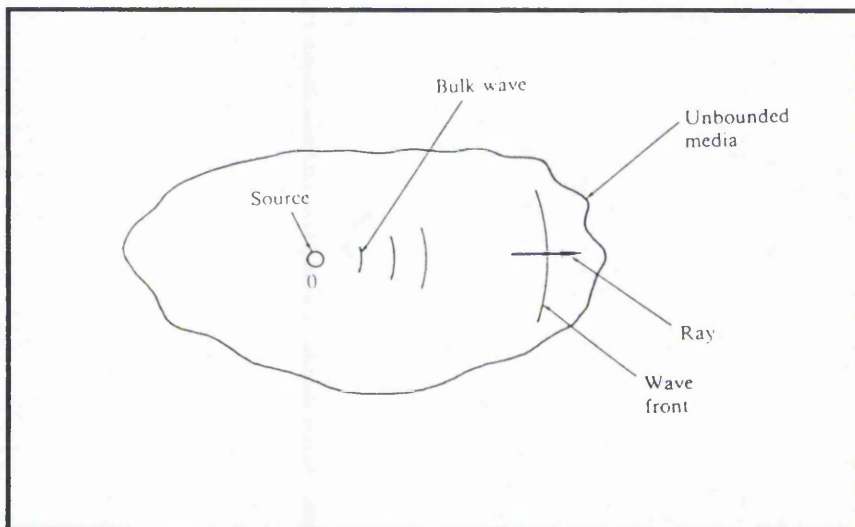
characteristics are described by a 3-dimensional field as compared to the 1-dimensional field of the plane waves. For the bulk situation, a pure longitudinal disturbance produces deformation in the lateral directions as well. A schematic of a bulk wave is illustrated in figure 2.5. [40]. The variations of wavetype are often significant when applying acoustic emission testing to specific applications and structures.

The problem is also complicated by the constancy and method of coupling of the transducer to the specimen surface and for a very rigid adherence, the transducer and specimen can act effectively as a single unit and the radial modes of a disk transducer could be excited. In general the actual situation will involve a combination of these two cases although in the small size specimen used in laboratory tests, it is the direct (i.e. bulk) wave which has usually the greater significance.

Finally, the transducer response depends on the type of couplant which is used. The effect on the propagation of sound in the couplant, can theoretically be omitted as long as the couplant exists as a thin layer compared to the wavelength of sound. However, in practice, this is not always true and therefore, it is a potential source of variability and uncertainty associated with piezoelectric transducers and AE measurement. In the case of this work, this particular uncertainty can be dealt with by introducing a spring clamp to clamp the transducer to each of the specimens under test in order to minimise the variation (and thickness) of the couplant thickness.



◆ **Figure 2.4: Generation of Lamb wave. Only in case (c) where a broad wavefront is reflected at the angle 'a', do the rays interfere constructively with the build up of a Lamb wave.**



◆ **Figure 2.5: Bulk wave excitation and propagation.**

2.5 Experimental Procedure.

2.5.1 Preparation of the Transverse Fibre Reinforced Composite

Material

Composite reinforcements used in this study include E-glass (Fiber Glass (UK) Ltd, Equerove, Silane sized, ECB, 600 tex) of nominal diameter 10-12 μm and Kevlar-49 (Du Pont (UK) Ltd, Den 2160, tex 2400, 1000 filaments, finish free) of nominal diameter 14.25 μm . The matrix material used was Crystic Polyester 272 resin, supplied by Scott Bader (UK) Ltd which is an isophathic unsaturated polyester resin developed for high performance applications since it offers high mechanical strength and excellent strength retention in wet environments at medium temperature up to 50 °C.

The composite materials were prepared following the recommended procedure: 100 parts Crystic Polyester 272 resin, 2 parts of Catalyst M (methyl ethyl ketone peroxide), 0.4-1.0 parts of cobalt Accelerator E in styrene. This resin was then poured into a dog bone shaped mould of silicon rubber. In this study, two types of composite specimen were investigated, using both glass and Kevlar fiber reinforcement. In the first category are the specimens cured for 7 days at room temperature and in the second, specimens which had been subjected to a further post-cure for 2-4 hours at 80 °C in an oven.

The fiber bundle composites used in the testing had a bundle of either fiber system centrally located with respect to the mould but oriented transversely to the longitudinal axis of the mould. All composite gauge dimensions were 40 mm x 5 mm x 2.5 mm.

2.5.2 Tensile Test Conditions.

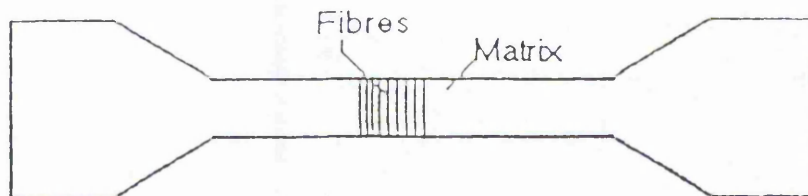
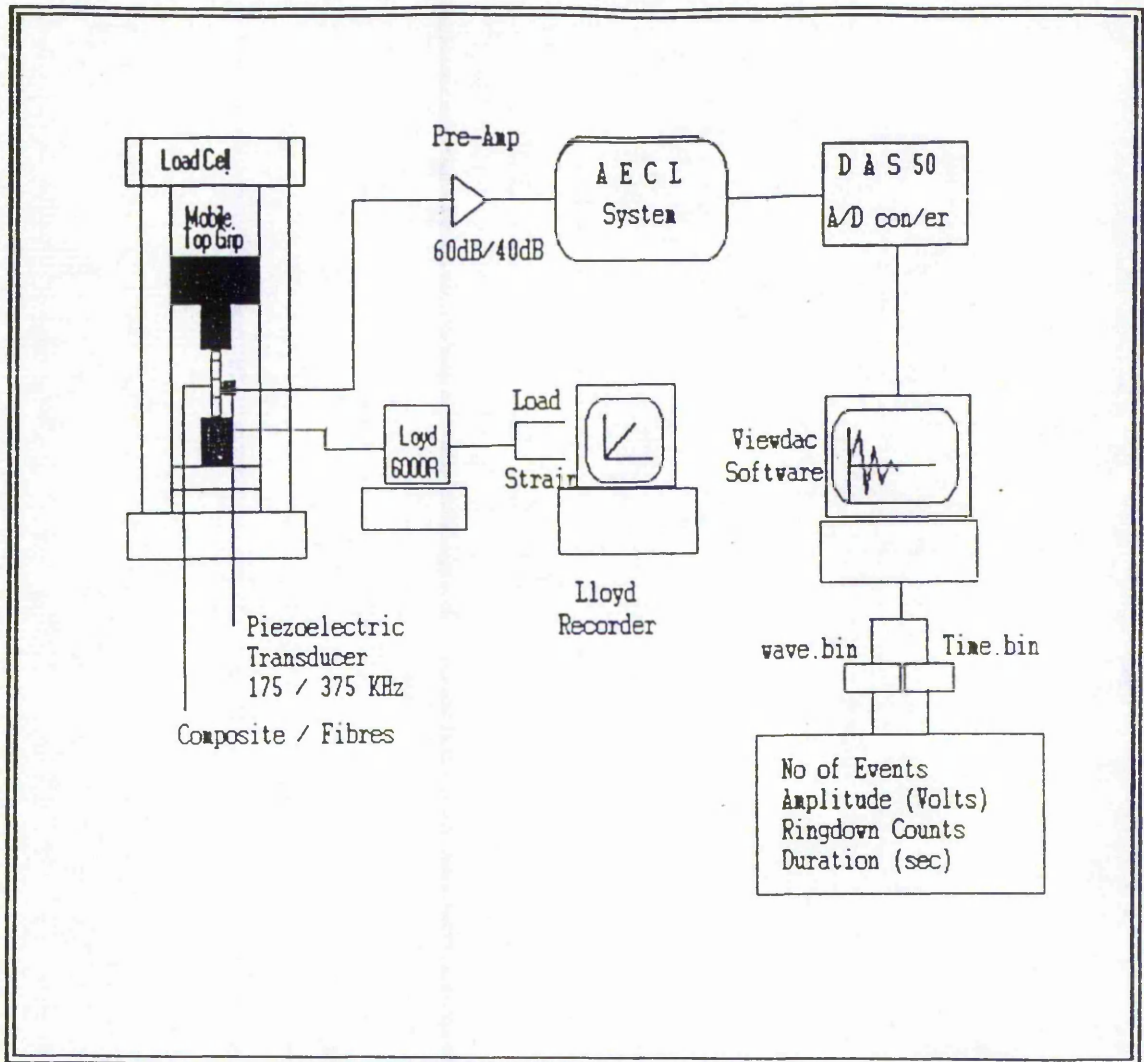
Mechanical tensile test were performed using a LLOYD-6000R test machine. The specimen were loaded at a constant speed of 0.5 %/min. (0.2 mm min.^{-1}), at a room temperature range of $20 \pm 5 \text{ }^\circ\text{C}$. The Acoustic Emission technique was employed during the tests as a mean of monitoring and distinguishing between the fracture mechanisms occurring during the deformation of the composite materials. AE can monitor active crack growth continuously, using transducers that can be tailored to work in confined spaces, hostile environments and so is well suited to industrial applications. AE is a sudden release of strain energy in the material as short bursts of elastic wave energy. These material displacements can be detected and converted into fluctuating voltage signals by sensitive piezoelectric transducers. The technique has previously [27, 28] been employed to monitor fiber failures and their mode (singlets, doublets, triplets, and so on) during tensile testing of fiber bundles in air, yielding the stress-strain response.

In this study, a commercial acoustic emission transducer (AC375L, resonant frequency 375 kHz, supplied by Acoustic Emission Technology Corporation) was utilised. As the stress wave caused by the deformation event travels across the surface of a material small movements of the surface occur. The role of the sensor is to convert these small movements of the test sample surface into useful electrical signal. The sensor was clamped in the middle of a dogbone shape specimen which was mounted in the bottom grip of the tensile machine. Silicon grease was used as a couplant in order to transmit the sample stress wave signals to the sensor.

The AE signal from the transducer, is in the form of decaying sine waves of given initial amplitude, frequency and decay constant, and these signals were preamplified by 60dB (AECL 2100/PA, 208-530kHz bandpass) and than processed using the AECL 2100 M acoustic emission system. The processed data then passed via an integral analogue to digital (A-D) DAS 50 board. This can accept data from up to 4 single-ended channels, can operate in Unipolar or bipolar mode with software selected input ranges of $\pm 2.5\text{V}$, $\pm 5\text{V}$, $\pm 10\text{ Volts}$. It has a maximum sample rate of 1,000,000 samples/sec and was set to record 200 samples per AE event. This board operated within a 486DX33 computer under the control of Viewdac software package which acquired data from the DAS board and could

easily handle large data sets, offering both high speed and long duration data acquisition. The software could analyse and graph data in real time with a feature of exploring the data with interactive graphics and a full complement of time, frequency and statistical analysis functions. The software was set up to provide information such as: number of AE events, and duration, amplitude, ringdown counts and energy of each AE event.

The system setting used were: threshold 0.2 Volts and dead time 0.2 msec. The former was chosen to minimise electronic background noise from the grips and from the tensile machine, thus ensuring that received signals were from the damage sources occurring in the composite been tested. For the ringdown counting (i.e. number of oscillations greater than the preset threshold level) and amplitude determination, an analysis window of 200 μ sec was defined. If at the end of the signal it did not pass the threshold for 0.2msec then it was taken to be the end of the event. Figure 2.6 shows a schematic diagram of the experimental system and specimen types.



Transverse bundle of fibres composite (TBFC)

◆ **Figure 2.6:** Schematic diagram of the experimental system together and a typical diagram of transverse fibre reinforced composite material.

CHAPTER 3

TESTING E-GLASS AND KEVLAR-49 COMPOSITE MATERIALS

3.1 Aim of the Tensile Testing on Composites

This chapter addresses the importance of interfacial properties in glass and Kevlar transverse fibre reinforced composites materials. Studies on curing and post-curing, for the glass fibre composites and fibre surface treatment for the Kevlar fibre composites, aim to modify the adhesion between the fibre bundle and the resin material. Such treatments can easily alter the bulk material properties via the fibre surface or the interface resin structure, and possibly by modification of surface defects and surface chemistry. This would ultimately influence the properties of the finished composite materials. The changes will then appear in the AE signature relative to the stress-strain response during tensile testing.

3.2 Curing and Post Curing Processes

Traditionally, thermoset polymers have been used as a matrix material for fibre-reinforced composites. The curing reaction for polyester resins is initiated by adding small quantities of catalyst to the liquid mix. With the application of heat the catalyst decomposes rapidly into free radicals, which react with the styrene molecules and break their C=C bonds. Styrene radicals in turn, join with the polymer molecules at their saturation points and eventually form cross-links between them. As a result liquid resins are converted into hard brittle solids by chemical cross-linking which leads to the formation of a tightly bonded 3 dimensional network of polymer chains. Heating curing used in order to achieve optimum cross-linking and mechanical properties, depends on the molecular units making up the network and the length and density of the crosslinks. This sudden and irreversible transformation from a viscous liquid to an elastic gel, which marks the first appearance of the infinite network, is called the gel point. From the processing standpoint, gelation is critical since the polymer does not flow and is no longer processable beyond this point. Gelation occurs at well defined and calculable stage in the course of the

chemical reaction, and is dependent on the functionality, reactivity and stoichiometry of the reactants. Curing reactions can take place until absolute exhaustion of reactive groups and only at temperatures above the glass transition temperature of a complete cured binder.

During the post-curing process, which is been carried-out in this investigation, it was particularly clear that the post-curing improved the elastic modulus, toughness and stress distribution of the matrix leading to the formation of a mechanically superior interface. Post-cure increased the polymer strength. However, it should be noted, that mechanical properties of thermosetting polymers can only be improved up to a limit with increasing cure temperature and time values. Further increases in cure and post cure temperature and time usually result in deterioration of mechanical properties. For example, the yield strength and elastic modulus when plotted against temperature behaves as a bell-shaped function: first it increases up to a limit and decreases at elevated post cure temperature, associated with a reduction of the fracture energy.[44].

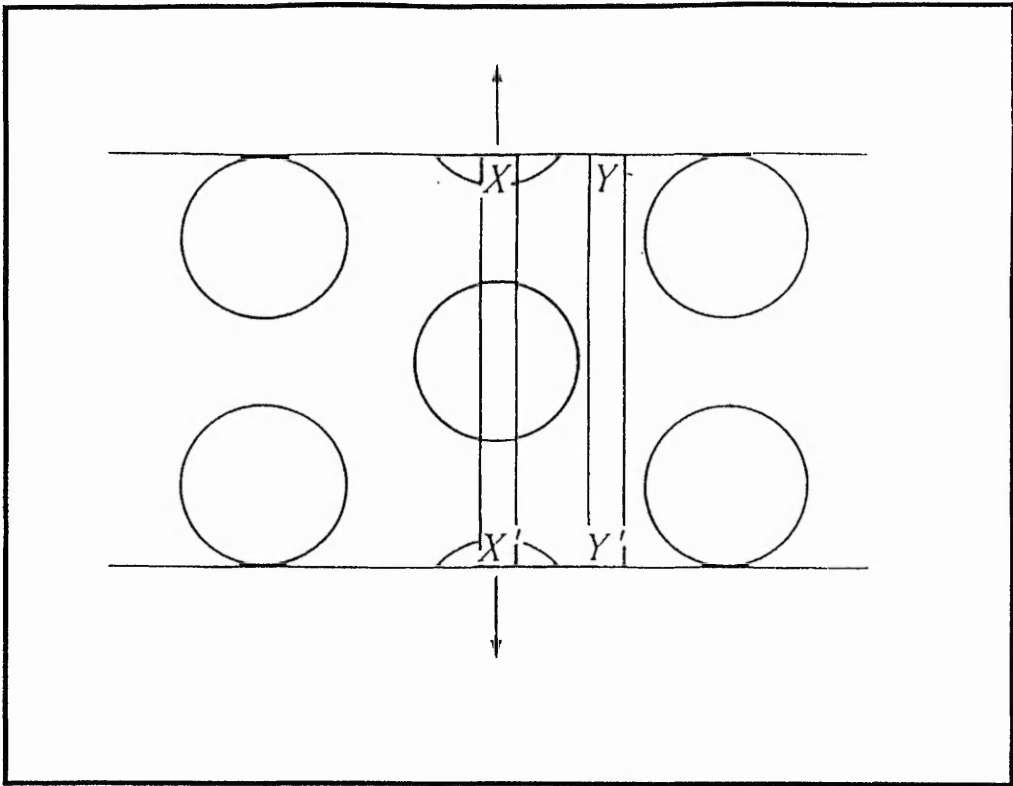
The stresses due to curing arise from a combination of resin shrinkage during the curing processes and differential thermal contraction after post curing at elevated temperature. Much of the resin shrinkage occurs while it is still liquid so that stresses do not develop. This shrinkage can lead to sink marks and other undesirable surface effects on plastic products. Resin shrinkage in the later stages of cure leads to microstresses which cannot be relieved. Microstresses are often sufficient to produce microcracking even in the absence of external loads.

3.3 Micromechanics of Transverse Reinforced Composites

A desired effect in composites is to maximise polymeric matrix-fibre adhesion along the interface. Undesirable effects may occur due to incompleteness of phase contacts and cracks. The interface is a geometric boundary between the fibres and the matrix, and the final properties will be influenced by the physical and chemical processes taking place during interactions of the fibre and matrix in the composite formulation stage. The interface condition and its structure, including, the concentration of defects, is affected by the physical, chemical and thermomechanical compatibility of the composite forming components. The first two define the phase contact completeness, via the nature, number and strength of the physical and chemical bonds, generated by the interaction of the polymeric matrix with the fibre surface. The effects of structure formation, the change of the matrix and fibre composition, and the properties in the boundary layers due to interdiffusion, the catalyst effect and the binder curing process can all influence the nature of the final interface.

Several authors have considered the influence of fibre spacing on the mechanical characteristics and performance of a composite materials[45-47]. Results of these studies indicate that decreased fibre spacing increases the magnitude of the local thermal stresses and consequently leads to an increase in microcracking. They also have demonstrated that the material properties of a thin interface region around the fibre has a significant effect on local thermal stresses.

Shrinkage of resin between closely packed fibres will also produce tensile stresses in the resin and across the fibre-matrix interface. Therefore, one of the primary reasons for the non uniform distribution of stress in the composite materials is the stress magnification and shrinkage which are obtained when the fibres are closely packed. As can be seen in figure 3.1 the strain in slice YY' which passes completely through the resin will be much smaller than in resin in slice XX' [48]. In other words there is a strain magnification in the resin between the fibres. The different strains in different parts of the resin lead to additional stresses and consequently non-uniform stress distribution.

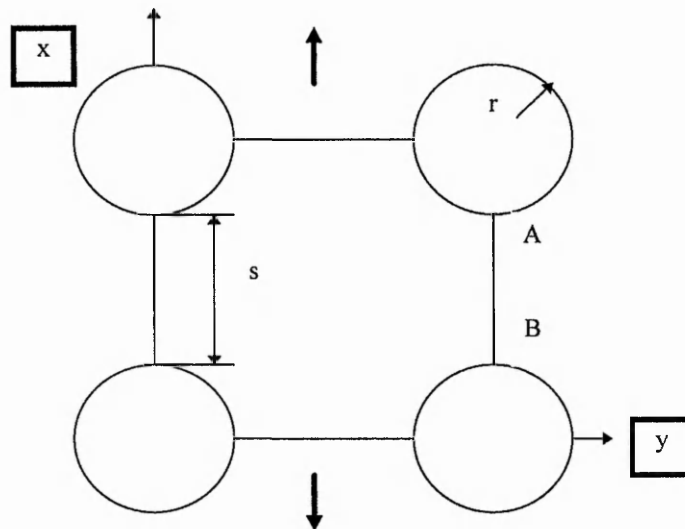


◆ **Figure 3.1: Schematic representation of strain magnification in a unidirectional lamina subjected to transverse load**

Kies [48], made one of the earliest quantitative estimates of the non-uniform distribution of strain in the matrix between the fibres, using the simple model illustrated in figure 3.2. When a square array is subjected to a simple tensile strain ϵ_x , the strain magnification in the resin along the line AB according to Kies is:

$$\frac{\epsilon_x}{\epsilon_x} = \frac{2 + \frac{s}{r}}{\left[\frac{s}{r} + 2 \cdot \left(\frac{E_m}{E_f} \right) \right]} \quad (3.1)$$

where s and r are defined in figure 3.2. From the above equation it is obvious that as the distance between the fibres, s increases the strain magnification reduces.

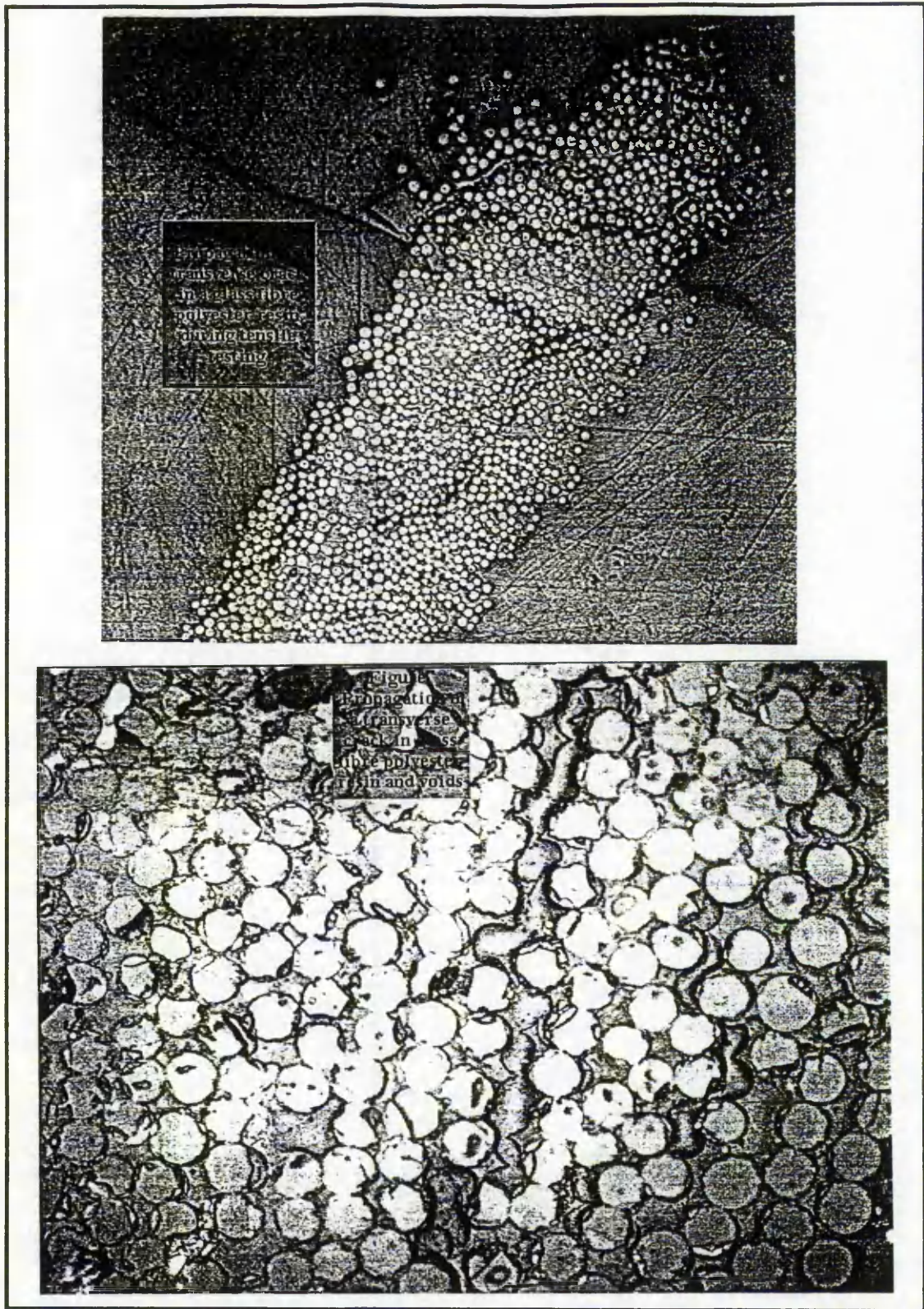


◆ **Figure 3.2: Square array model used by Kies, to calculate strain magnification.**

In the case of transverse fibre composites the crack is halted by the fibre, firstly because the high stiffness of the fibre inhibits further opening displacement of the matrix crack at the current level of load and secondly because the strength of the fibre is too high for it to be broken by the current level of stress concentration at the tip of the matrix crack. The matrix crack may bow around the fibre but it cannot move past the fibre until the critical matrix Crack Opening Displacement is exceeded. For further cracking to occur, therefore, some mechanism is required to permit an increased matrix COD.

Microscopic studies of the fractured specimen confirm that transverse cracks are nucleated in regions of dense packing and also propagate preferentially through such regions. Also apart from large cavities due to gross defects in the manufacturing operation there are voids in the composite material. These voids lie along individual fibres which are spherical or are elongated into ellipsoidal cavities parallel to the fibres. Voids arise from two main causes: firstly, incomplete wetting-out of the fibres by the resin; this results in entrapment of air and are more likely in systems where the dry fibres are closely spaced and the viscosity of the resin is high. The second source of voids is due to the presence of

volatile components produced during the curing cycle in resins. The void content distribution depends on fibre volume fraction and distribution, resin properties and processing conditions, such as temperature, pressure and time. The sequence of photographs in figure 3.3 a, b, were obtained from a microscopic examination of the region of the transverse bundle of fibres used in this work. They show resin containing fibres and clearly illustrates the presence of crack propagation. The variable distribution of fibres within the resin material and the variable packing between of the fibres, can be clearly seen: factors which influence the process and mechanics of transverse cracking.



◆ Figure 3.3 a, b: Microscopic examination of the E-glass transverse fibre polyester
 a) Crack propagation, b) Resin fibre distribution and dense packing between the fibres.

3.4 Transverse Cracking in E-glass Fibre Reinforced Composites

Transverse matrix cracking is of great interest and importance. As has been mentioned earlier these cracks cause stiffness degradation, which can be lifetime limiting damage mechanisms in stiffness dependent aerospace and automotive applications. However, it is well reported that there is no simple relationship for predicting the transverse strength of composite materials [15], [20], [37], [49]. Unlike the longitudinal tensile strength which is determined almost entirely by a single factor such as for example the fibre strength, the transverse strength is governed by many factors including the properties of the fibre and matrix, the interface bond strength, the presence and distribution of voids, and the internal stress and strain distribution due to the interaction between fibres and voids.

Virgin glass fibres are susceptible to water adsorption and to abrasive damage during processing so that a protective size is required. It is also important that the surface is fully wetted by the resin and that some bonding occurs. The fibres are given a size treatment which includes a silane coupling agent and a film forming resin. This ensures protection from water degradation and damage during injection moulding process. It is also possible to obtain some chemical bonding if there are reactive side groups of the molecules of the thermoset resin material.

3.4.1 Stress-Strain Data

There are two main approaches for the determination of the bond strength between glass or Kevlar and the resin material. One involves tests with single fibres, and the other unidirectional laminate and fibre bundles, such as in the present experiments. Although both test require very precise alignment of the fibres, single fibre testing is inherently difficult and unreliable because of the problems associated with specimen preparation. On the other hand, complete fibre bundles in resin, offer simplicity, convenience and show potential as a means of routine evaluation of adhesion in a variety of composite systems.

A number of samples were prepared using glass as the transverse reinforcing fibre and then tensile testing was applied. Table 3.1 includes the maximum stress, extension, and number of acoustic emission events for both the E-glass reinforced composites in the cured and post-cured conditions. Batches of samples were produced, labelled E1 and E2 and within the batches, some were tested as cured (C) and after post-curing (PC) as described in sections 2.5 and 3.2. This data, describes the failure stress of the samples in MPa. The tensile strain ϵ (%), can be determined by measuring the relative displacement of the two ends on a specimen with a displacement gauge. However, in the present experiments, the measuring displacement is not the relative displacement of the two end tabs but the displacement of the crosshead of the testing machine. The major contribution to this relative displacement occurs within the narrow section of the dogbone sample. Displacement of the crosshead is used to determine strain (extension %).

The role played by the resin-fibre interface is apparent from the composite stress-strain response. Examination of failed composites revealed that fracture occurred within the composite region containing the fibre bundle and nowhere else, clearly indicating that fibre-matrix interfacial failure initiated the composite failure.

3.4.2 AE System Monitoring of Transverse Cracking in Composite Materials

Acoustic emission testing was carried out on composite materials using specimens described in section 2.5. Since a single glass or Kevlar fibre bundle was encased in the centre of the dog bone sample, and transverse to applied load, the monitoring of acoustic emission provided intimate information on the fracture processes occurring within the transverse bundle. Having established [24], that it possible with the means of AE to monitor failure in the interface region during tensile deformation of TBFCs, the method is now extended to compare the level of adhesion between variously treated matrix material and different fibre systems.

The AE system and the testing of the samples were started simultaneously. Acoustic emission data was obtained by post processing each AE event to obtain, in this case the cumulative acoustic emission events counted, the amplitude per event and the ringdown counts per event respectively. The amplitude and ringdown counts values were evaluated from the AE events captured and are related to the relative acoustic energy released by the fracture events. Table 3.1 a, also includes the number of acoustic emission events which are highly variable since the nature of transverse glass fibre composite is complicated.

3.5. Experimental Results for Transverse Glass Fibre Reinforced Composite Testing.

Transverse matrix cracking is of such interest and importance because it is often the first mode of damage that occurs in engineering composites subject to tensile testing. The cracks cause stiffness degradation, which can be lifetime limiting mechanism and they may lead to initiation of delamination. However, interface debonding is the beginning of material failure. It is an important event because a composite with debonded interfaces has lost some integrity and its mechanical properties will be degraded significantly.

Any microcracking will also have a significantly effect on the life time performance and durability of the composite structure. For both room temperature curing and post-curing conditions, interfacial failure is controlled by interfacial debonding. However, the degree of debonding in the hot-cured composite is reduced due to the existence of thermal radial compressive stresses. From table 3.1 b it is obvious that the maximum stress sustained by the post cured treated composites which is on average 41.5 MPa, is significantly higher than for the room temperature 7-days cured materials which have an average of 27.6 MPa. Also, as can be seen from table 3.1 a, for some of the specimens the strain is highly variable since it is controlled by crack propagation within the fibre bundle. In the case of post-cured materials (table 3b), the average strain value is 3.5 % and it is greater than in the case of cured materials which have a 3.2 % strain value on average. This difference can be readily explained by the existence of a thermal compressive strain in the fibre in the hot-cured specimen, due to cooling down from the curing temperature. Extra strain has to be applied to recover the compressive strain before true tensile deformation results.

Together with the data described in tables 3.1 a, b, typical test information for E-glass cured and post-cured specimens embedded in polyester resin matrix are presented in figures 3.4a, b, c and 3.5a, b, c respectively. Figures 3.4 and 3.5 show the stress-strain response and superimposed AE data for the tested glass fibre reinforced composite materials.

In the case of the room temperature cured samples, as can be seen in figures 3.4, the data is characterised by a stress-strain graph which curves over, and is characteristic for the mechanical deformation of a polymer which dominates the deformation process. Each AE appears as occasional "early" events with a second, later region of AE activity beginning as the stress-strain curve begins to turn over occurring at a gross specimen strain rate of about 2.3%. It should be noted that this figure is after correction for the flat portion of the curve associated with specimen slip in the grips. This often occurred due to the nature of the polyester resin. It is significant that no AE events were detected in this region. It appears that any slight friction noise associated with this process was not detected acoustically and confirms the source of detected AE, which is from the transverse fibre region and specifically from the fibre-matrix interface. Intense AE activity is followed by final material failure. It is clear from these figures, that the amplitude and ringdown count values rise during the test but with large fluctuations. This rise is associated with a rise in the amount of acoustic energy released by the composite failure events.

Considering figures 3.5a, b and c, it can be seen that the stress-strain curve for the post-cured specimen is straighter indicating that the resin phase is more brittle than in the case of the cured samples. As already mentioned, from table 3.1 a, b, the maximum stress " σ_{max} ", the post-cured samples can sustain is much higher than for the normally cured specimen, indicating better adhesion properties between the fibres and resin, and better resin performance. High temperature curing improves the modulus and strength of the polyester resin. This is achieved since the density of the crosslink network is increased, together with the reduced mobility of polymer molecules, thereby promoting adhesion and better resistance to crack propagation.

It is noticeable that the gradient of the stress-extension curve is more linear together with the change in magnitude (Amplitude and/or ringdown counts values) with the events occurring earlier. In the case of post-cured sample, with a higher elastic modulus, the composite is generally stronger and in order to cause the same displacement higher load has to be applied. Consequently, the mechanical energy that has to be applied to the system is higher. Since the energy is transformed into acoustic emission energy, the

magnitude of the amplitude and/or ringdown counts values of the events would be expected to be higher. The data described by figures 3.4 and 3.5 confirms this.

For both types of curing and at about the maximum stress position, saturation of the ringdown count values occur for some of the tested samples. It is important to point out that for the post-cured type of specimen, (figure 3.5), events start at a lower strain value than for the cured specimen (figure 3.4). Also, the number of the events is higher and consequently many more events reach higher amplitude and ringdown counts values. However, in the case of post-cured specimens, the stress continues to rise, but AE activity subsides somewhat, in some specimens, picking up immediately prior to failure. As a general pattern the behaviour of these transverse samples can be characterised as “**quiet-then-noisy**” for room cured specimens and “**noisy-then-quiet**” for post-cured specimens, indicating better overall adhesion characteristics, sample modulus and resin toughness.

It is finally worth mentioning that AE occurs due to the impulsive propagation of damage centres within the material. The ultrasonic velocity is highly anisotropic in engineering composites as are the elastic properties. In attempting to model the ultrasonic response of a test material to damage propagation, no attempt has been made to account for these effects, since these are felt to modify the fine detail of any ultrasonic pulse propagation within the material, rather than detracting from the general arguments. In any event, most of the wave propagation path for the single bundle transverse composites tested, no fibres are present and propagation will be relatively isotropic and in the resin only. The ultrasonic pulse train associated with a single AE events carries information on the source position and source energy.

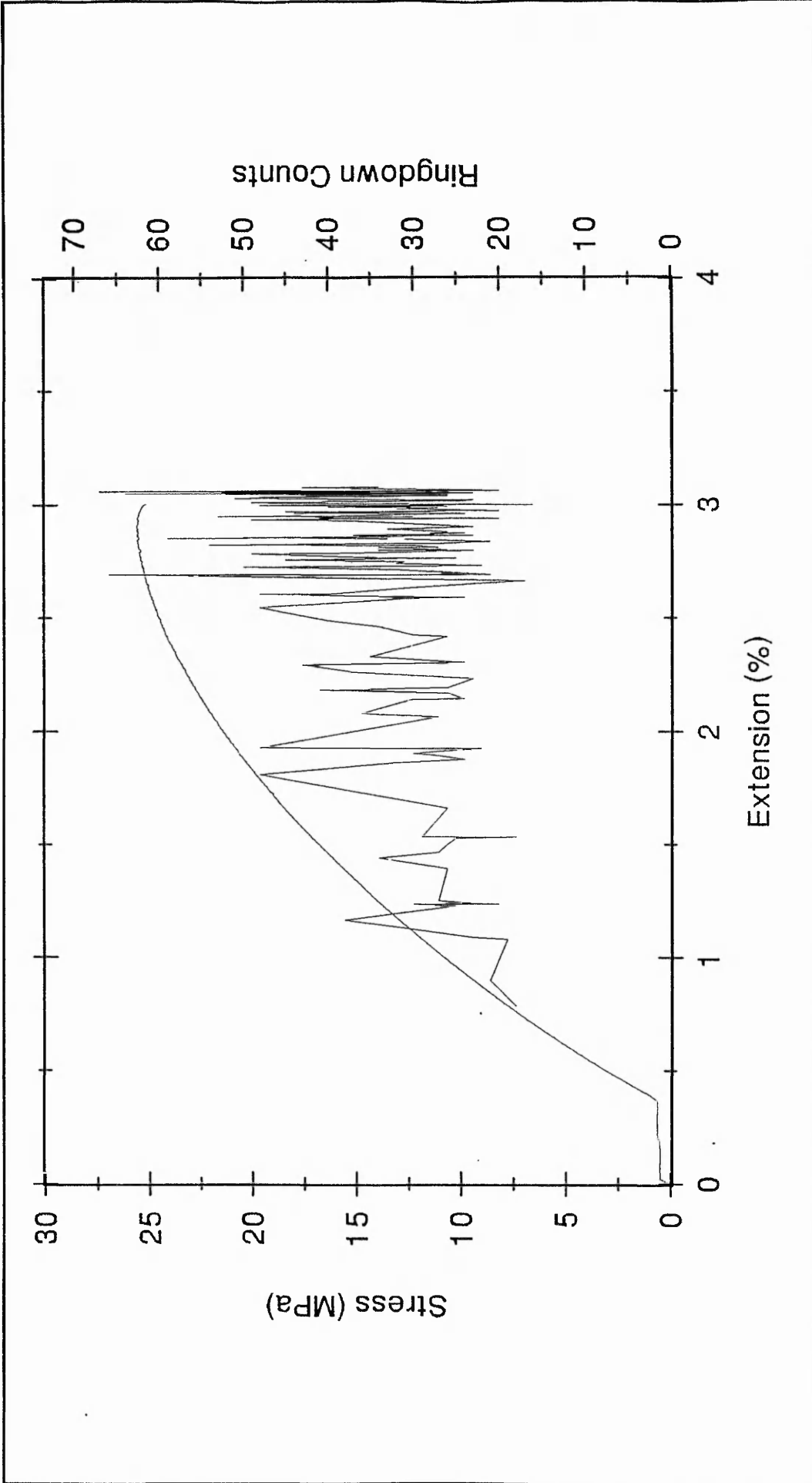
◆ **TABLE 3.1a**

Tensile properties and Acoustic Emission events for transverse glass-fibres reinforced composites - cured 'C' and post-cured 'PC' respectively for batches 1 and 2.

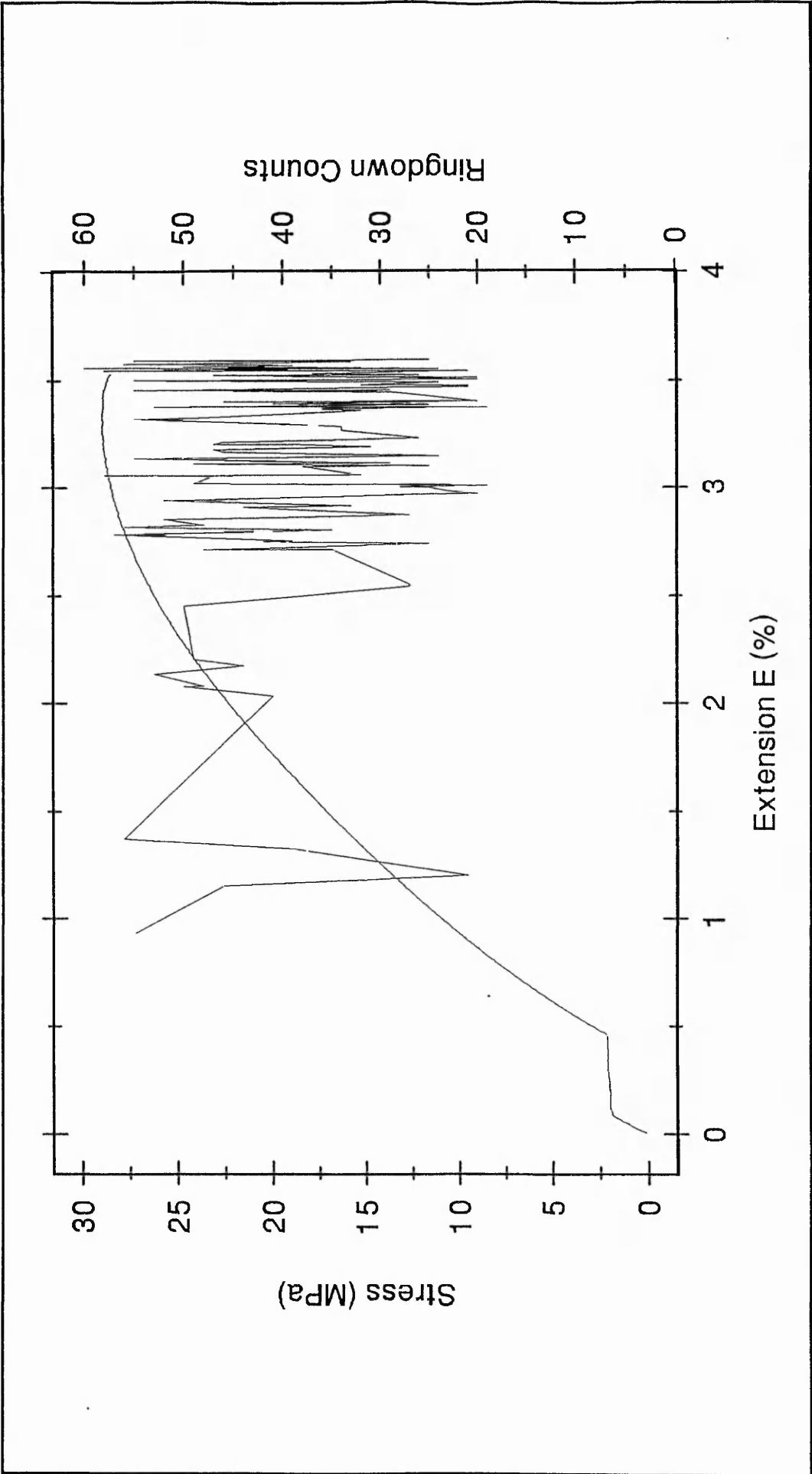
Specimen No	Stress MPa	Max Extension %	No of Events
E1-Glass 'C'	28.28	2.93	178
E1-Glass 'C'	25.56	2.91	55
E2-Glass 'C'	26.42	2.82	118
E2-Glass 'C'	28.86	4.02	75
E2-Glass 'C'	28.88	3.34	121
E1-Glass 'PC'	40.01	3.42	31
E1-Glass 'PC'	41.44	1.90	89
E1-Glass 'PC'	46.62	3.34	91
E2-Glass 'PC'	45.22	5.03	260
E2-Glass 'PC'	30.00	4.03	370
E2-Glass 'PC'	42.40	2.27	271
E2-Glass 'PC'	40.41	4.27	97

- ◆ **Table 3.1b:** Average values for maximum stress(MPa), strain (%) and number of events emitted during tensile testing, for cured (C) and post-cured (PC) transverse glass fibre bundle composite materials.

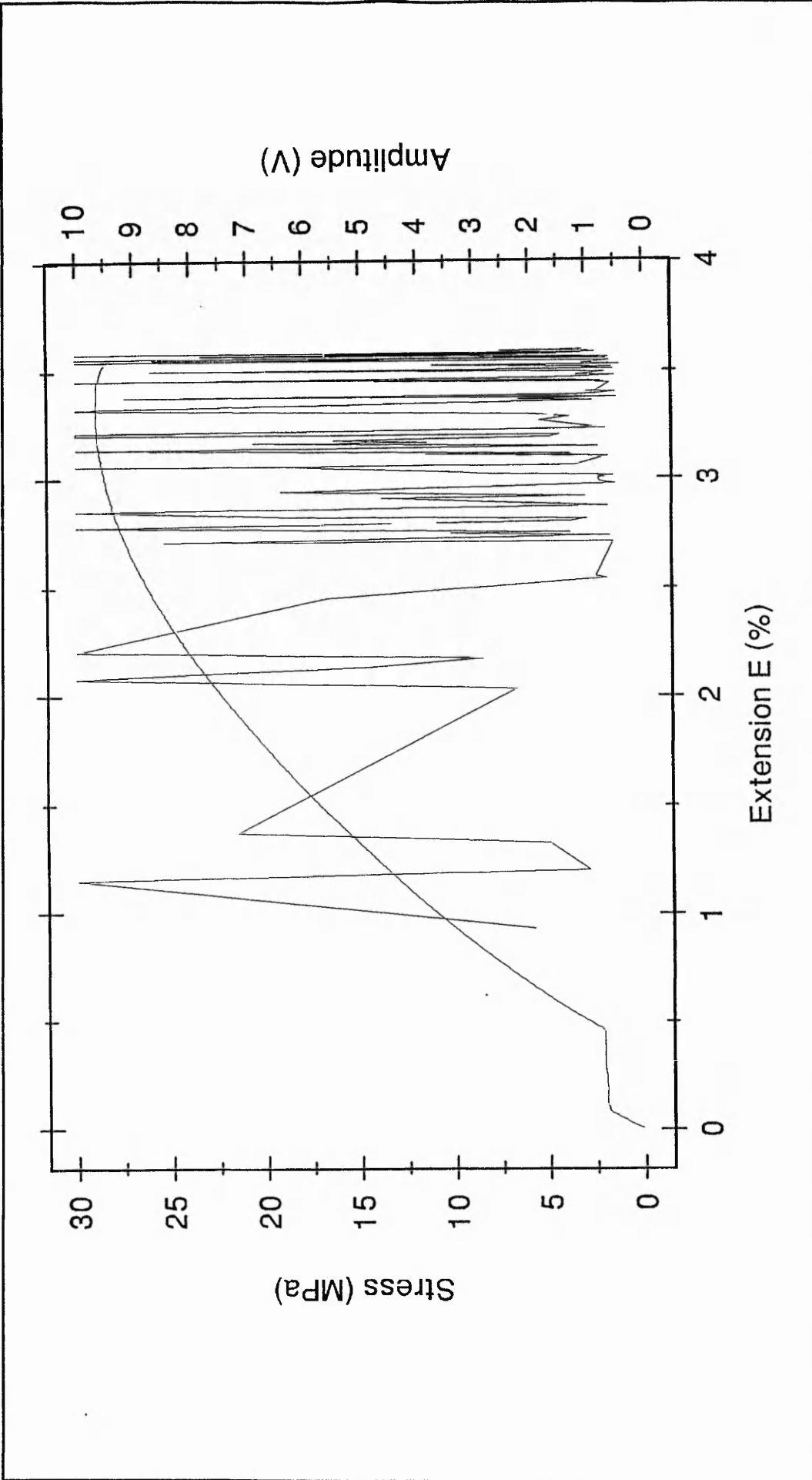
Sample Type.	Average Stress (MPa).	Average Extension (%)	Average No of events.
E-glass 'C'	27.6	3.20	109
E-glass 'PC'	41.5	3.50	173



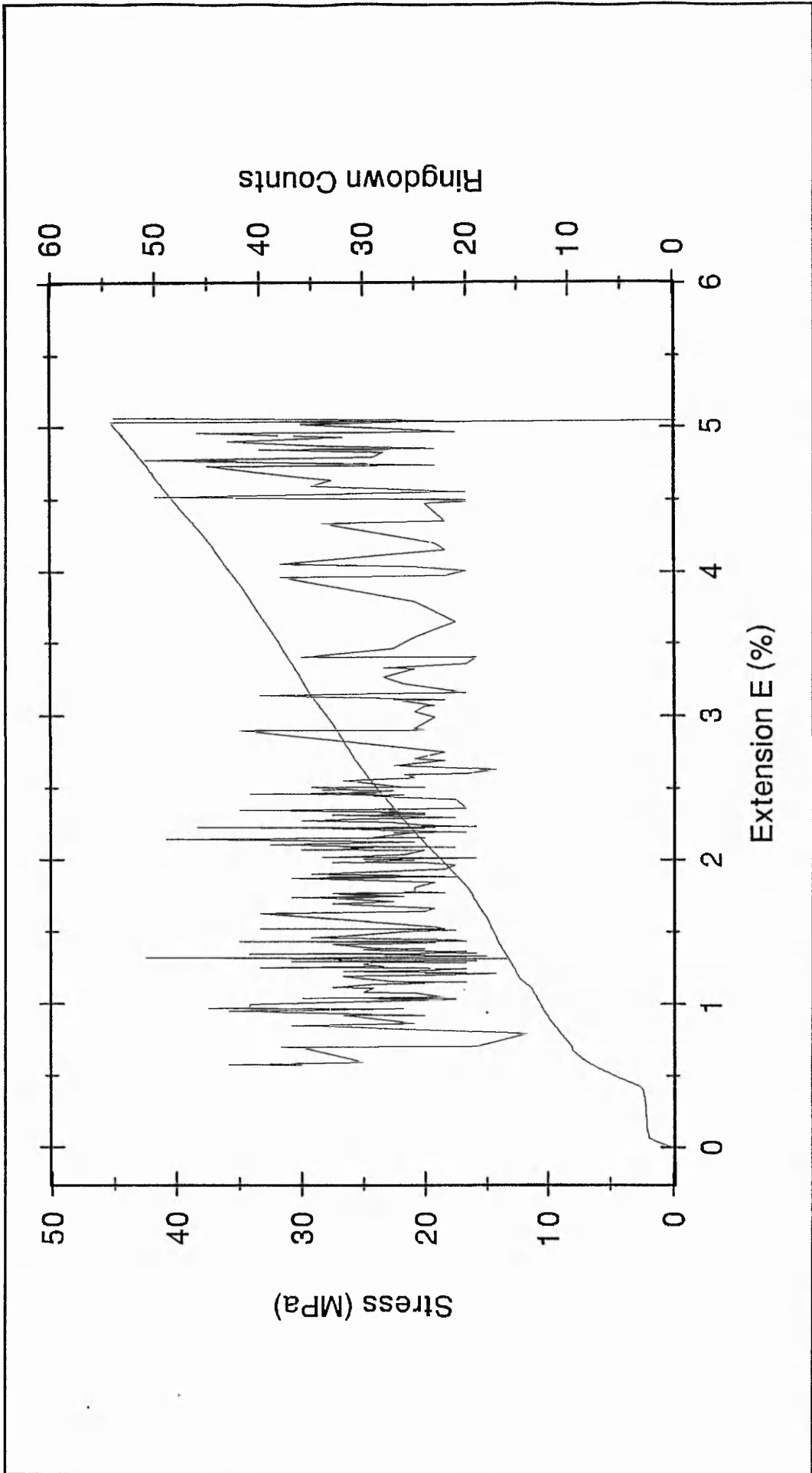
♦ **Figure 3.4 a:** Transverse fibre reinforced composite Stress-Strain and AE ringdown counts per event data for E-glass Cured composite materials.



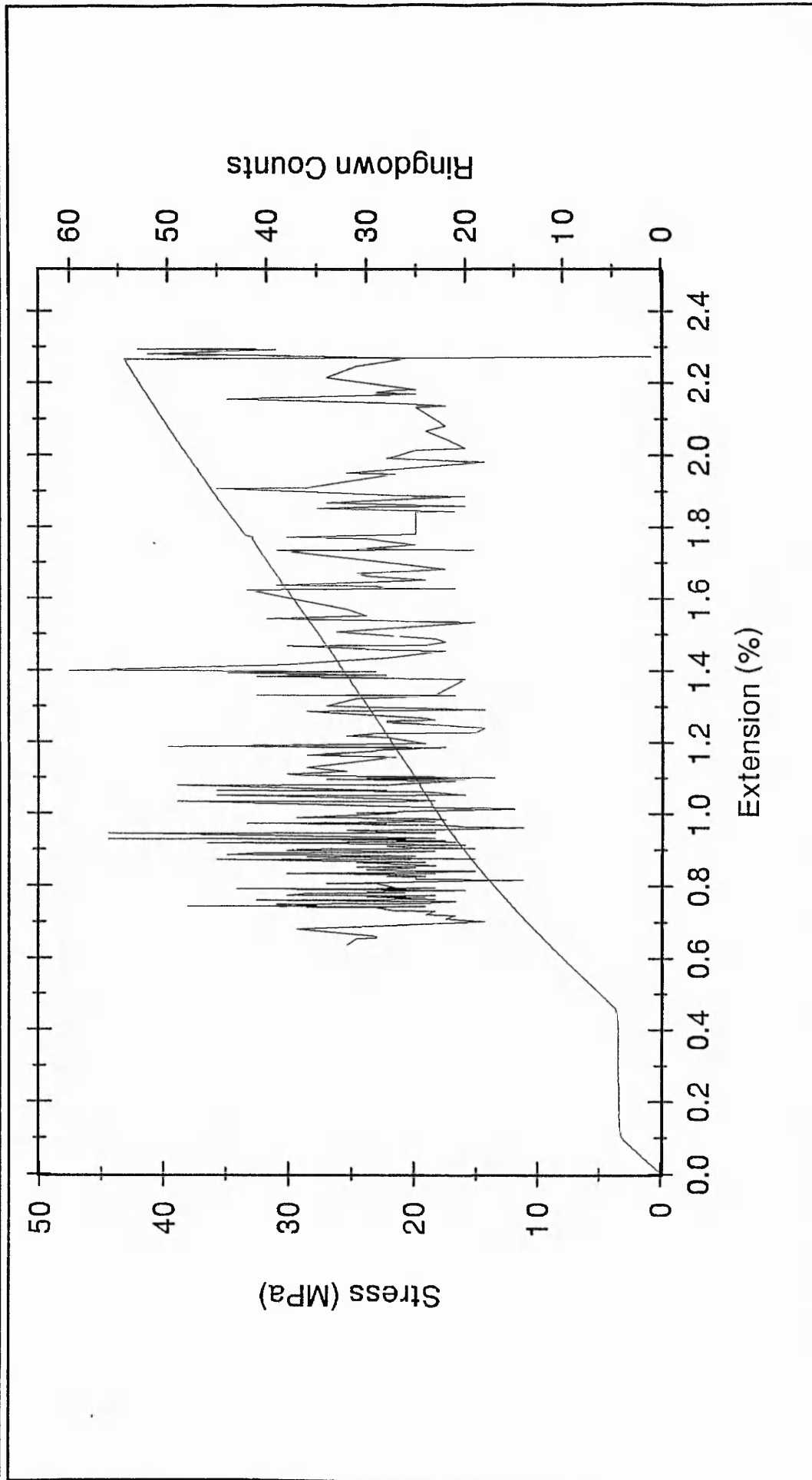
♦ **Figure 3.4 b:** Transverse fibre reinforced composite Stress-Strain and AE ringdown counts per event data for E-glass Cured composite materials.



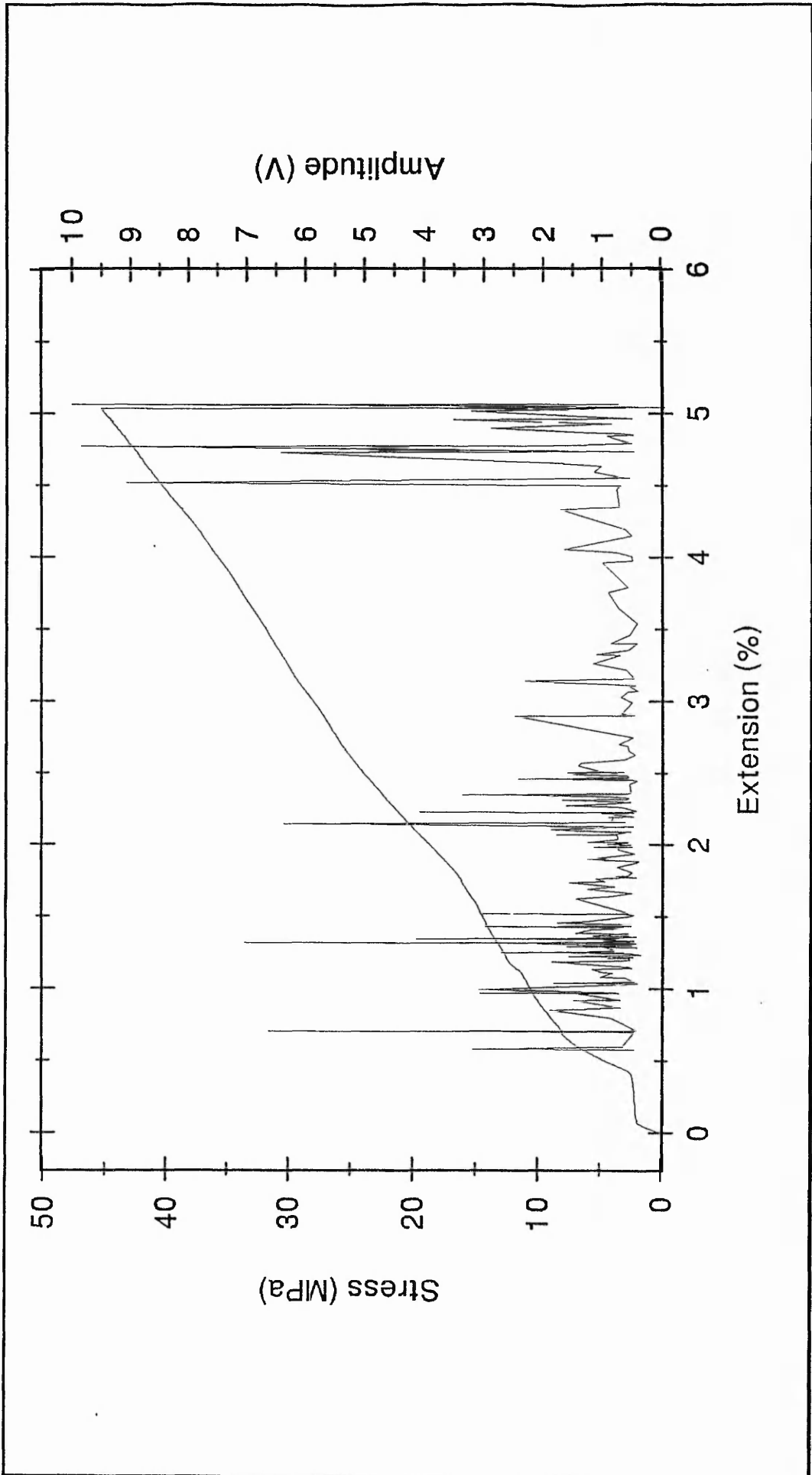
◆ Figure 3.4 c: Transverse fibre reinforced composite Stress-Strain and AE amplitude per event data for E-glass Cured composite materials.



◆ **Figure 3.5 a:** Transverse fibre reinforced composite Stress-Strain and AE ringdown counts per event data for E-glass Post-Cured composite materials.



♦ **Figure 3.5 b:** Transverse fibre reinforced composite Stress-Strain and AE ringdown counts per event data for E-glass Post-Cured composite materials.



♦ **Figure 3.5 c:** Transverse fibre reinforced composite Stress-Strain and AE amplitude per event data for E-glass Post-Cured composite materials.

3.6 Experimental Results for Transverse Kevlar-49 Fibre Reinforced Composite Testing.

This section reports studies on the interfacial properties of Kevlar-49 transverse fibre bundle reinforced composite materials. As for E-glass samples, acoustic emission data was obtained by post processing each AE event to obtain, the cumulative AE events counted, the amplitude per event and the ringdown counts per event respectively. For the data reported in this section, Kevlar-49 was the reinforcing fibre bundle and AE was monitored during specimen testing as described in section 2.5.

Specimens reinforced with Kevlar fibre bundles were of four types. The cured composites with 'as received' fibres (**K1-Kevlar'C'**), the cured composites with ultrasound treated fibres (**K3-Kevlar'CU'**), the post cured with as received fibres (**K2-Kevlar'PC'**), and finally the post cured with the ultrasound treated fibres (**K4-Kevlar'PCU'**). In the case of K3 and K4 type of materials, the fibre bundles were immersed in an ultrasonic bath containing distilled water for 15 minutes. The ultrasound induced cavitation would be expected to produce surface cleaning and erosion due to the formation and collapse of cavitation bubbles. The surface disruption caused by the ultrasound would be expected to cause a reduction in fibre strength, when compared to the as received fibres due to the increasing number of surface defects and the severity of existing defects as in reference [25], although, of course, fibre strength is not critical when considering transverse tests.

Table 3.2 a, gives a clear indication of the values for maximum stress, strain, failure strain and the number of AE events for the **seven days cured** (K1 and K3 types) and the **2 hours further post cured samples** (K2 and K4 types). As in the case of the E-glass transverse fibre composites, it can be seen that the specimens which were subjected to a post cured treatment can sustain much higher levels of stress than the normally room cured materials. As can be seen from table 3.2 b, together with figures 3.6a, b, and 3.7a, b, and the average failure stress for the as received Kevlar-49 room cured composite materials (K1-Kevlar'C') is 16.5 MPa at an average extension of 3.98%. The average Stress for the (K3-Kevlar'CU') type is been reduced to 16.2 MPa and 3.27 % extension since ultrasonic

treatment on the fibres was applied. The post cured type of samples show an increase in the failure stress, in comparison to the cured samples as can be seen from figures 3.8 a, b, and 3.9 a, b, and tables 3.2 a and 3.2 b. The average maximum stress was 27.5 MPa for the (K2-Kevlar'PC'), with a 0.99% extension, and 29.3 MPa with 1.02% extension for the (K4-Kevlar'PCU') type of samples. This proved that as in the case of E-glass composites, high temperature treatment improves the elastic modulus and strength of polyester resin but on the other hand the resin is very brittle. It also indicates that better adhesion exists between the fibres and the resin for the post-cured composite materials.

The elastic modulus for the four different types of Kevlar-49 fibre bundle reinforced composite materials were determined. In order to obtain the Young's modulus in this case the ratio of the normal tensile stress to the corresponding strain of $YM_{0.5}$ at 0.5% and YM_1 at 1% was taken. These Young's modulus values were determined as a secant modulus to allow for curvature of the stress/strain curve. The results (MPa) and for "as received" and ultrasound treated, cured and post-cured test samples as are shown in Table 3.3 a.

From figures 3.6, 3.7, 3.8 and 3.9 and table 3.3a, the increase of Young's modulus in the case of post-cured materials in comparison to the cured materials can be seen. Also table 3.3b includes the corresponding average values for each of the type of the treated composites. It is clear that the post-cured composites at 0.5 % have a modulus value approximately three times higher in comparison to the cured materials. This difference is also clear for the 1% modulus, where the post-cured samples have four times the value of the cured samples. This increase in Young's' Modulus is reflected in the AE ringdown counts and amplitude values where these values are higher towards the end of the stress strain curve. This is due to the fact that the steeper gradient indicates that the composite is tougher and in order to cause the same displacement higher load is required. This means that the elastic energy is higher and since this energy is transformed into AE energy the magnitude of amplitude and ringdown counts values are higher.

Interfacial properties are dominant factor in the fracture toughness properties of composite materials, also affecting their response to aqueous and corrosive environments. Composite materials with weak interfaces have relatively low strength and stiffness but

high resistance to fracture whereas materials with strong interfaces have high strength and stiffness but show a poor resistance to fracture. Part of the bond strength is attributed to mechanical effects and part to effects associated with chemical bonding. For example the polyvinyl acetate coating will be soluble in the polyester resin and the bond strength is similar to that obtained with the water affected surface.

For the transverse oriented Kevlar-49 fibre reinforced composites materials tested, assuming that the normal applied load acts equally on the fibre and the matrix (although this is unrealistic) [50], stress and/or strain range over which the interfacial failure AE events occurred can be regarded as an indirect indicator of the range of the fibre-matrix interface strength. This failure is also affected by strain magnification, as well as non-uniform loading of the interface, due to such effects as variable transverse fibre density, some degree of misalignment of the fibres, edge effects and voids. The paper by Okoroafor and Hill [24] suggested a close relationship between the level of adhesion, the occurrence of the first few events and the externally applied macrostress (MPa).

For composite materials, the stress and strain for the first detected AE events can be used as a measure of the interfacial strength between Kevlar-49 and Crystic 272 polyester resin. By varying the heat treatment of the composites (cured for seven days at room temperature and/or further post-cure for 3 hours at 80 °C), and the fibre surface condition by subjecting the fibre surface to insonification in a water filled ultrasonic bath for 15' minutes, variation in the mechanical behaviour of the interface was achieved.

The AE system and the loading of the specimen were started simultaneously. Having established that it is possible for AE to monitor interfacial failure during tensile deformation of the transverse bundle fibre composites (TBFCs), the method has been applied to compare the level of interfacial adhesion between differently treated matrix material and fibre systems. The typical information and AE data from the transverse oriented Kevlar bundle composites is presented in figures 3.6, 3.7, 3.8, 3.9 and in the table 3.2 a respectively.

It can be seen from table 3.2b column three, that the interface failure strength of

K1-Kevlar'C'/polyester is approximately 1.8 times of that of K3-Kevlar'CU'/polyester. A similar pattern is also seen for the two types of post-cured specimen, K2 and K4. It appears that the ultrasound treatment has affected not only the fibre properties [48], but also the interfacial characteristics of the transverse bundle composites. Similar comparisons can be made in any combination between any of the four types of composites since the AE and Stress-Strain characteristics are distinctly different in each case. Figures 3.6 and 3.7 for the room cured samples, and 3.8 and 3.9 for the post-cured samples can be compared, using AE events, and strain response. The recorded AE events would be expected to be mostly associated with interfacial failure. It is obvious that the two types of ultrasound treated fibre composites failed at lower strain values than the as received fibre composites. This is very clear, especially in the case of K1 and K3 types of materials as can be seen from the original specimen values (table 3.2 a) and the average values (table 3.2 b). This suggests that the as received fibre composite interface is much stronger than the treated fibre composite interface. The average interfacial failure stress (IFFS) for the as received cured composites (K1-Kev'C') is 7.70 MPa. The IFFS for the ultrasound treated fibres in room cure conditions (K3-Kev'CU') is clearly lower with an average value of 4.3 MPa indicating the reduction in adhesion performance between fibres and resin. Similarly, for the "as received" post-cured materials (K2-Kev'PC') the average IFFS is 8.0 MPa, which is significantly higher than the corresponding value for the ultrasound treated fibres in post-cure conditions (K4-Kev'PCU'), which is 2.9 MPa. It is apparent, that the ultrasound treatment modifies the nature of the interfacial bonding.

Finally, and especially in the cases of the post-cured composite materials, the Amplitude and/or Ringdown Count values rise during the test with large fluctuations. This rise is associated with a rise in the amount the A.E energy released by the composite failure events. It is important to notice that, in contrast to the E-glass fibre reinforced composite materials, the AE recorded in the case of Kevlar reinforced cured samples starts at relatively low strain levels and is produced throughout the test.

This study of variously treated Kevlar fibres using cured and post-cured resin materials indicated some interesting results. It is known that the adhesion between Kevlar fibres and polyester resin is not as strong as in the case of E-glass fibre/polyester composite [24], [30]. This could be in the main, a physical effect due to the resin shrinkage of the

fibres and the fact that the extension characteristics of the fibres are far superior to the resin. However, information from Scott Bader Ltd indicates Crystic resin 272 is one of the best polyester resin materials that can be found on the market in order to form Kevlar-49 fibre reinforced composite materials. It is important to notice, that during these experiments, each A.E signal will propagate in a similar acoustic mode, or mixture of modes, and be similarly attenuated in transit to the measuring sensor. Also it is to be expected that the electrical energy of the AE transducer, will be directly proportional to the elastic energy released in fracture of the composite materials. As a conclusion it has to be noted that the testing of Kevlar-49 composite materials provided a very clear picture of the characteristics and capabilities of acoustic emission for evaluating changes in adhesion between resin and fibre systems.

♦ **Table 3.2 a**

Macroscopic measurements of the maximum stress and corresponding strain, maximum strain, interfacial failure stress and corresponding strain deduced from the macroscopic sample stress giving initial A.E events, and total number of events emitted for four different types of Kevlar Fibre Reinforced Composites.

<i>Specimen Number</i>	<i>Max σ (MPa) Max ϵ (%)</i>	<i>Max Strain (%)</i>	<i>IFES (MPa) IFFE (%)</i>	<i>No of Events</i>
K1-Kevlar'C'	10.92/4.00	4.00	7.34/1.425	62
K1-Kevlar'C'	16.34/4.52	4.59	7.52/0.95	338
K1-Kevlar'C'	25.24/2.03	2.76	8.91/0.71	723
K1-Kevlar'C'	13.35/5.40	5.40	7.09/1.10	522
K2-Kev'PC'	23.30/0.93	0.94	11.94/0.67	81
K2-Kev'PC'	24.34/0.90	0.91	2.88/0.28	87
K2-Kev'PC'	34.78/1.13	1.14	10.11/0.61	164
K3-Kev'CU'	19.66/2.71	3.07	4.66/0.58	169
K3-Kev'CU'	10.78/3.89	4.12	3.56/0.72	222
K3-Kev'CU'	18.13/3.22	3.22	4.73/0.92	332
K4Kev'PCU'	24.23/0.93	0.94	1.35/0.12	59
K4Kev'PCU'	34.73/1.13	1.14	2.80/0.35	213
K4Kev'PCU'	28.93/1.01	1.02	4.55/0.39	99

◆ **Table 3.2 b**

Average values for the maximum stress (MPa), corresponding strain (ϵ), interfacial failure stress and corresponding failure strain for all the four type of transverse Kevlar-49 fibre bundle composite materials. 'C' signifies room temperature curing, 'PC' post-curing, and 'U' ultrasound treatment of the fibre bundle in distilled water for 15 minutes prior to composite manufacture.

Sample Type	Max σ / ϵ	IFFS (MPa)	IFEFE (%)
K1-Kev'C'	16.46 / 3.98	7.70	1.04
K2-Kev'PC'	27.47 / 0.99	8.00	0.52
K3-Kev'CU'	16.19 / 3.27	4.30	0.74
K4-Kev'PCU'	29.30 / 1.02	2.90	0.28

♦ **Table 3.3 a**

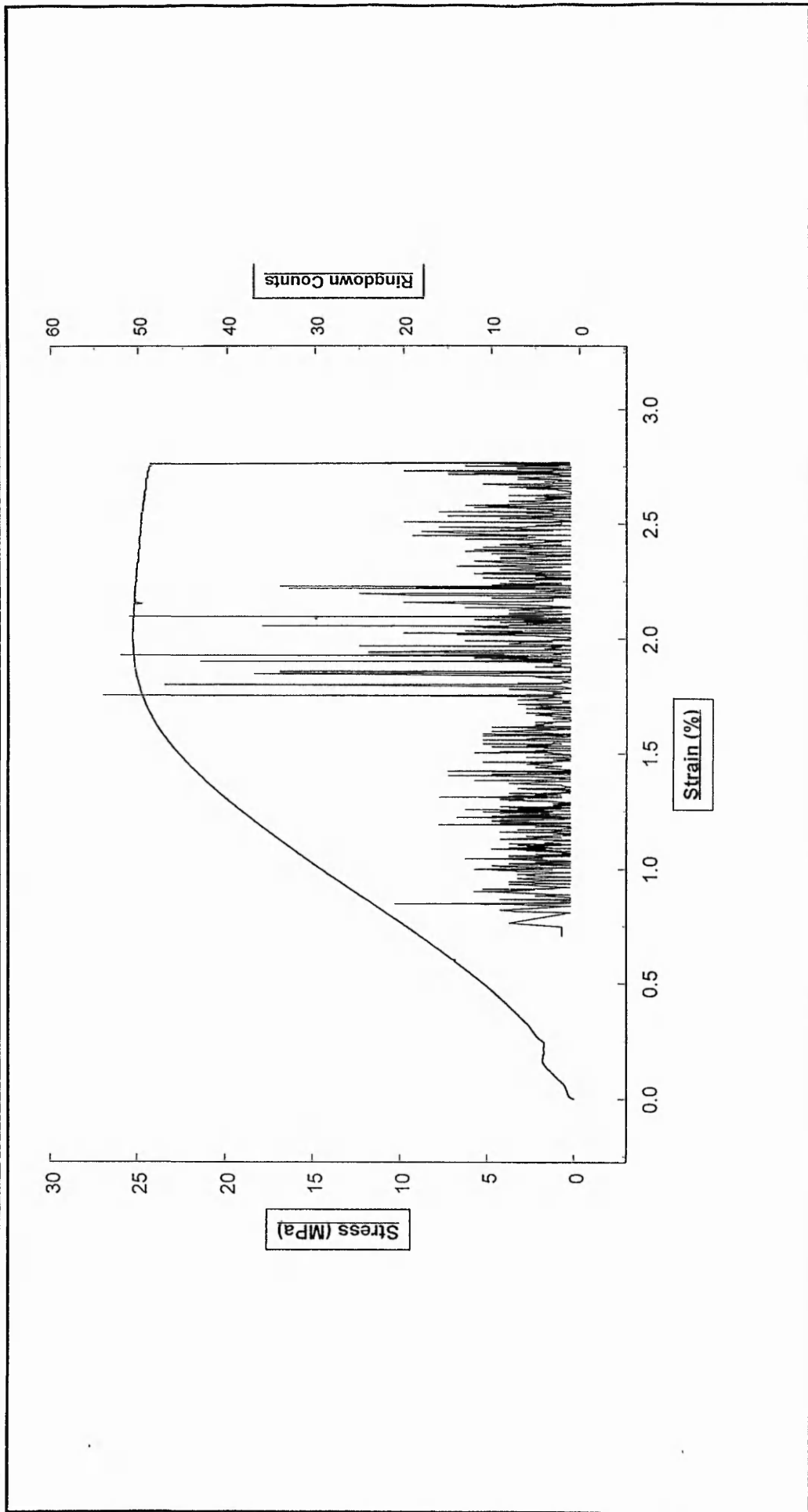
Measurements of the Young's Modulus in MPa. For K1 and K3 types $Y.M_{0.5}$ corresponds to 0.5 % secant modulus strain region and $Y.M_1$ to the 1 % secant modulus. As for the K2 and K4 types $Y.M_1$ and $Y.M_2$ correspond to the 0.5% and 1% strains respectively.

<u>Specimen No</u>	<u>Young's Modulus 0.5</u> (MPa)	<u>Young's Modulus 1</u> (MPa)
K1-Kevlar'C'	3.54	1.58
K1-Kevlar'C'	10.00	6.00
K1-Kevlar'C'	18.00	10.80
K1-Kevlar'C'	5.15	1.95
K2-Kevlar'PC'	24.70	45.10
K2-Kevlar'PC'	29.09	42.10
K2-Kevlar'PC'	28.57	52.00
K3-Kevlar'CU'	12.80	8.60
K3-Kevlar'CU'	4.59	2.03
K3-Kevlar'CU'	10.66	2.07
K4-Kevlar'PCU'	26.34	50.00
K4-Kevlar'PCU'	27.20	44.00
K4-Kevlar'PCU'	32.60	47.00

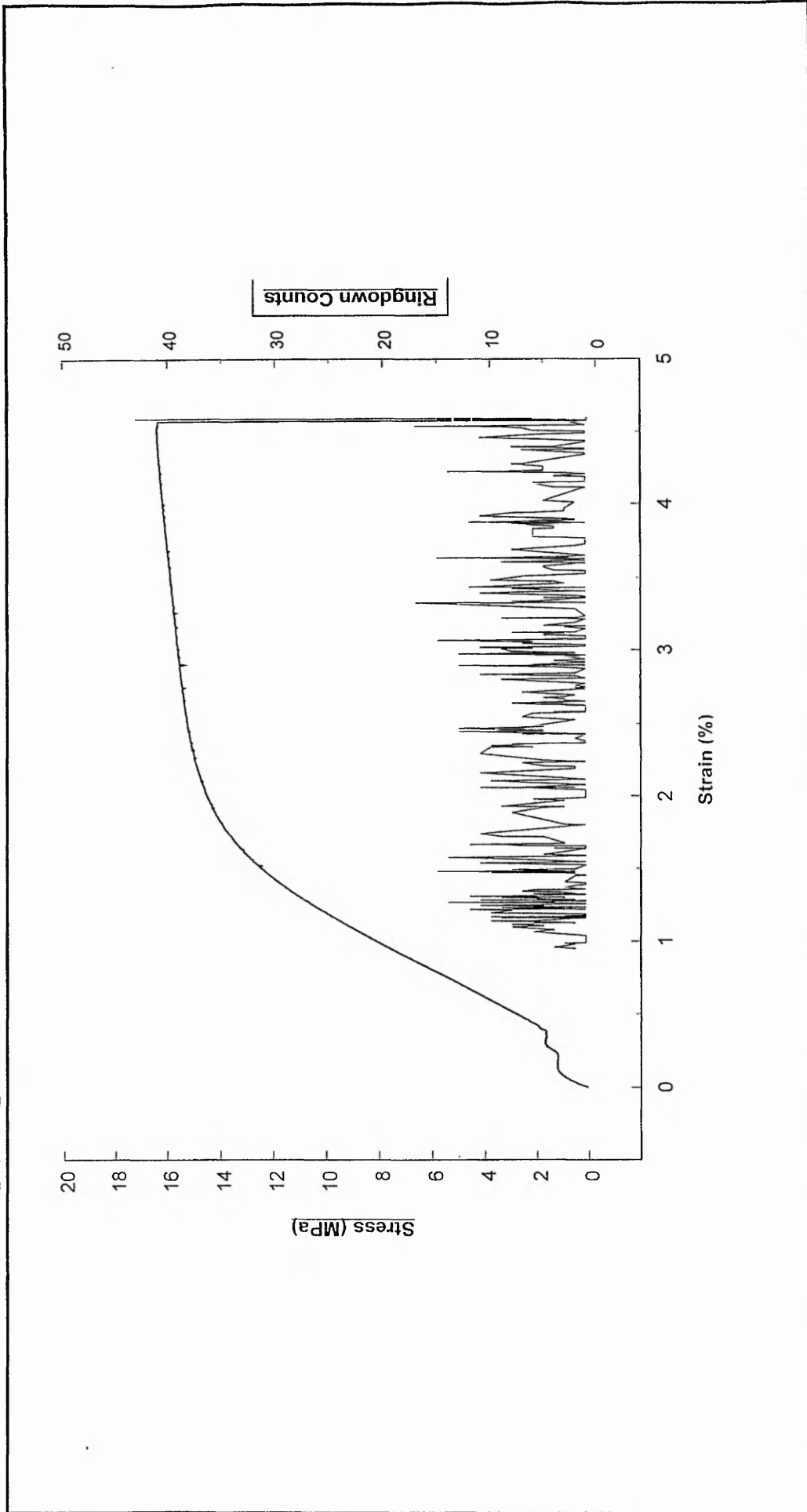
◆ **Table 3.3 b**

Average values calculated for the elastic modulus and each of the four types of composite materials, as cured, post-cured and ultrasound treated fibre bundles.

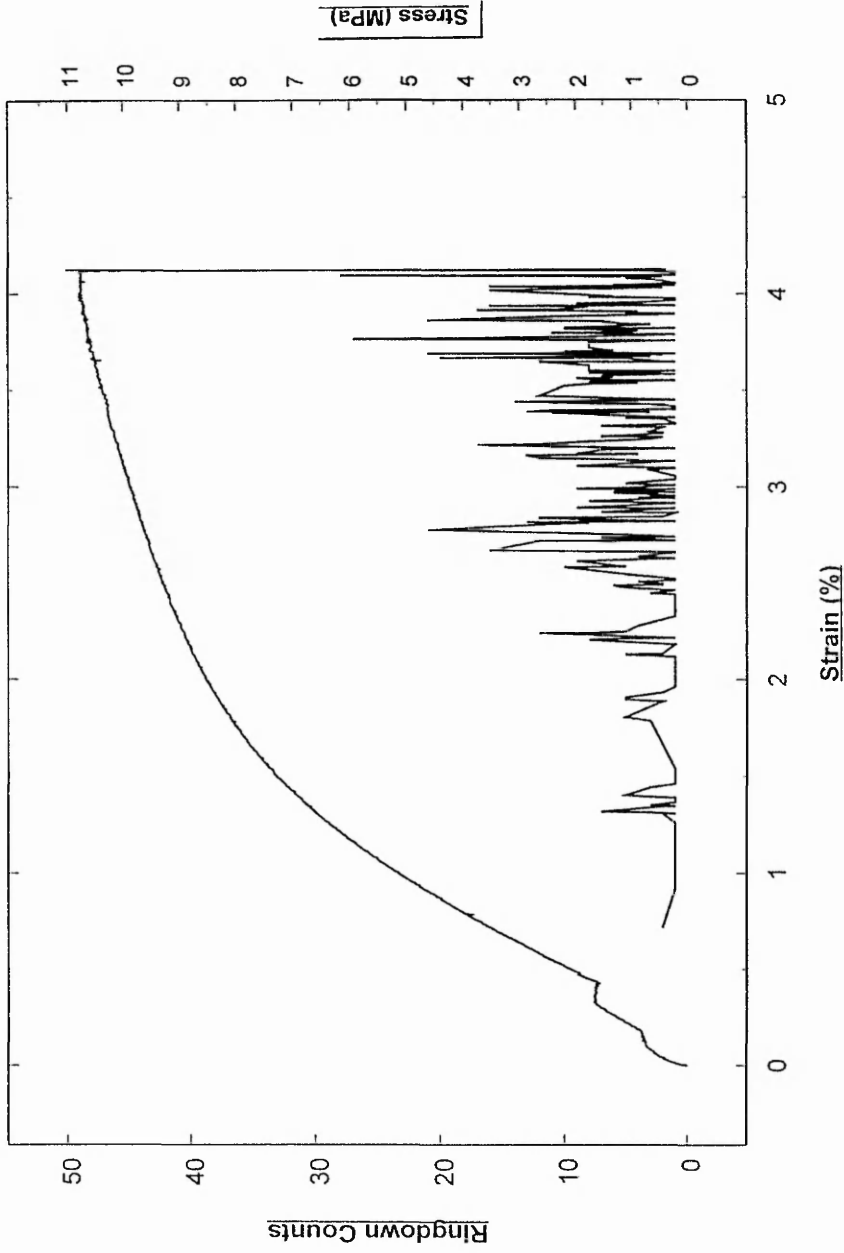
Sample Type	Y.M _{0.5} (MPa)	Y.M ₁ (MPa)
K1-Kev'C'	9.17	5.08
K2-Kev'PC'	27.45	46.40
K3-Kev'CU'	9.35	4.23
K4-Kev'PCU'	28.71	47.00



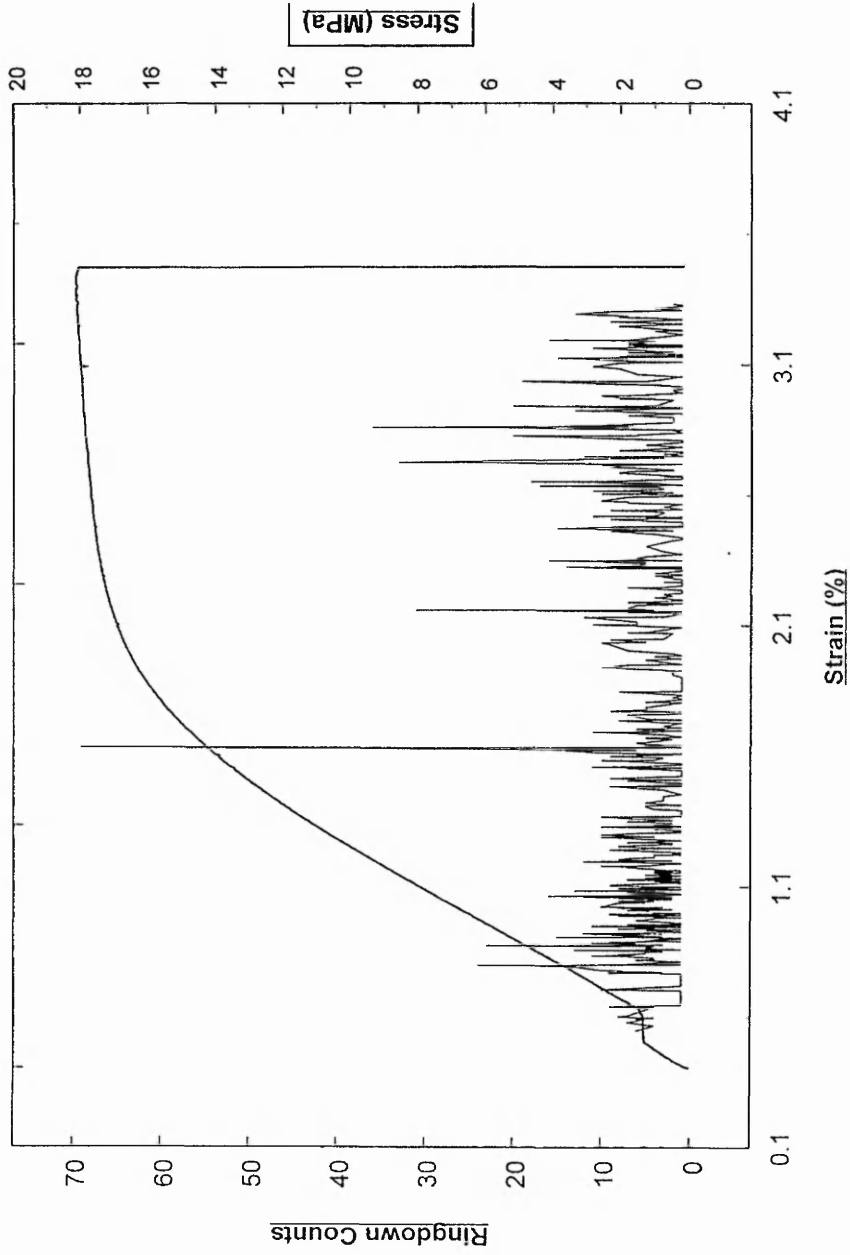
♦ **Figure 3.6 a:** Transverse fibre reinforced composite Stress-Strain and AE ringdown counts per event data for 'As received Kevlar-49 fibre' Cured composite materials.



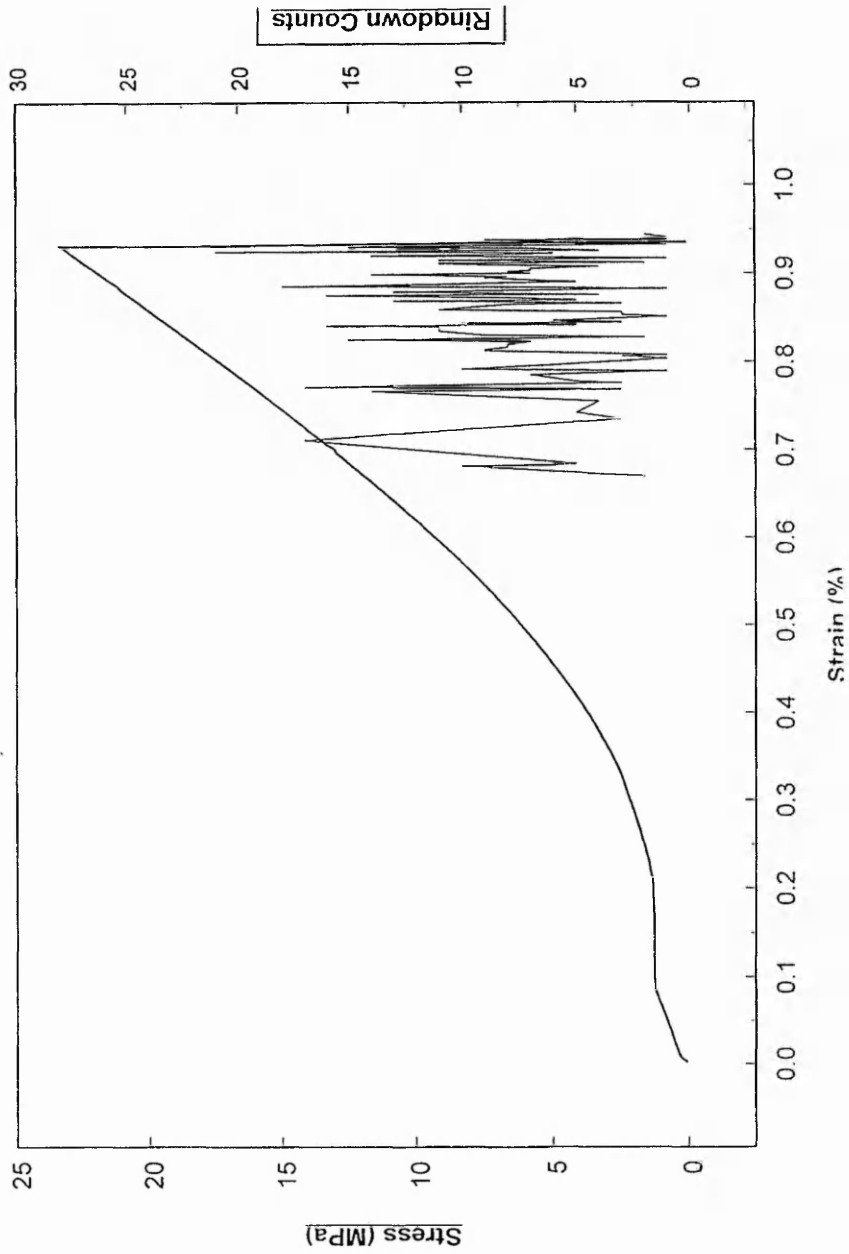
♦ **Figure 3.6 b:** Transverse fibre reinforced composite Stress-Strain and AE ringdown counts per event data for 'As received Kevlar-49 fibre' Cured composite materials.



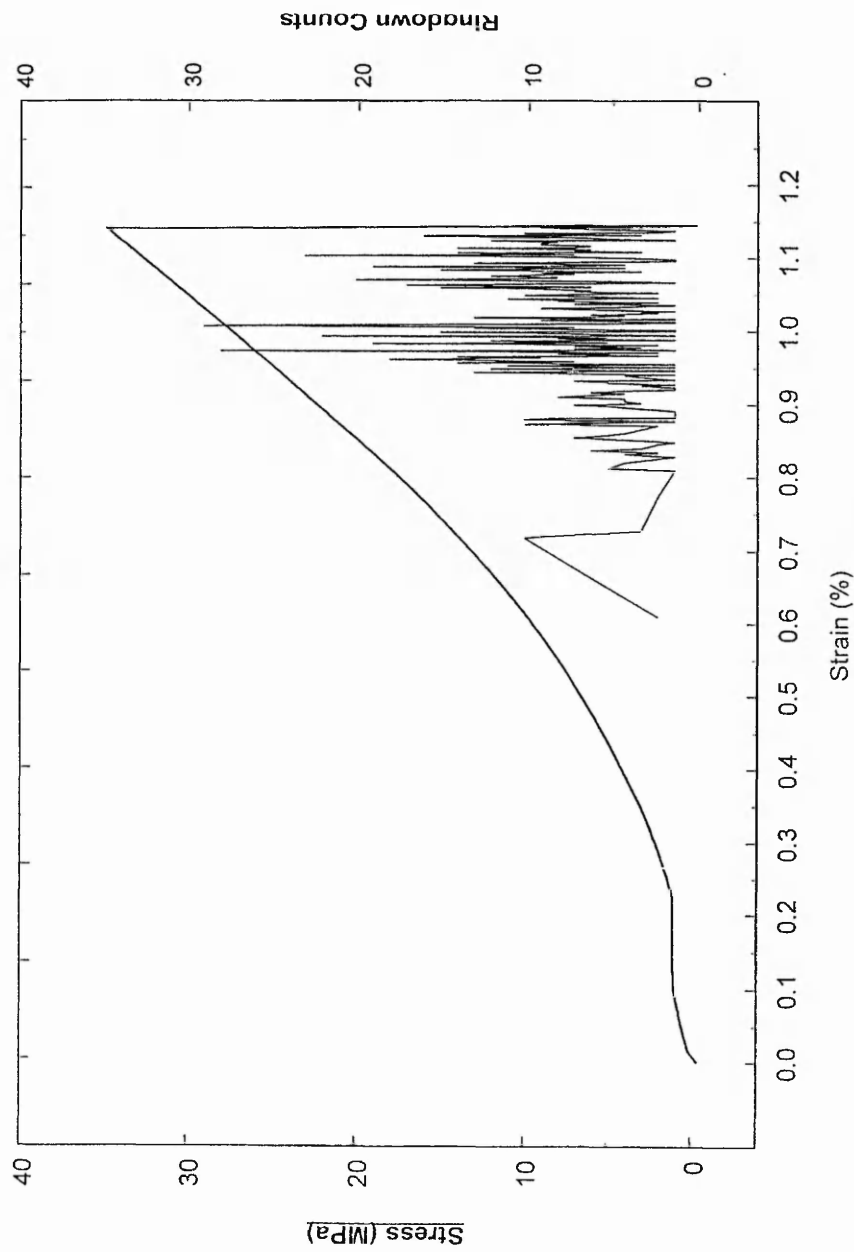
♦ **Figure 3.7 a:** Transverse fibre reinforced composite Stress-Strain and AE ringdown counts per event data for 'Ultrasound treated Kevlar-49 fibre' Cured composite materials.



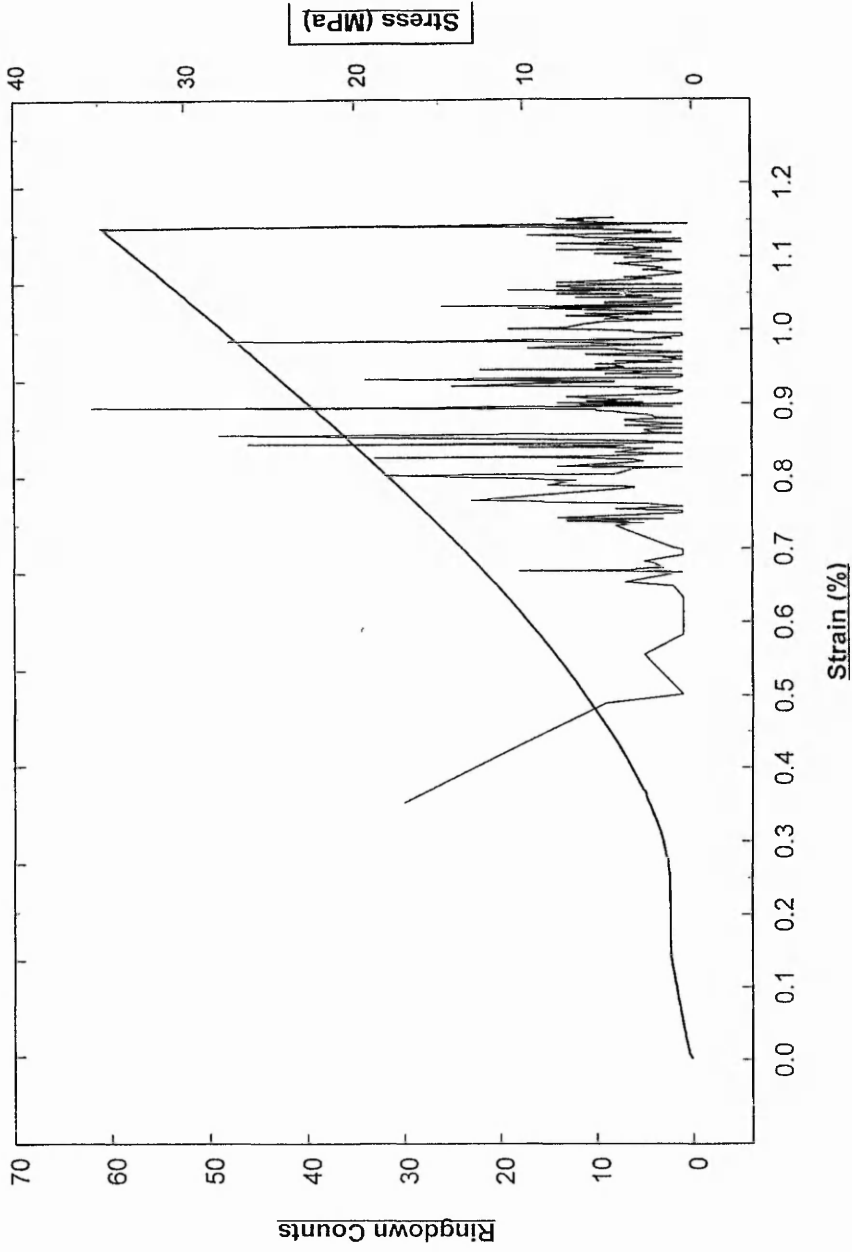
♦ **Figure 3.7 b:** Transverse fibre reinforced composite Stress-Strain and AE ringdown counts per event data for 'Ultrasound treated Kevlar-49 fibre' Cured composite materials.



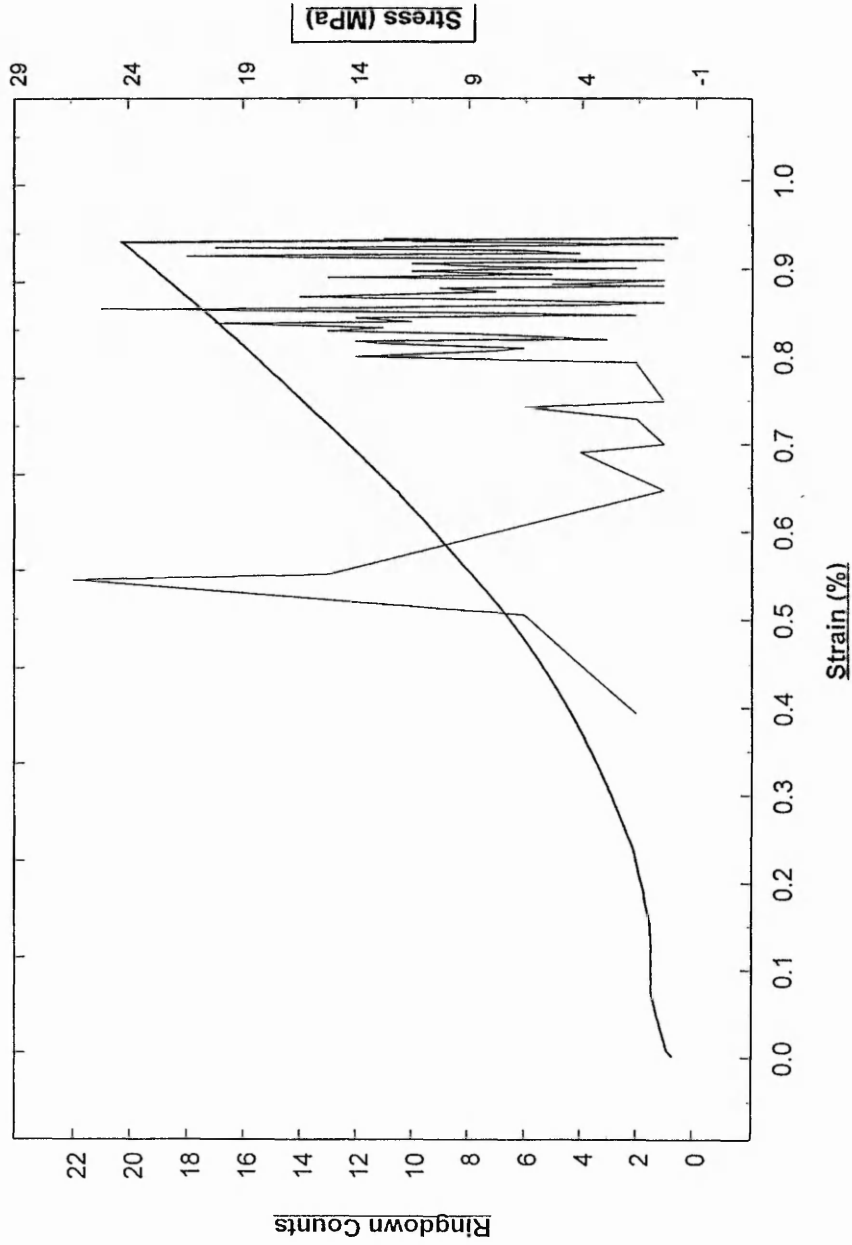
◆ **Figure 3.8 a:** Transverse fibre reinforced composite Stress-Strain and AE ringdown counts per event data for 'As received Kevlar-49 fibre' Post-Cured composite materials.



♦ **Figure 3.8 b:** Transverse fibre reinforced composite Stress-Strain and AE ringdown counts per event data for 'As received Kevlar-49 fibre' Post-Cured composite materials.



◆ **Figure 3.9 a:** Transverse fibre reinforced composite Stress-Strain and AE ringdown counts per event data for 'Ultrasound treated Kevlar-49 fibre' Post-Cured composite materials.



◆ **Figure 3.9 b:** Transverse fibre reinforced composite Stress-Strain and AE ringdown counts per event data for 'Ultrasound Kevlar-49 fibre' Post-Cured composite materials.

3.7 Conclusions

Mechanical tests of transverse oriented fibre composites in conjunction with suitable AE instrumentation has provided a clear idea of the level of resin-fibre adhesion and strength of the interface. In the case of E-glass composite materials it was clear that the post-cured samples can sustain higher stress (41.5 MPa), in comparison to the cured samples (27.6 MPa). This indicated a better resistance to crack propagation and better adhesion characteristics for the post-cured samples. Also when considering AE events superimposed to stress-strain data, the events for the post-cured samples emitted in much earlier strain levels and show a 'noisy-then-quiet' pattern, while the cured samples show a 'quiet-then-noisy' behaviour.

The next step of this study was the characterisation of the interfacial properties between a Kevlar-49 fibre bundle and the resin matrix. Experimental data showed that the average failure stress was higher for the as received fibre post-cured composite (27.5 MPa) in comparison to the room temperature cured samples (16.5 MPa). Post-curing seem to improve the strength and adhesion performance of the composites but they proved to be brittle.

With the use of the interfacial failure stress (IFFS) which combines stress-strain and AE data, it was possible to characterise the different interfacial performances between cured, post-cured and ultrasound treated samples. The average (IFFS) for the as received cured samples was 7.70 MPa, while for the ultrasound treated cured samples IFFS was reduced to 4.3 MPa. Similarly, for the as received post-cured samples IFFS was 8.0 MPa in comparison to 2.9 MPa for the ultrasound treated samples. It is thus become apparent that with the use of AE it is possible to examine the effect of the ultrasound treatment to the nature of the interfacial bonding

The work in this chapter shows that information relating to composite interfacial properties can be deduced using a simple multifibre transverse bundle composite rather than other methods such as a single fibre composite testing. Mechanical tests in

conjunction with suitably adjusted AE instrumentation has provided a clear indication of the characterisation of differently treated composite systems and especially their corresponding level of adhesion and the strength of the interface. When either, the composite treatment or the fibre system is modified, the AE characteristics of the modified system reflect this change and provide a method of tracking this change. The detail of the change is reflected in stress-strain responses but most importantly in the AE data profile with strain which may be used in addition to the Weibull statistical parameters, as will be demonstrated later.

CHAPTER 4

STATISTICAL TECHNIQUES USED FOR AE CHARACTERISATION OF TRANSVERSE GLASS FIBRE REINFORCED COMPOSITE MATERIALS

4.1 Aim of the Statistical Analysis.

All material properties are subject to statistical fluctuation. In the case of material strength, any set of samples tested will show fluctuations in their failure strength. In a similar way, the distribution of acoustic emission ringdown counts can be described by the applications of Weibull statistics. Weibull statistics have the advantage of a wide variability of shape, determined by parameters within the equations of the statistical distribution.

Weibull statistics has previously been applied to the fracture of composite fibre bundles [27], [29] and in this case the mathematics is extended to apply to situations where the Weibull statistics and ideas of the weakest link may not strictly apply. Also, by integrating stress-strain and AE data, it is possible to analyse a number of composite systems and obtain their distinctive differences and the severity of each of the AE events emitted during testing.

4.2 Weibull Theory.

Weibull statistics are based on a weakest-link hypothesis, which means that the weakest component determined, for example by the most serious flaw will lead to fracture and thereby control the strength of the material, [51]. The weakest flaw is the one which is subjected to the higher stress intensity factor. This means that both size of the crack and its orientation and shape, relative to the applied stress, will contribute to its severity.

The basic Weibull distribution is given by:

$$P_f = 1 - \exp \left[- \left(\frac{\sigma}{\sigma_0} \right)^m \right] \quad (4.1)$$

Where P is the fracture probability for stress " σ ", " m " is the Weibull modulus or shape parameter and " σ_0 " is the scaling parameter, sometimes referred to as the "characteristic strength" and corresponds to a fracture probability of 0.63.

Traditionally, in order to obtain reliable fracture statistics from equation (4.1), σ_0 and m have been determined from a set of measurements of the fracture stress. The evaluation of Weibull parameters is definitely not a trivial task. Four different methods could be used for their evaluation: linear least squares analysis (which is been used in this investigation), the weight function method applied to the linear least square analysis, the direct least square method, and the method of moments.

In the past, these methods have been extensively used for the characterisation of fibre bundles [52]. In a bundles of N_0 fibres tested for fracture strength the quantity " $P_f(\sigma)$ " may be estimated by noting the number of fibres " N_f " that have been fractured at stress σ or less. The probability of fracture of the N th fibre break may be expressed as:

$$P_f(\sigma) = \frac{N_f}{N_0} + 1 \quad (4.2)$$

So equation (4.1) becomes:

$$\left(N_f / N_0 + 1 \right) = 1 - \exp \left[- \left(\sigma / \sigma_0 \right)^m \right] \quad (4.3)$$

If N_0 is large then $N_0 + 1 \approx N_0$.

When a load “F” is applied to a bundles, some fibres may break and the resulting stresses in the fibres is given by:

$$\sigma = \frac{F}{A \cdot N_s} \quad (4.4)$$

‘ N_s ’ is the number of fibres surviving at the applied stress σ and A is the cross sectional area of a single fibre.

By using equation (4.3) and (4.4) and $N_f = N_0 - N_s$ yields:

$$F = \sigma \cdot N_0 A \cdot \exp \left[- \left(\sigma / \sigma_0 \right)^m \right] \quad (4.5)$$

Since ' $\sigma = E \varepsilon$ ' (4.6) then by using (4.3), (4.5) and (4.6) and at an applied strain “ ε ” the number of surviving fibres in a bundles which consists of N_0 fibres is:

$$N_s = N_0 \cdot \exp \left[- \left(\varepsilon / \varepsilon_0 \right)^m \right] \quad (4.7)$$

Equation (4.7) is the basic equation applicable to the Weibull Statistics of fibre bundle fracture.

4.2.1 Regression Analysis Applied to Weibull Statistics

The purpose of this analysis is to rearrange the Weibull equation (4.7) into a form providing a linear relationship, in order to deduce the shape parameter “m” and scale parameter “ ε_0 ” from the slope of the appropriate graphical display.

$$\text{From equation (4.7): } N = N_o \cdot \exp \cdot \left[- (\varepsilon / \varepsilon_o)^m \right] \Rightarrow$$

$$N = N_o \cdot \frac{1}{\exp \cdot \left[(\varepsilon / \varepsilon_o)^m \right]} \Rightarrow \quad \frac{N_o}{N} = \exp \cdot \left[(\varepsilon / \varepsilon_o)^m \right] \Rightarrow$$

$$\ln \frac{N_o}{N} = \left(\frac{\varepsilon}{\varepsilon_o} \right)^m \Rightarrow \quad \ln \cdot \ln \left(\frac{N_o}{N} \right) = \ln \cdot \left(\frac{\varepsilon}{\varepsilon_o} \right)^m \Rightarrow$$

$$\ln \cdot \ln \left(\frac{N_o}{N} \right) = m \cdot \left[\ln(\varepsilon) - \ln(\varepsilon_o) \right] \therefore y = mx + \text{const} \Rightarrow$$

$$\text{const} = -m \ln(\varepsilon_o)$$

So by plotting $\ln \ln (N_o/N)$ vs $\ln (\varepsilon)$, **m** is determined from the slope of the graph and from the Y-axis intercept, $-m \ln (\varepsilon_o) = p_1$, ε_o is determined, as can be seen from figures 4.1 and 4.2.

4.3 Weibull Statistics Applied to AE Data from Transverse Failure of Glass Fibre Reinforced Composites

Statistical techniques and distributions are often resorted to when dealing with materials that exhibit wide scatter in test data. One such technique is the two parameter Weibull cumulative distribution function. Based upon theoretical and empirical justifications, it has become a popular statistical model in engineering applications. In the past the fibre strength distribution has usually been described using a two parameter Weibull distribution function [27, 29, 53, 54]. By means of AE it is possible to monitor the failure of these fibre bundles, fibre by fibre if the measurement system is calibrated to do this (equation 4.7). Techniques using AE have been shown to be highly versatile and can be formulated to account for a range of statistical processes.

In the present experiments the micromechanics of failure can be described using a two parameter Weibull distribution function. The propagation of transverse cracks in the transverse fibre composites is complex and may not conform to the weak link ideas implicit in the use of Weibull Statistics. However, Weibull statistics will be applied to composite fracture problems such as transverse failure in an empirical way since it is accepted that transient elastic waves are generated by the release of stress or strain energy from localised source within the material. Information extracted using mechanical testing, combined with measurement of acoustic emission events, may give accurate information on the condition of the material.

The Weibull equations can be used to characterise the statistical failure of mechanical systems. In this case the equations have been formulated in terms of AE events with specific ringdown count and amplitude values. Suppose that AE events emitted during testing have a number of different ringdown count (RDC_1, RDC_n) and amplitude (AMP_1, AMP_n) values, then the number of events 'N' which correspond to a specific ringdown count (RDC), or amplitude (AMP) value can be expressed by the equations (where these equations have the usual mathematical form of a Weibull equation) :

$$N = N_0 \cdot \exp \left[- \left(\frac{RDC}{RDC_0} \right)^m \right] \quad (4.8)$$

$$N = N_0 \cdot \exp \left[- \left(\frac{AMP}{AMP_0} \right)^m \right] \quad (4.9)$$

where m and AMP_0 or RDC_0 ; are the Weibull shape parameter and scale parameter respectively. N_0 is the total number of AE events for each of the specimens tested. Shape parameter m is important for determining the breadth of the distribution of RDC or AMP. A large value for 'm' signifies a narrow distribution and a structure with uniform distribution of similar defects. It is obtained from the slopes of the logarithmic Weibull plots produced in the form $\ln \ln (N_0/N)$ versus $\ln (RDC)$ or $\ln \ln (N_0/N)$ versus $\ln (AMP)$ derived from the acoustic emission data. The intersection between the straight line from the graph and the Y axis is represented by : $p_1 = -m \ln (RDC_0)$ and/or $p_2 = -m \ln (AMP_0)$. The last step is to derive the values for the scale parameters RDC_0 and AMP_0 . These values seem to be in close agreement with the most frequent occurring ringdown count and amplitude value relative to the number of events.

The linearity of such Weibull plots over the entire strain range indicate that a Weibull treatment is applicable. The present work represents an attempt to find a better means of obtaining the statistical parameters used to describe the nature of the fracture and damage growth process of a composite system. A significant requirement for convenience is that the tests should be carried out using a constant crosshead speed.

From equations 4.8 and 4.9, the values for the shape parameter 'm', for the 7-days cured and 2 hours further post cured specimen for two different batches of glass fibre reinforced specimens can be calculated. The Weibull parameters are obtained using composite fracture data below maximum stress, after which saturation of the acoustic emission data can occur which would have distorted Weibull parameters obtained. Figures 4.1 a, b and 4.2 a, b show the logarithmic Weibull plots in the form of $\ln \ln(N_0/N)$ versus $\ln (RDC)$, and $\ln (AMP)$ respectively, derived from the acoustic emission data.

Weibull test data are given in tables 4.1 a, 4.2 b for each of the samples. Again batches of samples were produced, labelled E1 and E2 and within these batches, some were tested as cured (C) and after post-curing (PC). In the table the shape parameter 'm' is listed for cured materials and for post-cured materials. The values of m has been derived from the amplitude and the ringdown count AE data. The percentage of the linear regression signifies the accuracy of the data fall inside the regression curve and gives information on the scatter of the data. By examining table 4.1 a, it could be argued that the regression percentages where satisfactory. The calculation of the corresponding scale parameters AMP_0 and RDC_0 is also included.

Table 4.1 b shows the average values for the Weibull parameters and gives a clear indication of the nature of the results. From table 4.1 b, note that 'm-RDC' is greater than 'm-AMP' derived from both the equations 4.8 and 4.9, which correspond to amplitude and ringdown data. The difference between these two values is not great but in each case, indicative of a different parametric measure. The average value for the cured materials 'mC-AMP' is 0.56 in comparison to the value for the post-cured materials 'mPC-AMP' which is 0.75. The same pattern appears from the corresponding ringdown counts calculations where 'mC-RDC' is 1.28 in comparison to 'mPC-RDC' which is 1.68., The calculation of the scale factors RDC_0 and AMP_0 was carried-out simultaneously. From table 4.2, it can be noticed that again the corresponding values for the post-cured samples are higher on average in comparison to the vales describing the cured condition. In general, it could be said that the calculated values for AMP_0 and RDC_0 , signify the position of the amplitude and ringdown count distributions. Figures 4.1a, b and 4.2a, b, demonstrate some typical examples with logarithmic plots for cured and post-cured samples.

The difference in the shape parameter values 'm', between the post and the post-cured specimen signifies the different nature of the ringdown count and amplitude distributions, together with the nature of the tested materials. The greater the value of 'm' the narrower scatter of the data and the statistical distribution and the more uniform the defects inside the transverse glass fibre reinforced composite materials. Post-curing might be expected to achieve a better overall structure and improvement on the overall properties of the composite material, with a more uniform distribution of similar defects which cause the narrowing of the statistical distribution. The average values for 'm', derived from the

AE data and shown in table 4.1 b, suggests this. The higher value for RDC_0 and AMP_0 , in the case of the post-cure and consequently more brittle materials signifies the fact that the acoustic energy in a microcrack might be expected to rise, as this measure suggests.

The last step is to evaluate the precision of these calculations. By obtaining the values for 'm' and RDC_0 , AMP_0 , the events distribution is obtained using equations 4.8 and 4.9 and can be predicted. Comparison are shown between theoretically fitted values and the real number of emitted events. Keeping in mind the fact that Weibull statistics are applied to a transverse fibre bundle composite material with relatively complex structure and fracture behaviour, the results show a good correlation especially in the case of ringdown counts as can be seen from figures 4.3a, b and 4.4a, b for cured and post-cured samples correspondingly.

The failure of transverse glass fibre reinforced composites can be described using Weibull statistics and the associate parameters. There are a number of graphical methods which are preferred for accurate work and especially when characterising fibre bundle tensile strength [29, 52]. The application of one of these methods for the characterisation of the transverse fibre bundle composite materials has been demonstrated in order to distinguish the differences between the cured and post-cured specimen. For further improvement to these results, these graphs could be divided into low strain and high strain regions. The same methods could then been applied in order to obtain the Weibull parameters. However, due to the inherent instability of using $\ln \ln$ plots for determining parameters, particular methods should be used with care.

◆ **Table 4.1a**

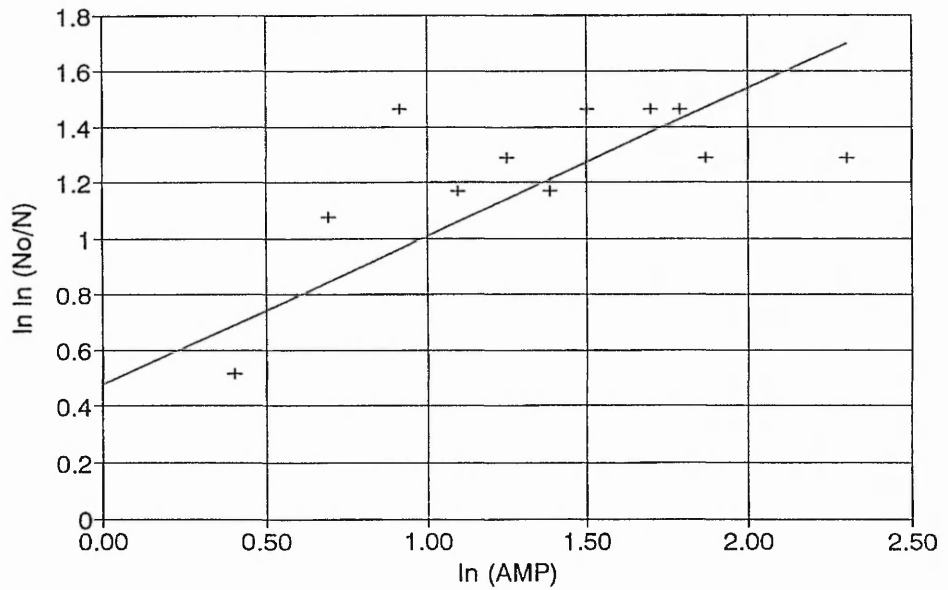
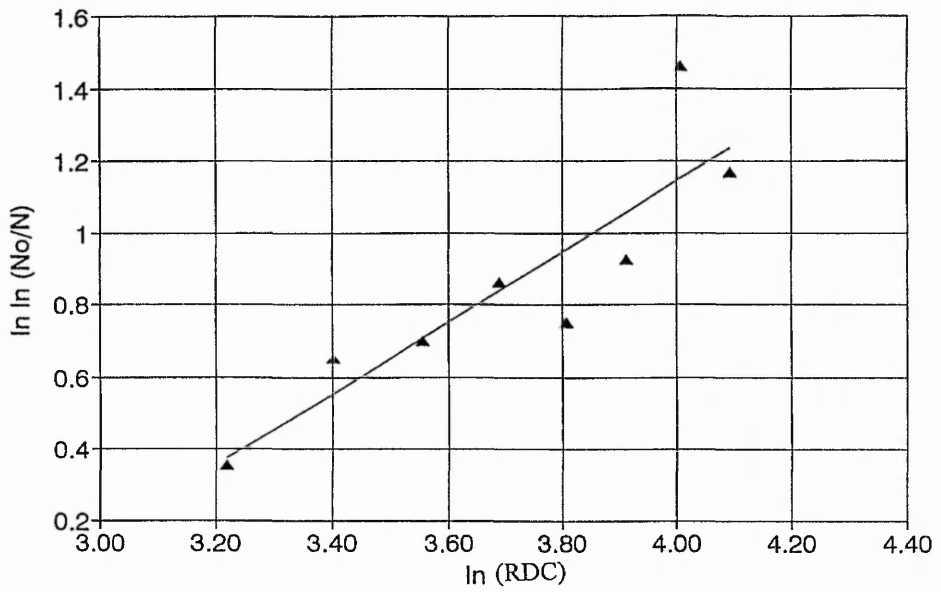
Weibull strength distribution parameters for transverse E-glass fibre reinforced composites- obtained from Amplitude versus Number of events and Ringdown counts versus Number of events for batches **1** and **2** together with the percentage of regression for each of the specimen. 'C' signifies room temperature cure samples and 'PC' post-cured samples.

Specimen No	m-AMP	% Regression	m-RDC	% Regression	AMP ₀	RDC ₀
E1-GC	0.627	85.2	1.41	85.8	0.581	23.47
E1-GC	0.528	69.1	0.484	47.0	0.524	6.84
E1-GPC	0.276	64.6	1.64	82.5	0.100	28.96
E1-GPC	0.727	76.7	1.81	99.2	0.730	26.09
E1-GPC	0.739	67.3	1.61	91.7	0.773	23.46
E2-GC	0.566	64.0	1.46	89.9	0.495	22.10
E2-GC	0.531	61.3	0.985	78.7	0.408	16.10
E2-GC	0.398	48.0	--	--	0.215	--
E2-GPC	0.699	71.8	1.71	98.9	0.612	23.66
E2-GPC	0.774	84.8	1.28	94.6	0.710	17.45
E2-GPC	0.813	74.6	1.71	95	0.773	23.94
E2-GPC	0.723	56.1	1.96	98.5	0.667	27.14

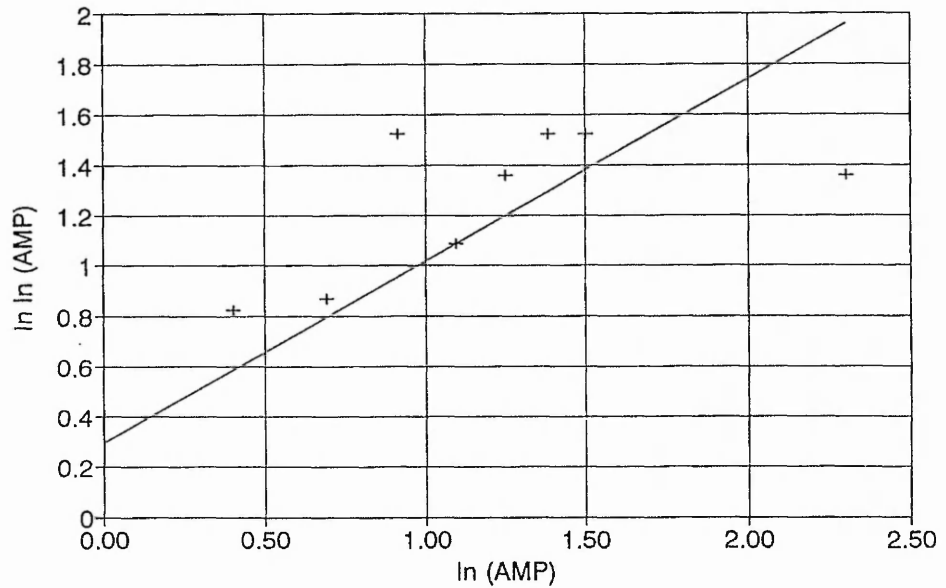
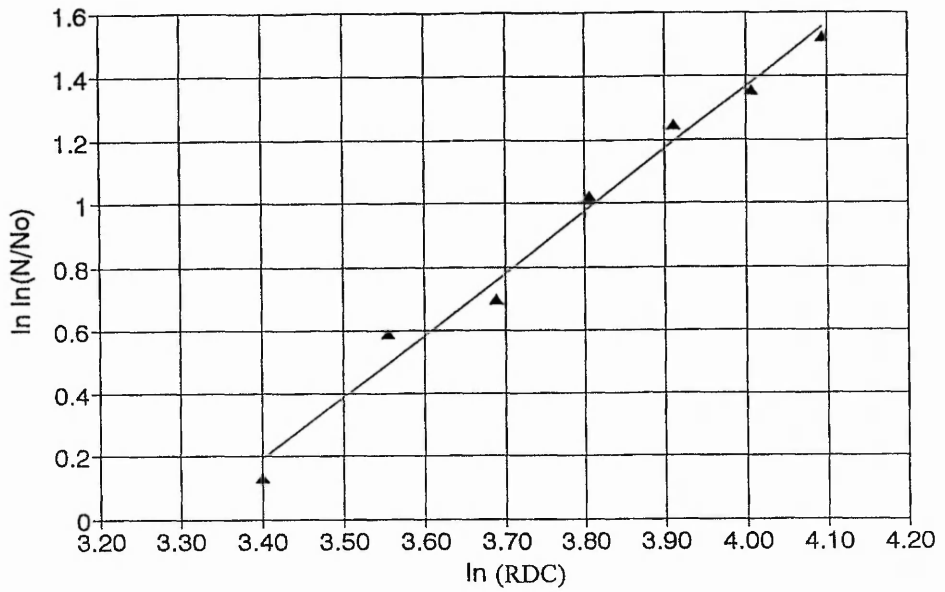
◆ **Table 4.1b**

Average values derived from the Weibull statistical data in table 4.1 a for cured and post-cured samples. 'm-AMP' and 'm-RG' derived from the AE amplitude and ringdown count data correspondingly.

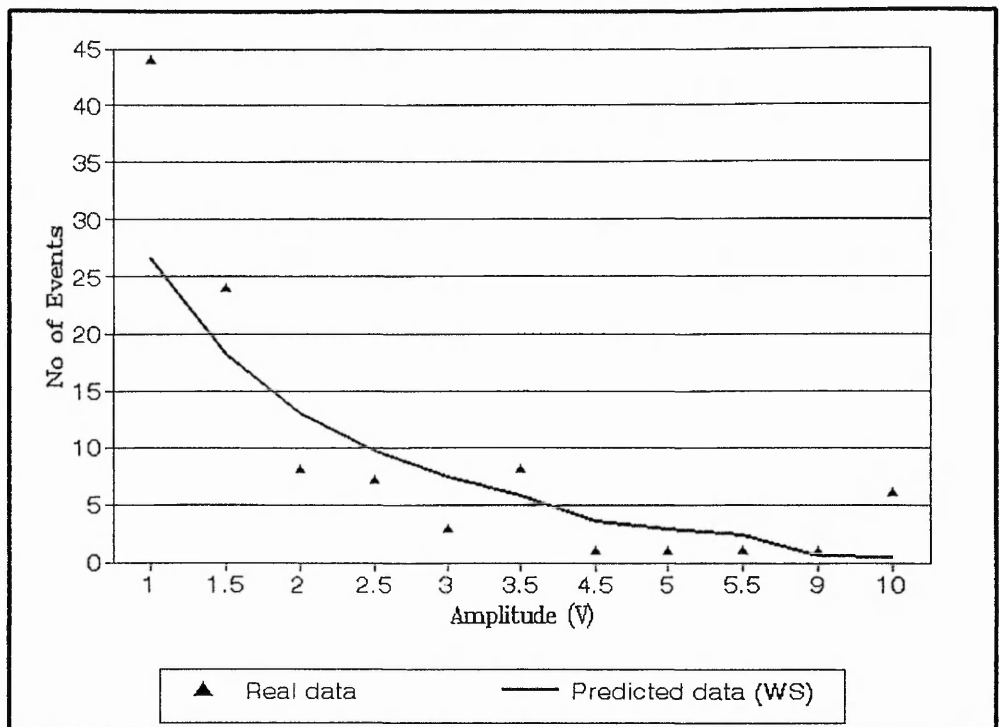
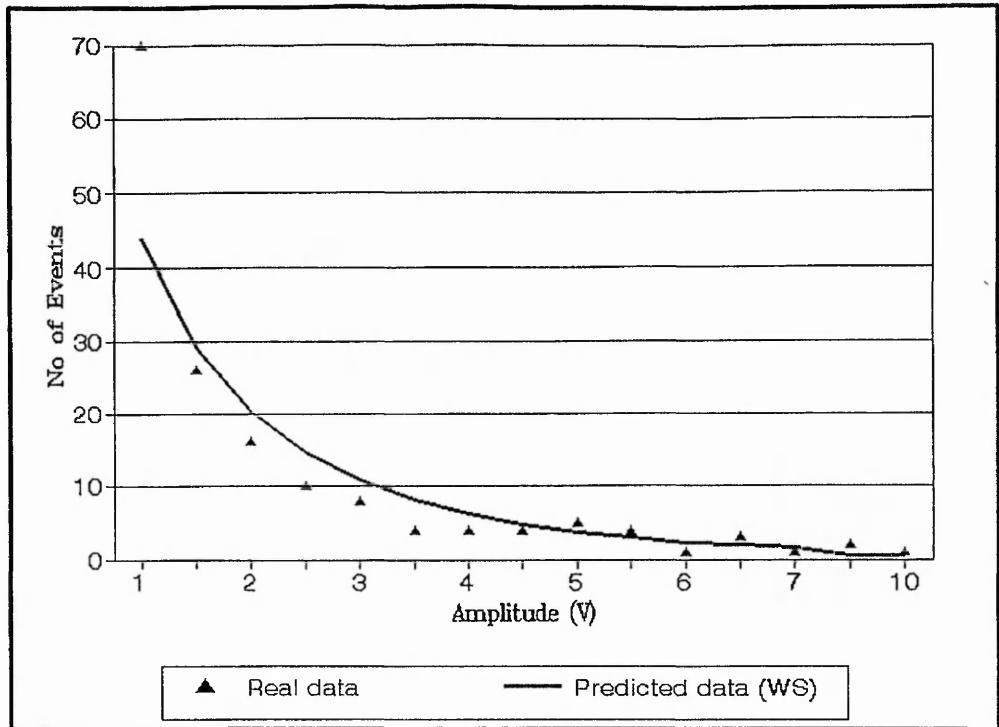
Type of Sample.	m-AMP	% Reg	m-RDC	% Reg	AMP ₀	RDC ₀
E-GC	0.56	70	1.28	84.8	0.50	20.55
E-GPC	0.75	72	1.68	96.3	0.71	24.54



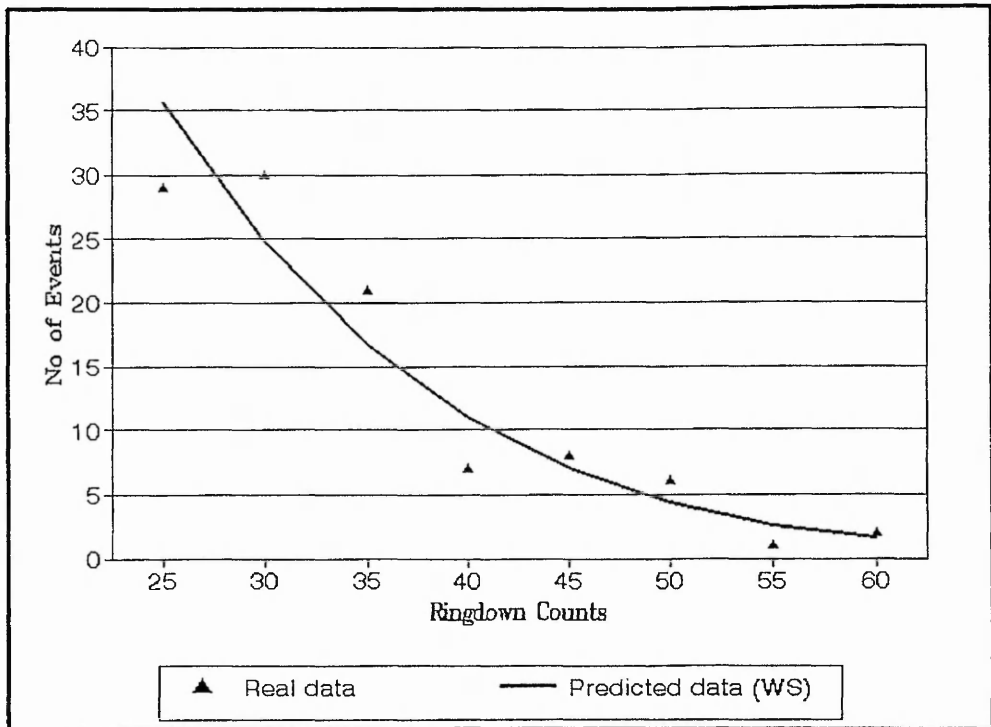
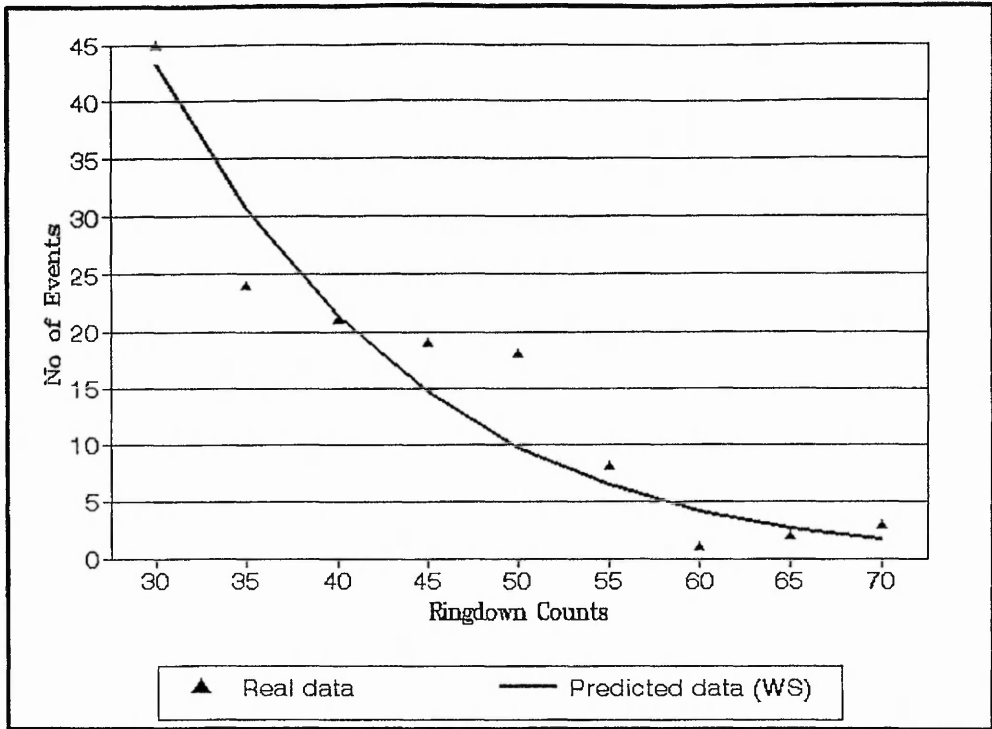
◆ **Figure 4.1 a, b:** Logarithmic Weibull plots in the form of 'ln ln (No/N) vs ln (RDC) or ln (AMP)', derived from tensile testing of Cured E-glass composite specimen.



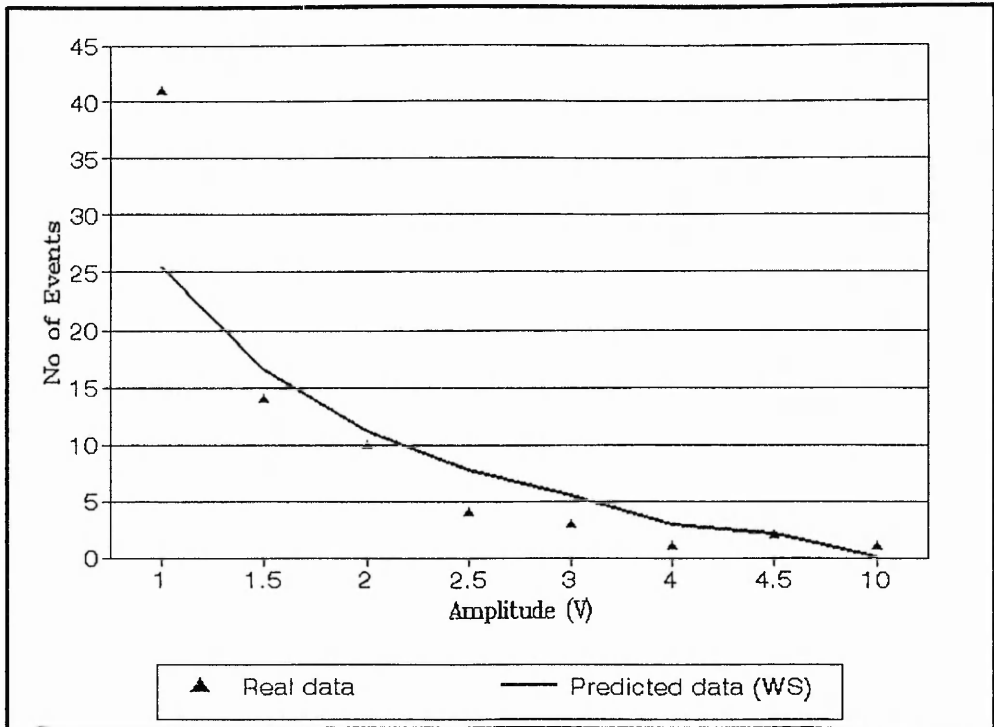
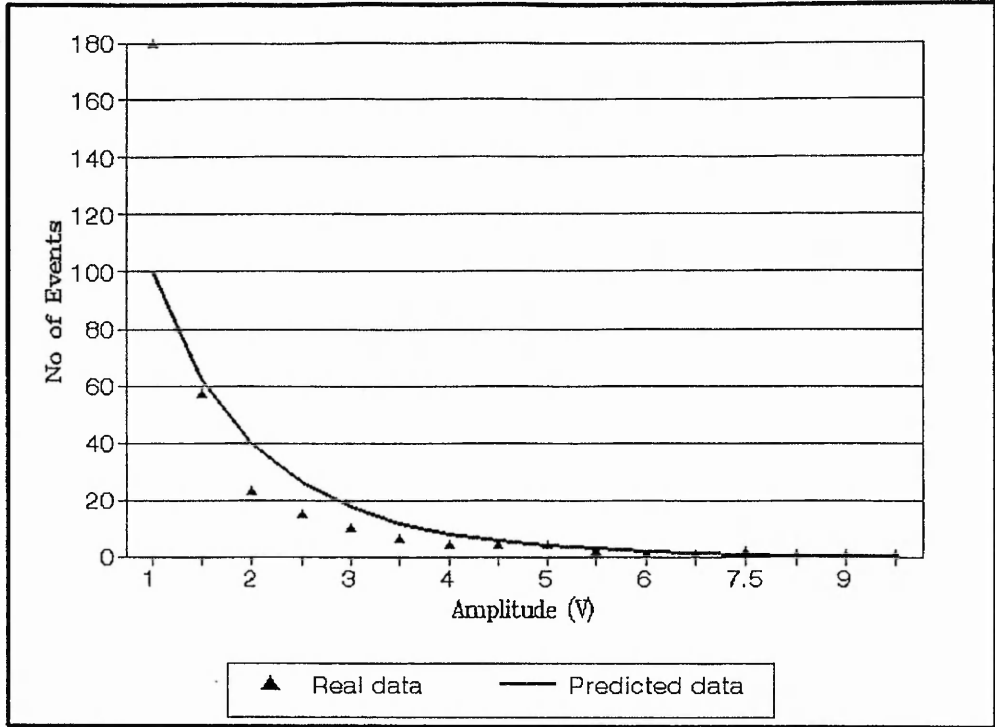
◆ **Figure 4.2 a, b:** Logarithmic Weibull plots in the form of ' $\ln \ln (No/N)$ vs $\ln (RDC)$ or $\ln (AMP)$ ', derived from tensile testing of Post-Cured E-glass composite materials.



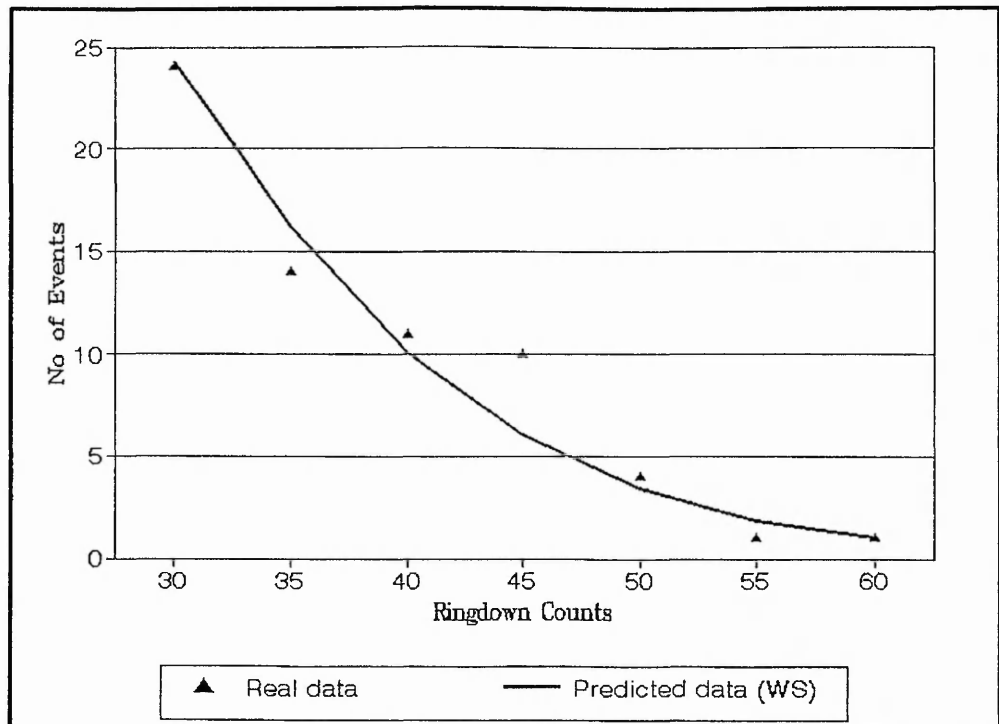
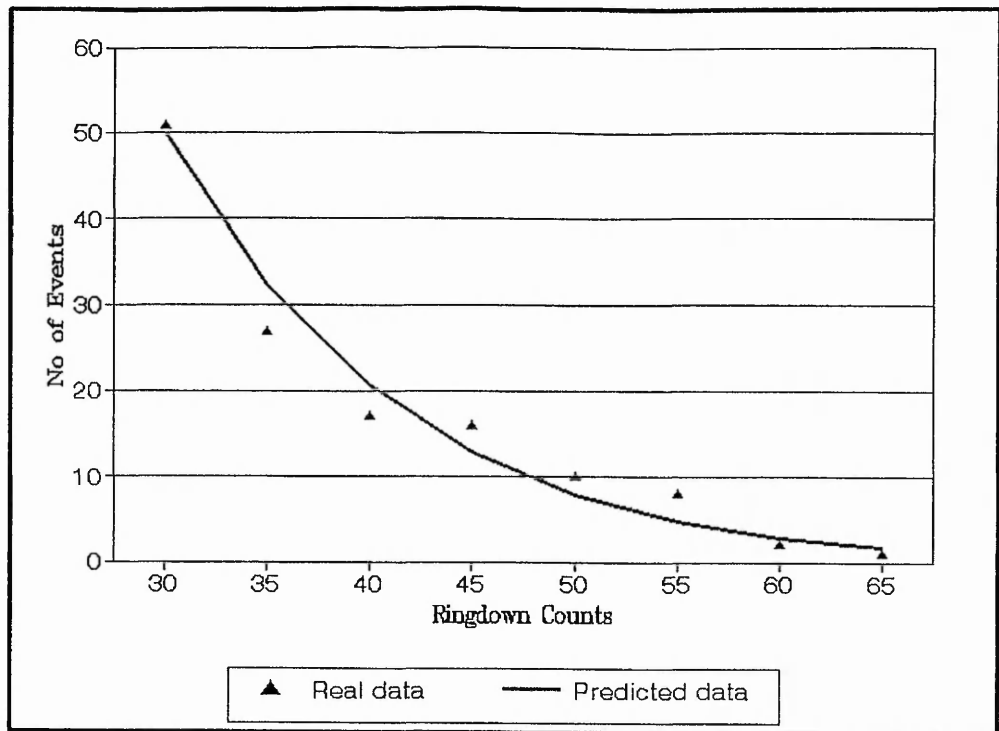
◆ **Figure 4.3 a:** Comparison of the real data versus the predicted data, calculated using Weibull equations 4.8 and 4.9, for E-glass Cured composite material.



◆ **Figure 4.3 b:** Comparison of the real data versus the predicted data calculated using Weibull equations 4.8 and 4.9 for E-glass Cured composite material.



♦ **Figure 4.4 a:** Comparison of the real data versus the predicted data calculated using Weibull equations 4.8 and 4.9 for E-glass Post-Cured composite material.



◆ **Figure 4.4 b:** Comparison of the real data versus the predicted data calculated using Weibull equations 4.8 and 4.9 for E-glass Post-Cured composite material.

4.4 AE Event Severity for the Characterisation of E-glass Composite Materials.

4.4.1 Aim of using a severity measure.

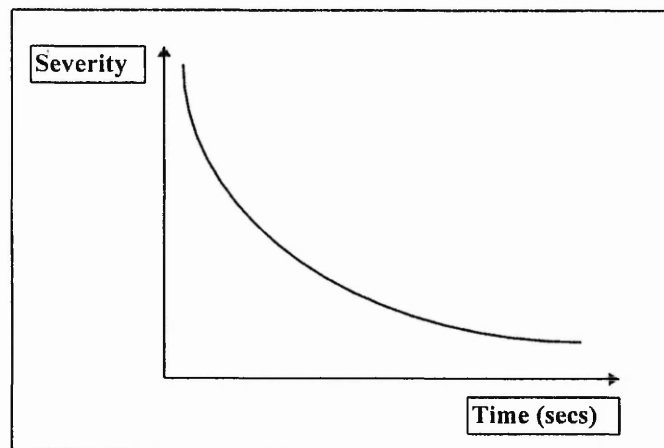
While conventional analysis techniques consider the time position of AE, they give no weighting to the stress applied during the testing of the transverse E-glass fibre reinforced composite materials. The applied stress provides the driving force for AE activity to take place. For instance, for two AE events with similar AE parameters, where one occurs at lower stress, then this event is likely to have a higher 'severity'. The term 'severe event' or 'severity', indicates the importance of the initiation of damage and the lack of integrity introduced at the microdamage site. Initial AE events emitted during tensile testing, are considered as severe, when they introduce the important damage sites and induced structural failure. In order to account for this, the mechanical energy of the sample is calculated and is used to estimate the AE event severity [15], [20], [22], [55-57].

4.4.2 AE Severity, Results and Discussion

An AE event may be caused by several material changes such as matrix cracking or interfacial debonding. During initial matrix cracking, the AE method has proved to be most suitable because it can continuously monitor any development of the material damage during tensile loading. Interfacial debonding is one aspect of the beginning of material failure. It is an important event because a composite with debonded interfaces is lacking integrity and its mechanical properties will be degraded significantly, leading to accelerated damage accumulation and ultimate failure. The combination of normal (σ) and shear (τ) stresses will determine the interface debonding. However, both ' σ ' and ' τ ' are formed from two contributions. One is the thermal residual stresses and the other is due to the applied stress. The effect of this complex stress distribution depends on the material properties which have been improved considerably in the case of the post-cure materials.

The stress-strain distribution carries information on the stored mechanical energy and from the AE parameters and the stored energy, it is possible to evaluate the degree of severity at any instant in time. Figures 4.5 a, b, and 4.6 a, b, plot the AE severity in terms of Amplitude/Energy or Ringdown counts/Energy versus time. The mechanical stored elastic energy has been deduced from the corresponding stress-strain graphs for each of the materials. It has the form of : $M.E.E_n = 1/2 \sigma \epsilon$ and it can be deduced for every time interval (t_{n-1}, t_n) . For the same time interval (t_{n-1}, t_n) , there is a corresponding value AMP_n or RDC_n . The severity of an AE event emitted at this time interval is: $S_n = AMP_n / M.E.E_n$. This process is then repeated for every single time interval (t_n, t_{n+1}) and the corresponding severity of every AE event in relation to the elastic energy is then estimated.

By plotting the severity graphs in the form of severity ' S_n ' versus 'time', a hyperbolic function is expected as is been shown in figure 4.7, in the hypothetical case where the emitted amplitude signal holds the same value during the experiment. Since the amplitude values vary, it is then expected several peaks will occur as is demonstrated in figures 4.5 and 4.6. The values and frequency of these peaks will then indicate the initiation of damage with the degree of severity of the event affecting the interfacial integrity of the material.



◆ **Figure 4.7:** Severity graphs where amplitude or ringdown count values emitted is constant during tensile testing of the material.

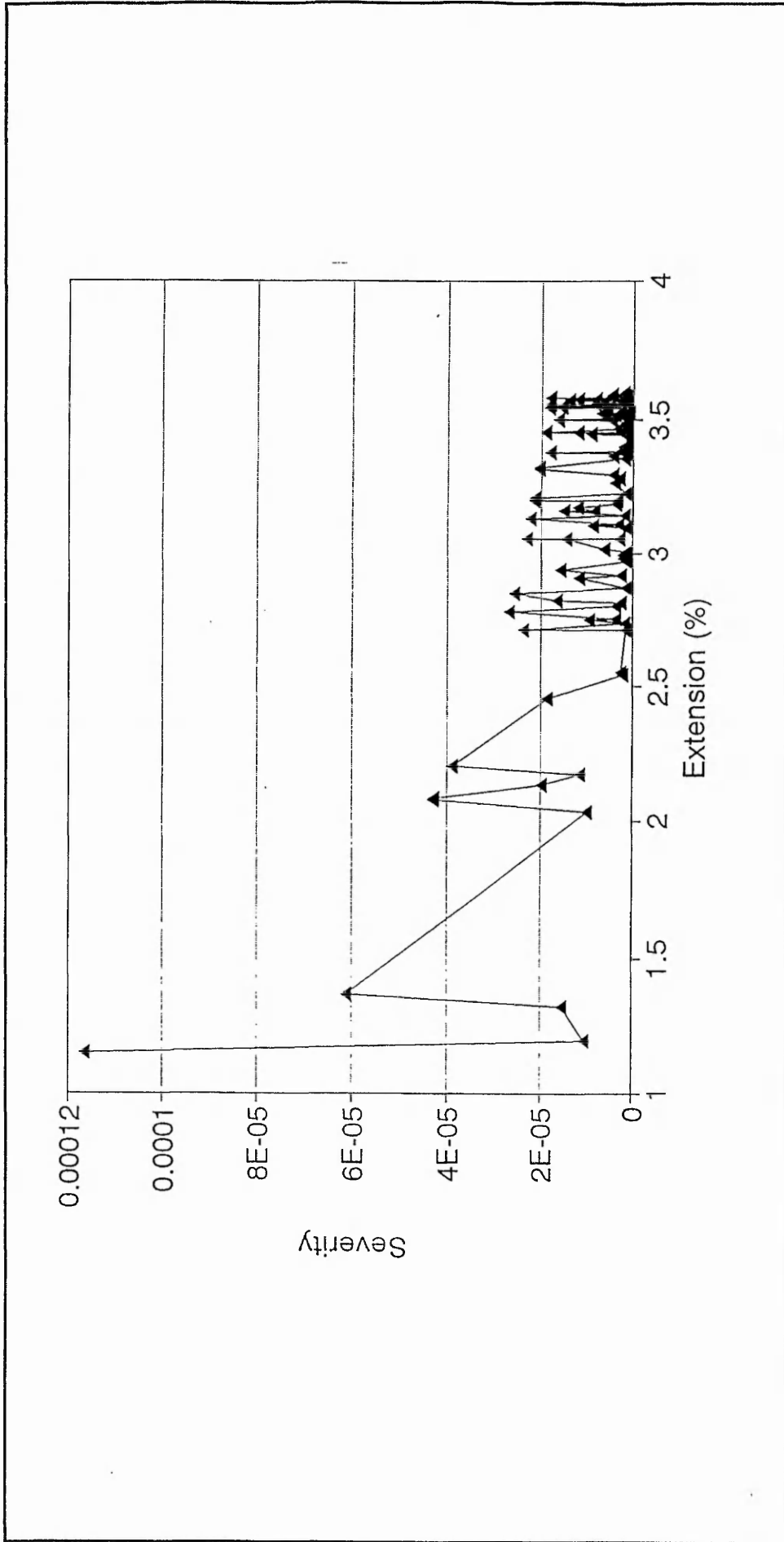
For all the calculations of severity, it is noticeable that these plots (figures 4.5 and 4.6) emphasise the initial events. The severity of the initial events is high which is as expected and may be due to the fact that the majority of cracks initiate from the free edges of the specimen and then propagate through the width of the material.

Data from transverse bundle samples using glass reinforcement were compared in the cure and the post-cure conditions using 'severity analysis'. It should be noted that many more initial events are severe in the case of the post-cure materials as is shown in figure 4.6. Once more, the adhesive properties between the glass fibres and the polyester resin prove to be considerably improved in the case of the post-cure materials which can sustain higher loads producing more severe events. In general, it could be said that the cured materials have a larger proportion of severe events towards the end of the corresponding curve and in comparison to the post-cured materials. Finally, it was particularly reassuring that a good correlation exists between the present method and the pattern recognition method (see section 4.5), in respect of identifying strong emitted signals, throughout the corresponding time period. In both cases, it is possible to identify a number of events with relatively high amplitude or ringdown count values. However, the present method has the advantage of relating the emitted signal to the stress-strain response of the tested material.

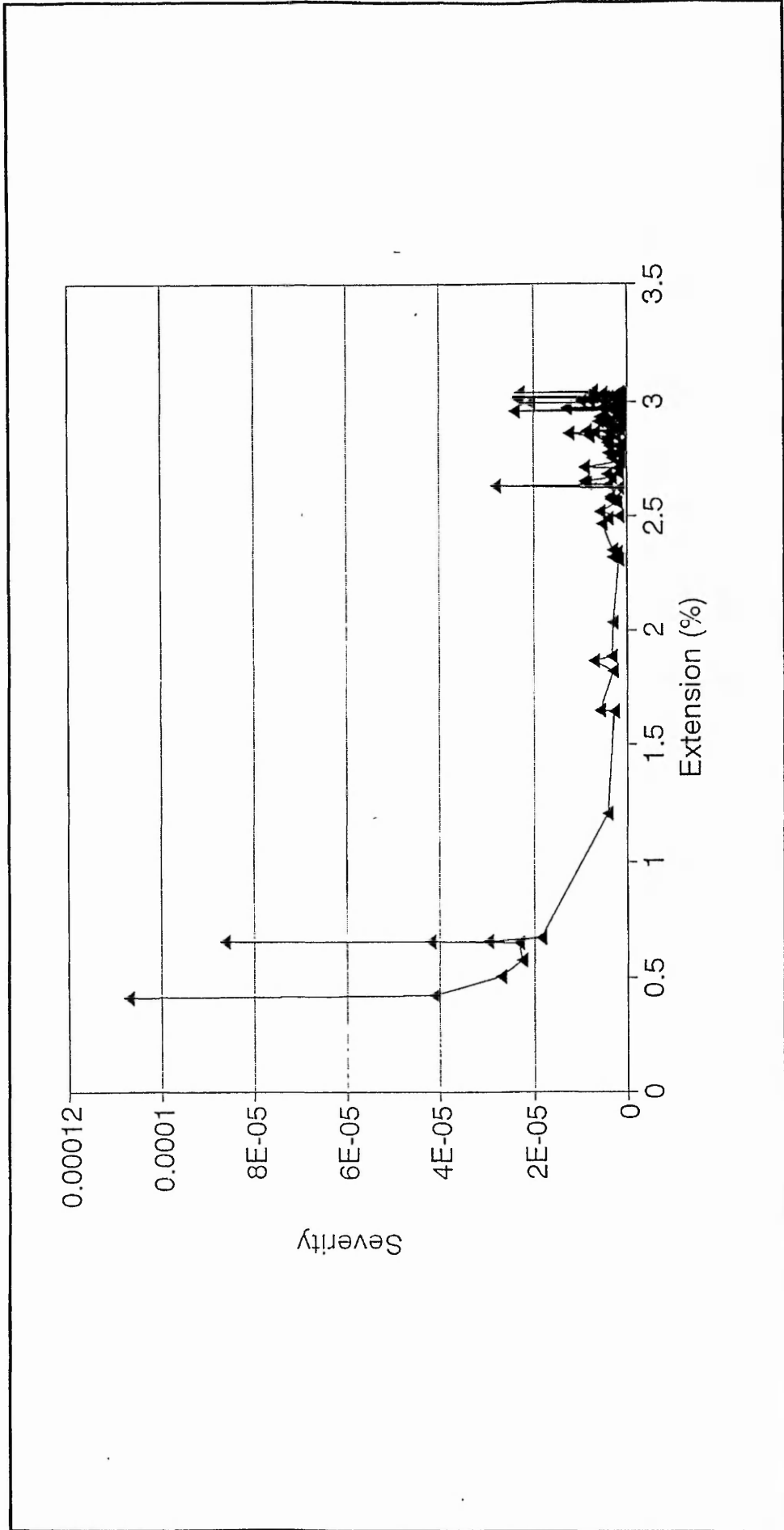
The reduction in transverse strength and early AE is accounted for in terms of the strain magnification which is maximum between the fibres. Very high strain magnification values are obtained when the fibres are close together. Transverse cracks are nucleated in regions of dense packing which propagate preferentially through such resins. A crack therefore spends relatively little time propagating through large zones of pure matrix. It is desirable that the distribution of the fibres in the resin in the region of the transverse bundle be uniform with good resin fibre adhesion to produce good, uniform material cracking.

As well as the above factors controlling cracking, matrix cracking may also be inhibited by the elastic constraint imposed on it by the presence of a rigid particle or fibre. In order for an increment of matrix crack growth to occur, a critical stress concentration factor at the crack tip must be exceeded. Initial crack/s are considered to be severe and would be expected to play a very important role to the later composite strength performance. In the case of transverse fibre composites the initial crack follows the fibre-

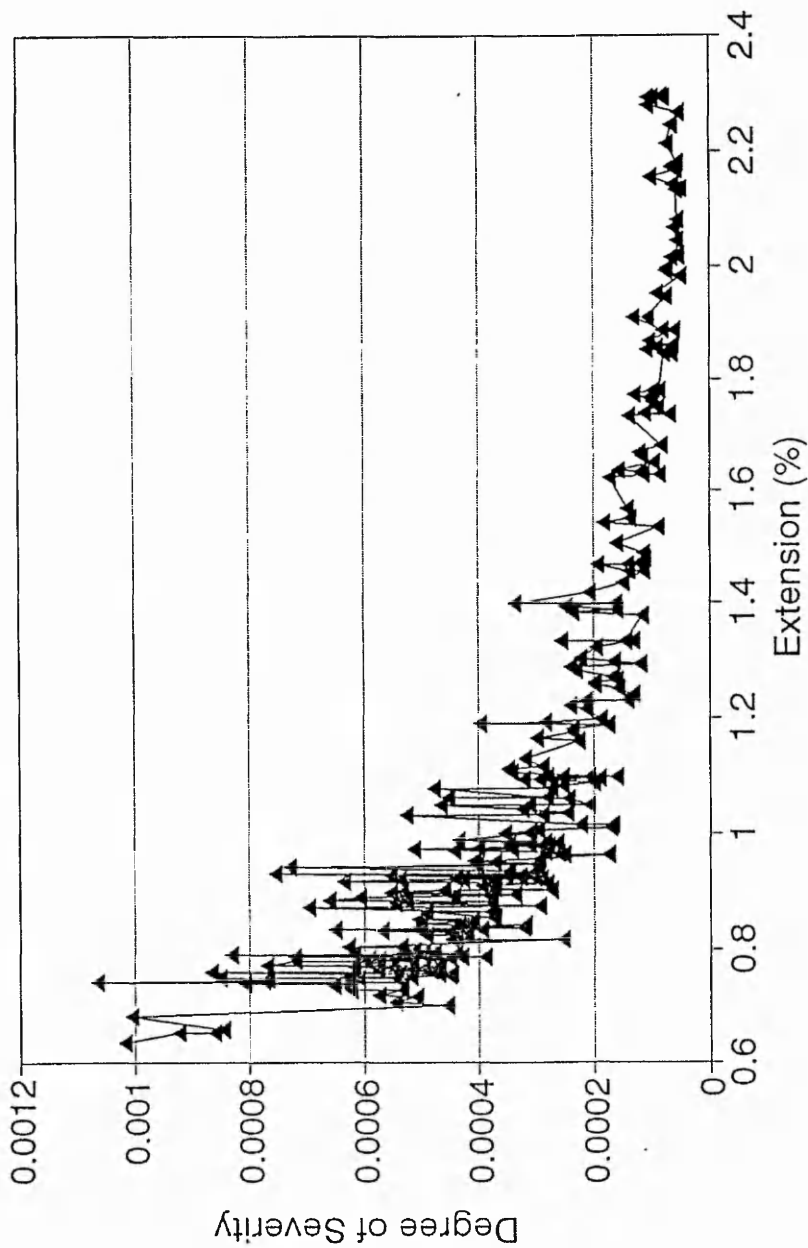
matrix interface and the cracks can nucleate ahead of the initial crack by debonding or by resin fracture very close to the fibre-matrix interface in regions of maximum radial tensile stress or strain. In other words once this initial crack occurs then its propagation is unavoidable and so the degree of severity of the damage to the material is high as can be seen from figures 3.3 a, b and severity figures 4.5 and 4.6. Here the majority of the cracks initiate from the free edges of the specimen and then propagates through the width of the specimen. Multiple cracks follow, and local matrix damage increases. The current method demonstrates the importance of identifying a number of emitted signals which show that structural failure initiates and propagates through the material interface.



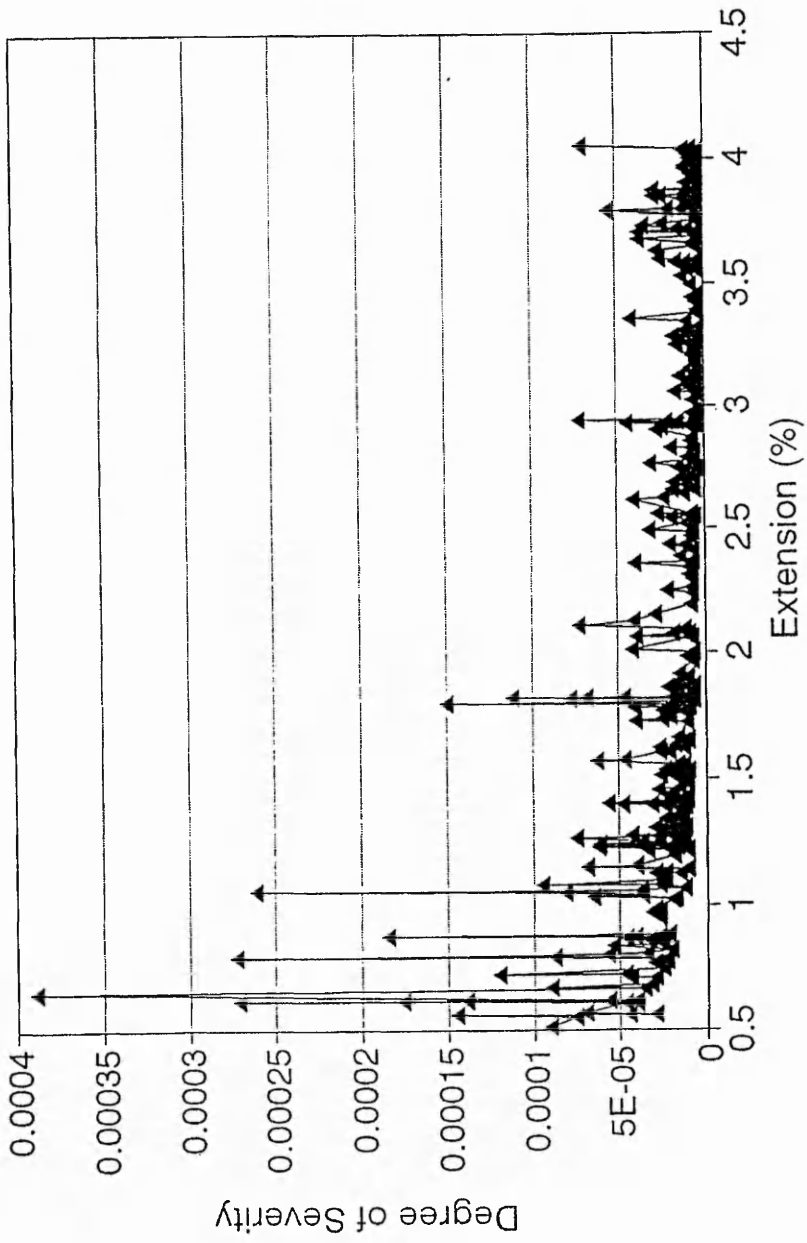
◆ **Figure 4.5 a:** AE Severity, derived from the amplitude data for Cured E-glass fibre reinforced transverse composite material.



◆ **Figure 4.5 b:** AE Severity, derived from the amplitude data for Cured E-glass fibre reinforced transverse composite material.



♦ **Figure 4.6 a:** AE Severity, derived from the amplitude for Post-Cured E-glass fibre reinforced transverse composite material.



♦ **Figure 4.6 b:** AE Severity, derived from the amplitude for Post-Cured E-glass fibre reinforced transverse composite material.

4.5 PATTERN RECOGNITION

4.5.1. Reasons for AE Signal Recognition

The aim of this section is to identify and categorise AE parameter values in such a way that it will be possible to determine different fracture mechanisms. Depending on the amplitude (Volt) and ringdown count value ranges, this study attempts to identify matrix cracking and fibre debonding. The study has limited application and further work could be undertaken, in order to achieve a proper scientific understanding.

4.5.2 Discussion of the Pattern Recognition Method and Results

The term “pattern recognition” is applied to a branch of artificial intelligence, where statistics and mathematics are applied to data, to store patterns in a computer and to compare new patterns with those that have been stored. It can be defined as the categorisation of identifiable classes in the input data via the extraction of significant features or attributes of the data from a background of irrelevant details. Generally, a pattern systems goes through a learning or training stage, in which a set of decision rules are developed. The goal is the classification of unknown signals into a set of pattern classes and it can perform the same function as a human expert in making a decision.

Acoustic emission monitoring, similarly generates a data set and is used because it allows real time analysis of damage accumulation in materials. The AE technique does not require special sample preparation (machining, mounting etc.) as might be expected in the case of metallography, or fracture surface studies.. Stress concentrations play a vital role in the mechanics of such systems and are generated, for instance, when fibres are oriented transverse to an applied load and are close together. If a composite of transverse fibres undergoes strain, the matrix between the fibres will elongate considerably more since the glass fibres are much more rigid. If the fibres are totally rigid, all the strain over the distance between the fibre centres (L) would be concentrated in the matrix between the fibres and hence a strain concentration generated. As the distance between the fibres

decreases, the stress concentration increases rapidly. In this work, details of the damage accumulation process have been studied by correlating the mechanical and acoustic emission response for each system.

First of all it has to be noted that the absolute values of the acoustic amplitudes and or ringdown counts are varying from system to system. Generally the literature is full of conflicting results concerning AE amplitudes and source mechanisms. However, from a number of authors [13], [17], [19], [37], it is well accepted that events which occur from fibre debonding, contain higher energy and therefore these events appear to have higher values for ringdown counts and amplitude than those events which purely caused by matrix cracking.

The AE amplitude and ringdown counts values versus time for both the 7 days cured and post-cured specimen are shown in figures 4.8 a, b, 4.9 a, b, and 4.10 a, b and 4.11 a, b, and are employed to give a better view of the damage evolution via A.E techniques. The AE events captured, due to the nature of the electronics used, have a range of values which are 0-10 volts and 0-60 ringdown counts. It could be argued that fibre debonding releases more energy than matrix cracking; hence it would be expected a fibre debonding signal would be more energetic.

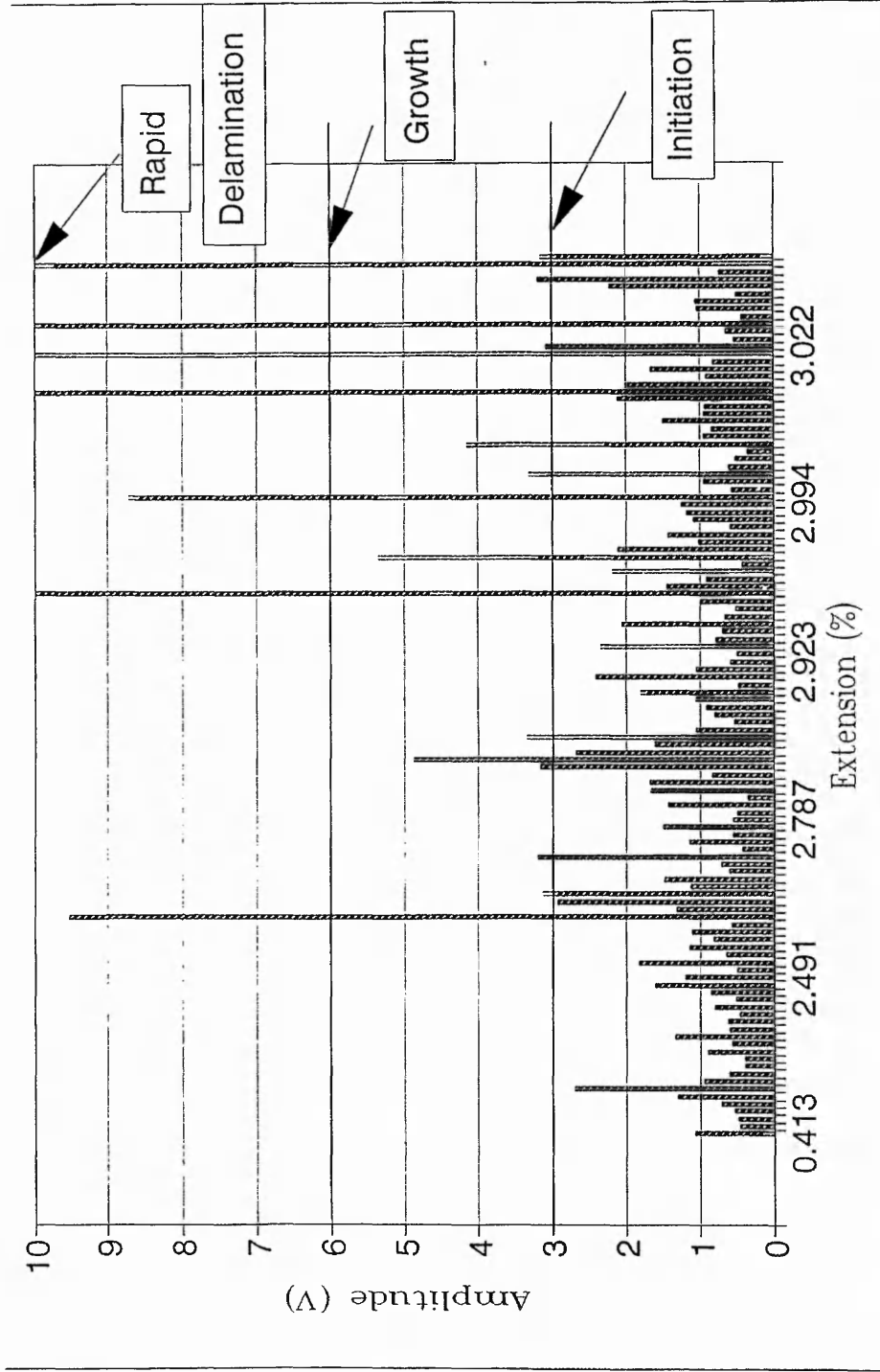
In the case of full engineering composites, the hypothesis that has been proposed is that, an AE signal within the range of 0-4 volts and 0-40 ringdown counts indicates matrix cracking, and that values in the range of 4-10 volts and 40-60 ringdown counts is linked to fibre debonding [13-14]. Also it is possible to say that for the low amplitude signals (0-3 V), (0-20 RDC), the initiation of delamination, takes place, for the medium range (3-6 V), (20-40 RDC), growth of delamination occurs, and the high amplitude events (6-10 V), (40-60 RDC), are caused by rapid advances of delamination. The latter case has been mostly obtained at the end of the stress-strain curve where the fibre debonding is reaching the final phase and the final fracture of the specimen is taking place. At this stage it is to be expected that there would be a build-up of interfacial failure leading up to the final fracture of the material. For both sets of data presented (figures 4.8, 4.9 and 4.10, 4.11) there was essentially no build up of high amplitude events. The suggested pattern is that low amplitude, short duration, low counts and energy data were due to matrix cracking, while

the high amplitude, long duration, high counts and energy data were due to fibre debonding.

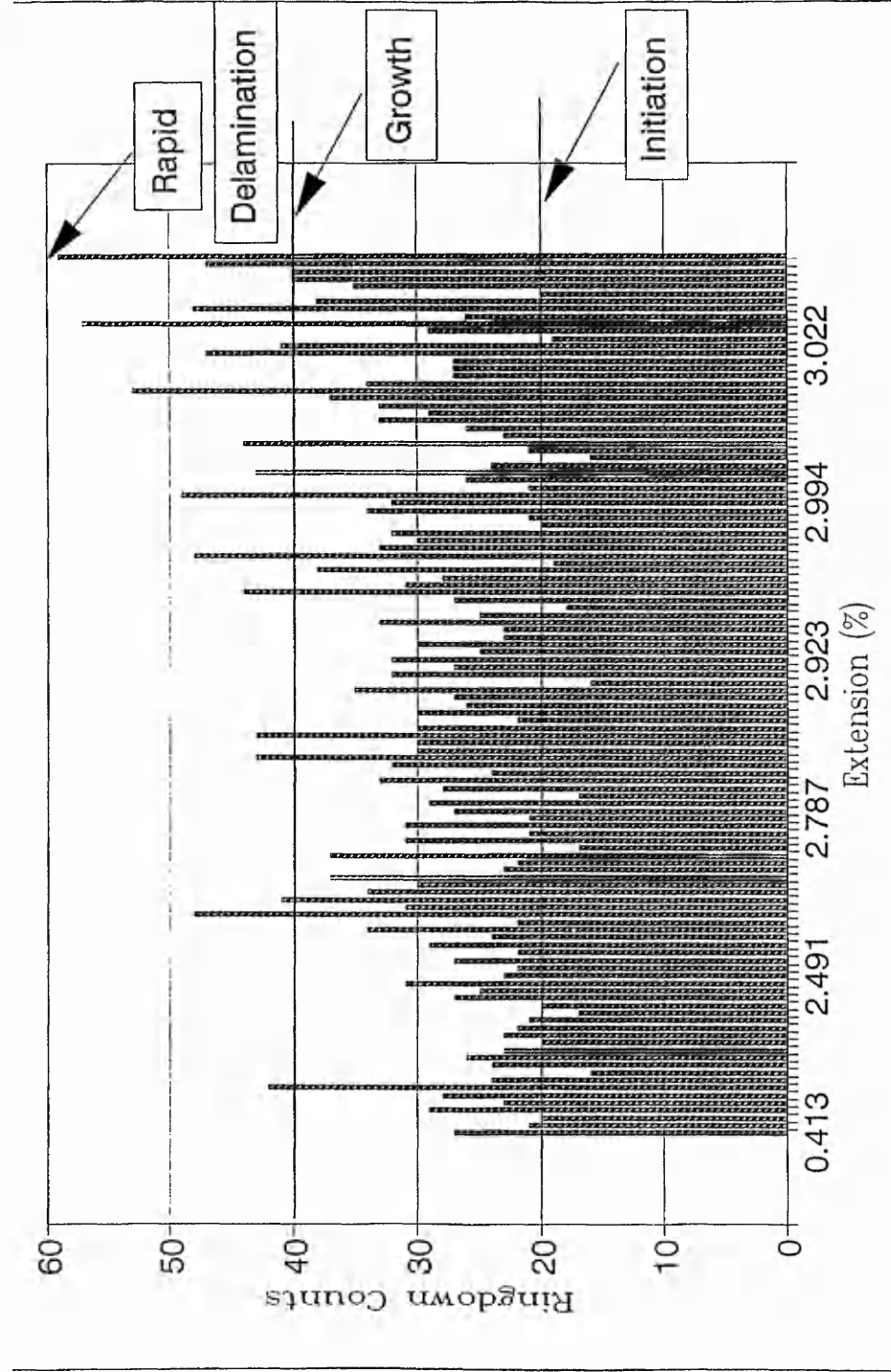
Continuous AE monitoring during loading provides information on first failure usually associated with the initiation of matrix cracking. The majority of cracks might be expected to initiate from the free edges of the specimen and then propagate through the width of the specimen. As part of this investigation, the severity of the initial events were examined (section 4.4). These events emit generally low amplitude and ringdown counts signals, but they do play a vital role in the initiation of the crack propagation and lifetime performance of the transverse glass fibre reinforced composite materials and in the practical case, full engineering composites.

Clearly, even in this investigation, analysis of data is complex since the detailed nature of the failure process for the transverse fibre composites is complicated. Noise signals were carefully eliminated from the AE data through the careful use of specific software filtering. This was basically achieved with the use of 0.2 V threshold level and the 200 μ sec data window. In some cases the very first AE events had unusual high amplitude and ringdown count values. These values fall well above the range of the average signal for the following events.

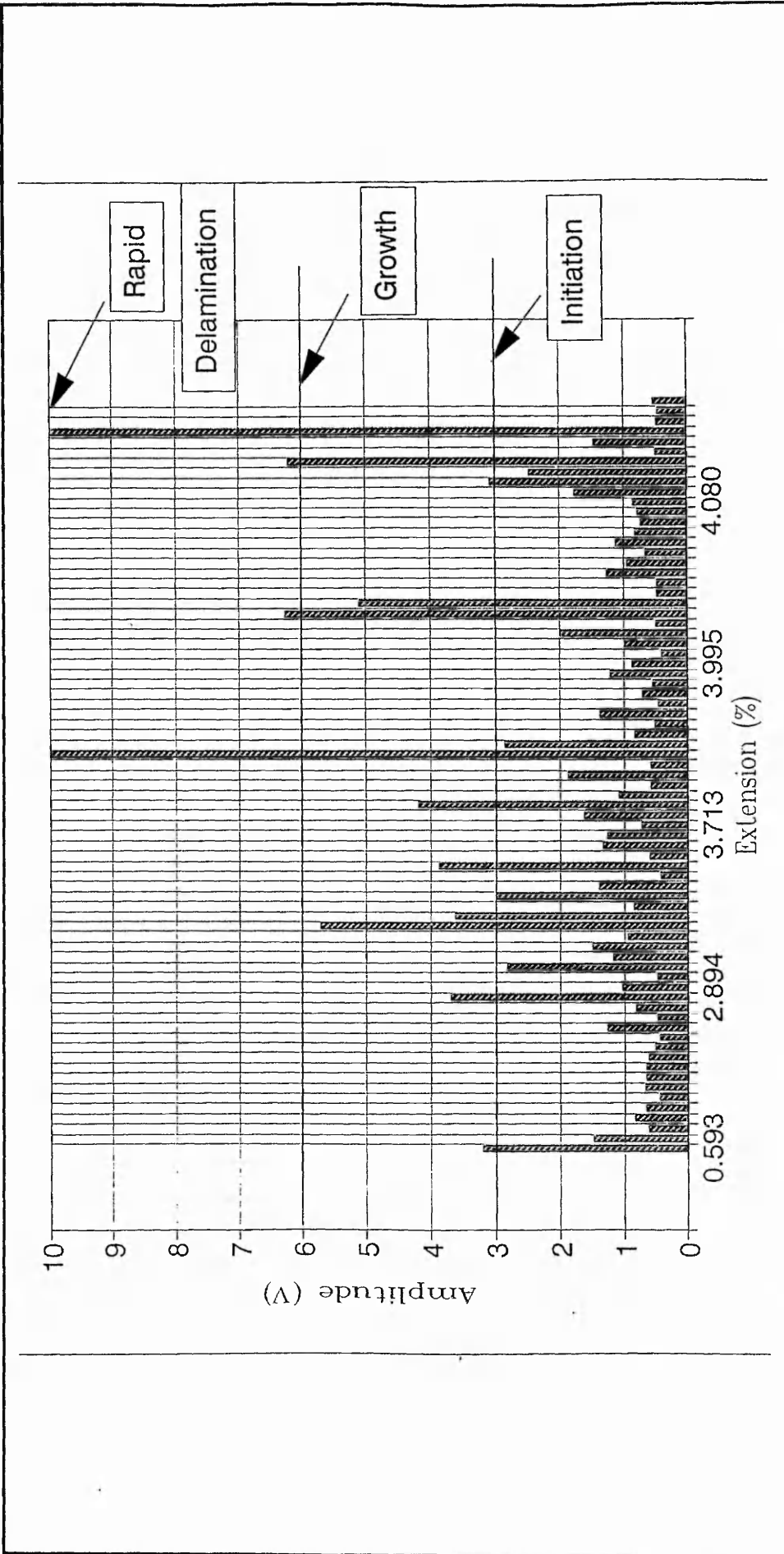
Since the duration of a noise (non AE) signal is long and the peak amplitude is low it is possible to eliminate such patterns [17], [58]. Finally, most studies on pattern recognition techniques applied to AE, do not have direct confirmation of the source mechanisms to compare with A.E data. Fracture energy considerations have been used in attempts to explain why a given source mechanism might produce larger or smaller amplitude acoustic signals, but the arguments have not been conclusive [37]. Also, the effects of wave propagation, such as attenuation, dispersion and multiple modes of propagation, have been largely ignored. In other words the corresponding pattern recognition applied to AE is not based on scientific understanding, but on empirical observations, which makes the whole subject incomplete. While the data in figures 4.8 and 4.11 suggest crack growth mechanisms associated with initiation, growth and delamination, pattern recognition applied to a time history appears less effective when compared to statistical methods discussed elsewhere in this thesis.



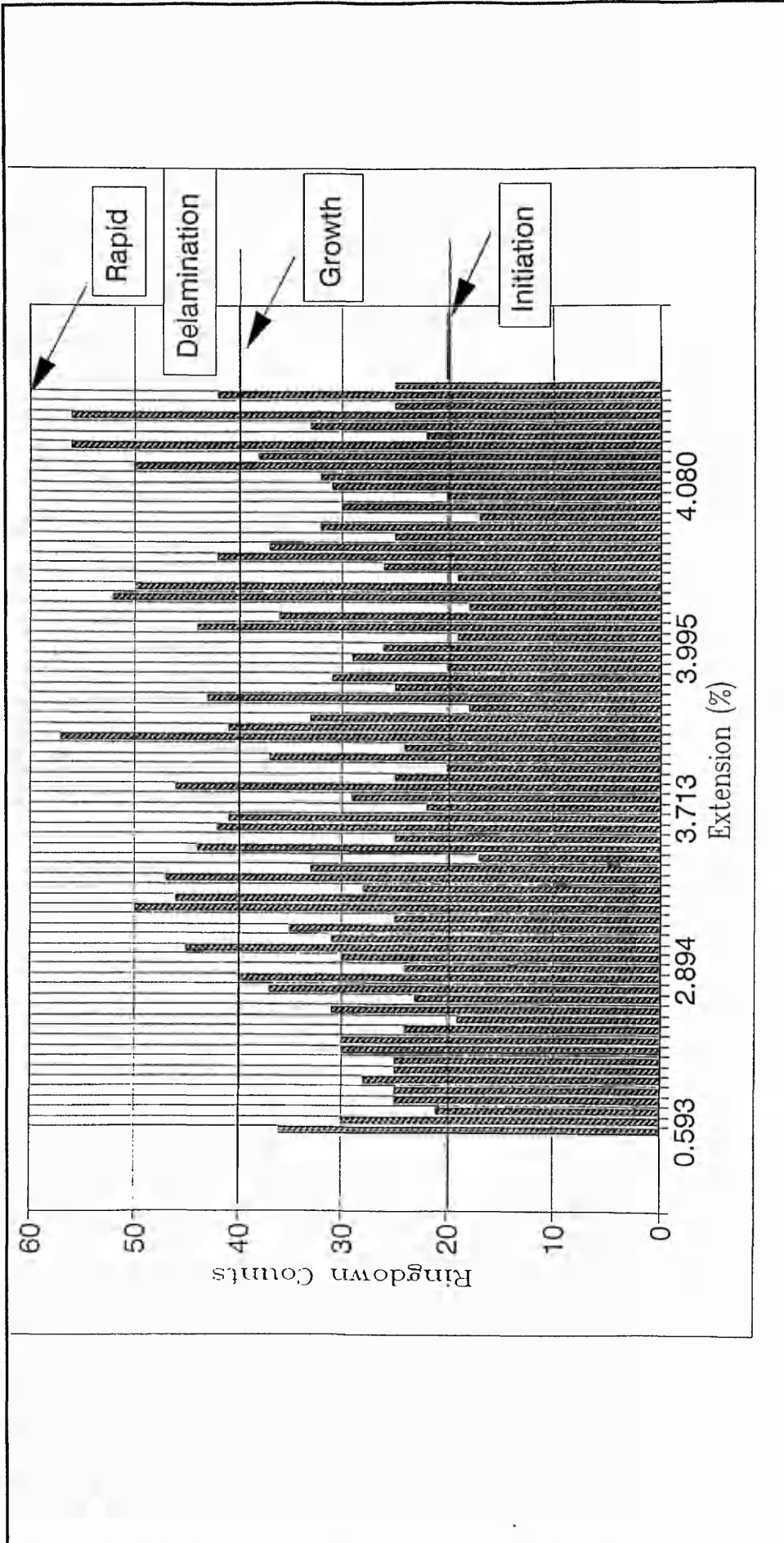
◆ Figure 4.8 a: AE amplitude versus specimen extension for Cured transverse E-glass fibre bundle composites.



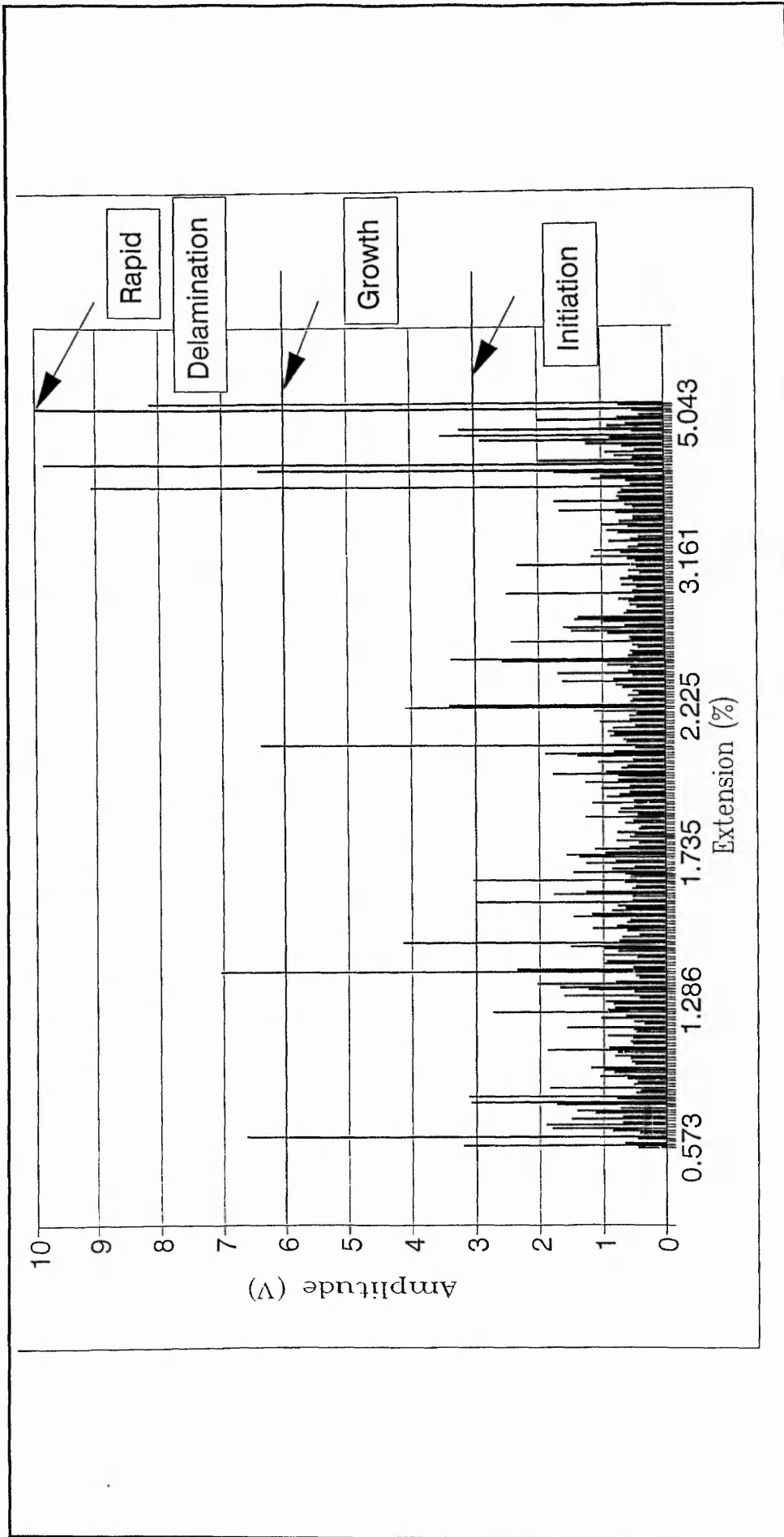
♦ **Figure 4.8 b:** AE ringdown counts versus specimen extension for Cured transverse E-glass fibre bundle composites



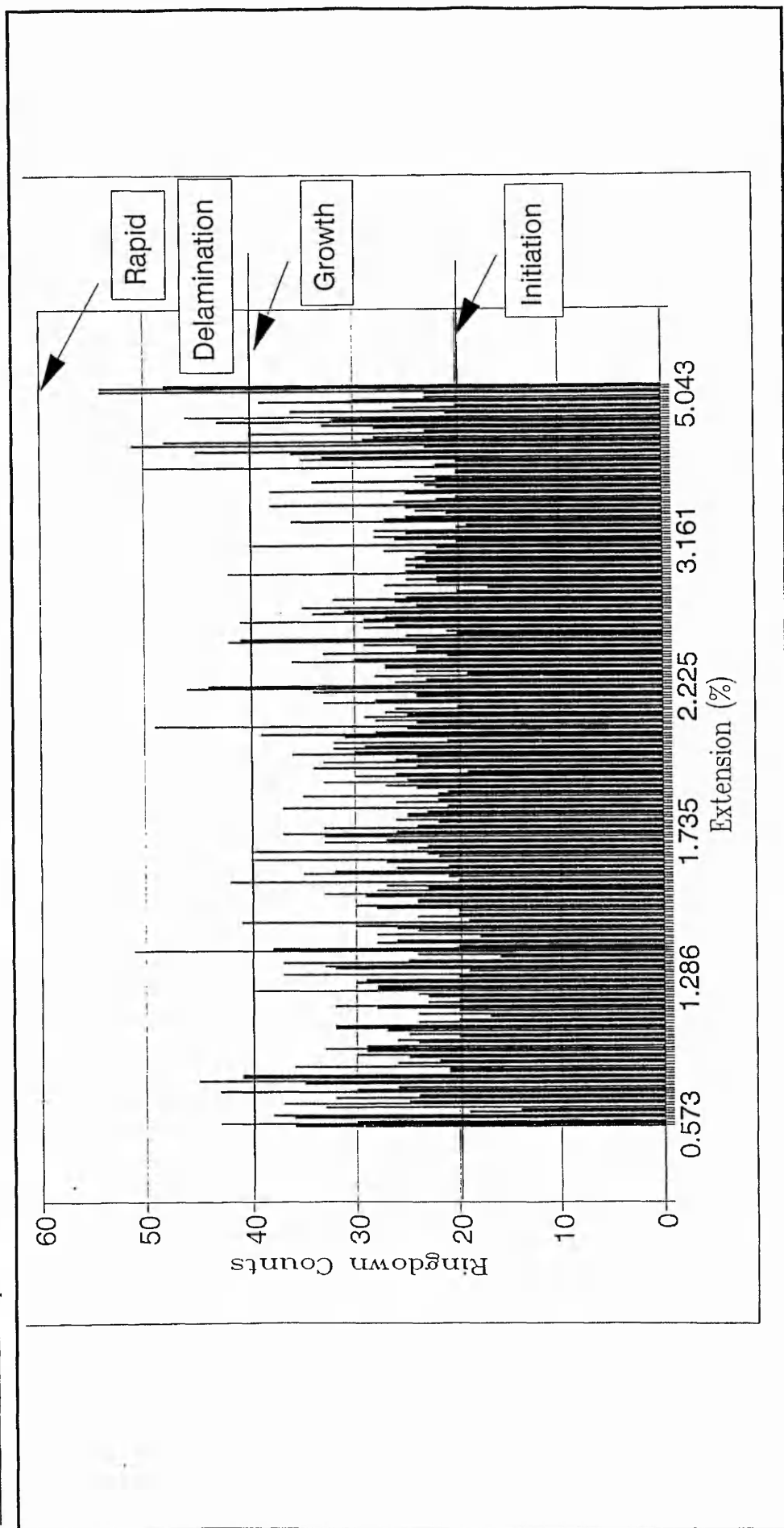
♦ Figure 4.9 a: AE amplitude versus specimen extension for Cured transverse E-glass fibre bundle composites.



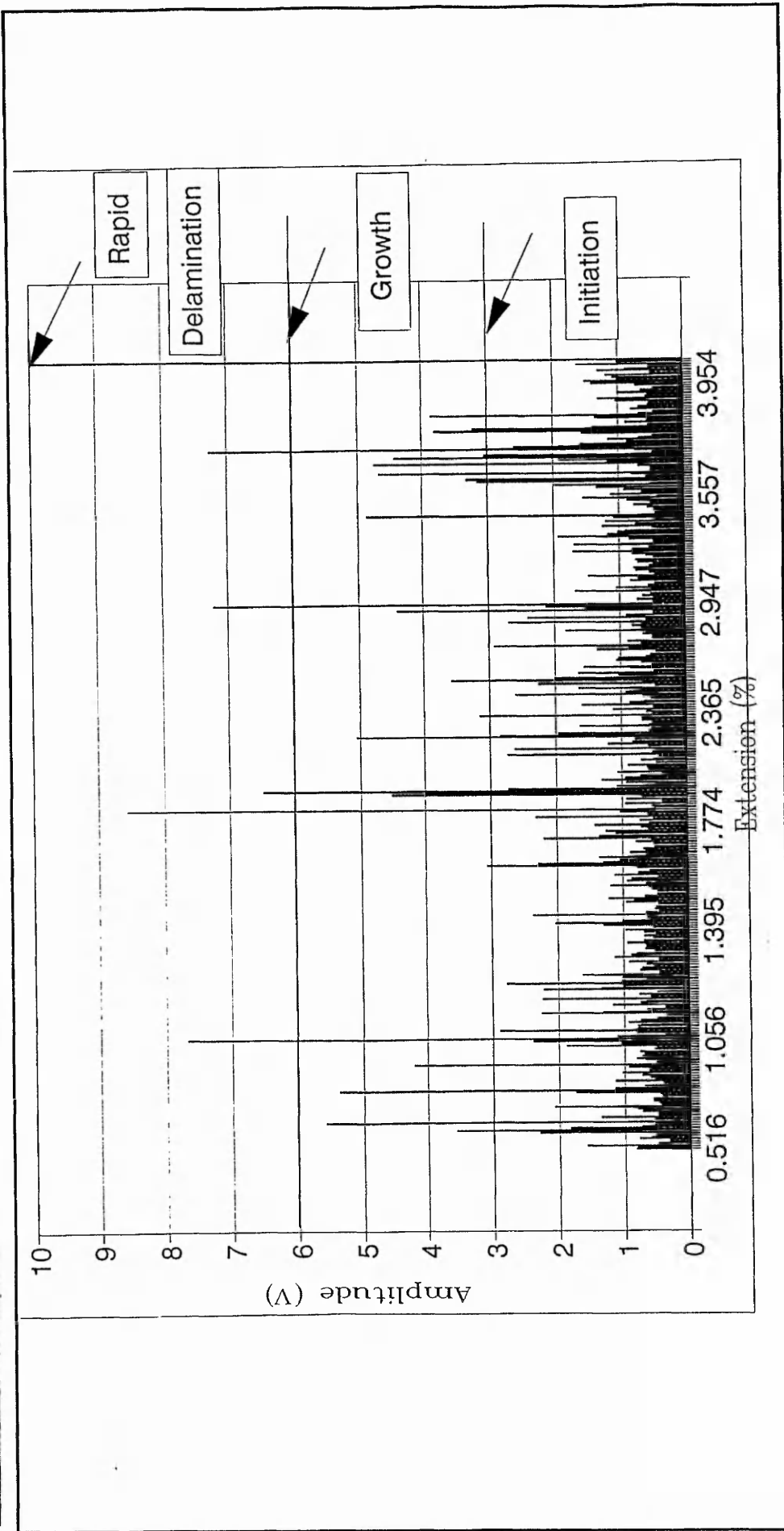
♦ **Figure 4.9 b:** AE ringdown counts versus specimen extension for Cured transverse E-glass fibre bundle composites.



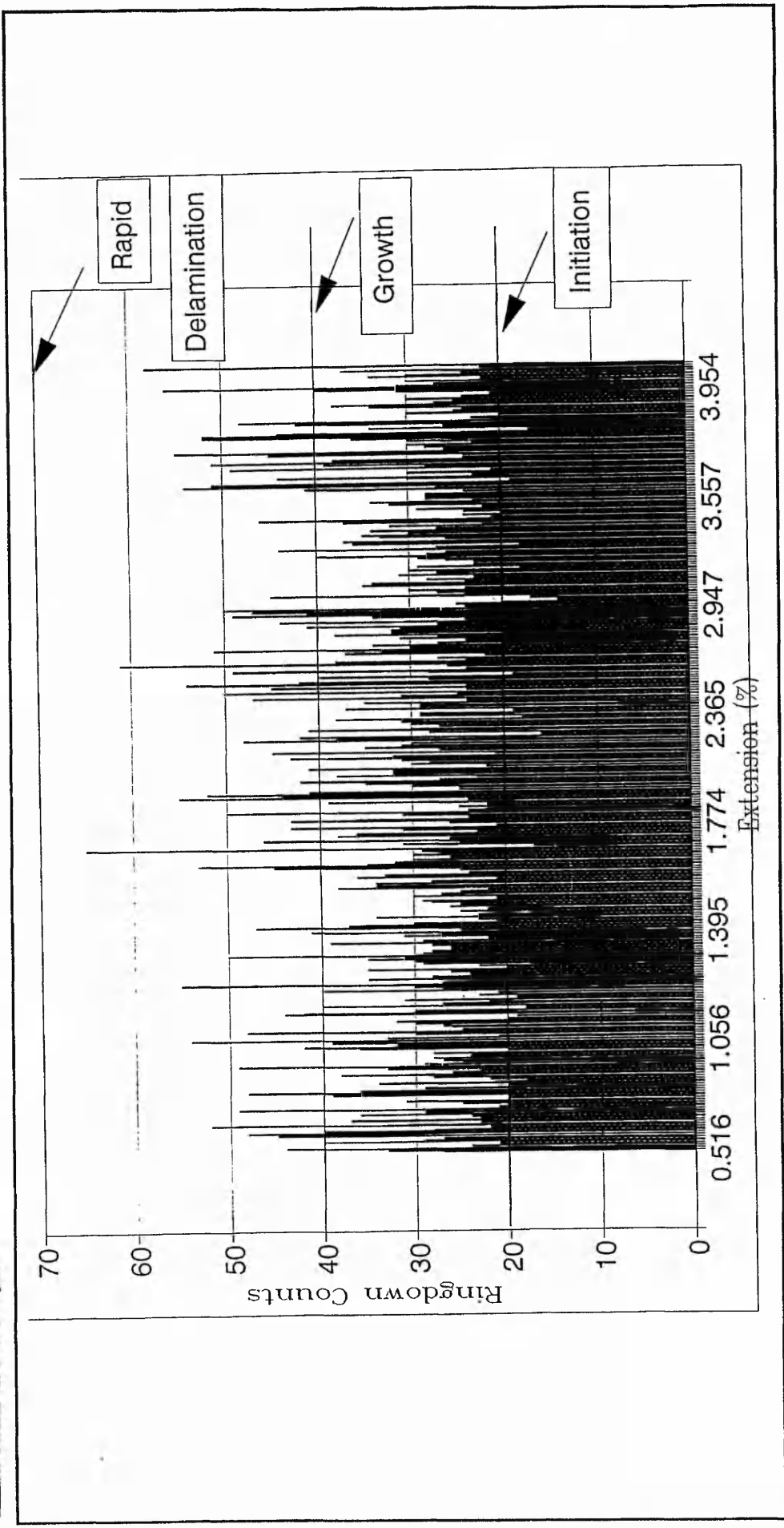
♦ **Figure 4.10 a:** AE amplitude versus specimen extension for Post-Cured transverse E-glass fibre bundle composites.



♦ **Figure 4.10 b.** AE ringdown counts versus specimen extension for Post-Cured transverse E-glass fibre bundle composites.



◆ **Figure 4.11 a:** AE amplitude versus specimen extension for Post-Cured transverse E-glass fibre bundle composites.



♦ **Figure 4.11 b.** AE ringdown counts versus specimen extension for Post-Cured transverse E-glass fibre bundle composites.

4.6 CONCLUSIONS FOR TESTING TRANSVERSE COMPOSITE MATERIALS

Chapter 4 has considered the characterisation of E-glass transverse bundle reinforced composite fracture mechanisms using statistical and pattern recognition techniques in order to analyse acoustic emission (AE) data derived from tensile testing. Samples were subjected to different treatments such as curing at room temperature, post-curing for 2-4 hours inside an oven and ultrasound treatment for 15 minutes in distilled water.

Weibull statistics were applied, to the AE data derived from the ringdown counts and amplitude distributions. Values for shape parameter 'm' and scale parameters 'RDC₀' and 'AMP₀' were obtained. The corresponding results for post-cured samples were 'm-AMP' = 0.75, 'm-RDC' = 1.68 and 'm-AMP' = 0.56 and 'm-RDC' = 1.28 for cured samples, giving a clear indication of the narrower amplitude and ringdown count distributions relative to the number of events, for the post-cured materials. This data suggests that for the post-cured condition a more uniform distribution of similar defects was achieved. The overall properties and resin/fibre adhesion characteristics of the post-cured samples were considerably improved. Using the 'm' and 'RDC₀' values, it was possible to predict/fit the Weibull equation to experimentation AE data distributions.

The severity of the events caused by the material displacements which are detected and converted into fluctuating voltage signals was also examined. The initiation of damage and the lack of integrity introduced in the fibre-matrix interface is considered to describe a severe event, which affects the overall performance of the composite material. By monitoring the acoustic emission events and especially the values from the amplitude and ringdown count data in relation to the stress-strain response, it is possible to estimate the degree of severity for both cured and post-cured types of samples. The number of the severe events in the case of post-curing is higher and start at a earlier extension rate. In order to give a clear view of the crack propagation microscopic examination was undertaken and demonstrated the existence of transverse cracks between the fibres.

The use of acoustic emission during composite testing developed in this work provides a quick, convenient and apparently reliable means of determining the evolution of damage in transverse glass and Kevlar fibre composites. The Weibull statistical methods proved effective in characterising material changes. It is probable that the technique considered here, could be used for tests on a variety of other fibre composite systems.

CHAPTER 5

APPLICATION OF AE TO THE TESTING OF FIBRE BUNDLES.

5.1 Introduction

When damage or failure occurs during loading of a material, only a part of the strain energy is recoverable. The remainder energy will be liberated, in part, in the form of a stress wave which travels through the material and can be detected at the surface of the material by suitable sensitive transducers. These acoustic or stress-wave emissions are a potentially powerful source of information about the internal processes of fracture in **E-glass and carbon fibre bundles**. It has been shown [25, 27] that monitoring such AE bursts ("events") provides a reliable means of identifying fibre fractures as they occur in a large bundle under tension. Thus AE provides the possibility of detecting fibre fracture and monitors the time of failure that otherwise would be difficult to achieve by optical methods, load drop or strain measurements.

Bundle testing of perfectly elastic fibres using a load/strain curve has recently been demonstrated [31, 54]. The AE technique has been employed in the study of a fibre system and has been able to determine the fracture stress of the individual bundles under tension. In this work the AE technique has been used, as described in chapters 3 and 4 to monitor transverse fibre bundle composite materials during tensile testing, providing information on composite fracture mechanisms. In the case of fibre bundles it is possible to relate AE signal parameters to the instantaneous fracture stress and hence analyse fibre systems by means of statistical techniques. The main focus of the work was the examination of AE ringdown counts and the relationship which exists between the number of counts and the number of physical events during damage propagation. It has been shown [28] that the statistical variation of the tensile properties of fibres can be obtained during fibre bundle testing which is preferred to single fibre testing, since it minimises the amount of handling and damage. However, using this method, statistical data on fibre strength would be expected to show some differences due to interfibre interactions and friction during fibre bundle testing [27, 29, 53].

The testing of complete fibre bundles has gained increased support in recent years, since the statistical data concerning fibre strength is much more conveniently obtained using complete fibre bundles and the data is more relevant to the situation which might prevail in a fibre bundle. When detecting AE from fibre bundle fracture, each fibre fracture has an associated AE. The main associated parameter chosen was the ringdown counts per AE event, which is emitted during tensile testing of glass and Carbon fibre bundles. From the AE data it was possible to obtain, the ringdown count distribution relative to the number of events. The corresponding distributions were examined and described using statistical approaches which aim to fit the distribution of the AE data to the equation for the statistical distribution. Therefore, by predicting this distribution it is possible to describe the nature of the failure processes within the fibre bundle. This can be approached by using a two parameter Weibull distribution function, [52, 61] since this function generally provides an adequate description of the failure processes. In this work, two additional statistical approaches have been considered:

- ◆ a) a two parameter log-normal distribution function [59] and
- ◆ b) a generalised Lambda distribution.

The latter method is a completely new approach proposed by W. Gilchrist [60]. The work in this thesis represents an empirical test of this new methodology.

5.2 Physical Dimensions and Defects in Fibres

Flaws usually found in fibres can be classified either as surface flaws or internal structural defects. Surface flaws are produced by abrasion, indentation or impact with harder materials, during manufacture or later during the handling stage. Although these flaws are small in size, they can act as severe stress concentration points. The fracture strength of any given fibre is limited by the physical dimensions and characteristics of the most severe defect present [62]. It is difficult to suppress the defects, despite major advances in both the manufacturing process and inspection techniques. This is mainly because of the inability of existing instruments to reveal submicron flaw sizes, and the unknown origin of defects, i.e. whether they occur during the manufacturing process or later during handling.

Griffith [63], used glass as a convenient model in his classical work to demonstrate that the “energy balance” criterion provided a satisfactory condition for the extension of a crack. He also showed that the strengths of materials, free from flaws were very much greater than those usually found in practice with an increase of the strength levels of up to 200%.

Additionally, a number of authors recognised the important fact that the fracture load, for a bundle is never greater than the product of the bundle area and the mean fibre strength. A notable attempt was made by Weibull [61] to establish a statistical theory for the strength of materials exhibiting a wide scatter in their fracture strengths. Daniel [53] investigated the relation between the strength of a bundle and its constituent fibres and developed in great detail the properties of the probability distribution of bundle strength. The assumption in Daniel’s model is that the fibre failure stress is independent of the rate of bundle loading and that the load, after failure of some fibres, is equally distributed among the surviving ones. In recent years, this basic assumption of “equal load sharing” has been analysed to allow for such features as interfibre frictional forces [32]. Coleman [64] considered the time dependence of mechanical breakdown in a fibre bundle by using the theory of “breaking kinetics”. He showed that classical theories, can be derived from the kinetic theory as special cases.

5.2.2 Fibre Diameter

Although glass and carbon fibres in a typical production run have similar diameters, the maximum variation from the mean being only about $\pm 10\%$, their strength may differ greatly. The most common fibre cross section produced is circular. Other shapes such as square, rectangular, I-beam and cross fibres are being considered for production as they permit closer packing in a composite and thus higher load bearing capability.

Thomas [65], while investigating the effect of surface on the glass fibre strength, found that the mean breaking stress of fibre bundles increases with decrease in the diameter of individual fibres. He postulated that thick fibres are more susceptible to surface damage and also include more internal flaws. However this investigation was not complete, since Thomas only used a range of diameters of 8 to 50 microns. Indeed it was later found [66] that the strength of a fibre increases with an increase in the diameter up to 7 microns and then decreases as the diameter increases.

5.2.3 Fracture Energy Models

For a fibre of length L of cross-sectional area A and elastic modulus E , fracturing at stress σ , the elastic energy released in fracture is [28]:

$$U_f = \frac{\sigma^2 \cdot A \cdot L}{2 \cdot E} \quad (5.1)$$

For each fibre fracture, as the energy is released, a similar fraction should appear as stress wave energy, after the energy is used to create new fracture surfaces. This AE energy will be propagated in similar acoustic modes or a mixture of modes, and will be similarly attenuated in transit to the measuring transducer. The electrical energy output by the AE transducer U_{AE} is assumed to be directly proportional to U_f .

5.3 Experimental Testing of Glass and Carbon Fibre Bundles.

5.3.1 Preparation of Materials.

As previously noted (see section 5.1), the characteristics of E-glass and carbon fibre bundles will be examined by the means of acoustic emission during tensile testing of a fibre bundle. The main characteristics for the two types of fibres are firstly that carbon fibres are far superior to E-glass fibres in terms of specific modulus. In the absence of air and other oxidising atmospheres carbon fibres possess exceptionally good high temperature properties while the properties of E-glass are likely to be reversible with temperature. Both types of fibres fracture in a brittle manner without any yield or flow.

Individually, and by comparing carbon to glass fibres, some of the main characteristics for E-glass fibres are the extremely high breaking strength, and elastic failure strain and the low fracture energy. Carbon fibres are popular materials due to their high strength and high specific Young's modulus as can be seen from a typical example which is described in table 5.1 [48]. The modulus of carbon fibres depends on the degree of perfection of alignment which varies considerably with the manufacturing process and conditions. These imperfections, together with surface and internal defects, act as stress raisers and points of weakness leading to a reduction in strength properties. Other sources of weaknesses, which are often associated with the manufacturing process, include pits and microcrystallites. Consequently, an important aspect of the statistical variability of the properties of fibre bundles is variability of the properties on individual fibres.

- ◆ **Table 5.1:** Properties of carbon and glass fibres at 20 °C. The information is obtained from manufacturer's data sheets.

Properties	Carbon PAN-based Type I	E glass
Specific Young's Modulus (Modulus/density)	200 ($\text{GNm}^{-2}/10^3\text{kgm}^{-3}$)	30 ($\text{GNm}^{-2}/10^3\text{kgm}^{-3}$)
Tensile Strength	2.2 (GNm^{-2})	2.5 (GNm^{-2})

Both E glass and carbon fibres used in this work were supplied by Les Fils d'A Chomarat & Cie (France). The first type of E glass fibre bundle is the 19S3 with 0.36 mm thickness. The second type is the 200T with 0.25 mm thickness. The carbon fibres tested are the 200C type. The fibre bundles were immersed into a silicone oil bath prior to testing, in order to reduce the interfibre friction during testing (which would decrease the strength of the bundle). As has been reported by Hill and Okoroafor, [27], dry bundles have been shown to induce some degree of co-operative failure. The effect of lubrication is to minimise this interfibre friction, which would come into play as fibres are drawn together by the applied load. The presence of friction induces failure due to frictional load transfers from fractured to unfractured adjacement fibres.

The ends of a bundle specimen to be tested were cemented to aluminium plates using the RS 159-3957 high strength epoxy adhesive taking care that the fibres were parallel in order to eliminate early buckling which would produce a reduction in their strength and performance. Figure 5.1 shows schematically the fibres aligned parallel to each other and cemented to aluminium plates. Work by Attou [51], considered which end plate material best transmits the AE signal to the sensor. The energy released during fibre fracture, was measuring using mild steel, brass and aluminium end plates. Aluminium was found to be the best when a wave travels from material "A" (the fibres) to material "B" (the end plates), some of the energy is reflected because of the acoustic impedance mismatch at the interface as can be seen in table 5.2. The energy reflected $[E_r]$ is:

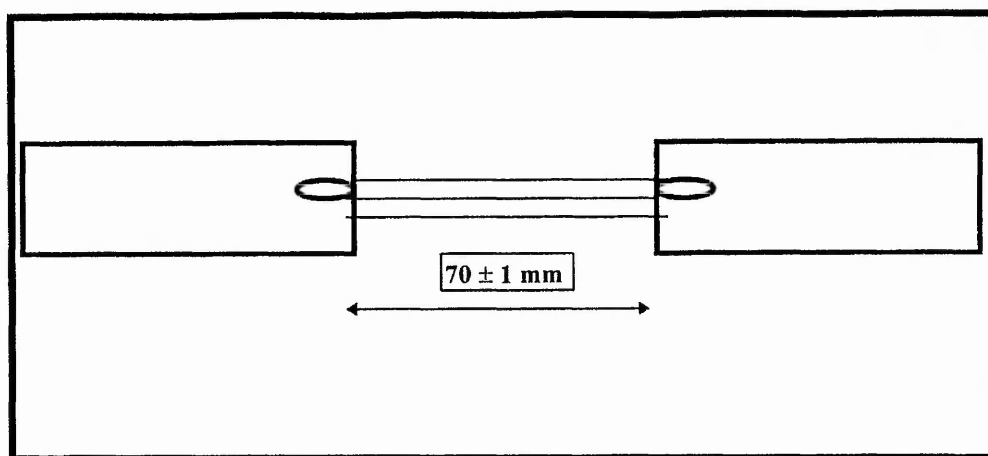
$$E_r = [(Z_1 - Z_2) / (Z_1 + Z_2)]^2$$

Where Z_1, Z_2 are the specific acoustic impedance of the materials.

- ◆ **Table 5.2:** Comparison of the materials suitable for the transmission of the AE signals resulting from fibre break.

MATERIAL	Specific Acoustic Impedance	% ENERGY REFLECTED
AL	17.3	1.0
BRASS	37	21.0
MILD STEEL	47.6	30.0
E - GLASS	13.7	--

The free length of the bundles to be tested were 110 ± 1 mm when cut from the "cake". The testing procedure was in each case identical. For variable fibre bundle length, the values of failure stress would be inversely proportional to the fibre length. The connection between the strength of a bundle and its flaw distribution, has been observed for a fixed length "l" which broke under normally distributed load. Different bundles of length "L" (greater than "l") would break under loads whose strength distribution is biased towards lower loads indicating an increase in the number of flaws in the longer sampled bundles.



◆ **Figure 5.1:** Schematic representation of glass and carbon fibre bundles aligned parallel to each other and cemented to aluminium plates.

5.3.2 Fibre Bundle Test Conditions

Fibre bundle tensile tests to failure were performed once more using a LLOYD-6000R testing machine, at a constant crosshead movement rate of 0.1%/min ensuring a constant strain rate. A commercial Acoustic Emission (AE) sensor - AET type AC 175L resonant frequency 175 kHz supplied by Acoustic Emission Technology Corporation - was utilised. Since the duration of the AE can be enhanced by stress waves reflected within the specimen / support system, it was found helpful if the AE sensor was mounted in the bottom testing machine grip using a spring clamp to minimise this effect. Silicone grease was used as a AE couplant. The AE signals from the transducer, in the form of decaying sine waves (as shown in figure 2.1 in section 2.2), of given amplitude, frequency and decay constant, were preamplified by a 40 dB (AECL 2100/PA,) [AECL Ltd "Manual for the use of the AECL AE system"]. Then the signals were processed using an AECL 2100M acoustic emission system. The sudden release of strain energy is converted into fluctuating small voltage signals which are amplified and then processed to be stored electronically on a computer. The threshold level applied was 0.2 Volts in order to try to eliminate the effect of any electronic and inherent background noise arising from the grips or movement of the crosshead of the tensile machine. The settings of the system threshold did not give exact correspondence between the emitted number of events and the number of fractured fibres. Although the data prove to have uniform distributions with well defined limits of 55-100 ringdown counts, occasionally the elimination of some weak fibre fracture data was necessary.

For the ringdown counts (i.e. the number of oscillations greater than the pre-set threshold level) and amplitude, a 400 μ sec window (400 data points) had been defined together with a 0.2 μ sec dead time. This means that if at the end the signal does not pass through the threshold for 0.2 μ sec then it is taken to be the end of the event. The system was configured so to calculate the value for ringdown counts of each acoustic emission event.

5.4. Fibre Bundle Testing

5.4.1 Aim of the Fibre Bundle Testing

With the use of tensile tests on lubricated glass and carbon fibre bundles an attempt has been made to monitor the fibre failure process. The aim of this work is to identify individual fibre breaks, to the last fibre in the bundle, without undertaking specific calibration to eliminate the frictional noise contribution to AE. Using AE together with the stress-strain responses it is possible to monitor the exact time and load of fibre breaks, since the breaking of each individual fibre is accompanied an associated AE signal with corresponding ringdown count data.

5.4.2 Bundle Fracture Processes

Experiments were carried out testing to failure fibre bundles of 70 ± 1 mm length for E-glass and carbon fibres. When a bundle of fibres is loaded in tension, the fibres break one by one starting with the weakest. Since the broken fibres do not carry tensile load the effective cross-sectional area of the bundle gradually decreases with the increasing load. The redistribution of stress leads to additional stresses on neighbouring fibres. As the load increases, this sequential fibre fracture continuous, leading to bundle failure.

The scattering of the fibre strength is very important in defining the maximum stress the bundle can sustain. As the fibres in the bundle break and its cross-sectional area reduces this results in multiple fibre breaks as the load increases. This phenomenon appears in the ringdown counts versus strain graphs where higher values of ringdown count are obtained as strain increases.

It is also noticeable that the fibres break when their stress reaches the fracture stress of the severest defect and the fracture stress of the severest defect varies according to the probability governing the population and the severity of the defects. It is assumed that the defects are distributed along the fibre length according to a spatial Poisson process which stated that:

- ◆ The defects are located at certain positions along the fibre length with equal probability.
- ◆ The location of the defect is independent of locations of any other defects.
- ◆ The severity of the defect is independent of its location.

For each fibre bundle fracture, as the elastic energy is released, a similar acoustic fraction of this energy should appear, with similar AE parameters. It should be pointed out that the resulting AE parameters show good agreement within each type of fibre bundles under tensile test.

5.5 Experimental Results and Discussion for Fibre Bundle Testing

A primary objective was to test glass fibre bundles, extend the testing to carbon fibres, assess the AE methodology when using full AE waveform capture and find out whether the fracture stress of a fibre or group of fibres could be correlated with some characteristics of the associated AE signals. A central difficulty here is that AE signals from similar source phenomena, such as fibre fracture at a given stress or stress intensity, are commonly found to have a wide scatter of ringdown counts, amplitude and duration. Even if the AE stress wave has energy proportional to the energy released at source there are, in general, losses such as plastic deformation, heating effects, creation of new surfaces, attenuation, and reflection at interfaces and boundaries. These effects have a strong presence in the case of dry bundles but they also take place in the case of the lubricated fibre bundles.

Typical mechanical and AE data for the two types of E-glass and carbon fibre bundles are presented in figures 5.2 a, b, c, 5.3 a, b, c and 5.4 a, b, c together with tables 5.3 a and 5.3 b which provide a complete set of data value and the average data values respectively. These figures show the stress strain response, and superimposed AE data. AE data was obtained by post-processing each AE event to obtain, in this case ringdown counts (per event) in order to relate the relative acoustic energy released by the fracture events. The test conditions mean that event saturation is represented by a ringdown count value of approximately 100. As has been reported [28] in the case of ringdown counts, it is possible, due to the occurrence and overlap of the various fibre failure modes as for example, singlets, doublets, triplets, at high strains that significant overlap of AE could be occurring. This will result in lower values of the ringdown counts that might be expected and explain the fact that this parameter saturates.

Each AE event appears as a point on the graph, with the points joined by straight lines, in order of increasing time (extension). It should finally be mentioned that these figures often show flat portion of the stress-strain curve associated with the aluminium tab slippage in the grips. It is important that no significant portion of AE events were recorded in this region and the flat portion has been subtracted from the final fracture strain value.

The maximum average failure strain, the maximum average failure stress, together with the corresponding strain and the number of emitted events during tensile testing are all presented in table 5.3 a together with figures 5.2 and 5.3 which correspond to the 19S3 and 200T glass fibre bundles. From table 5.3 b, it can be seen that the 200T E-glass fibres can sustain much higher levels of stress (1386.9 MPa) than the 19S3 type (833.2 MPa). However, for both types of glass fibre bundles the final strain values are similar with averages of 1.15 % and 1.02 % correspondingly (table 5.3 b).

The differences in data shown in table 5.3a are attributed to either the test procedure and/or the state of the fibre system prior to testing. Fibre bundle failure starts earlier on average for the 19S3 type (approximately 0.3% strain) compared with the 200T type (0.5% strain) as indicated by the AE record. The strain values at maximum load (fibre failure strain) occur in the same order (19S3 glass : 0.735% - 200T glass : 1.01%) as can be seen from table 5.3 b, the corresponding figures perhaps indicating a relationship between the commencement of fibre bundle failure and the bundle failure strain.

Tables 5.3 a and 5.3 b, describe the experimental data for 200C type carbon fibres. The carbon bundle shown similar levels of maximum stress as the 200 T type glass fibres with an average stress of 1275 MPa, strain of 0.827 % and maximum strain 1.02 % (strain on average). Carbon fibre data is shown in figure 5.4 a, b, c where the stress-strain response is superimposed with AE data such as ringdown counts.

By comparing figures 5.2 and 5.3 and using tables 5.3 a and 5.3 b the difference in the number of events between the 19S3-glass fibres and the 200T glass fibres, can be seen where the number of events are approximately 2-3 times more in the case of 19S3 E-glass fibres. The number of events for the 200C carbon fibres, fall into two different categories 600 and 1100. It is also important to notice the AE data signal pattern. Through the corresponding figures, it is possible to see that all three bundles can be characterised as having 'quiet then noisy' behaviour, with large fluctuations of the ringdown count values at low values of the stress-strain curve and higher ringdown count values as the stress-strain levels increased. This rise in ringdown counts also gives an associated rise in such AE parameters as events amplitude and event duration (assuming no event overlap occurs). In

general, the average ringdown counts for the fibre bundle failure events rises to a constant value, as applied stress increases, as can be seen from figures 5.4 a, b and c.

As has been mentioned earlier the number of events is affected by the selected threshold level. If the set value for the threshold level is too low and the duration window is too large, 'noise' events will be detected and can mask the 'good' events. If it is too high, some good events will be missed-out. Note also, that, as the AE signal duration is enhanced by stress-wave reflection within the specimen/support system [67], the attachment of the AE sensor to the aluminium end plate mounted in the immobile bottom grip of the tensile machine, was found to dampen the AE signals more rapidly. Also the AE energy released at source can be affected by general losses within the bundle system and reflection at interfaces and boundaries. Keeping in mind the above arguments and although it is difficult to give a precise correlation between the number of fibres in a bundle and the number of AE emitted during tensile testing, it could be said that the 19S3 glass bundle has approximately 650 fibres, while the 200T bundle has 250 and the 200C bundle has 800 fibres.

It is also important to point out that single fibre fractures are dominant at low stresses, while at high stresses multiple fibre fractures become predominant [28]. It is therefore possible that around the maximum stress position and beyond, overlap of the various fibre modes (singlets, doublets, triplets) of AE waveforms begins to occur. This will result in lower values of ringdown counts than might be expected as the stress on individual fibres continuous to rise beyond peak nominal stress.

Large values of ringdown counts in the AE signal, indicate that there is a large and sudden amount of stored energy released from the fibre bundle system. Also, there is a major difference between this experimental approach to testing fibres and the quasi-static test procedure undertaken by Cowking et al [30]. In the latter method, it is possible that load is equally shared in any configuration of failed and surviving fibres, hence minimising multiplet fibre failures. These factors, and possible energy loss factors, such as creation of the new fracture surfaces, acoustic reflection at interfaces and boundaries, signal attenuation in transit to the measuring transducer, and the rate at which the stored elastic energy is released in the failure process, play a significant in the value of ringdown counts. Thus, while the ringdown count values in general are expected to increase with rising fibre

failure stress and thus differentiate fibre failure stress, it could also exhibit large fluctuations. This is clear from the experimental data presented in the corresponding figures for glass and carbon fibre bundles.

It is noticeable the fact that as stress increases and then drops the remaining fibres can sustain the load. This indicates that there is not a catastrophic sudden failure of the bundle although individual fibres show sudden brittle fracture.

Finally in order to explain possible inconsistencies between the maximum stress-strain results for each of the fibre bundles, ICI and Owens Corning [51] have conducted an investigation on tensile strengths of fibre commercial rolls. They point out three significant variables such as:

- a) The effect of the chemical composition of the size on the strength of fibres.
- b) The strength variation in fibres taken from different positions within a roll (strength variation is believed to be due to different cooling rates between the surface layers and other layers within the roll).
- c) The differences in the strength between fibres taken from the turn around point and fibres taken from the centre of the cake. To make a fibre roll, a strand (bundle of fibres) is wound across the width of the roll, the edge is reached and the winding direction is changed to traverse back, continuing the winding up process. This traverse of the cake occurs at high speeds, thus inducing dramatic deceleration and acceleration in the strand at the edges of the roll. It is believed that as the winding angle changes at the edge of the roll, the fibres are curved over and thus susceptible to breaking because of their brittleness.

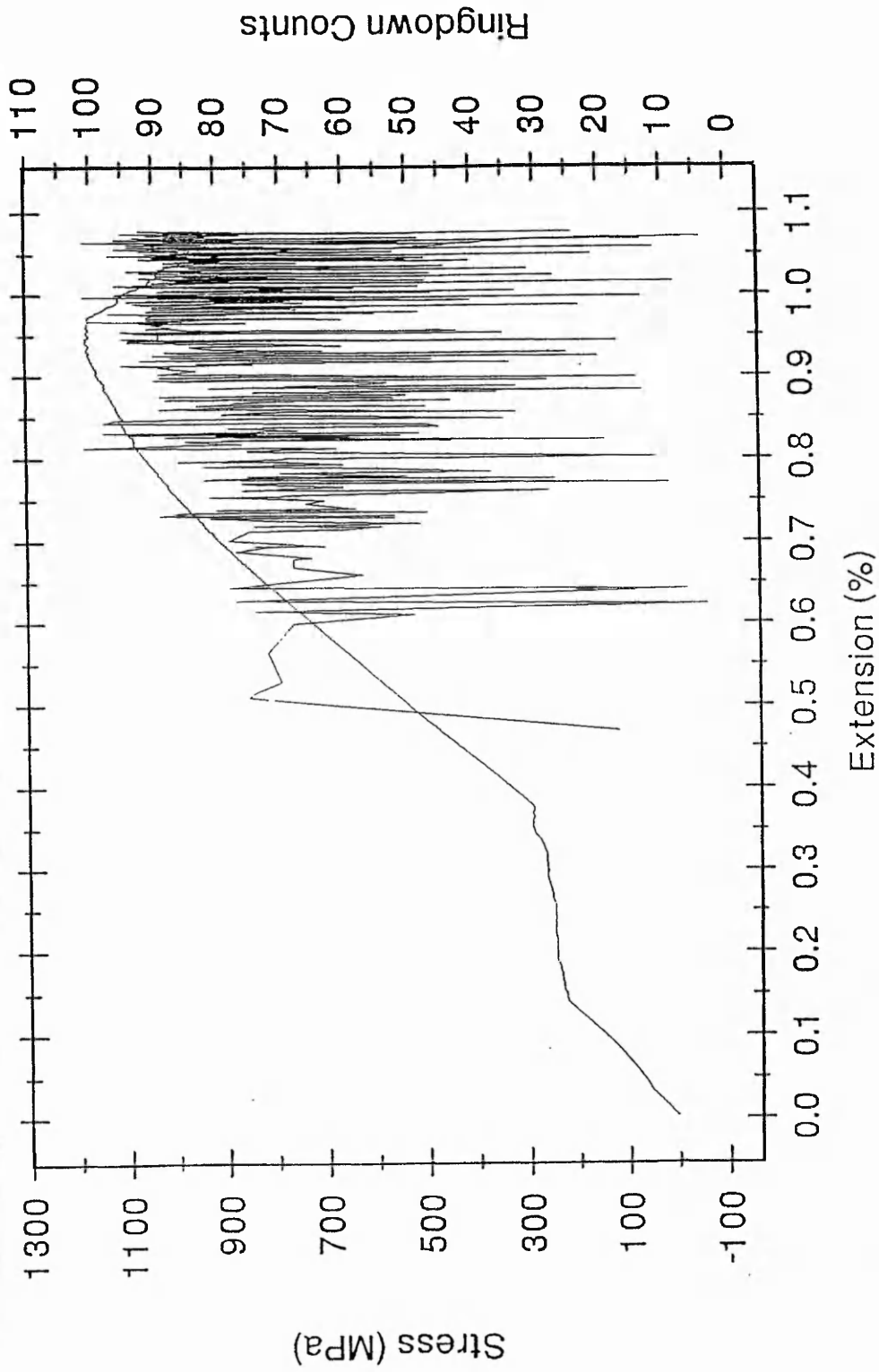
◆ **Table 5.3 a**

Tensile properties and acoustic emission events of: a) 19S3 glass fibres b) 200T glass fibres, and c) 200C carbon fibres.

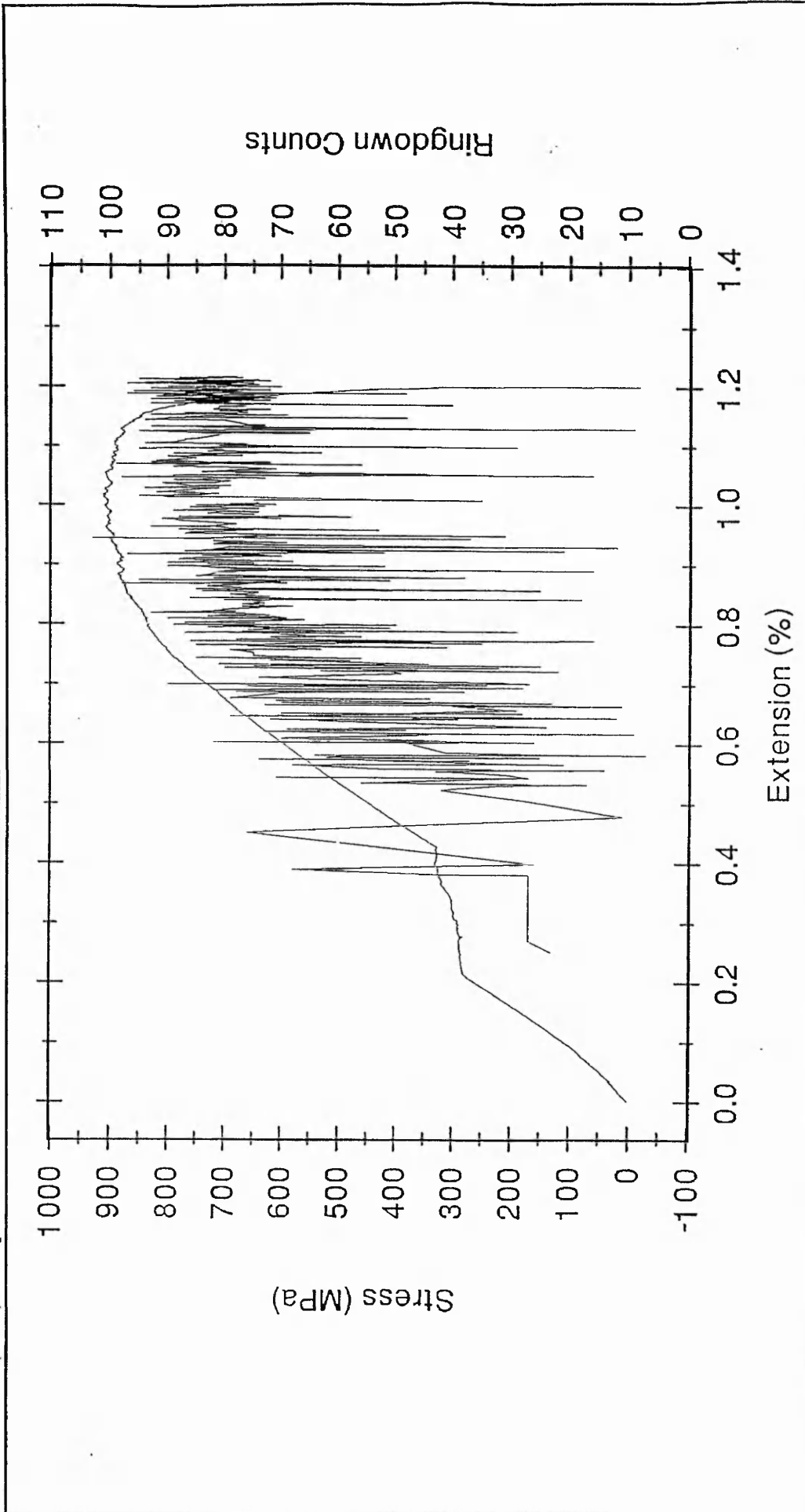
Specimen No.	Max Strain	Max Stress (Mpa) / Cor/ing Strain	No. of Events
19S3 - 1 glass	0.835	1184.2 / 0.713	580
19S3 - 2 glass	0.926	886.7 / 0.747	643
19S3 - 3 glass	0.9092	647.5 / 0.420	954
19S3 - 4 glass	0.996	911.7 / 0.812	614
19S3 - 5 glass	0.818	665.4 / 0.460	714
19S3 - 6 glass	1.418	751.5 / 1.007	861
19 S3 - 7 glass	1.112	785.3 / 0.984	527
200T - 1 glass	1.178	1306.5 / 0.983	293
200T - 2 glass	1.055	942.5 / 0.9257	217
200T - 3 glass	1.223	1545 / 0.997	346
200T - 4 glass	1.148	1602.2 / 1.082	204
200T - 5 glass	1.189	1538.6 / 1.063	233
200C - 1 carbon	0.898	1220.3 / 0.735	684
200C - 2 carbon	1.223	1301.3 / 0.883	546
200C - 3 carbon	0.964	1305.1 / 0.883	1032
200C - 4 carbon	0.996	1275.6 / 0.818	1250

- ◆ **Table 5.3 b:** Average values for maximum stress (MPa), strain (%) and number of emitted AE events during tensile testing for glass and carbon fibre bundles.

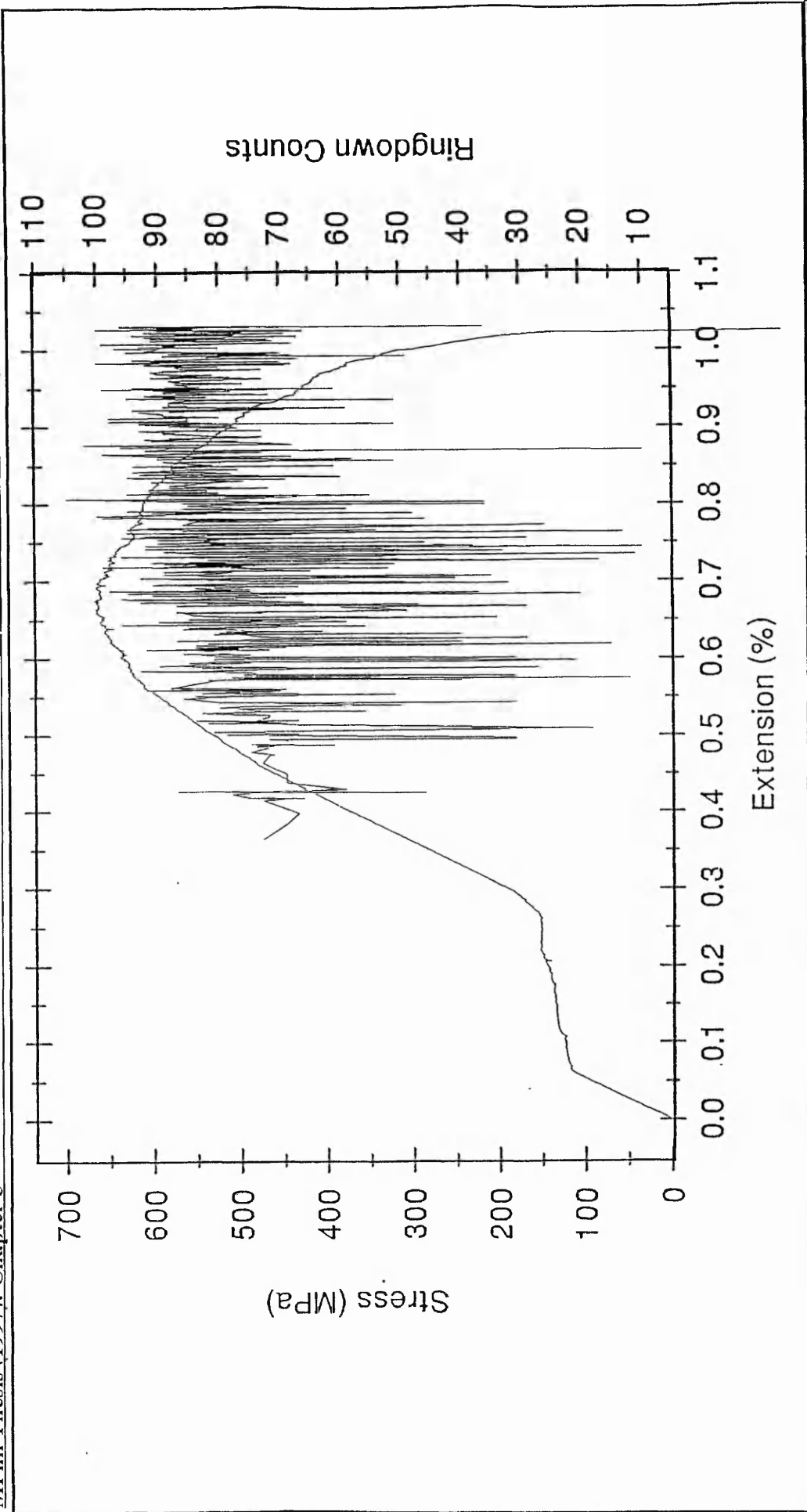
Sample No	Max Strain (%)	Max Stress(MPa)	No of Events
		Cor/ing Strain (%)	
19S3-glass	1.002	833.2 / 0.735	699
200T-glass	1.158	1386.9 / 1.01	259
200C-carbon	1.020	1275.5 / 0.827	870



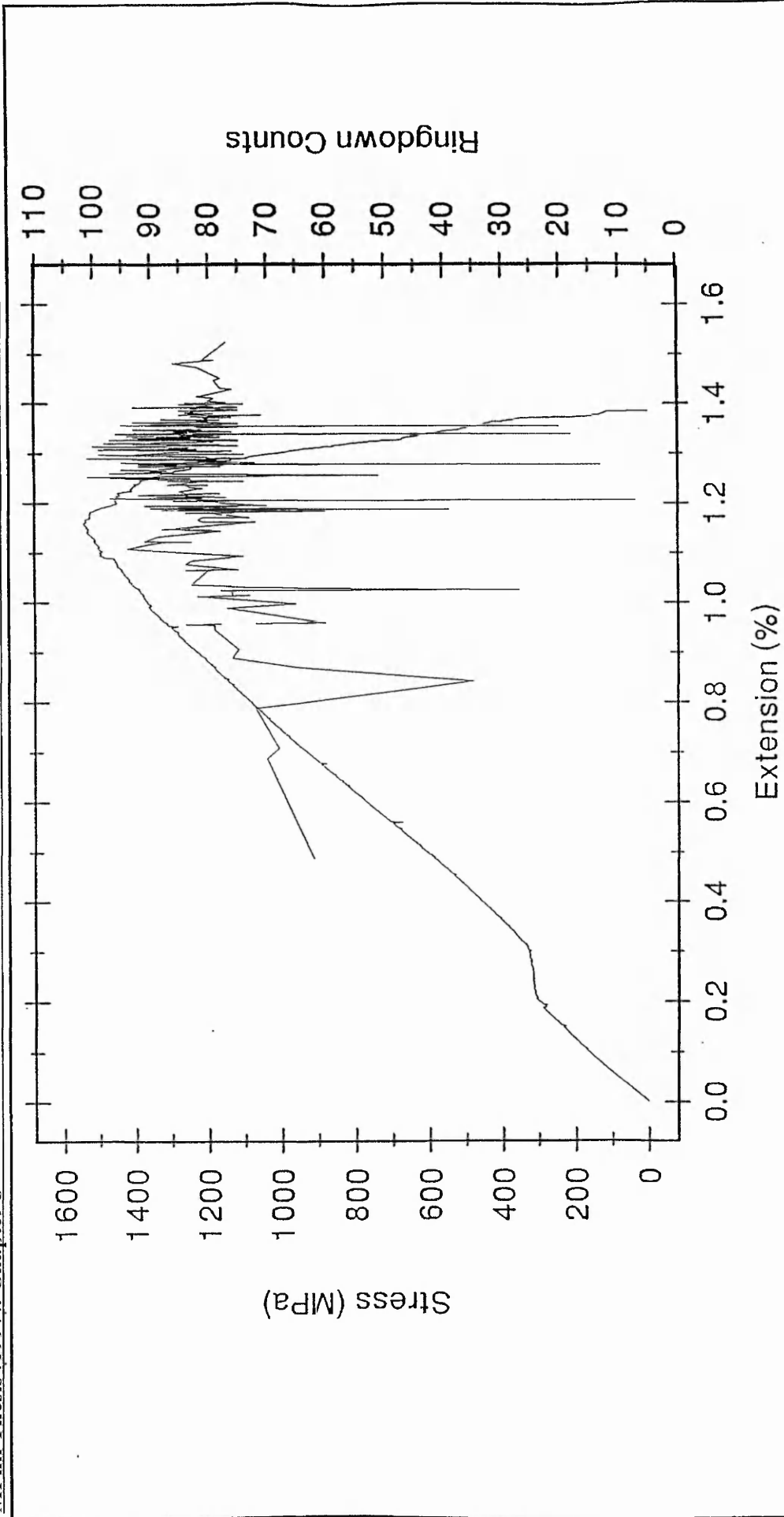
◆ **Figure 5.2 a:** Stress-Strain and AE ringdown counts per event data for 19S3-E-glass fibre bundle.



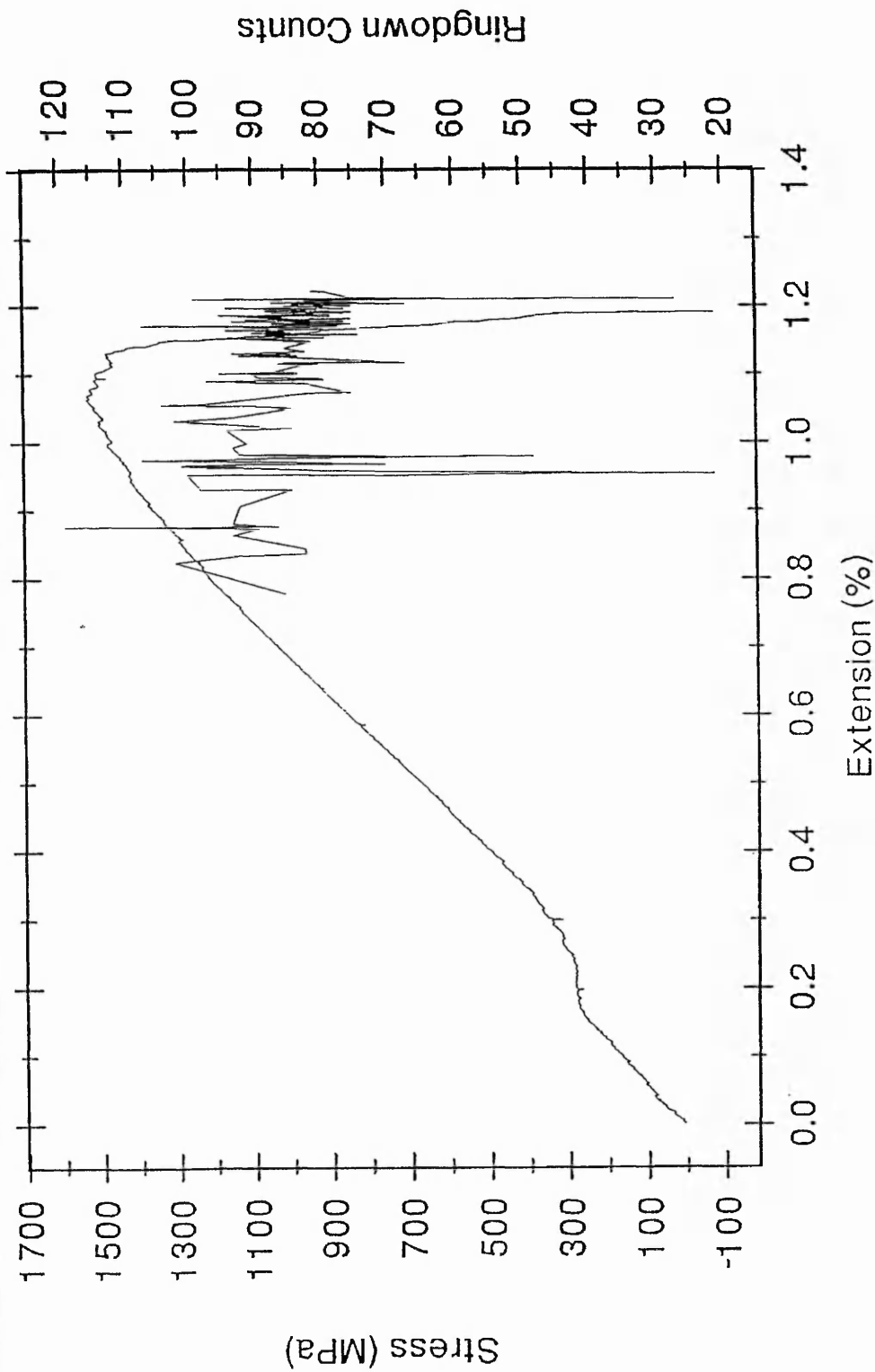
♦ **Figure 5.2.b:** Stress-Strain and AE ringdown counts per event data for 19S3-E-glass fibre bundle.



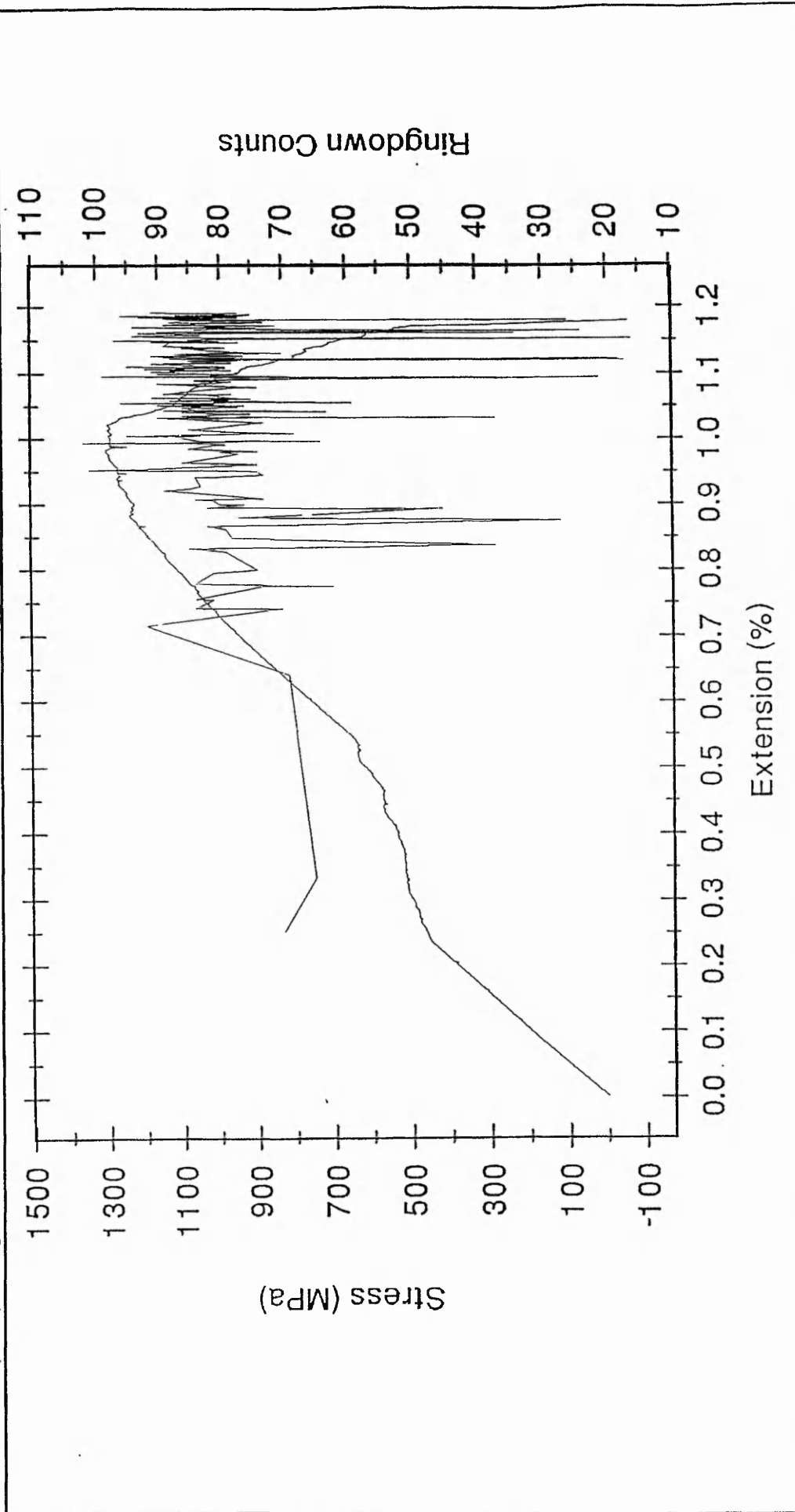
♦ Figure 5.2 c: Stress-Strain and AE ringdown counts per event data for 19S3-E-glass fibre bundle.



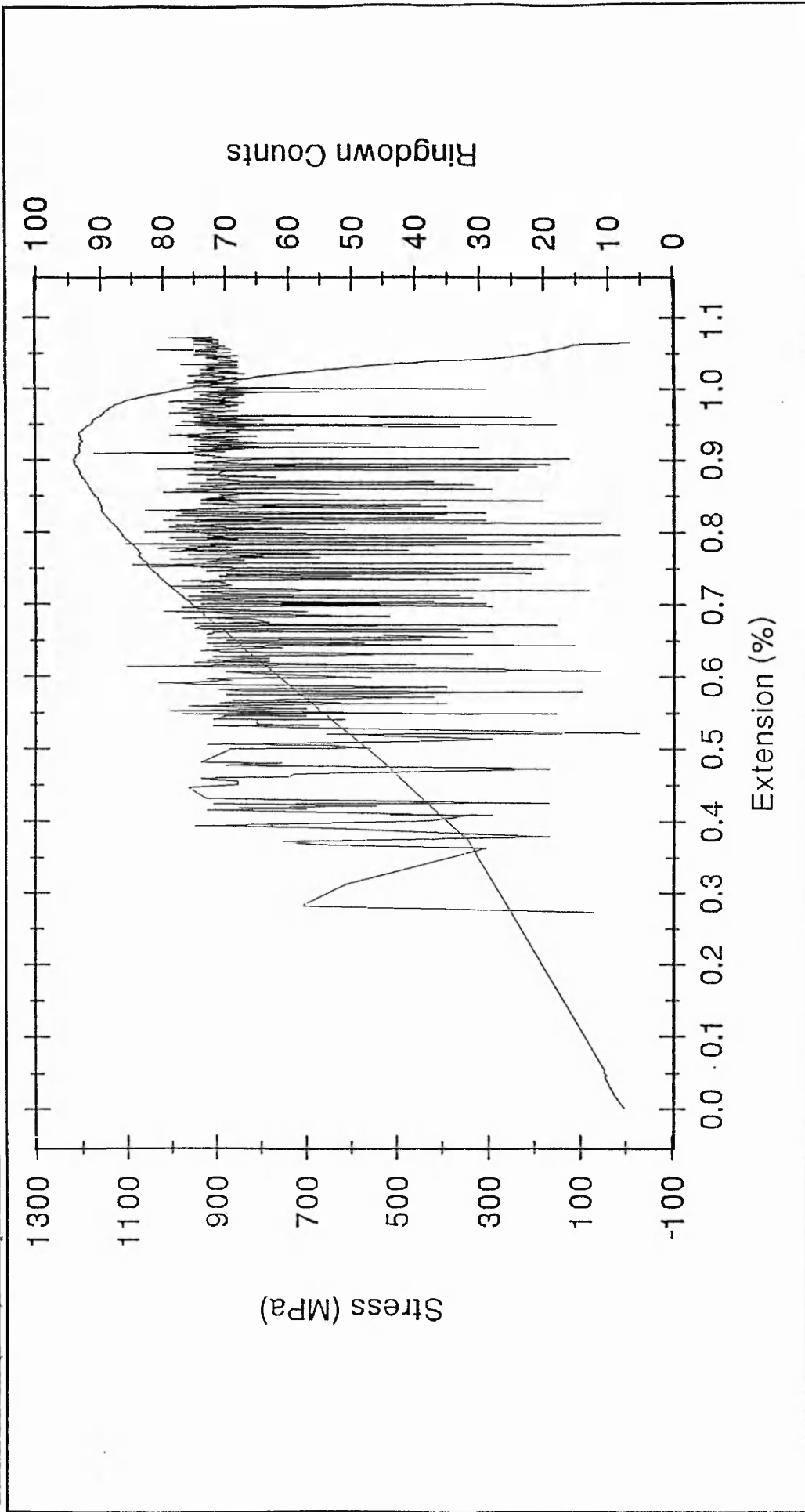
♦ Figure 5.3.a: Stress-Strain and AE ringdown counts per event data for 200T-E-glass fibre bundles.



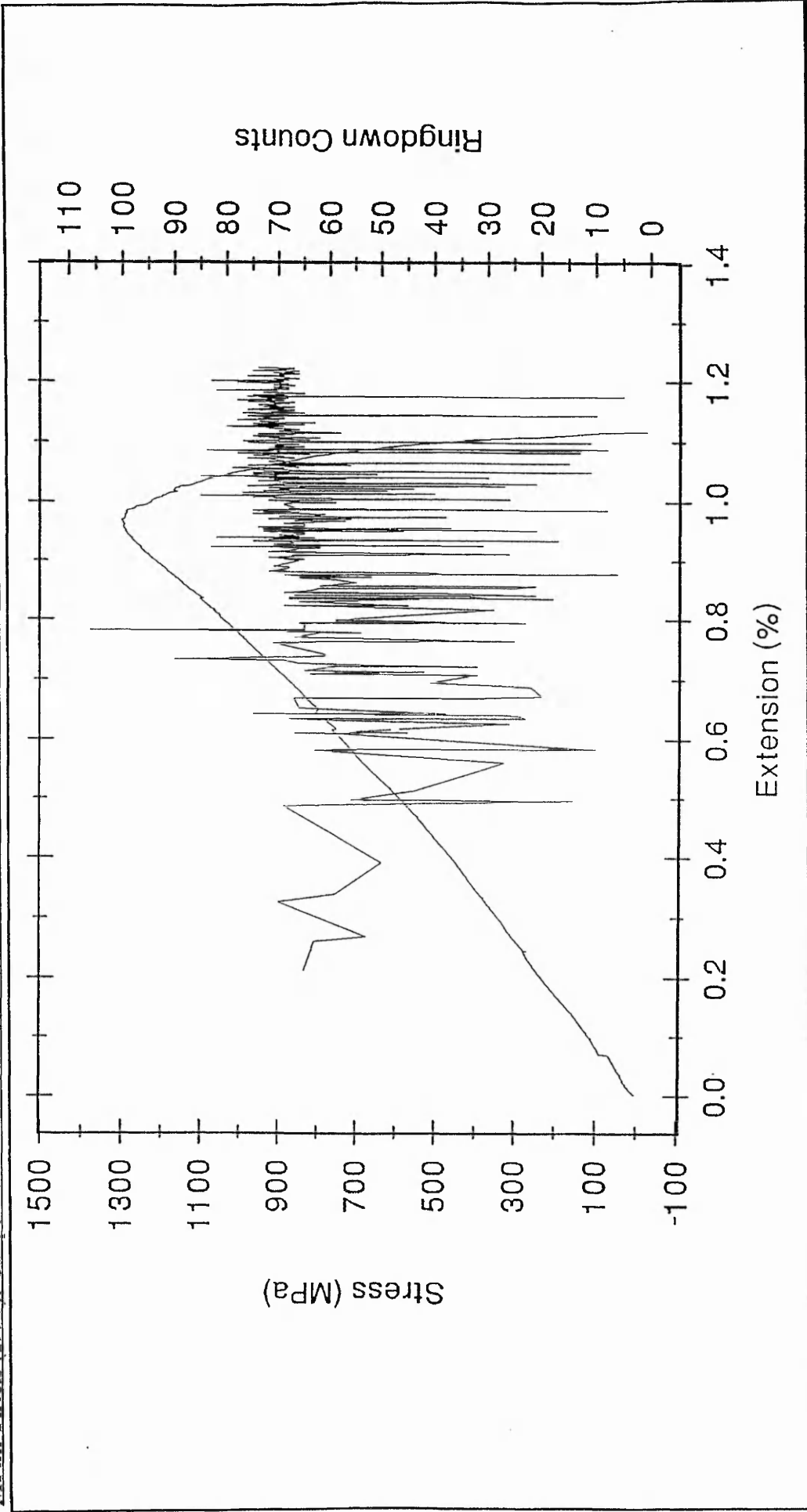
♦ **Figure 5.3 b:** Stress-Strain and AE ringdown counts per event data for 200T-E-glass fibre bundles.



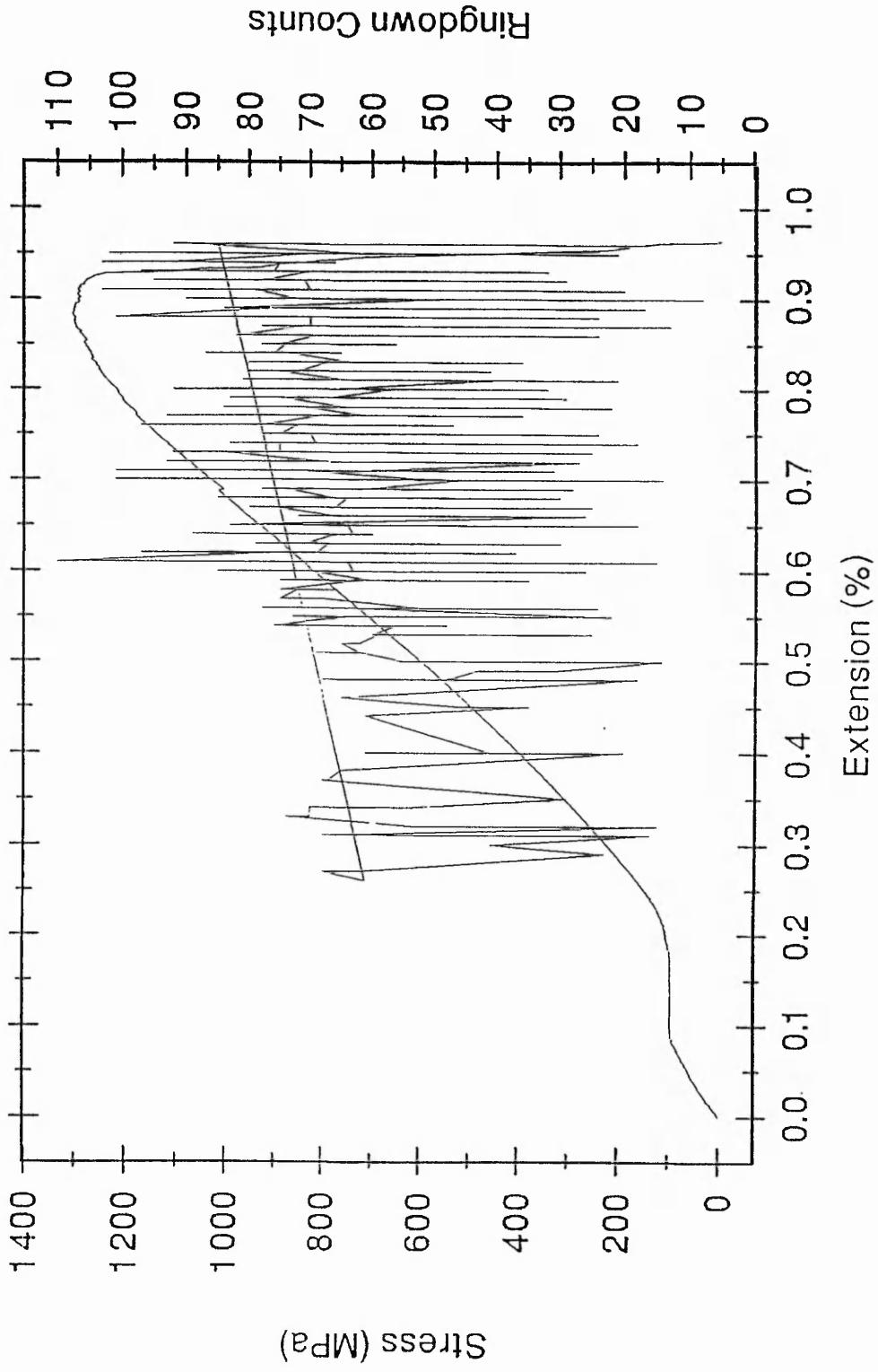
♦ Figure 5.3 c: Stress-Strain and AE ringdown counts per event data for 200T-E-glass fibre bundles.



◆ **Figure 5.4 a:** Stress-Strain and AE ringdown counts per event data for 200C carbon fibre bundles.



♦ Figure 5.4 b. Stress-Strain and AE ringdown counts per event data for 200C carbon fibre bundles.



◆ **Figure 5.4 c:** Stress-Strain and AE ringdown counts per event data for 200C carbon fibre bundles.

5.6 Conclusions

This chapter was based on the characterisation of glass and carbon fibre bundles (70 ± 1 mm length) fracture mechanisms with the use of acoustic emission and the associated parameters. The three different types of fibre bundles were subjected to silicone oil treatment in order to reduce the interfibre interactions and friction and consequently give a set of data which relates directly to fibre fracture. The AE data obtained, included useful information related to the number of emitted events during tensile testing and the associated ringdown counts and time (secs) of every event.

Initially, it was possible to obtain the stress-strain responses and superimposed AE data for the 19S3-glass, 200T-glass and 200C-carbon fibre bundles. It was clear that the 200T-glass fibres can sustain higher levels of stress (1387 MPa) than the 19S3-glass fibres (833.2 MPa), where the failure strain started at an earlier rate of 0.3 % in comparison to 0.5 % for the 200T-glass fibres. Similarly, the 200C-carbon fibre bundles failed at a stress level of 1275 MPa. From the corresponding plots of stress-strain and ringdown counts it is clear that there was a rise of ringdown counts with large fluctuations and large values of RDC, indicated a sudden released of stored energy inside the fibre bundle system. Generally, it was shown that stress-strain and AE characteristics reflect the difference between the fibre bundles. The AE technique provided a reliable mean of identifying fibre fracture in real time and it was able to monitor the fracture propagation in each fibre system.

CHAPTER 6

STATISTICAL DISTRIBUTION METHODS APPLIED TO AE

6.1. Aim of the Statistical Analysis of Fibre Bundle Failure

Chapter 5 discussed the acquisition of AE and stress-strain data from the fracture of two types of glass and one type of carbon fibre bundles. The number of fibres in the bundle were different in each case. Previous work [27-28], has set instrumentation thresholds, so that AE events reflect exactly the number of fibres present. The studies reported here have not tried to do this, with an arbitrary threshold used, providing perhaps a practical and more traditional approach to AE testing, where the electronic threshold is just used to eliminate environmental and electronic noise. Testing in this mode, would be expected to yield AE associated both with fibre breakage and interfibre frictional effects.

This chapter will consider the AE data associated with the failure of glass and carbon fibre bundles. These materials show fluctuations in their failure strength and AE parameters. The distribution of ringdown counts versus the number of events emitted during tensile testing will be examined and analysed. Statistical techniques will be applied to offer the possibility of characterisation and the prediction of the failure processes.

6.2 Distribution of AE Ringdown Counts and Events

AE related work described on chapter 5 and 6 concerns the characterisation of fibre bundles through the fracture energy released during tensile testing. The acoustic emission events recorded during the experiments leave a characteristic signature in terms of the corresponding ringdown counts. In this section the distributions of 19S3-glass, 200T-glass and 200C-carbon fibre bundles will be examined through plots of Ringdown Counts versus Number of Events. The characterisation of these distributions has been the topic of this investigation and a number of features such as interfibre friction, defects and manufacturing inconsistencies play a vital role in the results. The AE ringdown count distributions are shown in figures 6.1 a, b, 6.2 a, b, and 6.3 a, b, for the 19S3-glass, 200T-glass and 200C-carbon fibres, where the corresponding distributions appear to have an asymmetric nature.

By obtaining the corresponding plots for the three types of fibre bundles, it should be mentioned that the main peak of the ringdown count distribution starts at a value of about "55 to 65". The small relative number of emitted events prior to this region is attributed to a variety of noise sources. These noise sources as it is mentioned earlier could include frictional and de-adhesion effects within the fibre bundle and they were ignored in the statistical techniques which were applied in this research.

Comparison of the AE distributions for the three types of fibre bundles are considered in table 6.1 a where experimental data is illustrated. The statistical distribution is analysed in a simple way in terms of the percentage number of events above 55 and 65 ringdown counts respectively. This provides a simple indication of the shift of the distribution along the ringdown count axis. It is noticeable that the percentage ratio of the number of events between "55 or 65 to maximum ringdown counts" for the 200T type glass fibres is consistently higher than the 19S3 glass and 200C carbon types. From table 6.1 b, the average percentage of the number of events which is greater than 55 ringdown counts in relation to the total number of events for the 200T type is 96.85 % in contrast to 84.72. % for the 19S3 type and 85.25 % for the 200C type. The same trend follows for the number of events greater than 65 ringdown counts where the values are 97.55 % for the

200T, 89.7 % for 19S3 and 89.2 % for 200C types. In general, all three bundles show a narrow distribution of ringdown counts as could be expected since fibre tests should behave in a much more similar way than, for the transverse fibre composite materials.

The position of the distributions for similar materials were generally in good agreement to each other, considering AE signals from similar source phenomena, such as fibre fracture at a given stress or stress intensity are commonly expected to have a wide scattering of ringdown counts.[28, 67] This variability in the individual AE parameters is because even if an AE stress wave has energy proportional to the energy released at source there are in general variable losses which can attenuate the emitted signal. In general, AE bundle testing has again provided, a quick, convenient and reliable means of differentiating fibre systems.

◆ **Table 6.1 a**

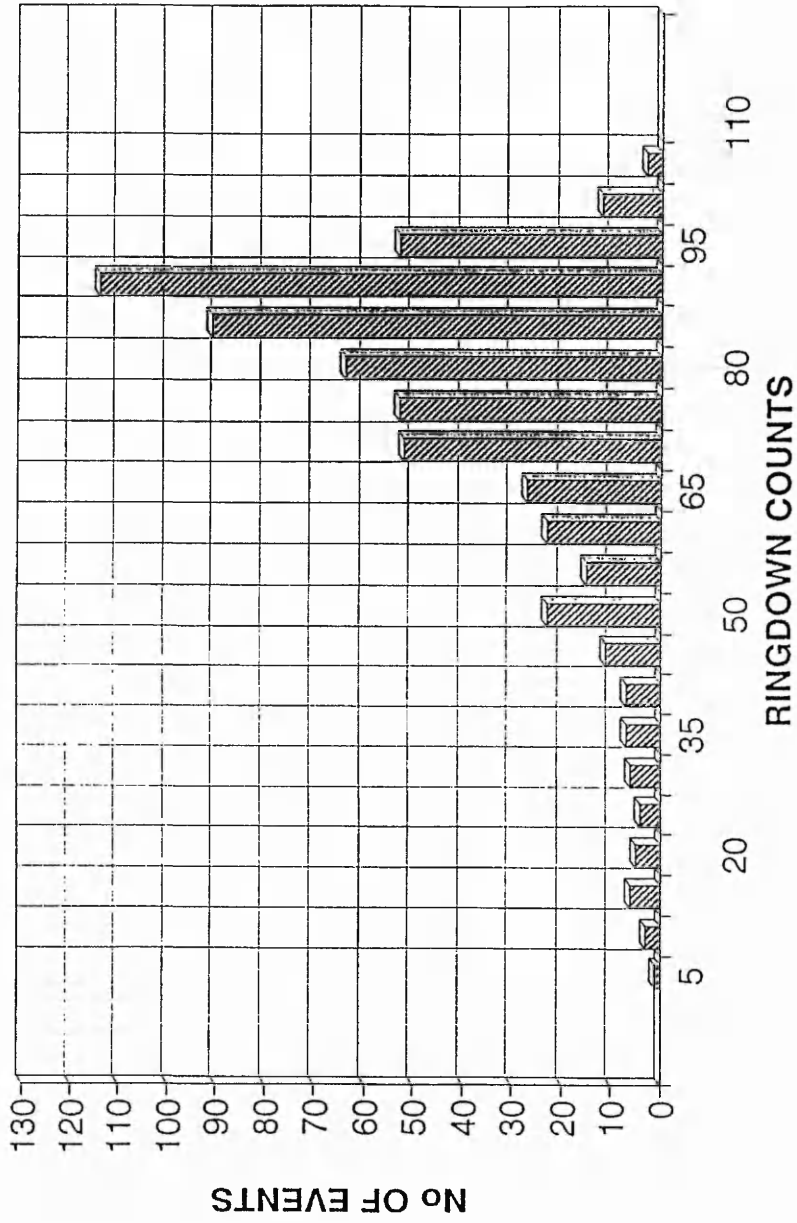
Number of events with ringdown counts above 55 and 65 respectively and in comparison to the total number of ringdown counts for: a) 19S3 glass fibres b) 200T glass fibres c) 200C carbon Fibres.

Specimen Number	No of Events above 65 RDC	No of Events above 55 RDC	RDC₆₅/ RDC_{total} Percentage %	RDC₅₅/ RDC_{total} Percentage %
19S3 - 1 glass	469 / 580	517 / 580	80.86	89.13
19S3 - 2 glass	582 / 643	603 / 643	90.51	93.77
19S3 - 3 glass	726 / 954	813 / 954	76.10	85.22
19S3 - 4 glass	504 / 529	529 / 614	82.08	86.15
19S3 - 5 glass	640 / 714	663 / 714	89.63	92.85
19S3 - 6 glass	677 / 861	730 / 861	78.62	84.78
19S3 - 7 glass	502 / 507	507 / 527	95.25	96.20
200T - 1 glass	280 / 293	282 / 293	95.56	96.24
200T - 2 glass	211 / 217	212 / 217	97.23	97.69
200T - 3 glass	336 / 346	339 / 346	97.10	97.97
200T - 4 glass	196 / 204	199 / 204	96.07	97.54
200T - 5 glass	229 / 233	229 / 233	98.28	98.28
200C - 1 car	560 / 684	593 / 684	81.87	86.70
200C - 2 car	462 / 546	485 / 546	84.61	88.82
200C - 3 car	875 / 1032	916 / 1032	84.78	88.78
200C - 4 car	1122 / 1250	1157 / 1250	89.76	92.56

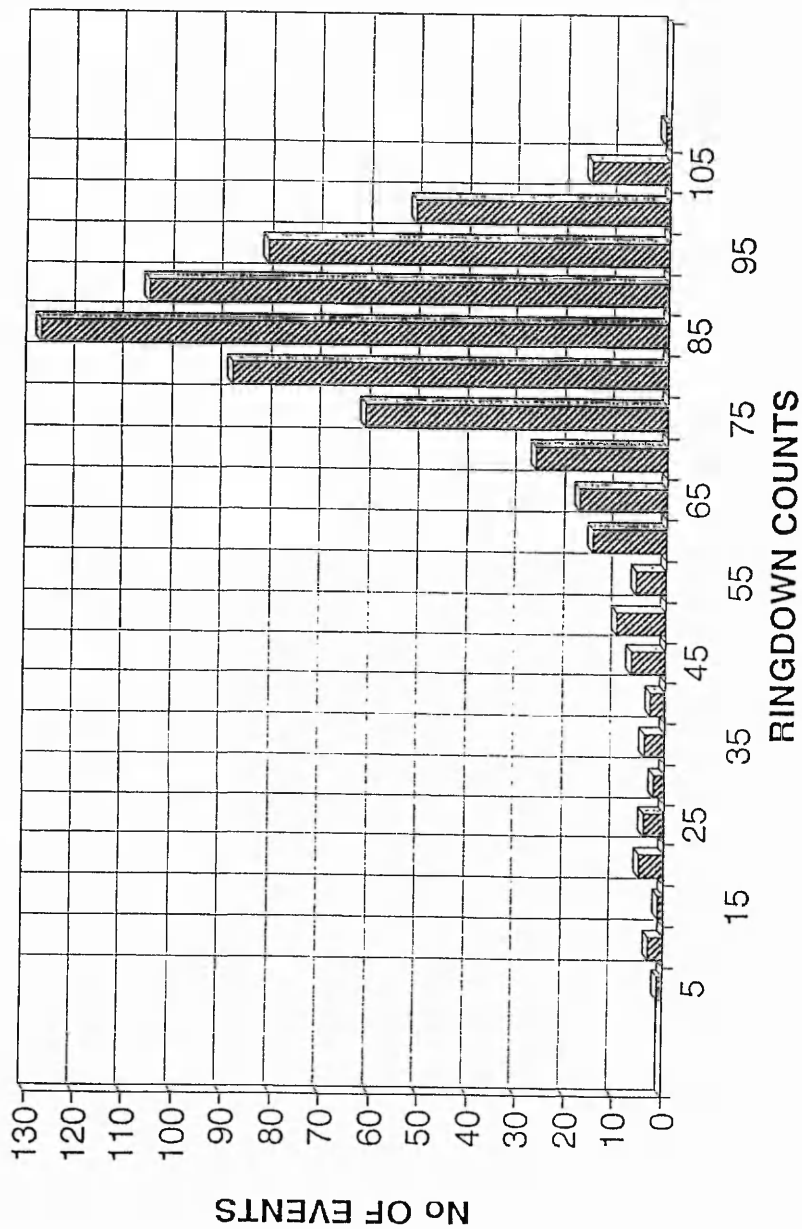
◆ **Table 6.1 b:**

Averages values derived from the corresponding ringdown counts versus number of events distributions in table 6.1 a. These values compare the number of events emitted above the 55/65 boundary and the total number of ringdown counts. The values include data for all the three types of bundles: 19S3-glass, 200T-glass and 200C-carbon fibres.

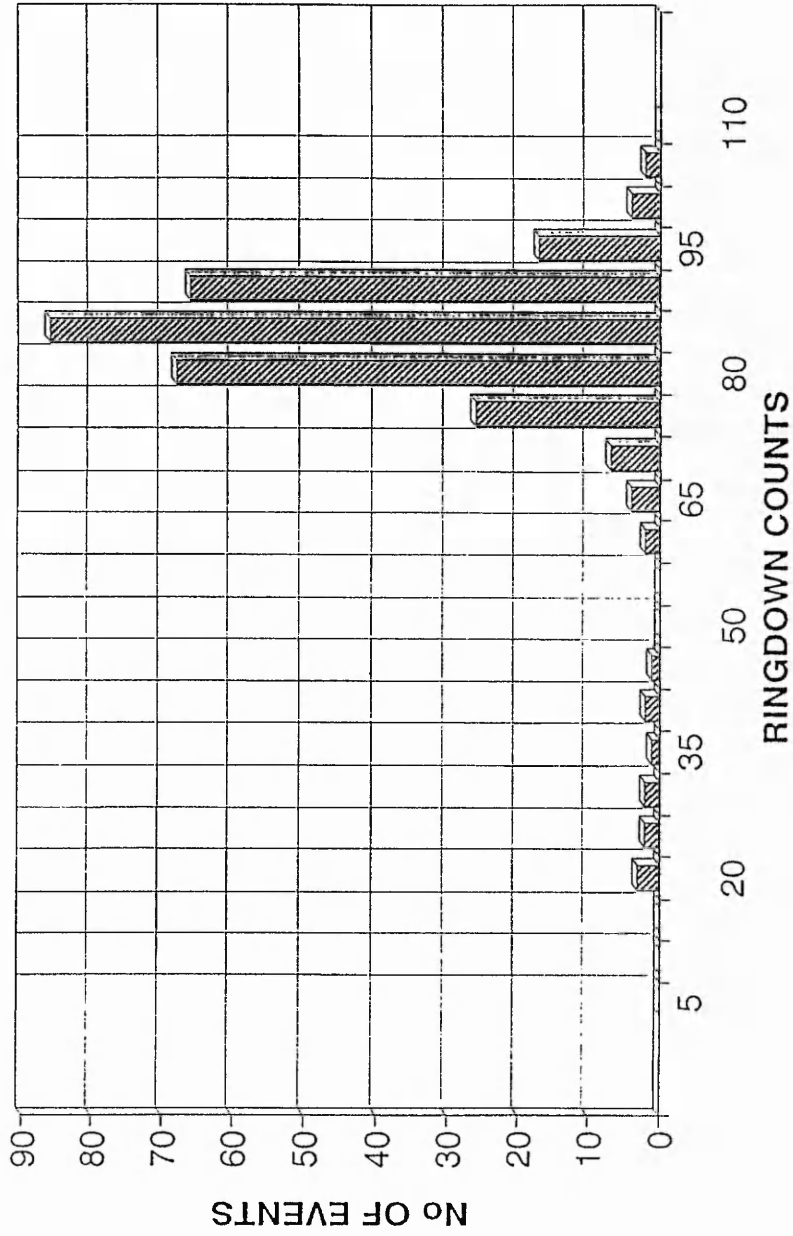
Sample Type	RDC '65-Total'	RDC '55-Total'	RDC 65-Total Percentage %	RDC 55-Total Percentage %
19S3-glass	4100/4893	4362/4893	84.72	89.72
200T-glass	1252/1293	1261/1293	96.85	97.55
200C-carbon	3019/3512	3151/3512	85.25	89.20



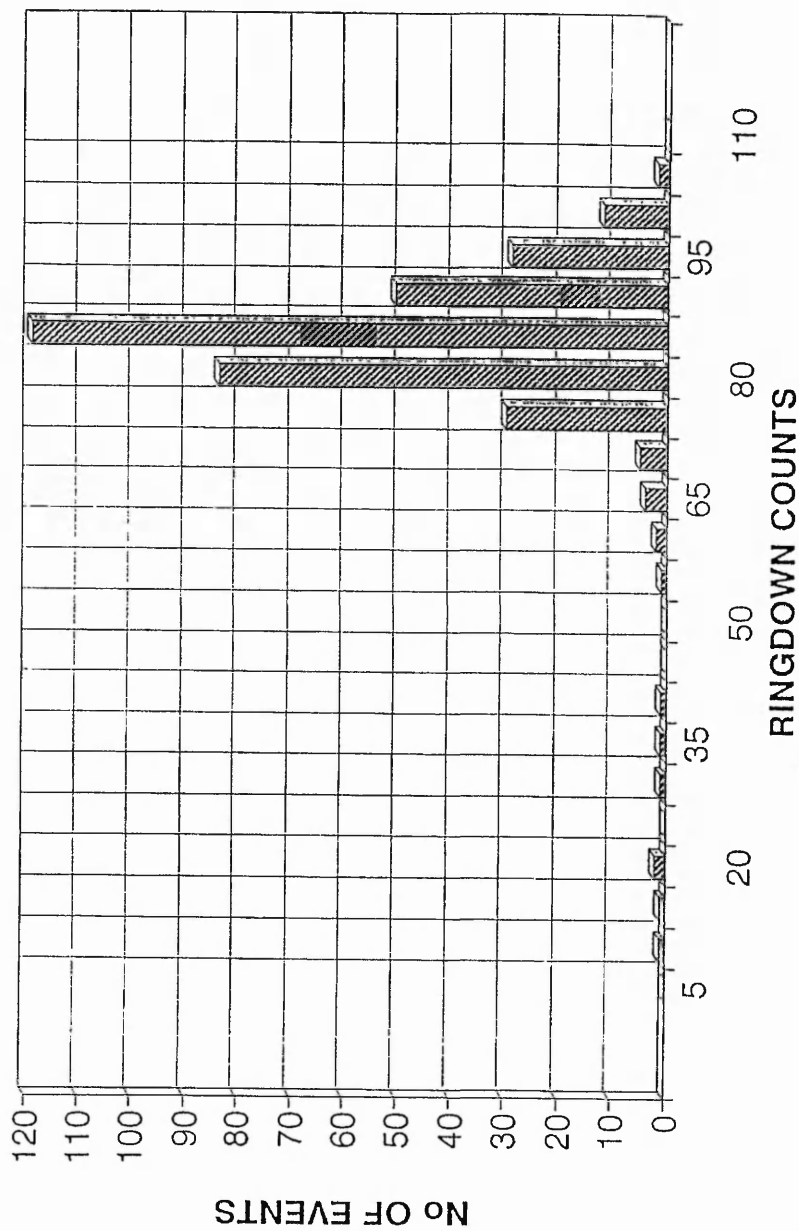
◆ **Figure 6.1 a:** Distribution of Ringdown Counts per AE event for 19S3 E-glass fibre bundles.



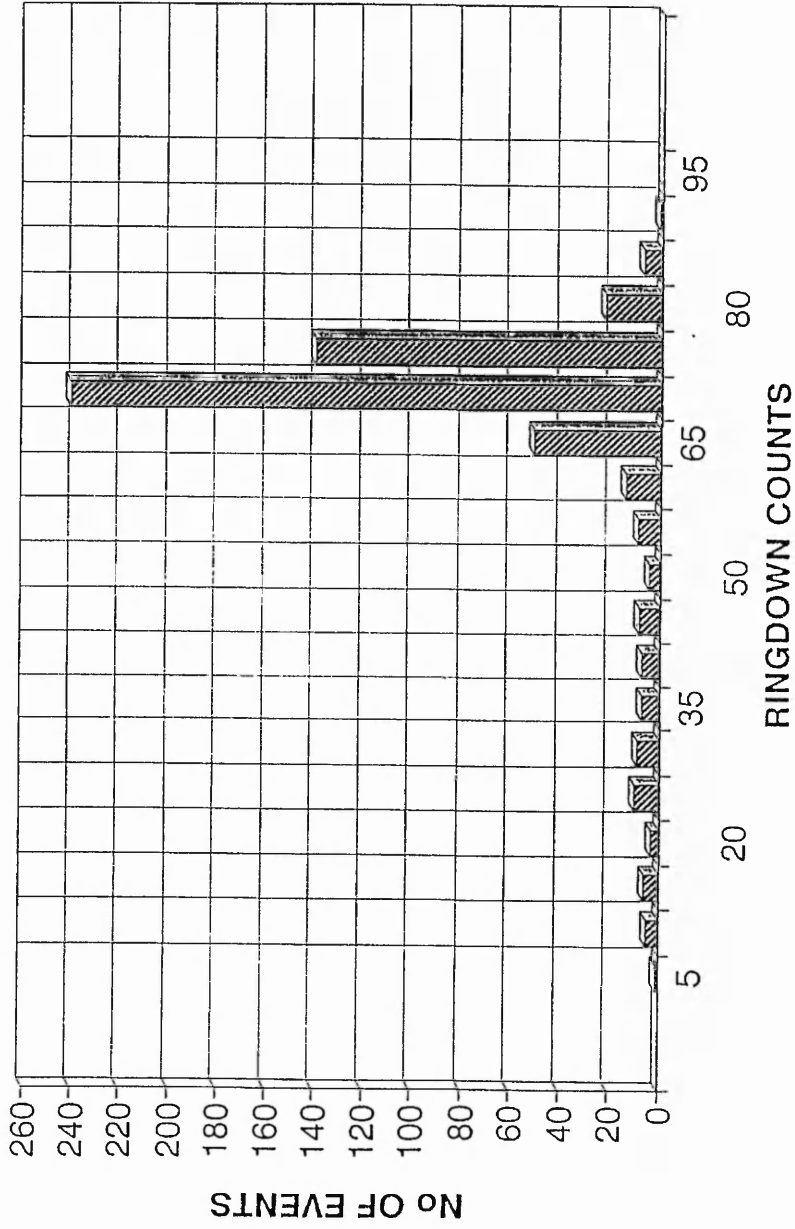
♦ **Figure 6.1 b:** Distribution of Ringdown Counts per AE event for 19S3 E-glass fibre bundles.



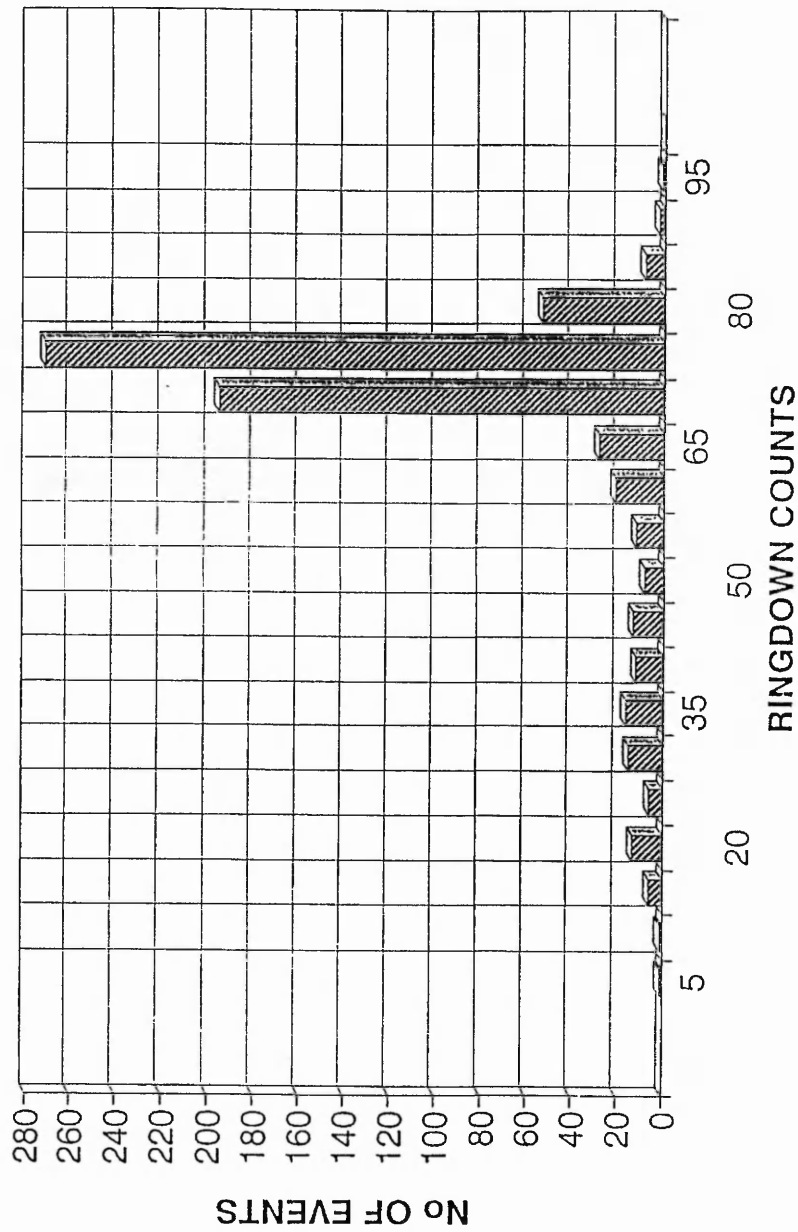
◆ **Figure 6.2 a:** Distribution of Ringdown Counts per AE event for 200T E-glass fibre bundles.



♦ **Figure 6.2 b:** Distribution of Ringdown Counts per AE event for 200T E-glass fibre bundles.



♦ Figure 6.3 a: Distribution of Ringdown Counts per AE event for 200C carbon fibre bundles.



♦ Figure 6.3.b: Distribution of Ringdown Counts per AE event for 200C carbon fibre bundles.

6.3 Statistical Analysis and Fibre Bundles

It is well documented [17, 25, 28, 30, 66.] that the fracture stress of brittle materials show a large variability. In order to use these materials for engineering purposes, the distribution of strength needs to be characterised. Based upon theoretical and empirical justification, Weibull Statistics has become a widely popular statistical model in engineering applications. In this part of the present work, a technique has been developed whereby AE monitoring of fibre bundles under tension, provides a method of obtaining strength characteristics [31]. The technique is convenient and quick. The fibres are tested in the form of a continuous “tow” and lubricated in silicone oil.

A procedure often adopted by researchers in determining fibre strength distribution is through the measurement of the average strength of a group of fibres of the same length. The Weibull shape parameter is then determined from the distribution of fibre average strength. There are shortcomings in such measurements. First, it is rather tedious to extract individual fibres from a bundle and to perform numerous tests on fibres with very small diameter. Second, the extraction of fibres from a bundle inevitably has “selected” the stronger ones, since the weaker fibres are prone to damage and fracture in the process. Third, it is difficult to determine the exact cross-sectional area of a single fibre. Experiments based upon laser diffraction fringes have shown that the measured fibre diameters vary along the fibre length due to fibre twist and non-circular fibre cross section [70].

In the past Hill and Okoroafor [26, 28] have investigated Kevlar and glass fibre bundles and shown that interfibre friction significantly reduces fibre bundle strength (σ_b) and the corresponding failure strain (ϵ_b). These fibre bundles were characterised and monitored by the use of a simple graphical (LST) method and by the use of Weibull statistics, which defined the shape of the fibre-bundles stress-strain response.

Statistical analysis of the relationship between the strength of a bundle and the strength of individual filaments is based on a number of assumptions:

- ◆ a) in a fibre, flaws of a range of severity either exists beforehand or are formed during loading. Each defect is equivalent to a crack of a given length.
- ◆ b) the strength of a fibre is determined by the most severe crack.
- ◆ c) the relationship between the applied stress and strain of a single fibre follows Hooke's law up to fracture.
- ◆ d) the applied load is uniformly distributed among the surviving fibres at any instant during the test and interactions between fibres such as friction and twisting are neglected.

6.4 The Weibull Distribution Function and AE Testing

Statistical techniques are often resorted to when dealing with material that exhibit wide scatter of data. One such technique is the two parameter *Weibull Cumulative Distribution function*. Based upon theoretical and empirical justifications, it has become a popular model in engineering applications [29]. In chapter 4 the growth of damage in composite materials have been described using a Weibull function since it provides an adequate description of damage growth in the composite material.

From chapter 4, the following equation was considered:

$$N_s = N_0 \cdot \exp \left[- \left(\varepsilon / \varepsilon_0 \right)^m \right] \quad (4.7)$$

Where “ N_0 ” is the number of fibres in a bundle, tested for fracture strength, “ N_s ” is the number of fibres that have been fractured at strain “ ε ”, “ m ” is the Weibull shape parameter and “ ε_0 ” the scale parameter.

The Weibull equation is highly versatile and can be formulated to account for a range of statistical processes. The use of this form of statistics in characterising composite failure has been entirely empirical, with the aim of extracting two material related parameters derived from AE data, which characterise and differentiate material conditions. As in the case of composite materials described in section 4, here the Weibull equations have been formulated in terms of AE events with specific ringdown count values. In order to be able to fit a statistical distribution to the ringdown counts versus number of events, (a bell shape distribution), a number of equations were modified. The initial step was the transformation of the original Weibull equation to a new one which is able to describe the total number of emitted events N_0 , the number of events at a RDC value N_i and of course the corresponding shape and scale parameters.

In the present section, the distribution of AE events and ringdown counts obtained during fibre bundle fracture could be described by the following equation:

$$N_i = N_o \left[1 - \exp \left(- \left(\frac{RDC}{RDC_o} \right)^m \right) \right] \quad (6.1)$$

Although equation (6.1) gave a good approximation to the right hand side of the bell shape ringdown counts versus number of events distribution, the results were not really considered to be successful. Because of that equation (6.1) was modified, in order to provide a better fit to the right hand side of the distribution. It also proved to be especially useful for the prediction of the number of events at the most frequently occurring value of ringdown counts. Equation (6.1) was finally used in the form of:

$$N_i = N_o \exp \left[- \left(\frac{RDC}{RDC_o} \right)^m \right] \quad (4.8)$$

As before, the shape parameter m is important for determining the shape of distribution of times to failure, the magnitude of size effect and the amount of scatter in the data. A large value of m signifies a narrow distribution. It is obtained from the slopes of the logarithmic Weibull plots produced in the form $\ln \ln (N_o/N_i)$ versus $\ln (RDC)$, derived from the tensile stress-strain response and the AE event response. The intersection between the straight line obtained from the corresponding plots and the Y axis is represented by: $p1 = -m \ln (RDC_o)$. It should be noted that equation 6.1 cannot be linearised, while equation 4.8 is of a form to only predict the shape of the right hand tail of a distribution such as that shown in figure 6.1a (for example).

6.5 Application of Weibull Statistics to Fibre Bundle Failure - Results and Discussion.

The linearity of such Weibull plots and the high percentage of regression obtained for the 200T E-glass and the 200C-carbon type of fibres, indicate that the Weibull treatment is applicable as can be seen in figures 6.4 a, b and 6.5 a, b, respectively. From equation (4.8) it is possible to obtain the values for the shape parameter m , and the appropriate scale parameters.

Figures 6.4 a, b and 6.5 a, b show the logarithmic Weibull plots derived from the tensile stress-strain and AE data for the two different types of fibres. From the corresponding plots in the form of $\ln \ln (N_0/N_i)$ versus $\ln (RDC)$, it is possible to derive the values for m and RDC_0 . Figures 6.6 a, b, 6.7 a, b, show a comparison between the real data derived from the tests and the predicted data obtained from the Weibull model using equation (4.8) where the predicted number of events N_i is calculated for each RDC value. It is noticeable that the predicted events are very close to the real data especially for the most popular value of ringdown counts.

Table 6.2a shows the calculated values of shape m and scale parameters RDC_0 , for each of the 200T-glass and 200C-carbon tested samples. The results for m and RDC_0 show some scatter, but it should not be forgotten that manufacturing flaws and handling inconsistency can easily alter the results since the fibre bundles are extremely sensitive to these effects. Table 6.2b includes the average values for the corresponding Weibull parameters. The final column, shows the percentage of linear regression for the graph of $\ln \ln (N_0/N)$ and $\ln (RDC)$. The comparison between the experimental data and the fitted Weibull model, is presented numerically in table 6.3 for both the glass and carbon fibre bundles. From table 6.3, it is important to note the average percentage of error between the real and the predicted data. For the 200T glass fibres, the average percentage of error was 10.5%, while for the 200C carbon fibres it was 7%.

By comparing the two types of fibres, the m values identify differences between the two fibre bundles. In the case where m appears to be larger, this indicates a narrower

scatter of data and the fact that the bundle has a more uniform distribution of similar defects and a lower coefficient of variation, as in the case of 200C-carbon fibres where $m_{200c} > m_{200T}$. The variations in the Weibull parameters associated with interfibre friction suggests that it induces some degree of co-operative failure reducing the bundle strength which in the case of lubricated bundles is minimised [27, 29]. The AE method used has the advantage that it will give the strength distribution of fibres whether or not the strength fits a Weibull or any other analytical expression, and the analytical expression can be employed for any fibre system, whether brittle, plastic, or with variable number of fibres.

All data reported in this section applies to lubricated fibre bundles. This type of investigation offers the possibility of describing the failure of the fibre bundles using Weibull statistics and the associate parameters. All the logarithmic Weibull plots derived over the right hand entire ringdown count distribution showed good linearity, with the Weibull parameter m obtained from the gradient of the corresponding plots. If a further method of analysis is desired then, these graphs could be divided into low strain and high strain regions. The same methods could then applied, in order to obtain the Weibull parameters and be able to predict the number of events at a particular ringdown count value. However, due to inherent instability in using $\ln \ln$ plots for determining parameters, particular methods should be used with care.

◆ **Table 6.2a**

Weibull ringdown count distribution parameters for 200C E-glass and 200T-carbon fibre bundles obtained from ringdown counts per AE event versus number of events together with the percentage of regression derived from the logarithmic plots, for each of the specimens.

Specimen No	Shape parameter <i>m</i>	Scale parameter <i>RDC₀</i>	% Regression
200T - 1 glass	9.56	87.97	95.90
200T - 2 glass	8.43	88.58	91.90
200T - 3 glass	9.24	88.28	96.90
200T - 4 glass	3.79	77.75	95.10
200T - 5 glass	5.80	85.48	91.10
200C - 1 carbon	13.20	80.34	81.10
200C - 2 carbon	9.89	73.50	96.90
200C - 3 carbon	4.21	70.23	91.10
200C - 4 carbon	15.90	74.30	96.30

◆ **Table 6.2b**

Average values derived from table 6.2, for the shape and scale parameters for the 200T-glass and 200C-carbon fibre bundles.

Sample Type	Average Shape Parameter <i>m</i>	Average Scale Parameter <i>RDC₀</i>	Average % of Regression
200T-glass	7.36	85.61	94.18
200C-carbon	10.8	74.60	91.35

◆ **Table 6.3**

Comparison between the real and the predicted number of emitted events derived during tensile testing for the 200T-glass and 200C-carbon fibre bundles.

Specimen 200T-1 glass		
<u>Ringdown Counts</u>	<u>Number of Events (Real)</u>	<u>Number of Events (Predicted)</u>
85	86	85.17
90	66	50.45
95	17	21.74
100	4	5.8
105	2	0.8

Specimen 200T-2 glass		
<u>Ringdown Counts</u>	<u>Number of Events (Real)</u>	<u>Number of Events (Predicted)</u>
85	60	54.80
90	25	35.40
95	20	18,30
100	3	6.90
105	3	1.70

Specimen 200T-3 glass		
<u>Ringdown Counts</u>	<u>Number of Events (Real)</u>	<u>Number of Events (Predicted)</u>
<u>85</u>	<u>119</u>	<u>105.30</u>
90	51	64.50
95	29	29.70
100	12	9.00
105	2	1.50

Specimen 200T-4 glass		
<u>Ringdown Counts</u>	<u>Number of Events (Real)</u>	<u>Number of Events (Predicted)</u>
<u>80</u>	<u>57</u>	<u>51.90</u>
85	41	39.00
90	23	27.70
95	14	18.65
100	9	11.80
105	9	7.00
110	5	3.80

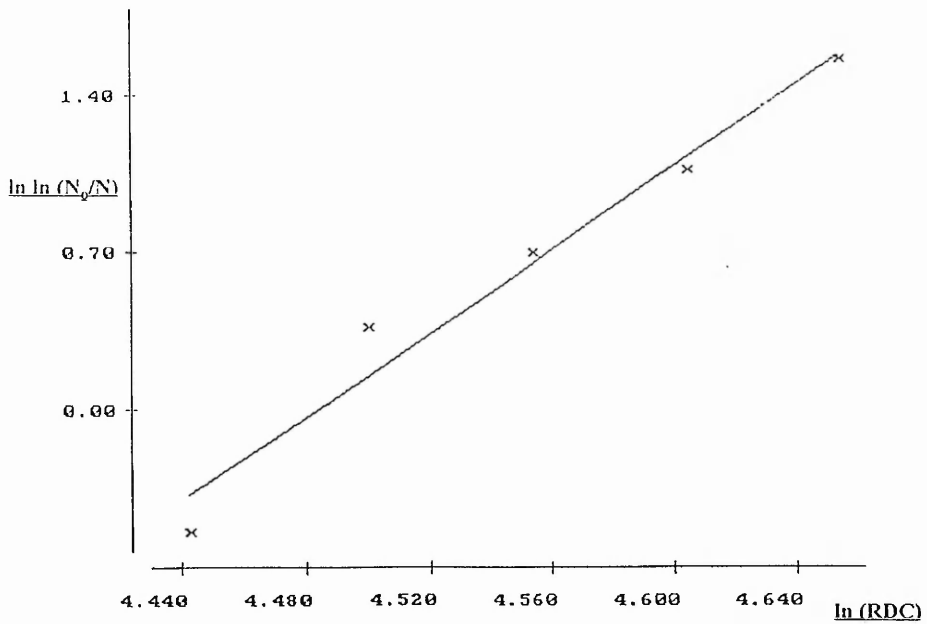
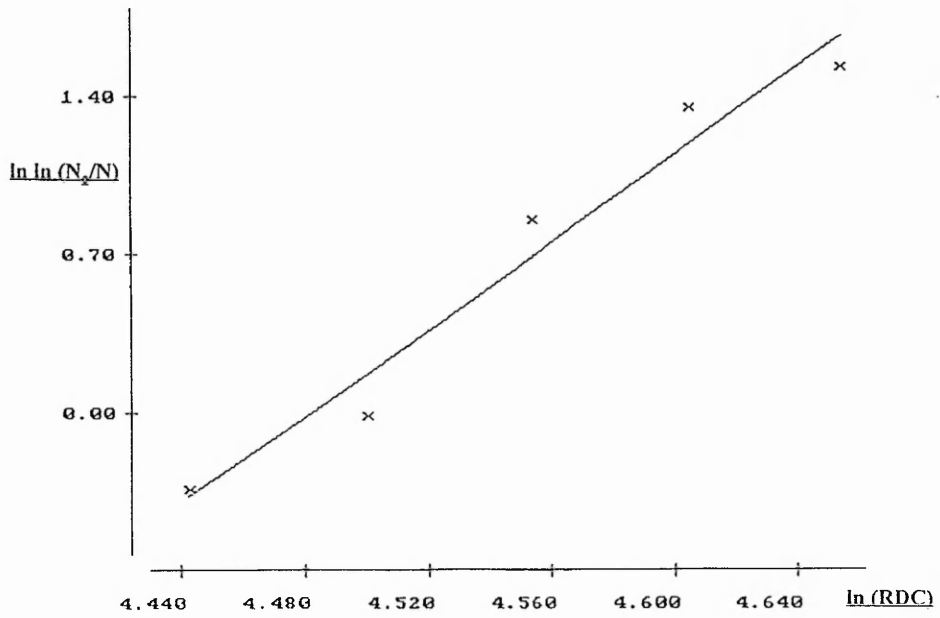
<u>Specimen 200T-5 glass</u>		
<u>Ringdown Counts</u>	<u>Number of Events</u> <u>(Real)</u>	<u>Number of Events</u> <u>(Predicted)</u>
<u>85</u>	<u>81</u>	<u>62.00</u>
90	44	42.40
95	24	25.75
100	7	13.60
105	4	6.05
110	2	2.20
120	1	0.15

<u>Specimen 200C -1 carbon</u>		
<u>Ringdown Counts</u>	<u>Number of Events</u> <u>(Real)</u>	<u>Number of Events</u> <u>(Predicted)</u>
<u>75</u>	<u>272</u>	<u>224</u>
80	53	130
85	8	40
90	2	3.8
95	1	--

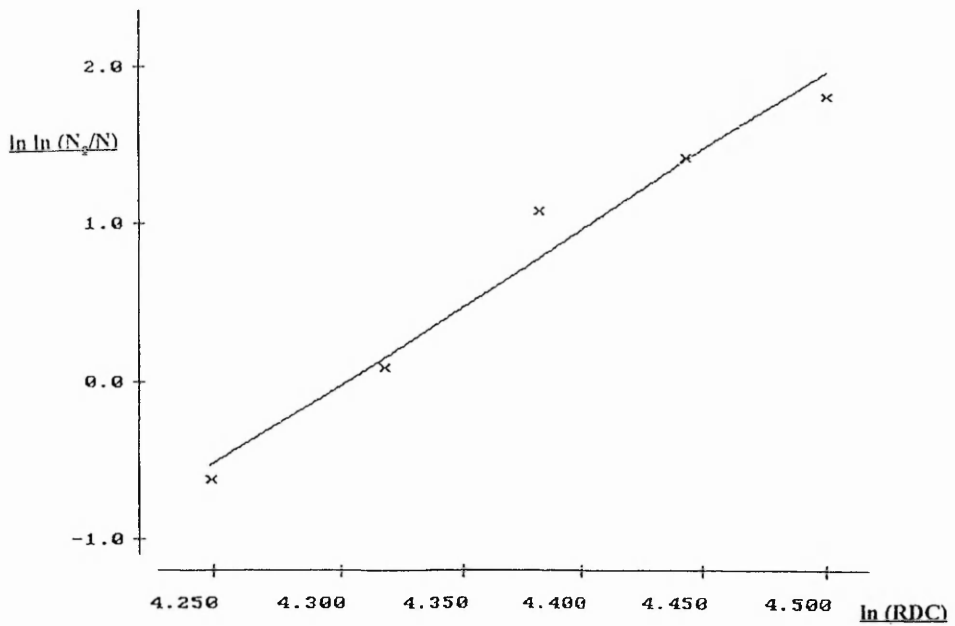
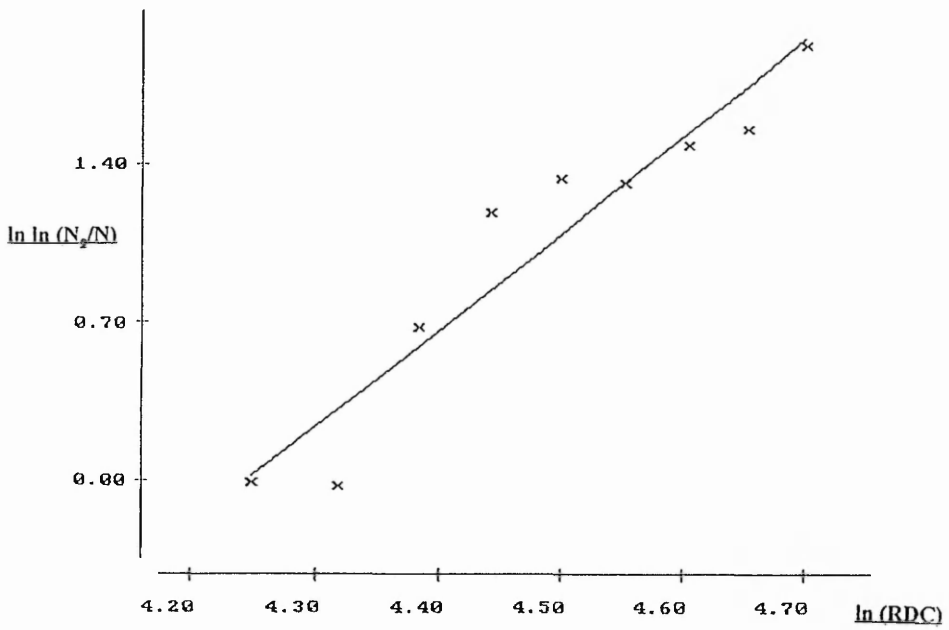
Specimen 200C - 2 carbon		
<u>Ringdown Counts</u>	<u>Number of Events</u> <u>(Real)</u>	<u>Number of Events</u> <u>(Predicted)</u>
<u>70</u>	<u>241</u>	<u>221.60</u>
75	140	121.20
80	22	40.60
85	7	6.09
90	1	0.25

Specimen 200C - 3 carbon		
<u>Ringdown Counts</u>	<u>Number of Events</u> <u>(Real)</u>	<u>Number of Events</u> <u>(Predicted)</u>
<u>70</u>	<u>287</u>	<u>287</u>
75	290	206
80	108	136.5
85	30	82.5
90	18	45.0
95	19	21.8
100	10	9.2
105	7	3.5

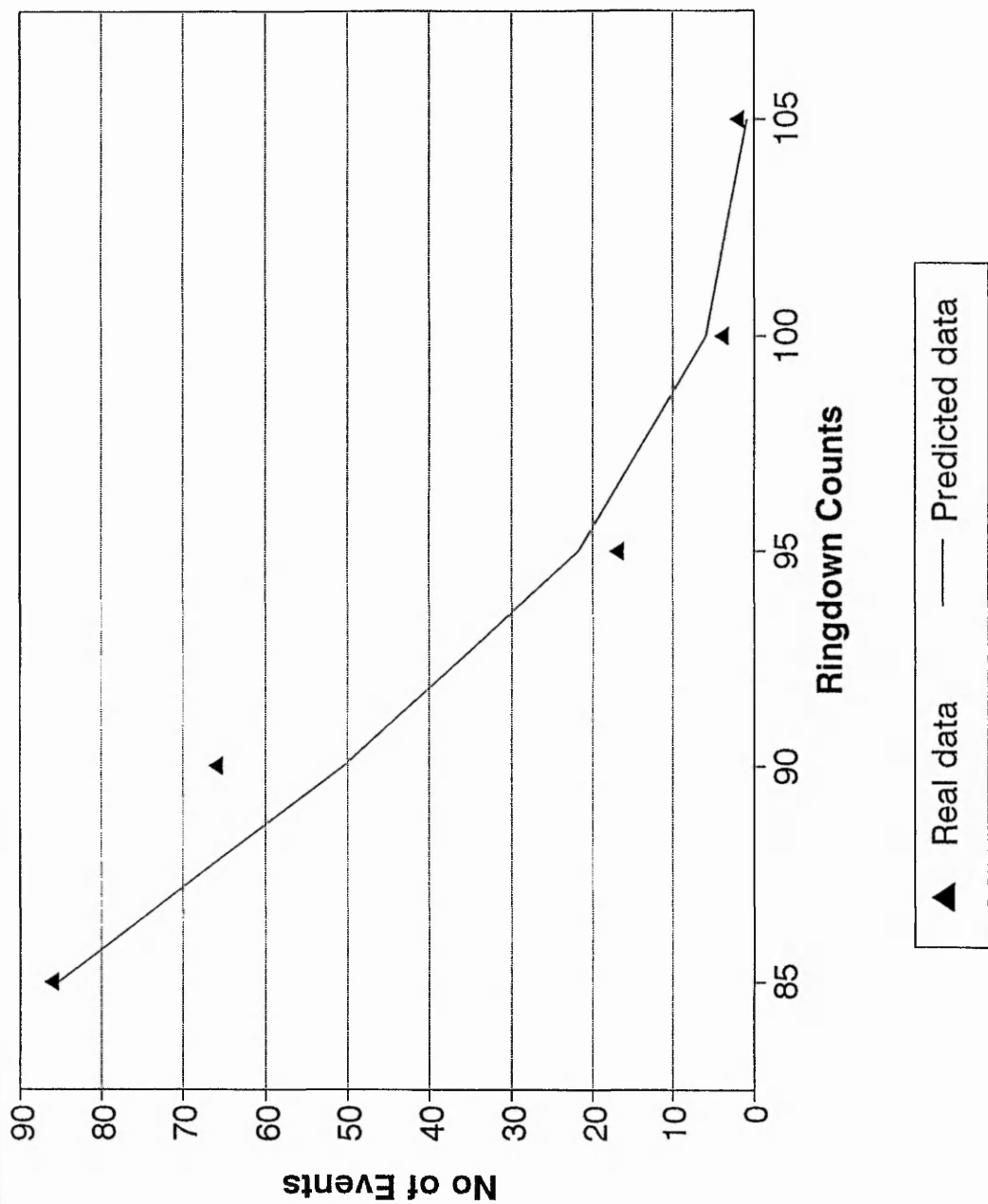
Specimen 200C - 4 carbon		
<u>Ringdown Counts</u>	<u>Number of Events</u> (Real)	<u>Number of Events</u> (Predicted)
<u>70</u>	<u>710</u>	<u>691</u>
75	299	319
80	8	40
85	1	0.2



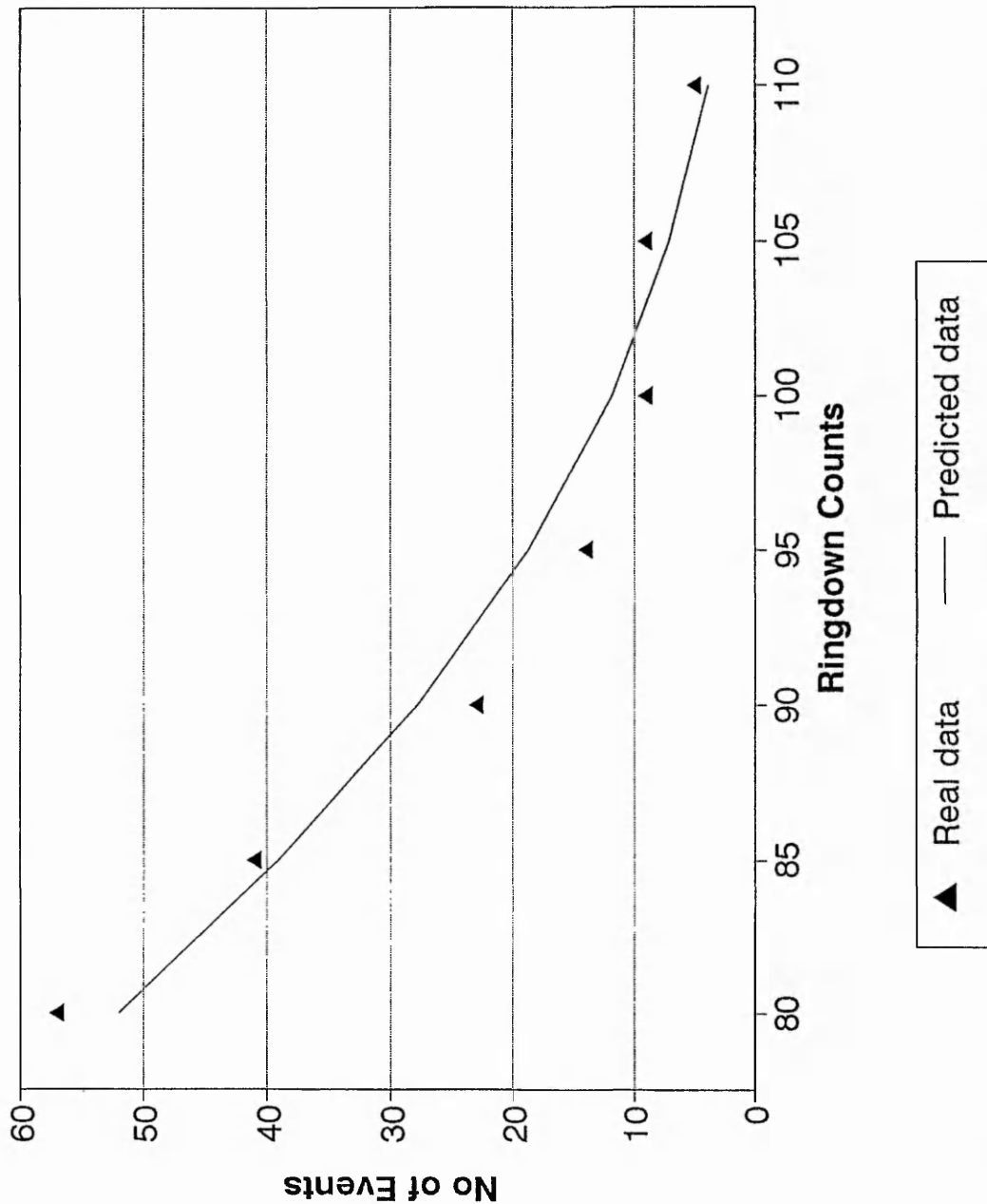
◆ **Figure 6.4 a, b:** Logarithmic Weibull plots in the form of $\ln \ln(N_0/N)$ vs $\ln(RDC)$, derived from the tensile testing of 200T E-glass fibre bundles.



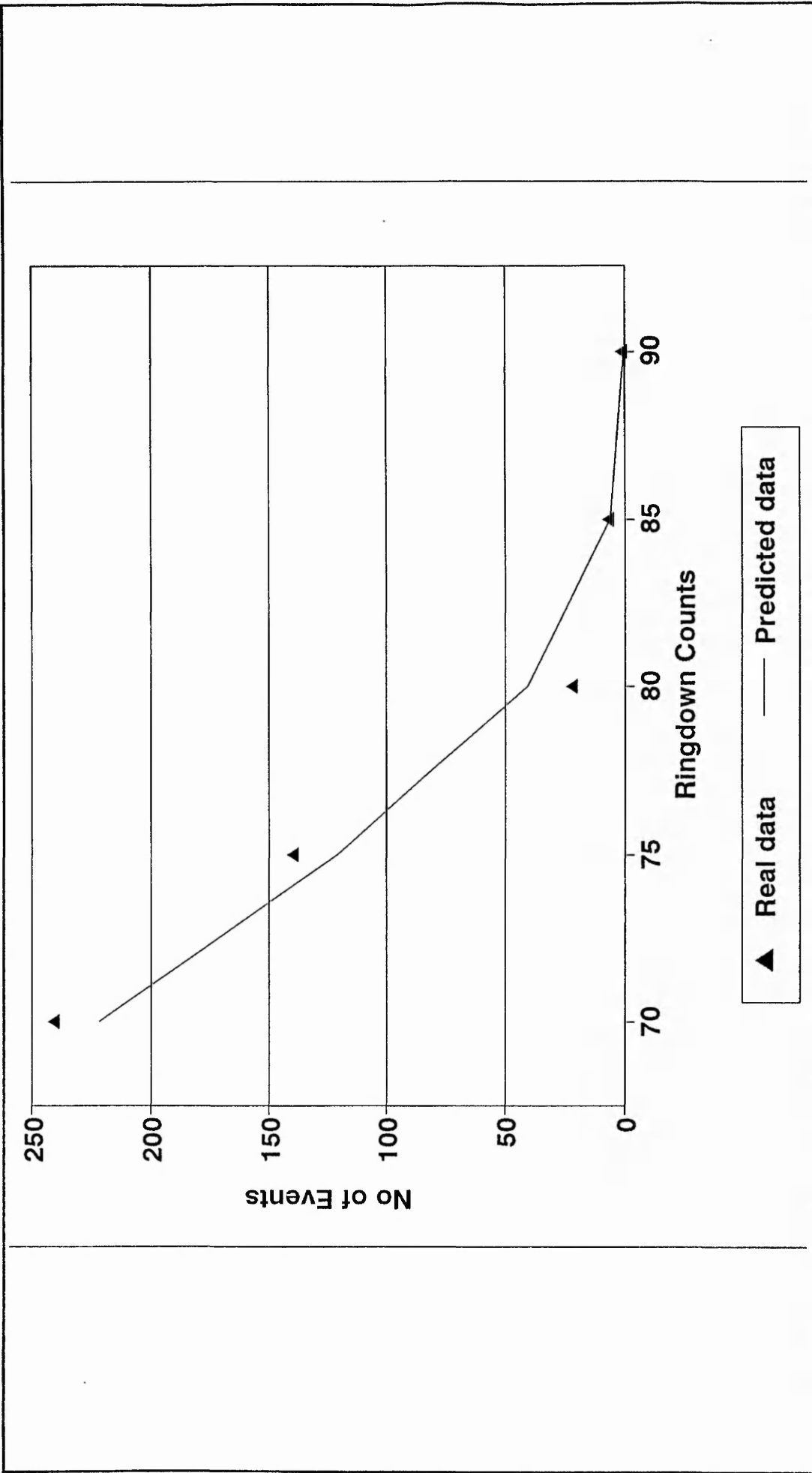
◆ **Figure 6.5 a, b:** Logarithmic Weibull plots in the form of $\ln \ln (N_0/N)$ vs $\ln (RDC)$, derived from the tensile testing of 200C carbon fibre bundles.



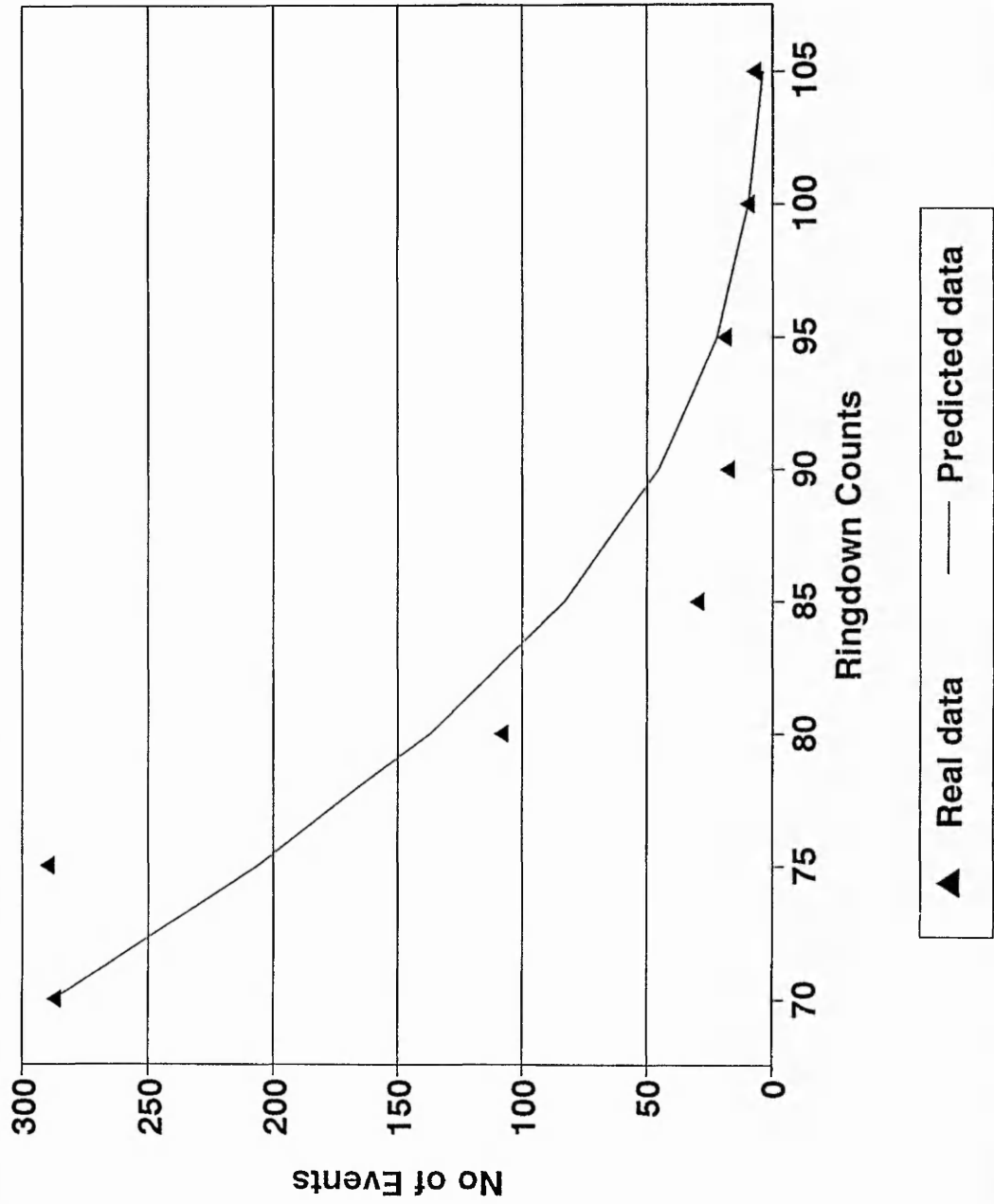
◆ **Figure 6.6 a:** Comparison of real data versus the predicted data, calculated using Weibullequation (4.8) for 200T E-glass fibre bundles.



♦ **Figure 6.6 b:** Comparison of real data versus the predicted data, calculated using Weibullequation (4.8) for 200T E-glass fibre bundles.



◆ **Figure 6.7 a:** Comparison of real data versus the predicted data, calculated using Weibullequation (4.8) for 200C carbon fibre bundles.



♦ **Figure 6.7 b:** Comparison of real data versus the predicted data, calculated using Weibullequation (4.8) for 200C carbon fibre bundles.

6.6 Two Parameter Log - Normal Function

One of the ways to indicate changes in the energy released during tensile testing of glass and carbon fibre bundles, is when the distribution of ringdown counts versus number of events is modified. This produces an asymmetric distribution which indirectly describes the distribution of energy due to fibre fracture. In this section, a different statistical distribution is used, -a two parameter log-normal function - in an attempt to describe the distribution of acoustic emission parameters and specifically the ringdown counts versus the number of events, statistically. In the previous section the use of a Weibull cumulative distribution function was under consideration. Although this mathematical model was used effectively, the method was only able to be fitted to the right hand tail of the ringdown count versus number of events distributions. By right hand tail, the calculation was applied from the most frequently occurring ringdown count value to the maximum ringdown count value emitted during the tensile testing as can be seen from figures 6.1, 6.2 and 6.6, 6.7. The use of the current method improves the accuracy of the prediction of the whole distribution, and provides another option in modelling the behaviour of fibre bundles under test.

The development of extreme value distributions proceeded to some extent outside the mainstream of statistical distribution theory, with early developments considering problems encountered in statistical inference. The extreme value theory is used to describe an enormous variety of applications involving natural phenomena such as rainfall, floods, wind gusts, air pollution and delicate mathematical results on point process and regularly varying functions.

The two parameter log normal function is used when the fitting data may be positively or negatively skewed. For the shape of AE data which was obtained throughout the experimental work and especially for 19S3 and 200T fibre bundle testing using AE, a basic probability density function can be applied in the form [59]:

$$p_x(x) = \Theta^{-1} e^{-(x-\xi)/\Theta} \exp\left[-e^{-\frac{(x-\xi)/\Theta}{\Theta}}\right] \quad (6.2)$$

where if: $\xi = 0$ and $\Theta = 1$ the distribution of: $Y=(x-\xi)/\Theta$, takes the standard form of:

$$p_y(Y) = \exp\left(-y - e^{-y}\right) \quad (6.3)$$

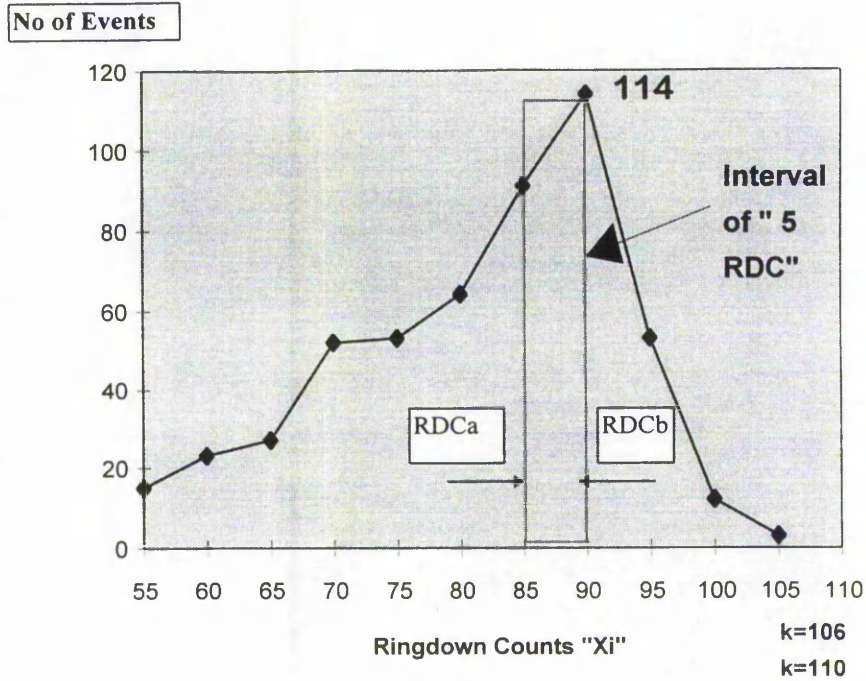
The standard probability density function of equation (6.3) is shown in figures 6.8 and 6.9. It is obvious that the shape is very closely mimiced by a lognormal distribution function. In order to characterise the statistical failure of mechanical system relevant to this work, and the description of the distribution of AE ringdown counts, the two parameter log-normal function takes the final form of [60]:

$$f(y)dy = \left[y \cdot c \cdot \sigma \cdot \sqrt{2\pi}\right]^{-1} \exp\left[-\frac{1}{2} \cdot (\log(y) - \Theta)^2 / c^2 \cdot \sigma^2\right] dy \quad (6.4)$$

Where: $\Theta = \frac{\sum f_i \cdot \ln(k - X_i)}{\sum f_i} \quad (6.4a)$

and $\sigma^2 = \frac{\sum f_i [\ln(k - X_i) - \Theta]^2}{\sum f_i} \quad (6.4b)$

Function $f(y)$ is the probability that a number of events can fall between a ringdown count boundary $[RDC_a, RDC_b]$, of values ± 5 Ringdown Counts. Factor k is the maximum ringdown count value emitted for each of the distributions. X_i is each of the ringdown count values. y is the difference between the maximum ringdown count value and a random RDC value, so that $y = k - x_i$ and finally c is just a scaling factor.



◆ **Figure 6.8 a:** Schematic representation of the a typical “RDC (Xi) vs. No of Events” distribution, showing the application of a two parameter log-normal distribution to the present method. $f(y)$ is the probability of “114” events falling between the ringdown count values of “85 to 90”. k is the factor derived from $RDC + 1 = 105+1 = 106$ or alternatively $RDC + 5 = 105+5 = 110$.

The first step in using the log-normal distribution was the calculation of Θ and σ^2 from equations (6.4 a) and (6.4 b). This was done by including all the values for the ringdown counts X_i and the associated total number of events for every sample in the corresponding series. Then from the main equation (6.4) it was possible to calculate the value for the two parameter log-normal function $f(y)$ for each RDC value. This calculation could be carried-out for each of the ringdown count values in order to estimate the predicted number of events in this range. However, it was carried out to determine for the propability of the most frequent occurring ringdown count value as has been demonstrated in the sixth column of tables 6.4a and 6.5a denoted as $f(RDC)_p$ predicted. It is important at this point to mention the role of k in the estimation of all the significant parameters Θ, σ

and $f(y)$. The values of k which are selected are either maximum ringdown count value plus one ($RDC_{\max} + 1$), or the maximum RDC value plus five ($RDC_{\max} + 5$).

However, as can be seen this method using equations (6.4) to (6.4b) is cumbersome. A more reliable and a faster approach to the problem was required and therefore a "Matlab" program was designed. This program is included in appendix 1 together with a detailed explanation. At this stage the two parameter log-normal function results denoted as $f(RDC)_p$ needed to be compared with the propability of the number of events emitted at the most frequently occurring ringdown count value denoted as $f(RDC)_R$ for the two types of glass fibre bundles. There are two different ways in which this comparison could be estimated. A typical example demonstrates each of the two possible ways of comparison.

From the real data the maximum value of $f(y)$ is detemined using the following equation (6.5) which is in the form of:

$$\mathit{max} f(RDC)_R = \mathit{max}(f / \mathit{sum}f \cdot 5) \quad (6.5)$$

where:

f: is the number of events at the most frequent occurring ringdown count value.

sum f: is the total number of events for the whole distribution curve.

For example for the first fibre sample 19S3-1G, at the most frequent occurring RDC value of 90, the total number of events emitted is 114 at this RDC value, and the total number in the distribution curve is 548. From equation (6.5) this is:

$$\mathit{max} f(RDC)_R = 114/548 \cdot 5 = 0.0416$$

By comparing $\mathit{max} f(RDC)_R$ which is 0.0416 to the $f(RDC)_p$ predicted which is 0.0346 and when $k = RDC_{\max} + 1$, the fit is 83.17%. This data is evident in table 6.4 a.

The number of events predicted (E) between an interval of $[RDC_a, RDC_b]$, could be given by the following equation:

$$E_{expected} = N \cdot \int_{RDC_a}^{RDC_b} f(y) \cdot dy \quad (6.6)$$

Where "N" is the total number of events.

For example for the same fibre bundle and for $k = RDC_{max} + 1$ equation (6.6) is on the form of:

$$E_{exp} = 548 \cdot 0.0346 \cdot 5 = 94.8 \approx 95 \text{ events}$$

This value of the predicted number of events which is 95 is compared to the real number of events which is 114 and gives a 83.17 % fit.

Tables 6.4a, b and 6.5a, b include the full analysis of AE data for the 19S3 and 200T glass fibre bundles, with this data corresponding only to the prediction of the probability of the number of events at the most frequently occurring ringdown count value. Also, figures 6.10a, b and 6.11a, b show typical examples of the total description of the corresponding distributions. It can be seen that, in general, the model of the predicted number of events proved to be accurate and close to the real data. In the case of 19S3-G glass fibre bundles the predicted number of events reached a 100% agreement in one case, while for the 200T-G glass fibres the predicted results reached a maximum agreement of 87% in one case.

Table 6.4 b shows the corresponding average values for the predicted maximum event probability. By comparing the corresponding results of the estimated values for the two k values, $k = RDC_{max} + 1$ and $k = RDC_{max} + 5$, it is obvious that the latter option proved to be more appropriate and in closer agreement to the actual data. The predicted average value, for the 19S3-G glass fibres and $k = RDC_{max} + 1$, was 0.0364, and achieved an 87.4% agreement to the real average value of 0.417, at the most frequently occurring ringdown count value. The accuracy of the calculation was increased for the $k = RDC_{max} +$

5 and giving an average value of 0.371 with a 89% agreement as can be seen from table 6.4 b and figures 6.10 a and b.

Similarly, table 6.5b describes the predicted average values of the maximum event probability for the 200T-g glass fibre bundles. The same pattern appears for the k values. For $k = RDC_{max} + 1$ the average predicted value was 0.0436 in comparison to the real value of 0.0628. This gives an 69.43% agreement between the two values. However, as k increases the predicted results are relatively closer to the real results. As can be seen from table 6.5b for $k = RDC_{max} + 5$ the average value increases to 0.0456 and for 72.61 % and $k = RDC_{max} + 10$ to 0.0462 and 73.7%. Generally, in both cases and for the prediction of the ringdown count distributions for the 19S3-glass and 200T-glass fibre bundles, it was clear that by increasing the k value from $RDC_{max} + 1$ to $RDC_{max} + 5$, the predicted distribution fitted closer to the real distribution derived from the AE data (see figure 6.11 a, b).

In the case of 200T glass fibres the percentage accuracy in the prediction of the maximum event probability has dropped by 15% on average in comparison to the 19S3 bundles, where the approximation proved to be more accurate. A big factor in this change is that, for 200T fibre bundles, the ringdown counts distribution is narrower. The narrower distribution could indicate that the 200T fibre bundle has a much more tightly defined fibre strength with fewer interfibre interactions/friction as AE events during fibre bundle testing.

In conclusion, the fibre system can be characterised using an alternative two parameter log-normal distribution function. The relationship obtained between the predicted and the real number of events at particular ringdown count values showed relatively good agreement in most of the cases for both types of glass fibre bundles considered. This statistical approach proved to be a useful tool and provided a quick and reliable mean of characterising material condition using the log-normal function.

◆ **Table 6.4 a**

Estimation of the parameters “k”, “ Θ ” and “ σ ”, together with the comparison of the experimental to the fitted data for the 19S3-glass fibre bundle and for the most frequent occurring ringdown counts.

<i>Two Parameter log-normal function / Glass Fibres</i>						
Specimen number	“K”	“Θ”	“σ”	f(RDC)_R Real	f(RDC)_P Predicted	f_R/f_P Ratio %
19S3-1 G	106	3.164	0.569	<u>0.0416</u>	<u>0.0346</u>	83.17
	110	3.341	0.455		<u>0.0338</u>	81.25
19S3-2 G	116	3.390	0.413	<u>0.0412</u>	<u>0.0354</u>	85.92
	120	3.353	0.346		<u>0.0360</u>	87.37
19S3-3 G	101	3.182	0.586	<u>0.0342</u>	<u>0.0333</u>	97.36
	105	3.362	0.442		<u>0.0341</u>	99.70
	110	3.535	0.363		<u>0.0342</u>	100.0
19S3-4 G	106	3.209	0.4495	<u>0.0453</u>	<u>0.0395</u>	87.19
	110	3.372	0.371		<u>0.0395</u>	87.19
19S3-5 G	106	3.083	0.507	<u>0.0394</u>	<u>0.0407</u>	96.80
	110	3.270	0.405		<u>0.0391</u>	99.23
19S3-6 G	111	3.467	0.470	<u>0.0302</u>	<u>0.0295</u>	97.68
	115	3.598	0.383		<u>0.0304</u>	99.34
19S3-7 G	111	3.148	0.440	<u>0.0602</u>	<u>0.0420</u>	67.74
	115	3.322	0.322		<u>0.0470</u>	75.80

♦ **Table 6.4 b**

Estimation of the average values of the predicted number of events for $k = RDC_{max} + 1$ and $k = RDC_{max} + 5$ for the 19S3-g glass fibre bundles.

Sample Type	"k"	Average $f(RDC)_R$	Average $f(RDC)_P$	f_R/f_P Ratio %
19S3-glass	$RDC_{max} + 1$	0.0417	0.0364	87.4
19S3-glass	$RDC_{max} + 5$	0.0417	0.0371	89.0

◆ **Table 6.5 a**

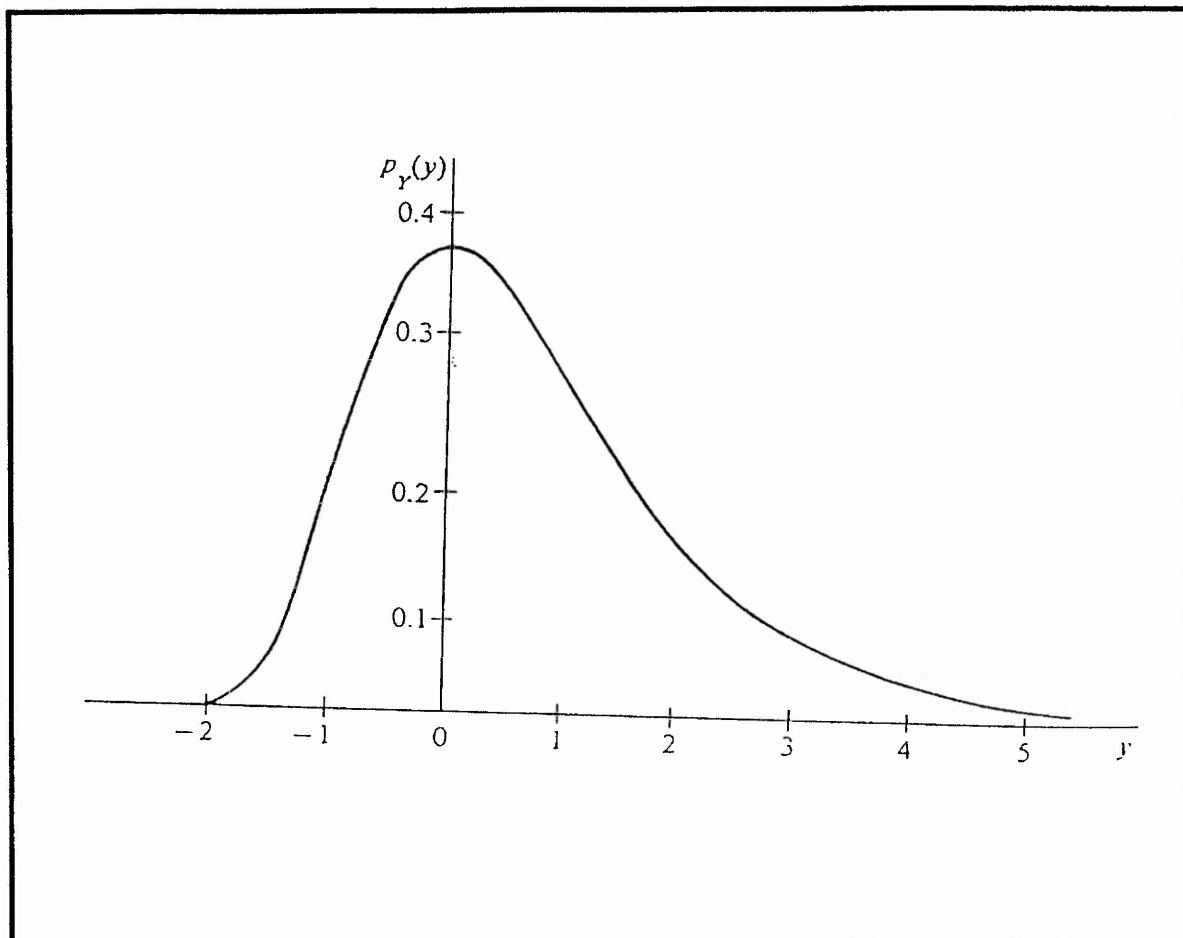
Estimation of the parameters “k”, “ Θ ” and “ σ ”, together with the comparison of the experimental to the fitted data for the 200T-glass fibre bundle and for the most frequent occurring ringdown counts.

Two Parameter log-normal function / Glass Fibres						
Specimen number	“K”	“Θ”	“σ”	f(RDC)_R Real	f(RDC)_F Predicted	I_R/I_F Ratio %
200T-1 G	106	3.018	0.415	0.061	0.050	82.62
	110	3.211	0.299		0.053	87.21
200T-2 G	106	3.050	0.513	0.056	0.042	74.02
	110	3.247	0.353		0.045	79.50
	120	3.588	0.231		0.048	86.22
200T-3 G	106	2.996	0.513	0.070	0.049	70.65
	110	3.195	0.323		0.051	72.65
	120	3.549	0.213		0.053	75.92
200T-4 G	111	3.142	0.669	0.057	0.032	55.85
	115	3.340	0.449		0.032	55.85
	120	3.519	0.348		0.036	63.00
200T-5 G	121	3.658	0.231	0.070	0.045	64.21
	125	3.759	0.199		0.047	66.47
	130	3.872	0.172		0.048	67.75

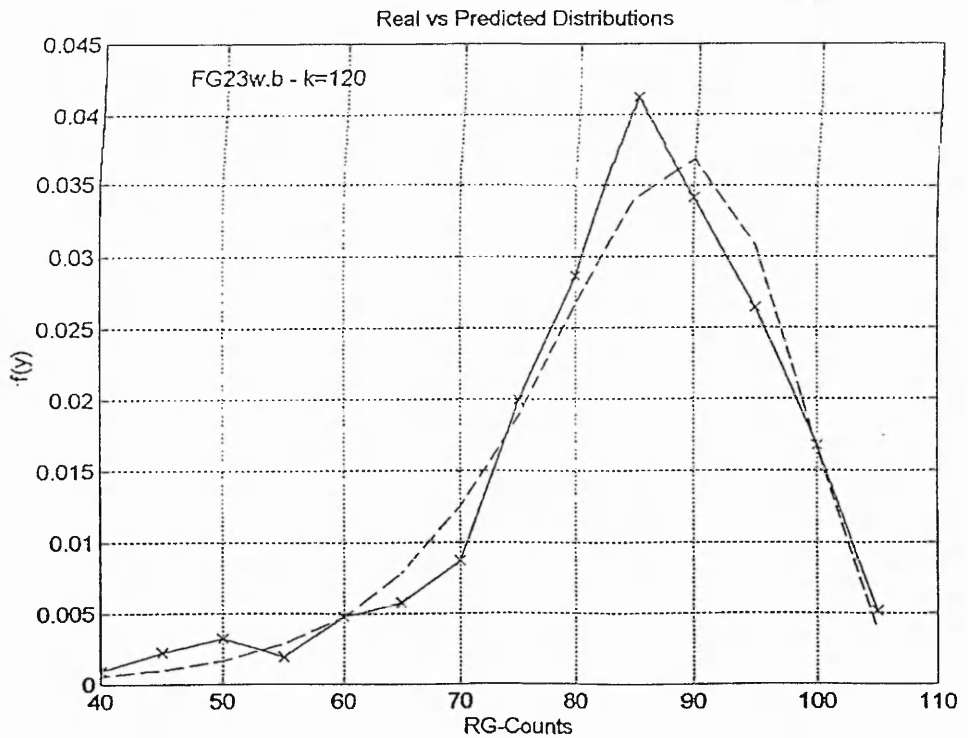
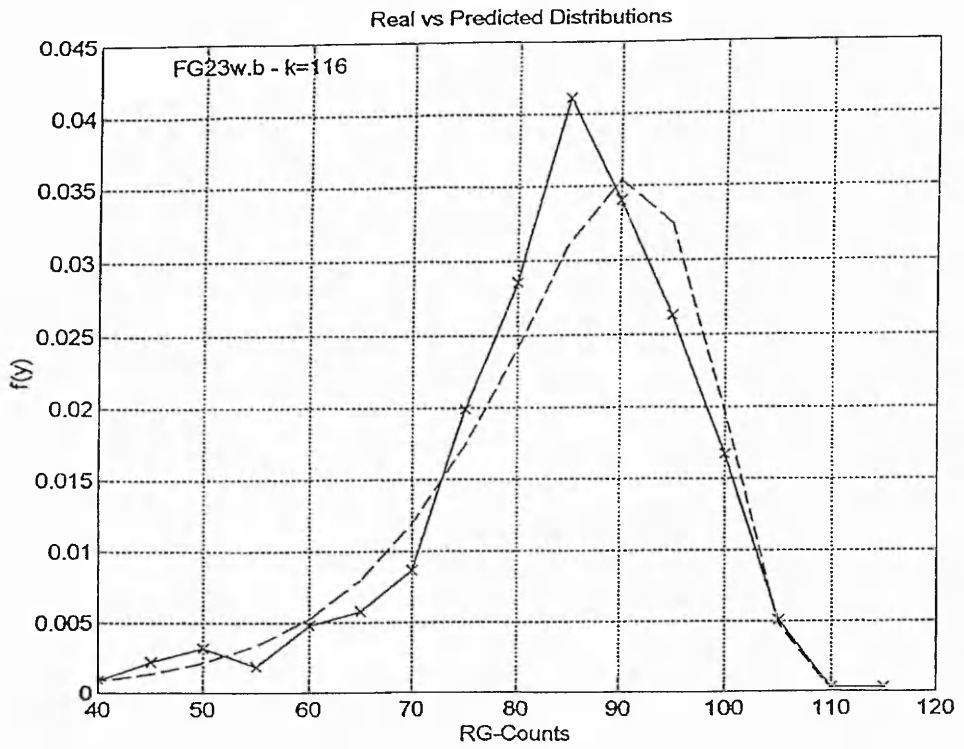
♦ **Table 6.5 b**

Estimation of the average values of the predicted number of events and for k_1 , k_2 , k_3 , for the 200T-glass fibre bundle.

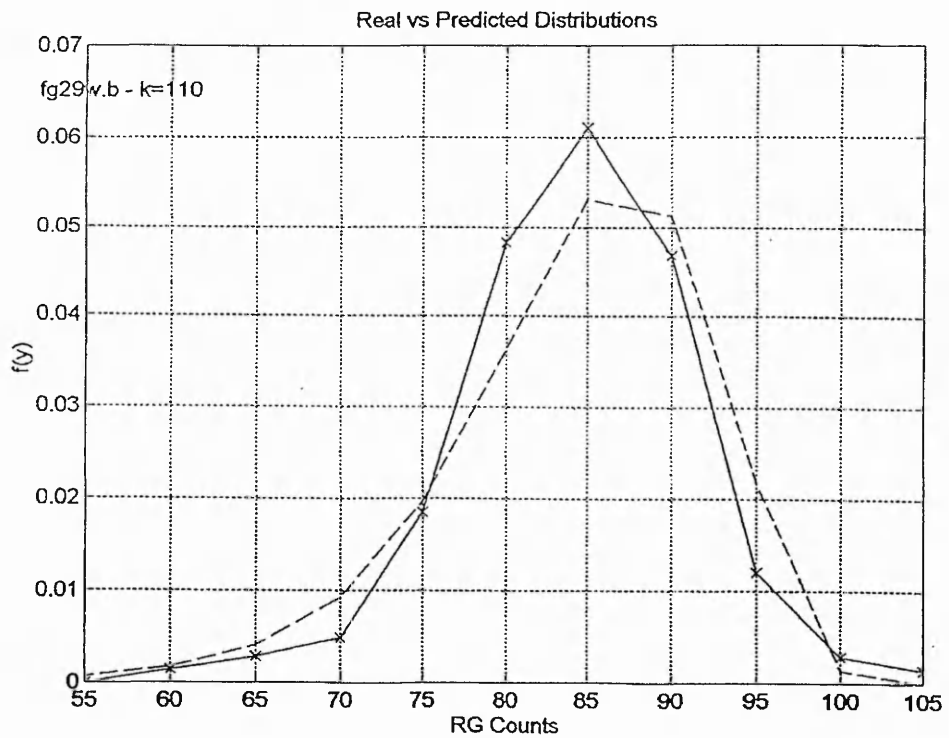
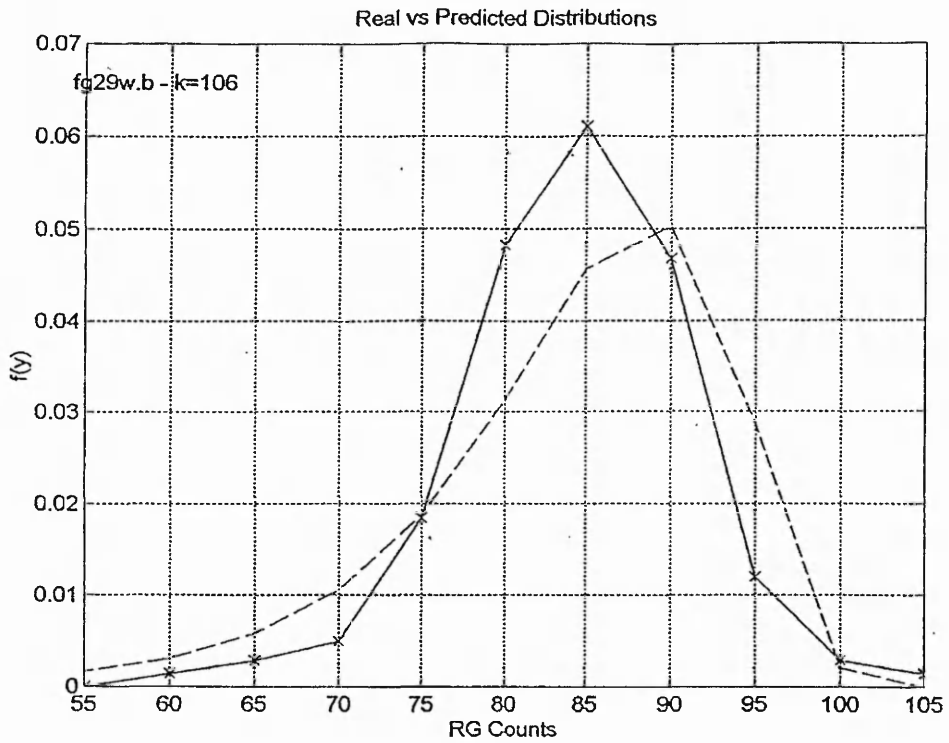
Sample Type	"k"	Average $f(RDC)_R$ Real	Average $f(RDC)_P$ Predicted	f_R / f_P Ratio %
200T-glass	$RDC_{max} + 1$	0.0628	0.0436	69.50
200T-glass	$RDC_{max} + 5$		0.0456	72.60
200T-glass	$RDC_{max} + 10$		0.0462	73.70



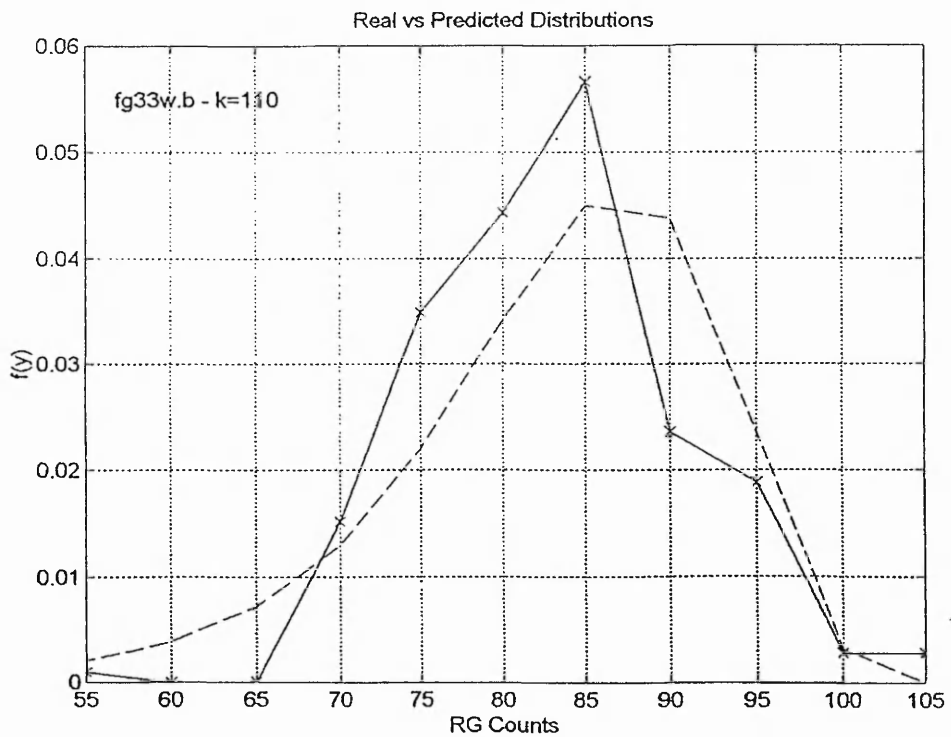
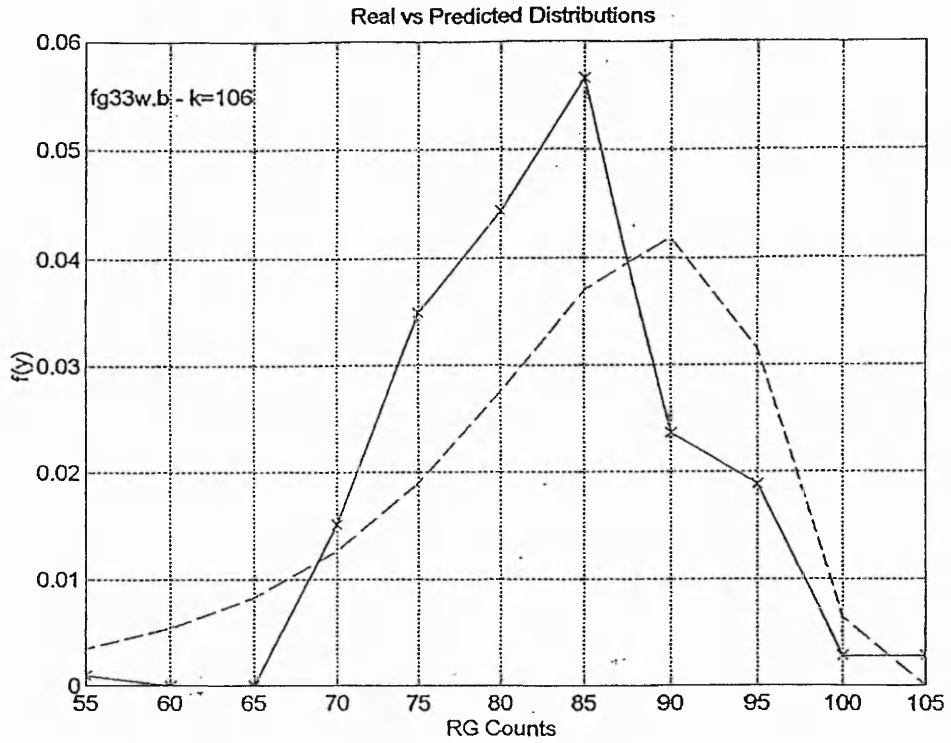
◆ **Figure 6.9:** Typical example of a probability density function in an assymmetric form



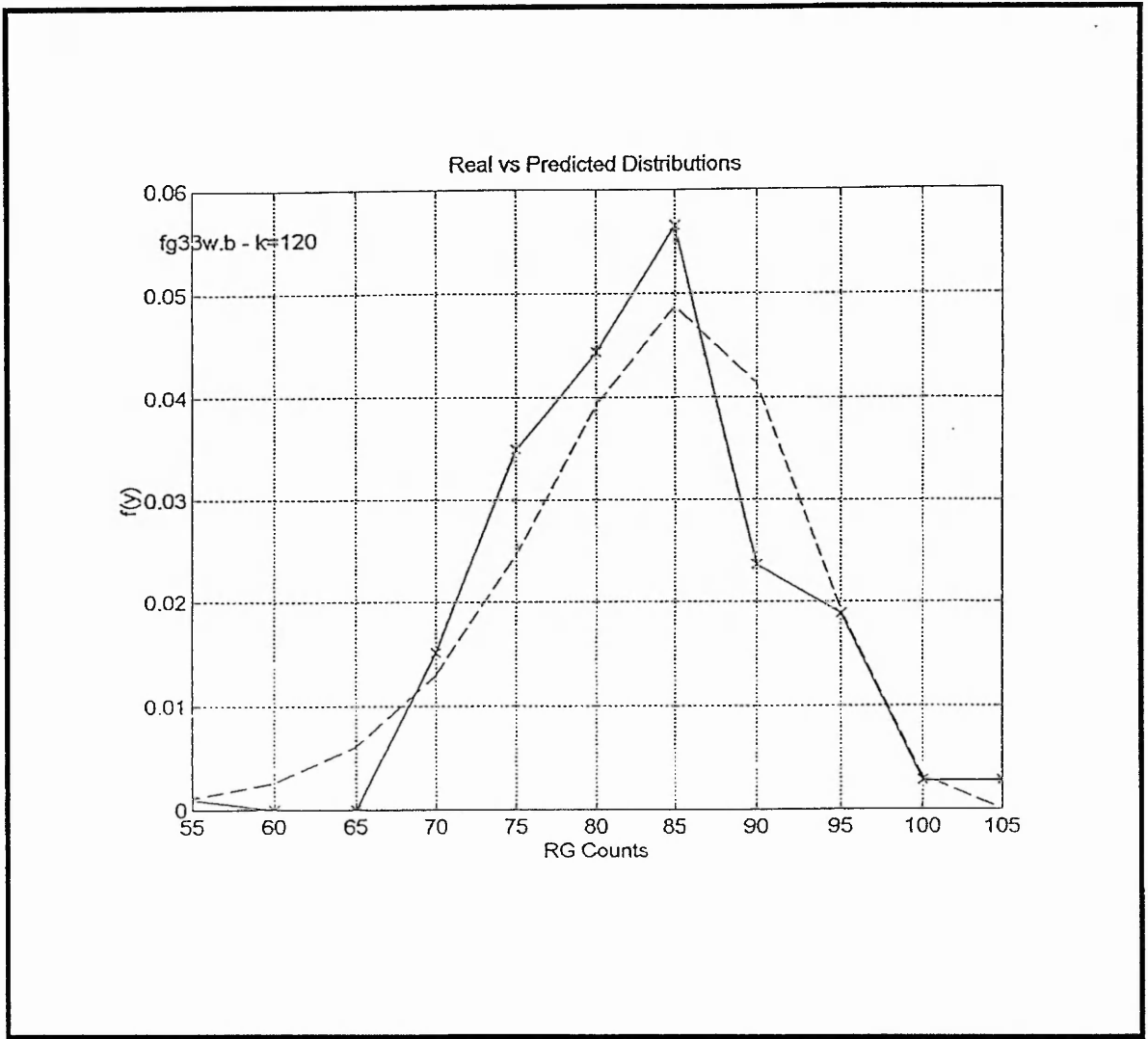
◆ **Figure 6.10 a:** Two parameter log-normal function plots for 19S3 E-glass fibre bundles. Example a) shows a theoretical prediction (---) using $RDC + 1 = K = 116$ and $RDC + 5 = K = 120$.



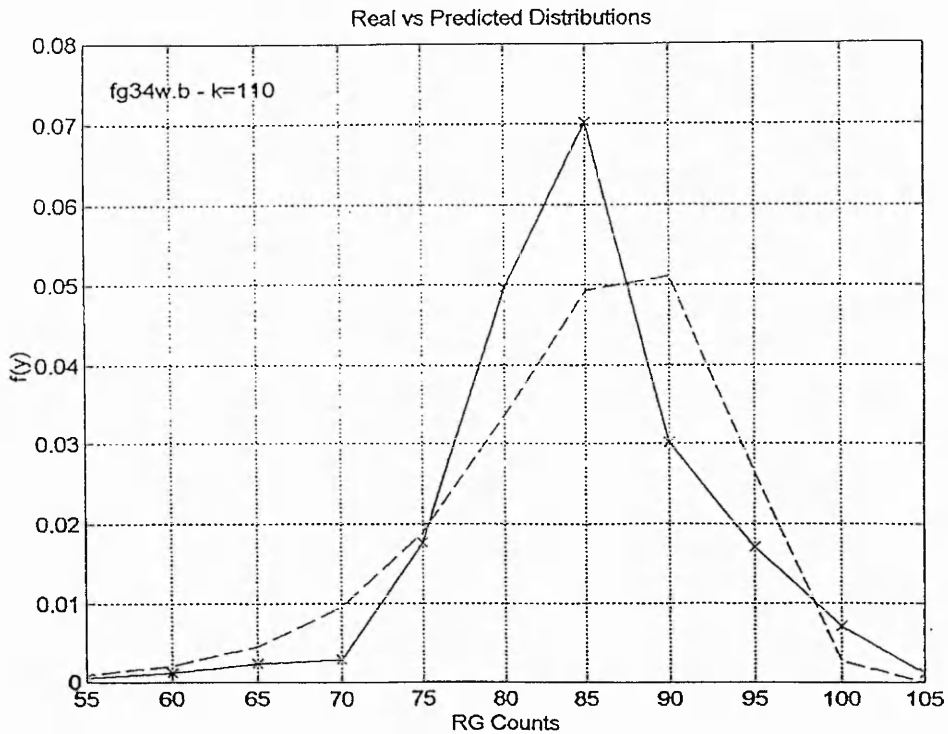
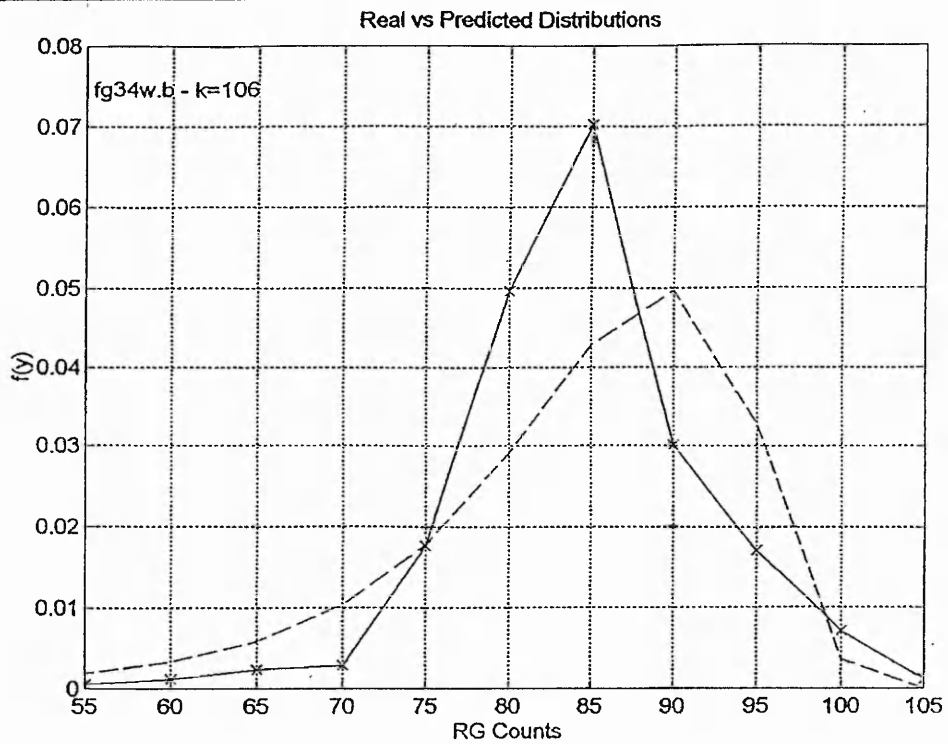
◆ **Figure 6.10 b:** Two parameter log-normal function plots for 19S3 E-glass fibre bundles. Example a) shows a theoretical prediction (---) using $RDC + 1 = K = 106$ and $RDC + 5 = K = 110$.



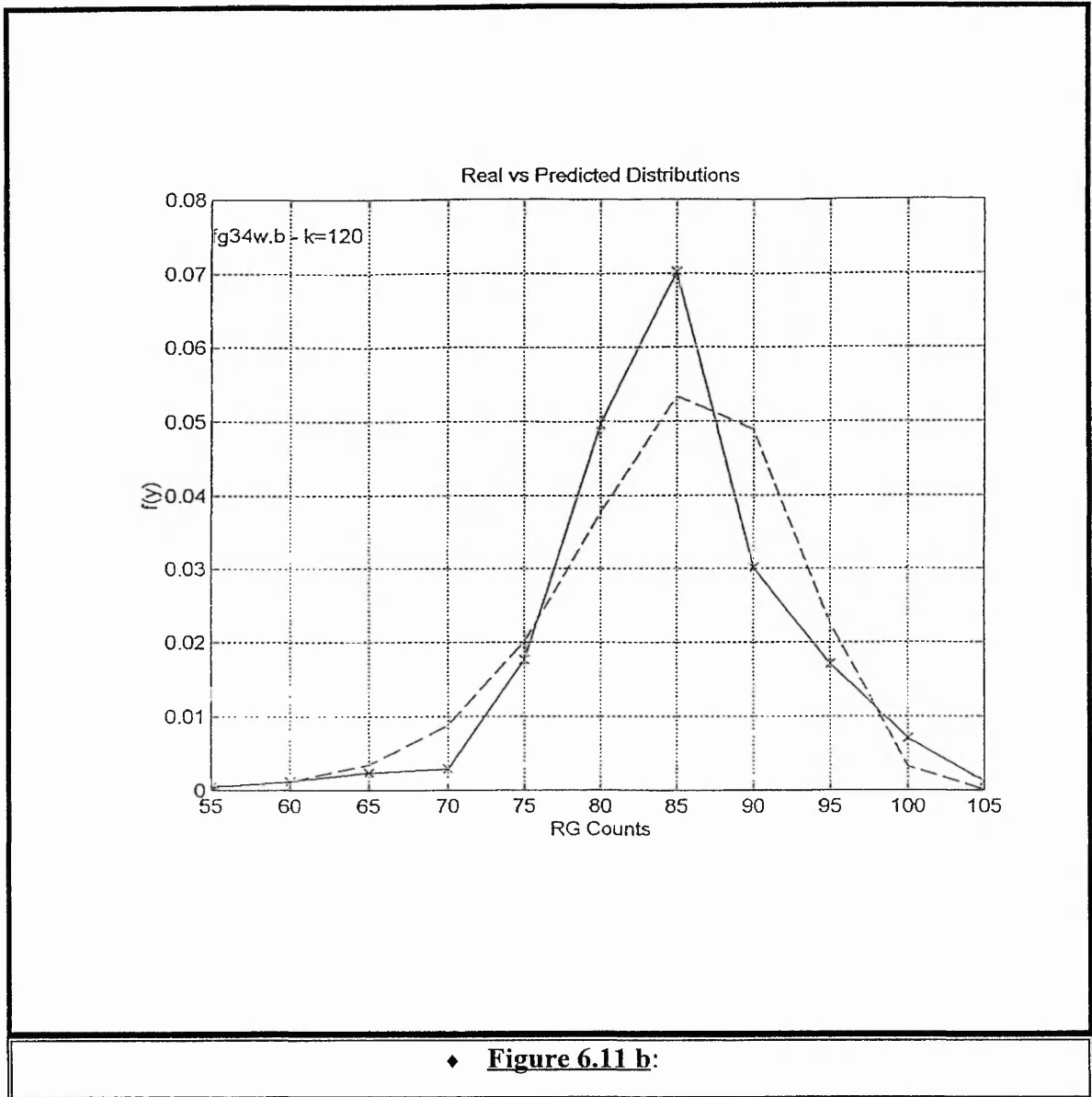
◆ **Figure 6.11 a:** Two parameter log-normal function plots for 200T E-glass fibre bundles. Example a) shows a theoretical prediction (---) using $RDC + 1 = K = 106$, $RDC + 5 = K = 110$ and $RDC + 15 = K = 120$.



◆ **Figure 6.11 a.:**



◆ **Figure 6.11 b:** Two parameter log-normal function plots for 200T E-glass fibre bundles. Example a) shows a theoretical prediction (---) using $RDC + 1 = K = 106$, $RDC + 5 = K = 110$ and $RDC + 15 = K = 120$.



6.7. The Quantile Distribution Function

In the previous two sections, two techniques have been considered for the characterisation of fibre bundles through the corresponding ringdown counts versus number of events distributions. At first by the means of a two parameter Weibull cumulative distribution function, it was possible to fit/predict accurately the right hand side of the asymmetric distributions, as shown in figures 6.6 and 6.7. The second method offered the possibility of improving the accuracy of the prediction by characterising the whole distribution of ringdown counts, as can be seen in figures 6.10 and 6.11. Now a third statistical technique will be examined which has to be resorted to when dealing with materials that exhibit wide scatter of data. This technique is called 'Quantile distribution function'.

As it has been mentioned earlier, statistical techniques are often useful when trying to explain behaviour in materials that exhibit wide scatter in test data. The main purpose of using the statistical models described in this section can be conveniently summarised as follows:

- I. **Description** - The use of the model to display important features in the data.
- II. **Exploration** - The use of the model and other techniques to investigate the behaviour of the data.
- III. **Prediction** - the use of the model to ask very specific 'what if?' questions, particularly in relation to experimental conditions that have not been observed.
- IV. **Decision** - Enabling the user to take more informed decisions.

The well known cumulative distribution function (cdf) is defined by the probability distribution function of [60]:

$$p = F(x) = \text{prob} \cdot (X \leq x) \quad (6.7)$$

The quantile distribution function (qdf) is its inverse given by:

$$x = F^{-1}(p) = Q(p) \quad (6.8)$$

The derivative of $F(x)$ is $f(x)$, the probability density function and the derivative of $Q(p)$ is $q(p)$, the quantile density function. The relation between these functions is:

$$f(x) = \frac{1}{q(p)} \quad (6.9)$$

The quantile distribution function offers a simple approach to many aspects of statistical theory, it provides a natural tool for the construction and choice of statistical models to fit data. It can be shown that quantile distributions can be added [60] resulting in another quantile distribution. This means that it is possible to combine left and right tails of distributions to make a new distribution which is asymmetric as can be shown from figures 6.12a and b. For example, the qdf of the exponential distribution $f(x) = a e^{-ax}$ ($x \geq 0$) is: $x_p = \frac{-\log(1-p)}{a}$. This is a right tail form (Q_p) say. The corresponding left tail form can be found from $-Q(1-p)$ and these can be added to get a two tailed symmetric distributions. If it is assumed without loss of generality that $a=1$, then a two tailed logistic distribution will be obtained, of the form of:

$$Q_1(p) = \log p - \log(1-p) = \log\left(\frac{p}{1-p}\right) \quad (6.10)$$

The flexibility afforded by quantile distribution function theory, means that it is possible to create a skew logistic quantile distribution function in the form of:

$$X_p = Q_2(p) = \lambda + \eta \left[(1+\delta) * (-\log(1-p)) + (1-\delta) * \log(p) \right] \quad (6.11)$$

Where : “ λ “: Controls the position of the distribution.

 “ η “: Control the scale-spread.

 “ δ “: Control the skewness.

This is called generalised lambda distribution. It is possible with the use of the model described by the equation (6.11) to estimate a broad range of models that can

approximate the distribution of data obtained for the 19S3-E-glass and 200C-carbon fibre bundles, distributions which are described in section 6.2 and the corresponding figures 6.1 and 6.3.

6.7.1. Model Estimation

The data obtained from the experimental investigation of glass and carbon fibre bundles is discrete, whereas the model described by the equation (6.11) is appropriate for continuous data. By using the skew logistic it is possible to approximate the discrete data obtained for 19S3-glass and 200C-carbon fibres. The method used evaluates the parameters in (6.11) is non linear and has been employed using the non-linear routine provided by Microsoft Excel Version 5.

The first step is to order the observations in increasing order of magnitude. Thus in the form of:

$$X_{(r)} = Q_{(r)}(p) = Q(p_{(r)}) \quad (6.12)$$

where $X_{(r)}$ is the r th ordered ringdown count value, $Q(p)$ is the QDF of X and $P_{(r)}$ is a mathematical function of r , n and p . In this case, r , is the number of events at a ringdown counts, X and n is the total number of events.

Appendix 2 shows the method of solution in more detail and a number of examples are given. An initial estimation of λ , η , δ is required to enable the non linear procedure to be applied. The equations which are used for this purpose are applied for both the left and right tails of the QDF.

Equation (6.12) describes the distribution of any ordered observation and this fact has been utilised in order to obtain the initial estimates of the corresponding parameters λ , η , and δ , in equation (6.11). The median or middle value, of the distribution can be found by putting $p=0.5$ in a QFD. This result holds for all reasonably behaved continuous distributions. Similarly the upper and lower quantiles and the interquantile range can be

used to obtain initial estimates of the parameters. The trick is to equate model values, with those observed in the data. Set IQR denotes the interquantile range, D the quantile difference and M the median. Appendix 3 describes a number of equations used for the estimation of median, M, upper quantile, UQ, lower quantile, LQ, IQR, quantile difference and Galtons skewness. Then from equation (6.11) and after some algebra, it can be shown that, the quantile distribution function parameters can be obtained as:

$$\hat{\delta} = \frac{D_{data} / IQR_{data}}{D / IQR} \quad (6.13)$$

$$\hat{\eta} = \frac{IQR_{data}}{IQR} \quad (6.14)$$

$$\hat{\lambda} = M_{data} - (D_{data} / D) \cdot M \quad (6.15)$$

where the subscript data corresponds to the values observed from the data observed through the tensile testing of the corresponding fibre bundles.

The non-linear solver in Microsoft Excel is used to minimise

$$S = \sum \left| (X_{(r)}) - M_{(r)} \right| \quad (6.16)$$

Where $M(r)$ are the so-called median Rankit obtainable from equation (6.10) and initial values are provided by equations (6.13), (6.14) and (6.15).

Table 6.6 includes the final estimates for λ , η and δ together with the average error and the error at most and the second most frequently occurring ringdown count, in relation to the number of events. Also as is mentioned earlier, appendix 2 gives a number of examples describing the results obtained by using the quantile distribution function.

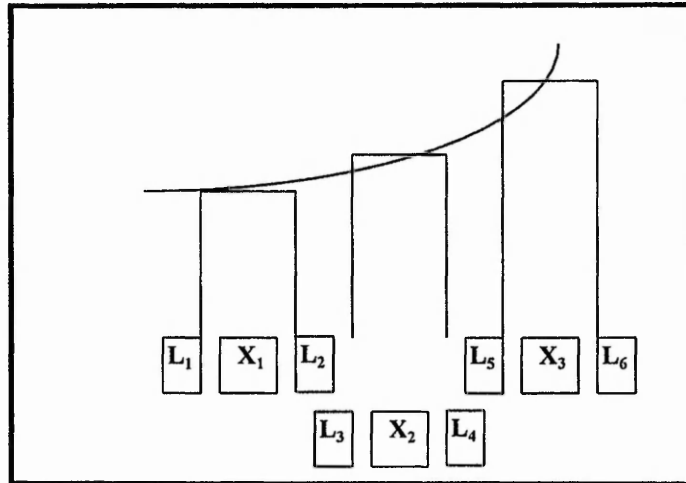
♦ **Table 6.6**

Estimation of Lambda (λ), Eta (η) and Delta (δ) for 19S3 E-glass and 200T carbon fibres, together with calculation of the average error and error at the most frequently occurring (MFO) and second most frequently (SMFO) occurring ringdown count value.

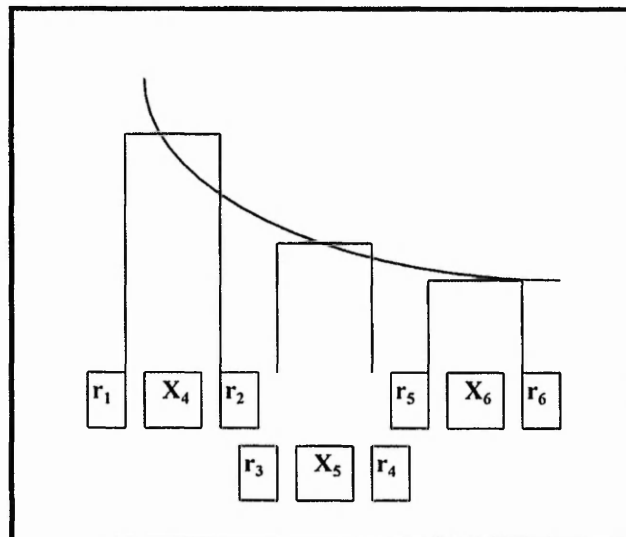
Spc/en Number	Lambda " l"	Eta "h"	Delta "d"	Average Error %	Error @ MFO RDC %	Error @ SMFO RDC %
19S3-1g	83.02	14.89	-0.53	1.63	2.76	1.27
19S3-2g	87.73	14.16	-0.45	1.39	0.246	0.29
19S3-3g	77.39	14.23	-0.44	1.28	3.28	1.75
19S3-4g	83.68	14.02	-0.58	1.59	0.48	0.004
19S3-5g	83.78	6.40	-0.85	0.95	0.69	0.008
19S3-7g	84.35	8.35	-0.012	0.84	0.90	8.7×10^{-6}
200T-1c	72.49	8.24	-0.25	1.86	0.03	3.73
200T-2c	69.80	17.75	-0.49	6.45	6.76	9.8×10^{-4}
200T-3c	70.89	12.61	-0.09	1.92	2.45×10^{-5}	3.46
200T-4c	70.11	10.87	-0.72	5.98	2.46	0.38
200T-5c	62.92	15.62	-0.49	3.76	0.58	2.54

6.7.2 Prediction

The discrete nature of the data means that the smooth curve implied by the model (6.11), will be sub-optimal in general to describe the AE distribution data. Figures 6.12a and 6.12b show how the left and right tails of a distribution may need different treatment in order that smooth curve can well approximate the data in that region.



◆ **Figure 6.12a:** Schematical representation of a left tail distribution.



◆ **Figure 6.12b:** Schematic representation of a right tail distribution.

By obtaining the data which correspond to the corresponding fibre bundles, it is clear that, the left tail has a much shallower slope than the right, reflecting the asymmetric nature of the data. Suppose that it is required to predict $P(X = x_1)$, for example. This value is given approximately by the area under the probability density function between L_1 and L_2 . For the localised region of the left tail it may well be that $(L_2 - L_1) = (L_4 - L_3) = (L_6 - L_5)$, so that the area of approximation will be the same for x_1, x_2, x_3 . However, in the right tail $P(X = x_4)$ will be given approximately by the area r_1 and r_2 under the smooth curve, but $(r_2 - r_1)$ will not be the same as $(L_2 - L_1)$. In predicting $P(X = x_1)$ can be obtained by: (area up to L_2 - area up to L_1). These will be P_{L1} and P_{L2} as for example:

$$L_1 = \hat{\lambda} + \hat{\eta} \cdot \left[(1 + \hat{\delta}) \cdot (-\log(1 - p_{L1})) + (1 - \hat{\delta}) \log p_{L1} \right] \quad (6.17a)$$

and

$$L_2 = \hat{\lambda} + \hat{\eta} \cdot \left[(1 + \hat{\delta}) \cdot (-\log(1 - p_{L2})) + (1 - \hat{\delta}) \log p_{L2} \right] \quad (6.17b)$$

Each of these equations is non-linear in P_{L1} and P_{L2} . A MATLAB programme was written to solve these equations. Appendix 4 describes the programme used. For the set of data which corresponds and characterises the two types of fibre bundles, it is important to decide the values of L_1, L_2 in the left tail and r_1, r_2 in the right tail. The values which were chosen by comparing the observed proportion of counts with a range of proportions (estimated probabilities) obtained by solving equations of the form (6.17a, b). Table 6.7 summarises the corresponding results for just a couple of the 19S3-glass fibre bundles samples.

♦ **Table 6.7:**

Comparison between the predicted probability model and the real (experimental) probability data for 19S3-glass fibre bundles.

Specimen Number	RDC Values	Real Prob/ies	Integral $(L/r_1 - L/r_2)$	Predicted Prob/ies	Percentage of success
19S3-g2	40	0.004	± 0.5	0.004	90.90
624 events	50	0.016	± 1	0.014	83.21
	60	0.024	± 1	0.021	85.41
	70	0.043	± 1.5	0.043	100.0
	80	0.142	± 4	0.143	99.60
	90	0.169	± 5	0.177	95.75
	100	0.083	± 3.5	0.087	94.95
19S3-g4	50	0.017	± 1	0.017	98.30
562 events	60	0.017	± 0.5	0.013	70.05
	70	0.064	± 2	0.066	95.78
	80	0.225	± 6	0.231	97.02
	90	0.145	± 4.5	0.144	99.30
	100	0.0012	± 1	0.014	84.70

6.7.3. Conclusions

In this section a relatively new technique was used, “the quantile distribution function”, to approximate the observed distribution of ringdown counts in relation to the number of events emitted during tensile testing of 19S3-glass and 200C-carbon fibre bundles. The method enabled the asymmetric behaviour of the data to be modelled. The estimated skew logistic distribution enabled predictions to be made of ringdown counts in areas when no experimental data could be collected. It was found that a good approximation to observed behaviour could be achieved by allowing the intervals of approximations to change, reflecting the asymmetry and extreme peakedness of the data. It is therefore possible to characterise fibre bundles, such as glass and carbon, during tensile testing and predict the corresponding distributions accurately.

6.8 Conclusions from the Statistical Analysis of Fibre Bundles

This chapter has considered the characterisation of glass and carbon fibre bundles with the use of the statistical distribution of AE data. The distribution of ringdown counts versus the number of events emitted, during tensile testing, were examined and analysed using Weibull statistics, the two parameter log-normal function, and the quantile distribution function.

Weibull statistics were applied to AE data derived from the corresponding ringdown count distributions. The method was applied successfully to the tail of the asymmetric distributions. By using the modified two parameter Weibull function, it was possible to predict the number of events from the most frequently occurring ringdown count value to the maximum ringdown count value. Values for the shape parameter, m and scale parameter RDC_0 were obtained. The results for the 200T-glass fibre bundles were $m = 7.36$ and $RDC_0 = 85.61$, and for the 200C-carbon fibres, $m = 10.8$ and $RDC_0 = 74.60$. This gives a clear indication of the narrower ringdown count distributions for the 200-C type of fibres. Also it has been shown that for 200C-carbon fibres, that a more uniform distribution of similar defects was present. Finally, the value of RDC_0 gives an accurate indication of the position of each distribution for each type of fibre bundles. This offers the possibility of predicting the ringdown count distribution relative to the AE events and therefore obtain a measure of the properties of the tested fibre bundle systems.

Weibull statistics were able to fit the right hand side of the ringdown count distributions. An additional technique was also investigated and this was the two parameter logarithmic- normal function (equation 6.4). The advantage of this approach was the ability to predict the whole asymmetric distribution rather than the right tail as before. This statistical approach proved to be reliable in predicting the number of events for the 19S3-glass and 200T-glass fibre bundles. Results show that on average a 88% and a 70 % agreement was achieved between the real to the predicted (fitted), data respectively.

Finally, with the use of a skew logistic quantile function and specifically the generalised lambda distribution function, it was possible to improve the fit of the ringdown count distributions. The skew logistic distribution function was in the form of :

$X_p = Q_2(p) = \lambda + \eta \left[(1 + \delta) * (-\log(1 - p)) + (1 - \delta) * \log(p) \right]$, where λ controls the position of the distribution, η controls the scale spread and δ controls the skewness. Typical information given in table 6.7, demonstrated 91%-92% agreement between the real and the predicted ringdown count distributions.

7.1. OVERALL CONCLUSIONS AND FUTURE WORK.

7.1.1. Testing of Transverse E-glass and Kevlar-49 Reinforced Composite Materials Using Acoustic Emission.

In the work carried-out and reported in this thesis, it has been shown that acoustic emission can be used as a convenient means of determining the fracture characteristics of both transverse composites and fibre bundles under tensile testing. AE events were detected and distinguished from each other by either the peak amplitude or ringdown counts, combined with stress-strain data recorded simultaneously.

AE monitoring of E-glass and Kevlar-49 transverse fibre reinforced composite materials under tension has enabled the level of adhesion and the strength of the fibre-resin bond to be determined. This was done for two different E-glass fiber composite systems, cured for seven days at room temperature and post-cured for two hours at 80 °C inside an oven. Experimental results show that the fracture stress for the post-cured samples was significantly higher and a 'noisy-then-quiet' pattern of AE events was recorded, in contrast to a 'quiet-then-noisy' pattern for the cured samples, indicating better adhesion characteristics between matrix and fibre bundle. Also, it was clear that many more severe events were emitted during the low levels of stress-strain curve and higher ringdown counts values were obtained in comparison to the cured samples.

The procedure also provided evidence on the Kevlar-49 resin composite system. Post-cured Kevlar-49 samples exhibited a better level of adhesion than the cured samples. It is also shown that ultrasonic treatment on fibre bundles prior to testing significantly reduced the level of adhesion and interfacial failure stress. Generally, when either, the composite treatment or the fibre system is modified the AE characteristics of the modified system reflect this change together with corresponding, changes in the stress-strain response.

Weibull statistics have been adapted to characterise the amplitude and ringdown count distribution of E-glass composite AE events, by using the associated scale and shape parameters m , RDC_0 or AMP_0 . Weibull parameters extracted from the ringdown count distributions for cured and post-cured samples suggest a tightening of the AE ringdown

count distribution when the sample is post-cured coupled to higher RDC values suggesting a more energetic AE source associated with the more brittle resin phase. Also, they gave accurate information on the most frequently occurring ringdown count value expected and were a useful statistical tool on the prediction of the ringdown count distributions. Generally, it can be said that AE data combined with Weibull statistics provides simple parameters relating AE to changing material condition and can be used for routine evaluation of the level of adhesion and providing monitoring of degradation at the resin-fibre interface.

7.1.2. Testing of E-glass and carbon fibre bundles using AE.

Work has been carried-out determining the strength distributions of E-glass and carbon fibres in a bundle under tension. The three different types of fibre bundles were coated in silicone oil in order to reduce the interfibre interactions and friction and consequently give a set of data which relates more closely to fibre fracture. Fibre break AE events were easily detected and distinguished from other AE events by their relative ringdown count values and it was also possible to monitor the time of AE event occurrence.

The resulting ringdown counts distributions were examined and analysed by the methods of Weibull statistics, two parameter log-normal function and quantile distribution functions. Initially, by using a modified version of the two parameter Weibull cumulative function, it was possible to characterise the fibre systems from the associated Weibull parameters and predict the shape of the corresponding distributions. However, the two later methods improved the accuracy of the fitted ringdown count distribution relative to the real ringdown count distribution and in some cases a 100 % agreement was achieved.

The AE bundle testing technique developed in this work provides a quick, convenient and apparently reliable means of determining the fracture stress and corresponding ringdown count distributions of E-glass and carbon fibre bundles while avoiding many problems associated with the measurements on single fibres. Also, the number of composite materials and their application worldwide increases, so does the challenge of controlling their performance characteristics. It is possible that the technique

investigated in this thesis could be used to characterise a variety of fibre bundles and composite systems and offers the possibility of improved material quality control.

7.1.3. Future Work.

One of the main section of the present thesis was the testing of post-cured E-glass and Kevlar-49 fibre reinforced composite materials inside a conventional electric oven at 80 °C. An alternative method which is possible to use is 'Microwave heating in the manufacture of composites'[73]. Microwave heating, offers inside-out, rapid and uniform heating by interaction of the material with a high frequency (2450 MHz) electromagnetic field. It is important that with this method, power dissipated and temperature rise in the material is uniform achieving a volumetric heating of the composite system.

Heat transfer considerations show that microwave heating is increasingly more efficient than conduction as the material thickness increases, and the thermal conductivity decreases. This happens particularly when the temperature difference between the surface and core of the material is not great. Microwave heating is therefore ideal for most composites. Also low cost of the generator and low pulling forces arising from the use of short dies, makes the process extremely attractive, especially for manufacture of simple but large profiles. Finally, shear strength increase by 10-20 % in comparison to the conventional means and fully crosslinked reaction process can be achieved.

Finally, it is worth mentioning the possibility of extending the statistical methods of the two parameter log-normal function and quantile distribution function to composite materials. This could also be combined with testing in different environments where composites are applied in acid/alkaline environments where glass fibres have recently been developed especially with enhanced corrosion resistance.

<u>APPENDIX 1.</u>

Matlab program designed for the solution of equations 6.4 to 6.4 b. Necessary explanation points are given.

FUNCTION PHYS3 (K)

```
1. % Examples: for K=105:110, k, phys3(K); pause; end;
2. % phys3(110);

3. f = [1 3 6 5 4 6 7 7 11 23 15 23 27 52 53 64 91 114 53 12 3];
4. x-[5:5:110];

5. length (f)
6. length (x)

7. f = f (8:21);
8. x = x (8:21);

9. sumf = sum (f);
10. plot (x, f/(5*sumf));
11. hold on;
12. plot (x, f/(5*sumf), 'yx');

13. c=1;
14. t = sum (f. * log (K-x)) / sumf
15. s = sqrt (sum (f. * (log(K-x)-t ^ 2) / sumf ).

16. y = K - x;

17. z = exp (-0.5 * (log (y) - t). ^2 / (s * s * c * c)). / (y * s * c * sqrt (2 * pi) );

18. maxy = max (f / (5 *sumf)).
19. maxz = max (z).

20. plot (x, z, 'c--');
21. hold off;
```

Analysis of the Program

1. Perform the following operation/procedure for **K=105** to **K=110** and show the results for every step taken.
2. Name of the file/program.
3. '**f**' indicates the number of events for each ringdown count value.
4. '**x**' indicates the steps which should be taken, up to maximum ringdown count value of each distribution - in this example, steps are taken from '5 -110'.
5. Show the length of '**f**' function.
6. Show the length of '**x**' function.
- 7, 8. Calculate and control the distribution from the 8th to the last RDC value and for step number 3. Fit the predicted to the real distribution.
9. Calculate the total number of events.
10. Plot **RDC (x) versus the number of events (y)** - but scale at the same time the Y axis, by dividing it by (Total number of events * 5).
11. Plot the '**real versus the predicted data**' at the same X-Y axis.
12. Plot data.
- 13-15. Equations for the calculation of θ (theta) and σ (sigma).
16. Call **y = K-x** - Chosen constant minus RDC value.
17. Basic density function '**f(y)**'.
18. Show the **maximum for the real events**.
19. Show the **maximum for the predicted events**.
20. **Plot real and predicted distributions**.
21. **End of the program!**

APPENDIX 2.

Examples of Skew Logistic Function and mainly equation 6.11.

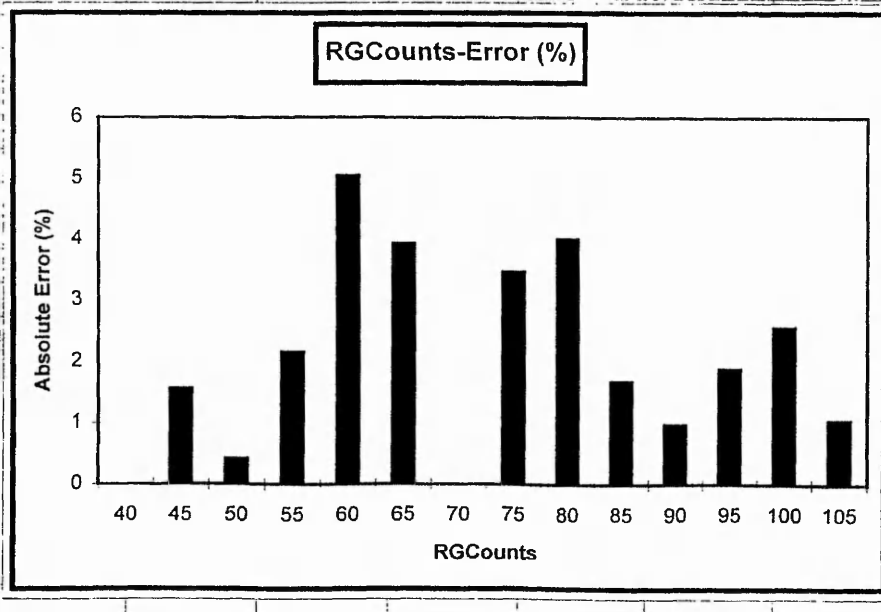
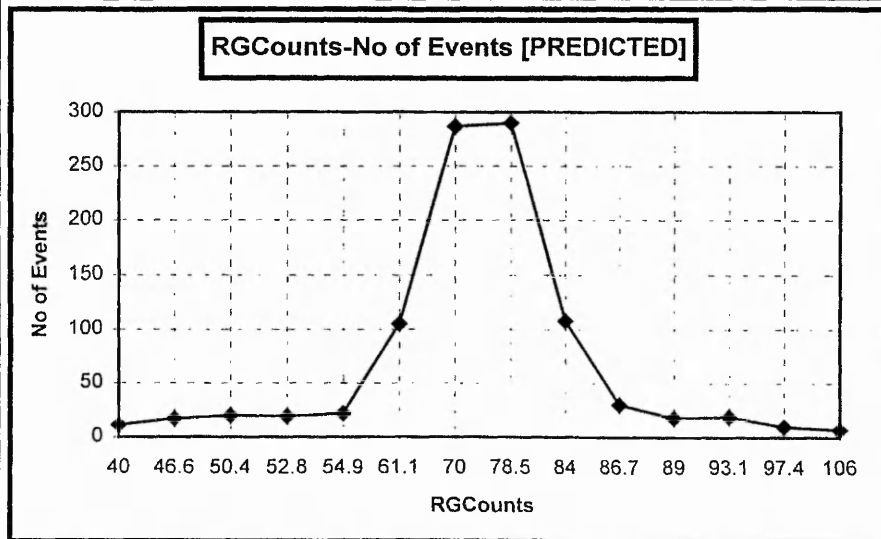
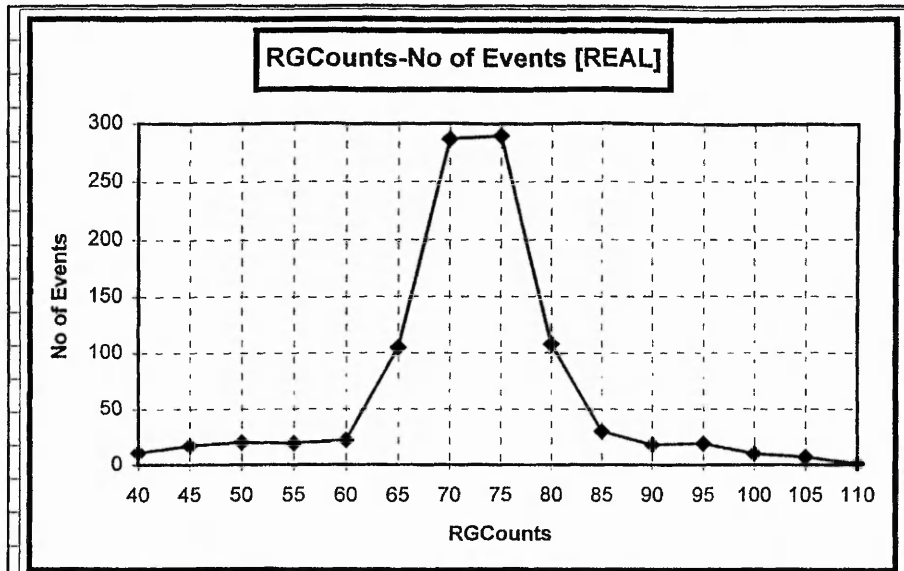
Typical examples are given for a number of 19S3-glass fibre bundles and 200C carbon fibre bundles.

◆ Initial Estimation of Parameters λ, η, δ .

Fitting by the Method of Percentiles							
			Model	"x=lambda+(neta/2)*((1+del)RE+(1-del)LE			
Parameters			Estimated	LQ	LE	RE	Data
			70	Median	-0.69626	0.690043	70
		Position l	7.247268	UQ	-0.15889	1.147157	72.5
		Scale n	0	IQR	0.755463	0.689915	5
		Skewnes d	965	D	0.319275	0.224312	0
		n=		GSk	0.422622	0.325129	0
x	r	r/(n+1)	ln(p)	"-ln(1-p)			
40	11	0.011399	-4.47423	0.011464			
45	17	0.029016	-3.53992	0.029445			
50	20	0.049741	-3.00093	0.051021			
55	19	0.06943	-2.66744	0.071958			
60	22	0.092228	-2.38349	0.096762			
65	105	0.201036	-1.60427	0.22444			
70	287	0.498446	-0.69626	0.690043			
75	290	0.798964	-0.22444	1.60427			
80	108	0.910881	-0.09334	2.417781			
85	30	0.941969	-0.05978	2.846776			
90	18	0.960622	-0.04017	3.234542			
95	19	0.980311	-0.01989	3.927689			
100	10	0.990674	-0.00937	4.674904			
105	7	0.997927	-0.00207	6.178981			
110	1	0.998964	-0.00104	6.872128			

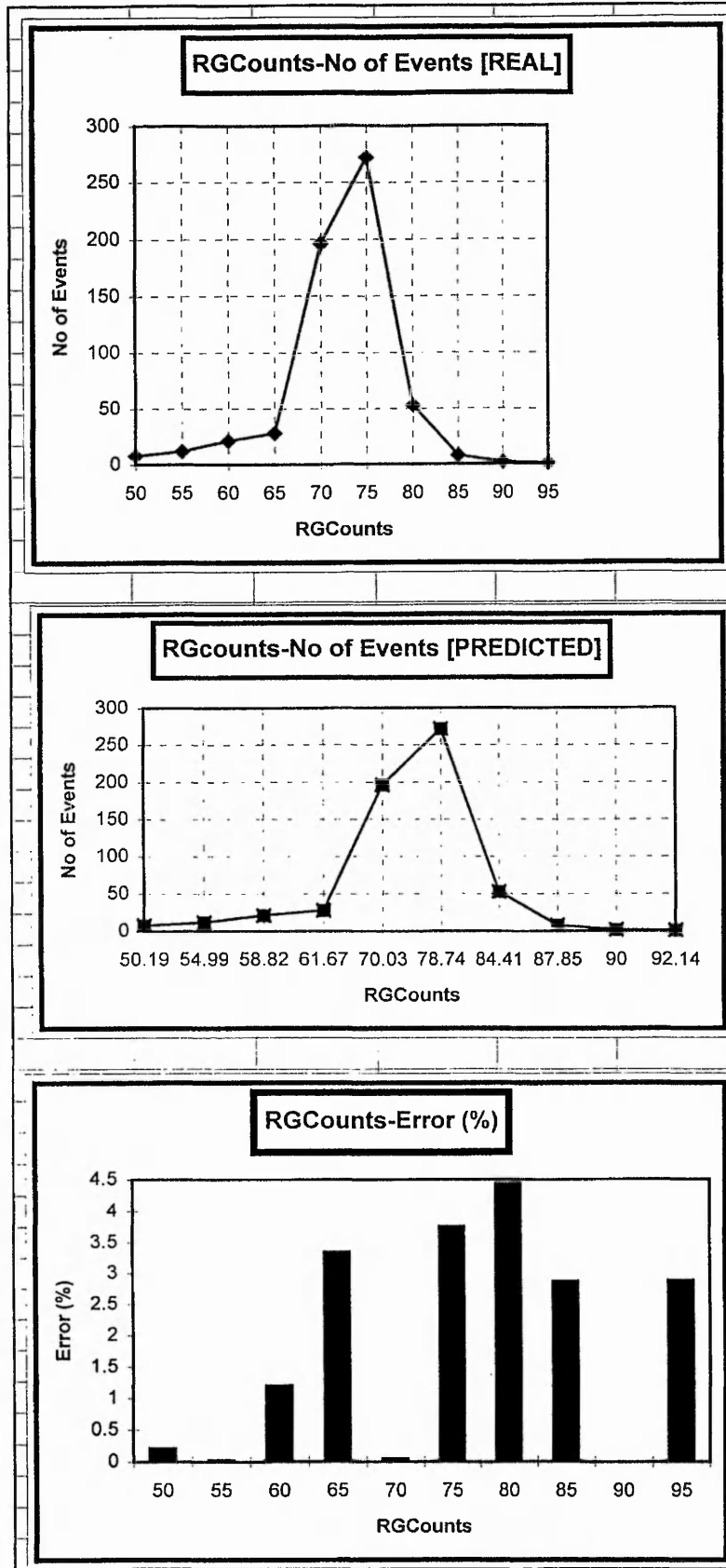
◆ Final Estimation of the Required Parameters.

Fitting by Least Absolute values									
			Model	"x=lambda+(neta/2)*{(1+del)RE+(1-del)LE					
Parameters				Estimated					
	Position	l		70.88959					
	Scale	n		12.61121					
	Skewnes	d		-0.09728					
	n=			965			sumabse	28.75873	
x	r	r/(n+1)	ln(p)	"-ln(1-p)	Q(p)	Error	ABSerror	r	
40	11	0.011399	-4.47423	0.011464	39.9976	0.002397	0.002397	11	
45	17	0.029016	-3.53992	0.029445	46.56444	-1.56444	1.564443	17	
50	20	0.049741	-3.00093	0.051021	50.41658	-0.41658	0.416577	20	
55	19	0.06943	-2.66744	0.071958	52.84319	2.156813	2.156813	19	
60	22	0.092228	-2.38349	0.096762	54.94898	5.051015	5.051015	22	
65	105	0.201036	-1.60427	0.22444	61.06719	3.932807	3.932807	105	
70	287	0.498446	-0.69626	0.690043	70.00002	-2.5E-05	2.45E-05	287	
75	290	0.798964	-0.22444	1.60427	78.46853	-3.46853	3.468525	290	
80	108	0.910881	-0.09334	2.417781	84.00625	-4.00625	4.006255	108	
85	30	0.941969	-0.05978	2.846776	86.68039	-1.68039	1.680389	30	
90	18	0.960622	-0.04017	3.234542	89.0233	0.976698	0.976698	18	
95	19	0.980311	-0.01989	3.927689	93.10922	1.890781	1.890781	19	
100	10	0.990674	-0.00937	4.674904	97.43527	2.564727	2.564727	10	
105	7	0.997927	-0.00207	6.178981	106.0473	-1.04727	1.04727	7	
110	1	0.998964	-0.00104	6.872128	110	1.21E-05	1.21E-05	1	
							28.75873		



◆ Initial Estimation of Parameters λ, η, δ .

Fitting by the method of Percentiles								
			Model	"x= $\lambda + (\eta/2) * \{(1-\delta)RE + (1-\delta)LE\}$ "				
		Parameters			LE	RE	data	
			Estimate	LQ	-1.49334	0.350955	67.5	
		Position	λ	70	Median	-0.82053	0.580175	70
		Scale	η	4.752549	UQ	-0.46739	1.403022	72.5
		Skewnes	δ	0	IQR	1.025946	1.052067	5
			n=	602	D	-0.31968	0.593629	0
					GSK	-0.31159	0.56425	0
x	r	r/(n+1)	ln(p)	"-ln(1-p)"				
50	8	0.013289	-4.32082	0.013378				
55	12	0.033223	-3.40453	0.033787				
60	21	0.068106	-2.68669	0.070537				
65	28	0.114618	-2.16615	0.121736				
70	196	0.440199	-0.82053	0.580175				
75	272	0.892027	-0.11426	2.22587				
80	53	0.980066	-0.02013	3.915351				
85	8	0.993355	-0.00667	5.013963				
90	2	0.996678	-0.00333	5.70711				
95	1	0.998339	-0.00166	6.400257				



APPENDIX 3

Equations describing parameters which lead to the calculation of λ , η and δ .

The search of the Median or middle value, of the distribution can be found by putting $p=0.5$ in order to give the Median Rankit of $M(r) = Q(P_{(r)}, M)$. This result holds for all reasonably behaved continuous distributions and the values of the Median Rankit are together easily obtained through the following set of equations which describe the rest of the variables too.

$$\text{Median} = M = \lambda + \left(\frac{\eta}{2}\right) \cdot 2 \cdot \delta \cdot 2M_R = \lambda + \eta \cdot \delta \cdot M_R \quad (\text{a})$$

$$\text{Upper Quantile} = UQ = \lambda + \left(\frac{\eta}{2}\right) \cdot \left[(1 + \delta) \cdot R\left(\frac{3}{4}\right) - (1 - \delta) \cdot R\left(\frac{1}{4}\right) \right] \quad (\text{b})$$

$$\text{Lower Quantile} = LQ = \lambda + \left(\frac{\eta}{2}\right) \cdot \left[(1 + \delta) \cdot R\left(\frac{1}{4}\right) - (1 - \delta) \cdot R\left(\frac{3}{4}\right) \right] \quad (\text{c})$$

$$IQR = \left(\frac{\eta}{2}\right) \cdot \left[(1 + \delta) \cdot IQR_R + (1 - \delta) \cdot IQR_R \right] = \eta \cdot IQR_R \quad (\text{d})$$

$$\text{Quantile Difference } D = UQ + LQ - 2 \cdot M \quad (\text{e})$$

$$\text{Galtons Skewness} = D / IQR = \delta \cdot G_R \quad (\text{f})$$

APPENDIX 4

Description of the MATLAB programme designed for the calculation of the quantile distribution function parameters.

A) MATLAB PROGRAM

```
function y=peqn(p)
```

```
lambda = 'Give the final estimated value);
```

```
xp =('Give xp1 - xp2');
```

```
eta =('Give the final estimated value');
```

```
delta =('Give the final estimated value');
```

```
y = lambda + eta * ((1+delta) * (-log(1-p)) + (1-delta) * log(p)) -xp;
```

A1) Execution of Bisection method

“ bisect ('peqn',0,1,20,0.01,1,0) “.

It is algorithm to find a root of $f(x)$ by the bisection method with ' 0 ' and ' 1 ' as starting guesses.

where: 'peqn' holds the equation of ' y '.

20: It is the maximum number of iterations.

0.01: It is the required tolerance.

1: defines the type of stopping criterion - selects a test based on the size of the function value.

REFERENCES

- [1]. T.F Drouillard.
Introduction of acoustic emission
Material Evaluation, Vol. 46, (1988), pp 178-179.
- [2]. D. Henning.
Kaiser.J-His achievements in acoustic emission research.
Material Evaluation, Vol. 46 (1988), pp 193-195.
- [3]. H.C Kim, A.P Neto, R.W.B Stephens.
Some observation on AE during continuous tensile cycling of Carbon fibre/epoxy composite.
Nature Physics Science, Vol. 27, No. 74, May 29, (1972), pp 78-80
- [4]. J.M Carlyle.
AE testing F-111.
NDT International, Vol. 22, (1989), pp 67
- [5]. S.L McBride et al.
Journal of Acoustic Emission, Vol. 4, (1985), pp 151-154.
- [6]. T.J Fowler.
R.S Scarpellini, Chemical Engineering, Nov, 1990.
- [7]. R.K Miller.
Tank-bottom leak detection in aboveground storage tanks by using AE.
Material Evaluation, Vol. 48, (1990), pp 822-828.
- [8]. K.P Nerz.
XVth meeting of AWGAE, pp 56-57.

- [9]. I. Sato et al.
Journal of Acoustic Emission, Vol 2, (1983), pp 1-10.
- [10]. W.D Jolly.
Sensor listens for impedance failure of turbo pump bearings.
Material Evaluation, Vol 46, (1988), pp 153.
- [11]. P.T Mc Gowan.
Analysis of failure mechanisms in glass fibre reinforced plastic and AE correlation with a transverse resin crack model.
First international symposium on AE from reinforced composites, The society of plastics industry, Inc. July (1983), pp 19-21,
- [12]. K.Ono
AE behaviour of flawed unidirectional carbon-fibre epoxy.
Proceedings 2nd International Symposium on AE from reinforced composites (Montreal), July (1986), pp 22-28.
- [13]. S.Barre, M.L Benzegagh.
On the use of A.E to investigate damage mechanisms in Glass-fibre reinforced polypropylene.
Composite Science and technology Vol. 52, (1994) pp 369-376.
- [14]. K.Ono, Q.Huang.
Pattern recognition analysis of AE signals.
Progress in AE VII, The Japanese society for NDI, (1994), pp 69-75.
- [15]. W.H Prosser, K.E Jackson et al.
Advanced waveform based AE detection of matrix cracking in composites.
Materials Evaluation, Sept (1995), pp 1052-1058.
- [16]. T.M Ely, E.K Hill.
Longitudinal splitting and fibre breakage characterisation in graphite using AE data.
Materials Evaluation, Feb (1995), pp 288-294.

- [17]. K.Kawamoto, K.Ono.
Pattern recognition, analysis of AE signals from Carbon fibre/epoxy composites.
5th International symposium & exhibition, Society for Advancement of Materials and Process Engineering, (1990), pp 230-239.
- [18]. N.Laws.
Progressive Transverse cracking in composites laminates.
Journal of Composite Materials, Vol 22, Oct 1988, pp 900-915.
- [19]. M.A. Hamstad, R.L. Moore
Journal of Composite Materials, Vol 20, (1986), pp 46-66.
- [20]. B.Harris.
Micromechanisms of crack extension in composites.
Metal Science, Aug-Sept, (1980), pp 351-361.
- [21]. L.Lorenzo, H. Thomas.
Journal of Acoustic Emission, Vol. 5, (1986), 15-24.
- [22]. D. Sheng Li, M.R Wisnom.
Factors Controlling the transverse tensile properties of unidirectional SiC/Ti-6Al-4V.
Composite Engineering Vol 5, No 3, (1995) pp 235-255.
- [23]. J.E Ashton, J.C Halpin and P.H Petit.
Primer on Composite Materials.
Analysis 2nd edn (1984) (Lancaster, PA:Technomic).
- [24]. E.U Okoroafor, R. Hill.
Determination of fibre-resin interface strength in fibre-reinforced plastics using the acoustic emission technique.
J. Phys. D: Appl. Phys. Vol 28 (1995) pp 1816-1825.

- [25]. R. Hill, E.U. Okoroafor.
Relative AE signal parameters to the strength of fibres used in manufacturing of polymeric composites
Ultrasonics, Vol. 32, No. 2, (1995).
- [26]. A.N Netravali, Z.F Li, W. Sasche.
Determination of fibre/matrix interfacial shear strength by an AE technique.
Journal of Material Science, Vol 26, (1991) pp 6631-6638.
- [27]. R. Hill, E.U Okoroafor.
Surface conditions of Kevlar and glass and mechanical properties studied by Weibull statistics and AE.
Composites, Vol.25, No. 10, (1994) pp 913-916.
- [28]. E.U Okoroafor, R. Hill.
Investigation of complex failure methods in fibre bundles during dynamic mechanical testing using acoustic emission and Weibull statistics.
Journal of Materials Science Vol. 30 (1995) pp 4233-4243.
- [29]. R Hill and E.U Okoroafor.
Weibull Statistics of fibre bundle failure using mechanical A.E testing. The influence of interfibre friction.
Composites Vol 26 (1995) pp 699-705.
- [30]. A. Cowking, A. Attou, A. M. Siddiqui, M. A. S. Sweet, R. Hill.
An acoustic emission study of failure by stress corrosion in bundles of E-glass fibres..
Journal of Materials Science Vol 26 (1991) pp 301-306.
- [31]. Z. Chi, T. Weib.
Determination of single fibre strength distribution from fibre bundle testing.
Journal of Materials Science, (1984), pp 3319-3324.

[32]. R.L Smith, R.L Phoenix.

Asymptotic distributions for the failure of fibrous materials under series-Parallel structure and equal load sharing.

Journal of Applied Mechanics, Vol 48, March (1981) pp 75-82.

[33]. P.S Theocaris, J.C Seferis.

Definition of Interface in Composites, In the role of the Polymer Matrix.

The Processing and Structural Properties of Composite Materials, Ed, Plenum Press, New York, (1983).

[34]. P.J Herrera, L.T. Drzal.

Composites Vol. 23 (1992).

[35]. Testing Standard - E1316-97 a.

Non Destructive Examinations, American Society for Testing Materials.

[36]. F.J Guild, M.G Phillips, B.Harris.

AE studies of damage in GRF.

NDT International, Oct (1980).

[37]. M.R Gorman, S.M Ziola.

Plate waves produced by transverse matrix cracking.

Ultrasonics, Vol 29, (1991) pp 245-251.

[38]. Ohara et al

Design of AE transducer by 1-3 piezoelectric composite.

Journal of Ceramic Society of Japan, Int. Edition, (1994) pp.368-374.

[39]. N. Guo, P. Cawley

Transient response of piezoelectric discs to applied voltage pulses.

Ultrasonics, Vol.29, May, (1991) pp 208-217.

[40]. D.E Bray, R.K Stanley

Nondestructive evaluation

McGraw-Hill, (1989)

[41]. Piezoelectric Technology, Data for Designers.

Published by the Vernitron Piezoelectric Division, Bedford, Ohio, a division of Vernitron Corp., © (1981).

[42]. AE Standardisation-A comparison method for calibrating of AE transducers.

Proceedings of the Institute of Acoustics, July, (1981), London.

[43]. R.S Geng.

AE investigations of phase transitions in condensed matter.

Phd Thesis University of London, (1983).

[44]. E.Sancaktar, M.Ma.

Viscoelastic and processing effects on the fibre matrix interface strength part III: The effects of postcure.

Journal of Adhesion, Vol. 38, (1992), pp 131-151.

[45]. D.F Adams.

A micromechanics analysis of the influence of the interface on the performance of polymer-matrix composites.

Journal of Reinforced Plastics and Composites, (1987), pp 666-688.

[46]. A.H Rezaifard.

Investigation of the transverse properties of a unidirectional carbon/epoxy laminate-part 2 laminate properties.

Composite Science and Technology, Vol 52, (1994), pp 287-295.

[47]. D.L. Hiemstra, S.R Sottos.

Thermally-Induced interfacial microcracking in polymer matrix composites.

Journal of Composite Materials Vol 27, No 10 (1993) pp 1030-1051.

[48]. D. Hull.

An Introduction to composite materials. (1981), Cambridge University Press.

[49]. R.L Mehan, J.V Mullin.

Analysis of composite failure mechanisms using acoustic emissions.

Journal of Composite Materials, Vol 5, April (1971), pp 266.

[50]. S.L Phoneix, E.M Wu.

Statistics dependent failure of Kevlar-49/epoxy composites; mechanical modelling and data interpretation; UCRL-53365, Lawrence Livermore National Laboratory, Livermore, Ca, (1983).

[51]. A.Attou

Cracking and stress corrosion cracking in glass fibre materials using acoustic emission.

Phd thesis, CNAA, Sept. (1990).

[52]. B. Bergman.

How to estimate Weibull parameters *Engineering with ceramics*.

2nd meeting Vol 37, part 39, (1987) pp 175-187.

[53]. H.E Daniels.

The Statistical theory of the strength of bundles of threads.

Proceedings of Royal Society London, A 183, 1945, pp 405-435.

[54]. E.U Okoroafor, R.Hill.

Relating AE signal parameters to the strength of fibres used in manufacture of polymeric composites.

Ultrasonics 1995, Vol 2, pp 123-131.

[55]. K.V Steiner, et al.

Ultrasonic NDE techniques for the evaluation of matrix cracking in composite laminates.

Composites Science and Technology, Vol. 53, (1995), pp 193-198.

- [56]. B.Harris, A.D Ankara.
Cracking in composite of glass fibre and resin.
Proceeding of Royal Society (London), (1978) pp 229-250.
- [57]. D.S Li, M.R Wisnom.
Factors Controlling the transverse tensile properties of unidirectional SiC/Ti-6Al-4V.
Composite Engineering, Vol 5, No 3, (1995), pp 235-253.
- [58]. Q.Huang, K.Ono.
Pattern Recognition analysis of AE signals. Progress in AE VII.
The Japanese Society for NDI, 1994, pp 69-78.
- [59]. L.N Johnson, S. Kotz, Balakrishnam
Continuous distributions 2nd Edition, Interscience Publication, (1994), Vol 2.
- [60]. W.Gilchrist.
Modelling with quantile distribution function.
Journal of Applied Statistics, Vol 24, No 1, (1997), pp 113-122.
- [61]. W.Weibull
Journal of Applied Mechanics, 18 (1951), pp 293.
- [62]. B.Sugarman.
Strength of glass (A review).
Journal of Material Science, Vol. 2, (1967), pp 275-283.
- [63]. A.A Griffith.
The Phenomena of rupture and flow in Solids.
Phil. Trans. Roy. Soc. a221 (1920), pp 163
- [64]. B.D. Coleman
Journal of Applied Physics, 29, (1958), pp 968-983.

- [65]. W.F. Thomas
An investigation of the factors affecting the strength of glass fibre strand, Part 4. The effect of surface area.
Glass Technology, Vol 13, No 5, Oct (1995).
- [66]. N.Sato
3rd International Symposium on AE Composite Materials (1989), Vol 42 Paris.
- [67]. M.A Hamstad
Fundamentals of AE edited by K.Ono (UCLA, California), (1979), ch. 9, pp 229-259.
- [70]. B. Harris, A. Fuwa.
An evaluation of AE techniques applied to carbon fibre composites.
Journal of Physics D, Vol. 9, (1976), pp 353-364.
- [71]. P.W Manders, T.W Chou
Journal of Reinforced Plastic Composites, Vol 2, (1983), 43.
- [72]. O.L. Davies, P.L. Goldsmith.
Statistical Method in Research and Production.
ICI Longman Group Ltd, (1980).
- [73]. J.M Methren.
Microwave heating in the manufacture of composites.
Material Technology 9, no (7/8), July/August (1994) pp 163-165



Characterization of transverse failure in composites using acoustic emission

R. Hill ^{a,*}, R. Brooks ^b, D. Kaloedes ^a

^a Centre for Research in Materials Science and Engineering, Department of Chemistry and Physics, The Nottingham Trent University, Clifton Campus, Nottingham, NG11 8NS, UK

^b Department of Mechanical Engineering, University of Nottingham, Nottingham, NG7 2RD, UK

Accepted 30 July 1997

Abstract

Composites materials provide a strong, lightweight material suitable for engineering applications. Degradation of these materials is by propagation of a range of defects which ultimately control failure. Acoustic emission (AE), an ultrasonic method for materials characterization, provides one of the most sensitive techniques for monitoring this material degradation and has advantages over both conventional ultrasonic and radiographic methods. Since composite materials used for engineering applications are manufactured by cross-ply methods, transverse failure is an important damage mechanism in controlling the initiation of damage in a complete composite. These defects cause stiffness degradation which may be lifetime limiting in, for instance, stiffness dependent aerospace applications, ultimately leading to initiation of delamination. Transverse samples of glass-polyester resin have been monitored using acoustic emission as they are taken to mechanical failure. Results presented consider the AE produced by transverse composite material in cured and post-cured conditions. The pattern of AE indicates the fact that the resin toughness has increased due to post cure. Weibull statistics have been applied to acoustic emission event parameters in the case of a transverse composite, although this particular application of the statistics does not bear a fundamental relationship to the microscopic damage mechanisms. Weibull statistical parameters associated with AE signals have proved useful in signalling the changing condition of these materials and monitoring the onset of damage. Transverse cracking in fibre bundles is considered, with acoustic emission providing a sensitive method for real time detection of cracking. AE provides a unique view into the micromechanics of defect initiation and growth. © 1997 Elsevier Science B.V.

Keywords: Author please supply keywords

1. Introduction

Acoustic emission operates using resonant or wide-band transducers in the ultrasonic frequency range from 100 kHz to 1 MHz. It has been widely used to monitor polymeric composites and has the advantage of being highly sensitive to the initiation and growth of damage within these materials. Polymeric composites are usually a two-phase system consisting of a thermosetting resin and bundles of reinforcing fibre, which might be glass, Kevlar, carbon, etc. The function of the fibres is to enhance the stiffness of the composite in the load direction and increase the strength [1-3]. To deal with the need for multi-axial loading of these materials and the elimination of mechanically weak directions, com-

plex patterns of fibre lay-up may be used. When a composite is subject to mechanical loading, although the longitudinal fibres bear the load, transverse cracking can occur between the transverse fibres and resin. This damage mechanism may have an effect on the ultimate survival of the composite, modifying the material elastic modulus, affecting the service lifetime of the material in, for instance, the case of aerospace applications of composites and when the material is used in a hazardous environment, affecting the service lifetime of the material, where transverse cracking can provide a route for ingress of fluids.

The fibre system used consists of bundles of fibres with diameters of the order of 10-15 µm. Fibre adhesion is usually evaluated using single fibres [4], although in the case of the testing reported here, a complete fibre bundle is used with the load applied transverse to the resin fibre interface. By using a complete fibre bundle,

* Corresponding author. Fax: +49-115-948-6636; e-mail: roger.hill@ntu.ac.uk

the system more accurately reflects the situation in an engineering composite. Transverse strength evaluated in this way is of interest since the testing of transverse composites, combined with acoustic emission, has been proposed by us as a way of evaluating the 'quality' of the resin–fibre interface [5]. Although a number of other methods exist based on the use of single fibres of glass, Herrera and Drzal [4] suggested that these methods have difficulties, which we believe can be resolved or clarified, using transverse testing and AE. Acoustic emission, as a technique of materials evaluation, has the advantage of being 'real time' and sensitive, providing the opportunity for continuous monitoring of materials.

The work reported here considers the mechanical testing of transverse composites consisting of a bundle of fibres set in a polyester resin. The acoustic emission produced by the transverse composite was obtained during testing to mechanical failure to evaluate the AE and mechanical characteristics of the material and assess the effect of material changes such as post-cure of the composite.

2. Aims of the work

Mechanical information on composite materials is obtained using mechanical testing to failure with stress–strain information monitored. Acoustic emission is able to provide more detailed information about intimate changes in the damage structure within these materials as load is increased. AE is able to monitor material properties such as interfacial bonding between resin and fibres and micro-crack propagation.

To carry out this evaluation of the test material using AE, parameters are usually extracted from AE signals since the AE signal often consists of discrete AE events. Our work has been aimed at characterizing material changes by detecting general changes within the AE profile and by detecting changes within the statistics of these AE parameters. One effective means to do this has been to use statistical parameters associated with Weibull statistics. Weibull statistics enables the quantification of two associated statistical parameters extracted from AE data (scale and shape parameters), which can be used to characterize the material change

3. Acoustic emission–mechanical testing system and materials

The acoustic emission system and mechanical testing system used is shown in Fig. 1. A monotonic load was applied to samples at a strain rate 0.5% per minute using a Lloyds 6000R tensile testing machine under computer control, with load and strain acquired automatically. Acoustic emission emanating from samples

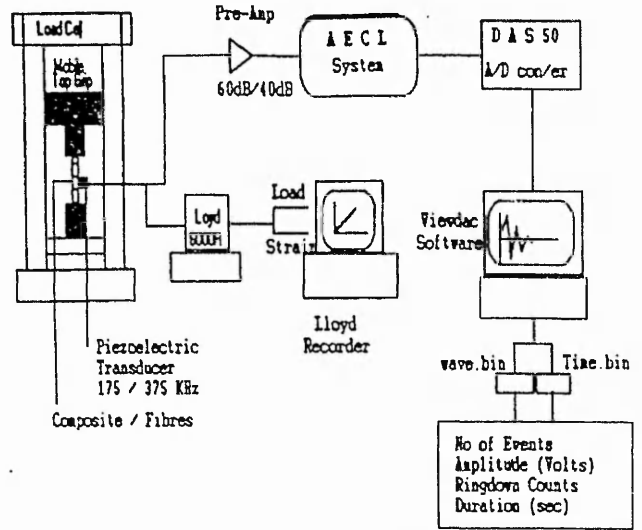


Fig. 1. System used for mechanical and acoustic emission testing of transverse bundle fibre composites.

was detected by a 375 kHz transducer attached to the test specimens. AE was pre-amplified and post-amplified followed by waveform capture using a DAS50 analogue-to-digital converter board. Computer software (VIEWDAC) allowed the capture of AE event waveforms into a file 'wave.bin' with an associated time stored in 'time.bin'. The software allowed signal parameters such as amplitude, ringdown-count and duration to be evaluated from these captured waveforms.

The specimens tested were 'dog-bone' shaped (Fig. 2), with composite gauge dimensions being 40 × 5 × 2.5 mm. A single fibre bundle was cast into the centre of the narrow cross-section and transverse to the applied load. All damage events and associated AE emanated from this transverse fibre region associated with microcrack generation.

The polyester resin used was provided by Scott Bader Co. Ltd and consisted of 100 parts Cristic Polyester 272 resin, 2 parts catalyst M with 0.4–1.2 parts of cobalt accelerator E in styrene. The resin was poured into prepared dog-bone-shaped moulds and cured for 7 days at room temperature. Post-cured samples were placed in an oven for 2 h at 80°C. A cross-section of the fibre bundle, obtained by optical microscopy, is shown in Fig. 3. This clearly shows the presence of interfibre

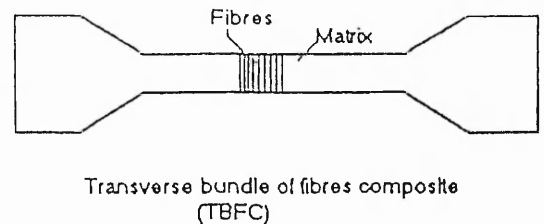


Fig. 2. Geometry of the transverse fibre bundle composite.

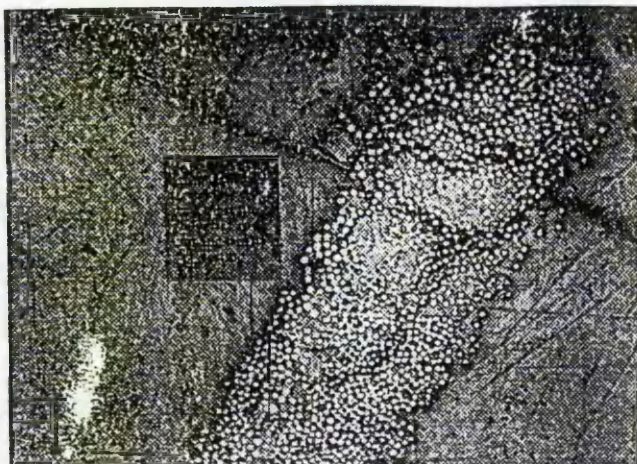


Fig. 3. Cross-section of a fibre bundle showing interfibre cracks responsible for acoustic emission.

The data from these room-cured samples are characterized by a stress-strain graph which curves over and which are characteristic of the mechanical deformation of a polymer. The main component of the test sample is, of course, polymer. Each acoustic emission event appears as a point on the graph, with the points joined by straight lines in order of increasing time (extension). In Figs. 4 and 5, the AE appears as occasional 'early' events. A second, later, region of AE activity begins as the stress-strain curve begins to turn over occurring at a gross specimen strain of $\sim 2.3\%$. It should be noted that this figure is after correction for the flat portion of the stress-strain curve associated with specimen slip in the grips. This often occurred due to the nature of the polyester surface. It is significant that no AE events were detected in this region. It appears that the likely slight friction noise associated with this process was not detected acoustically and confirms the source of detected AE, which is from the transverse fibre region of the sample.

Figs. 6 and 7 show acoustic emission and mechanical test data for specimens which had been further 'post-cured' in an oven at 80°C for 2 h. This is a procedure sometimes adopted in composite manufacture, causing the cross-linking chemistry to complete. It can be seen, from Figs. 6 and 7, that the stress-strain curve straightens up (evidence that the resin phase has become more brittle). It is also worth noting that the failure stress rises from ~ 27 MPa in the case of room-cured samples, to over 40 MPa in the case of post-cured samples.

In the case of the room-cured specimens (Figs. 4 and 5), intense (late) AE activity is followed by material failure. In the case of the post-cured specimens, intense AE activity begins at a relatively low gross sample

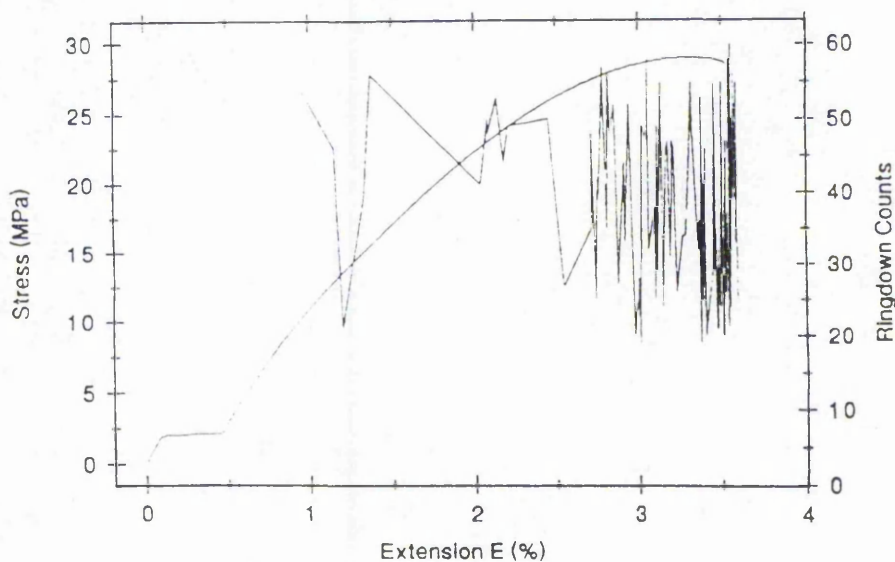
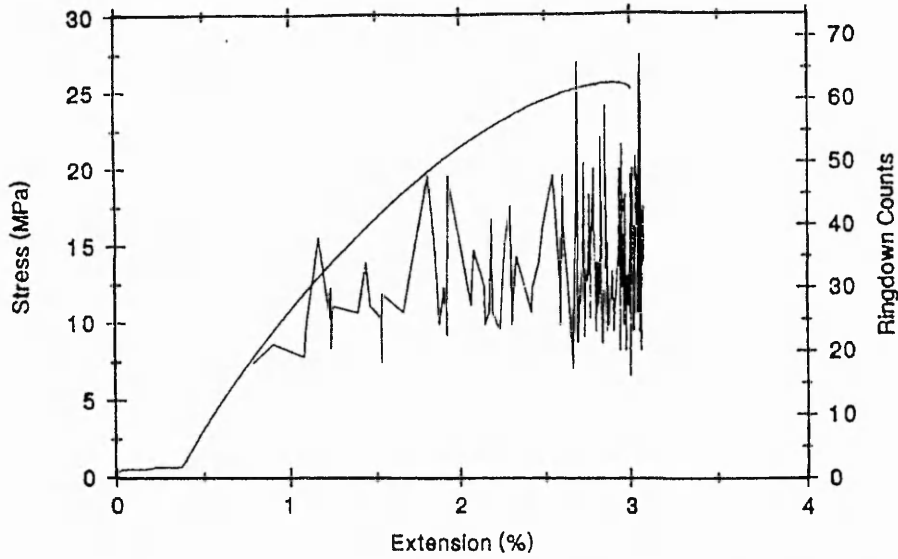
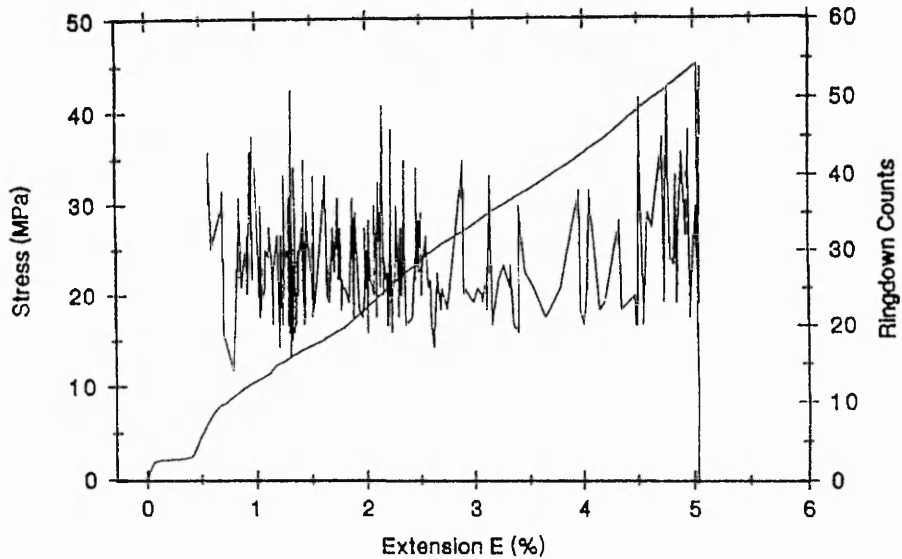


Fig. 4. Stress-strain (extension %) data and AE data (ringdown counts per AE event) for a 7 day room-cured transverse composite.



29
30

Fig. 5. Stress-strain (extension %) data and AE data (ringdown counts per AE event) for a 7 day room-cured transverse composite.



34
35
36

Fig. 6. Stress-strain (extension %) data and AE data (ringdown counts per AE event) for a 7 day room-cured and 2 h post-cured transverse composite.

203 strain. However, in this case, the stress continues to rise,
204 but AE activity subsides somewhat, while in some
205 specimens it picks up again immediately prior to speci-
206 men failure.

207 Clearly, the effect of post-curing the specimens has
208 been to increase the stiffness of the resin, but also the
209 toughness of the resin. Defects and damage begin to
210 propagate at an early stage during the mechanical testing
211 of the specimen and, in most cases, a rising AE rate is
212 an indicator of imminent failure. In this case, the damage
213 is arrested by a tough interfibre resin phase, the AE
214 event rate falls, and only picks up again close to failure.
215 The AE behaviour of transverse specimens appears as

'quiet- noisy' for room-cured specimens and
'noisy-quiet' for post-cured specimens.

5. Weibull statistic applied to composite material systems

Our work has previously considered the application
of Weibull statistics to the failure of composite material
systems using acoustic emission in unique ways [6-8].
One component of the composite is the fibre system.
Fibre bundles of hundreds of fine fibres are used to
reinforce composites in the longitudinal direction, and
the statistical spread of the fibre strength is an important

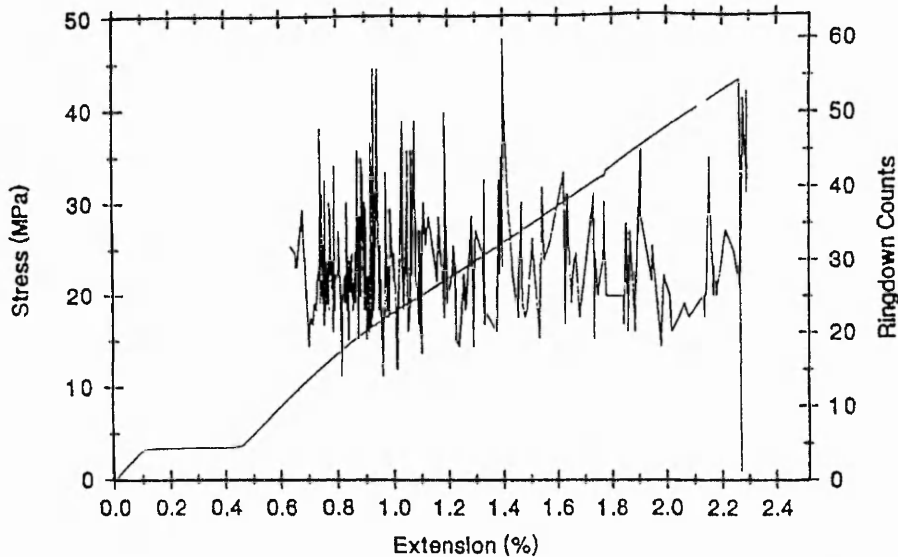


Fig. 7. Stress-strain (extension %) data and AE data (ringdown counts per AE event) for a 7 day room-cured and 2 h post-cured transverse composite.

factor for material quality control. We have studied the statistics of fibre failure using acoustic emission [6,7].

When using Weibull statistics on fibre bundle failure [6], the stress-strain curve can be predicted using an equation of the form:

$$\sigma = E_f \epsilon \exp[-L(\epsilon/\epsilon_0)^m], \quad (1)$$

where σ is the instantaneous fibre bundle stress, ϵ is the instantaneous fibre bundle strain, ϵ_0 is the Weibull distribution strain-scale parameter and m is the Weibull shape parameter with L being the normalized fibre length. This equation predicts the shape of the fibre bundle stress-strain curve and the shape is determined by the underlying statistics of fibre failure. Acoustic emission can monitor the failure of these fibres, fibre by fibre, if the measurement system is calibrated to do this. In this case, the surviving fibre number in the fibre bundle, N_s is given, in terms of increasing bundle strain ϵ , by the Weibull equation:

$$N_s = N_0 \exp[-L(\epsilon/\epsilon_0)^m], \quad (2)$$

where N_0 is the initial number of fibres.

6. Application of weibull statistics to transverse failure

The Weibull equation is highly versatile and can be formulated to account for a range of statistical processes. The propagation of transverse cracks in the transverse fibre bundle is complex and does not conform to the weak link ideas implicit in much of the use of Weibull statistics. Our use of the statistics in characterizing transverse failure has been entirely empirical, with the aim of extracting two material-related parameters

derived from acoustic emission data, which characterize and differentiate material condition. Our use of the equations has been formulated in terms of the number of AE events with a specific ringdown count value (RG) and the number of AE events with a particular amplitude (AMP).

In this case, the appropriate Weibull equations become:

$$N_s = N_0 \exp[-(RG/RG_0)^m], \quad (3)$$

in terms of ringdown counts, and

$$N_s = N_0 \exp[-(AMP/AMP_0)^m], \quad (4)$$

in terms of AE amplitude. Logarithmic plots of these equations can be used to extract the equivalent Weibull scale and shape parameters.

An example of this kind of plot is shown in Fig. 8, where $\ln \ln(N_s/N_0)$ is plotted against $\ln(RG)$. The data are used in the form of the number of AE events plotted as a ringdown count distribution. The values of m and RG_0 can be obtained from Fig. 8. On back substitution of m and RG_0 , the relatively good agreement between the theoretical and experimental data is seen. (Fig. 9).

The average values for m and RG_0 are given in Table 1. Although the specimen numbers are relatively small, the values do suggest expected changes. A high value of m signifies a tighter statistical distribution. Post-curing might be expected to generate a resin with more uniform mechanical and fracture characteristics. The values for m in Table 1, derived from acoustic emission data suggest this.

RG_0 , significantly, moves to a higher value. The RG_0 value indicates the position of the distribution on the ringdown count axis (Fig. 9). For a more brittle mate-

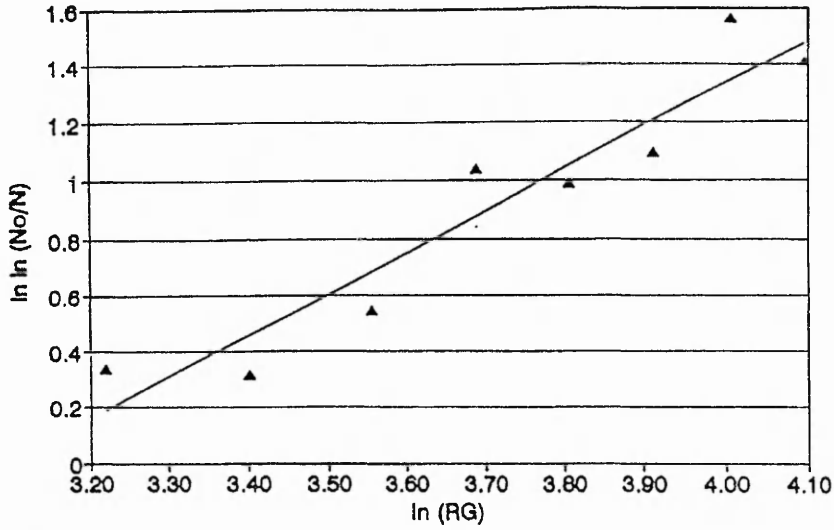


Fig. 8. Ln Ln plot of number of event against ringdown counts linearized to allow evaluation of Weibull parameters.

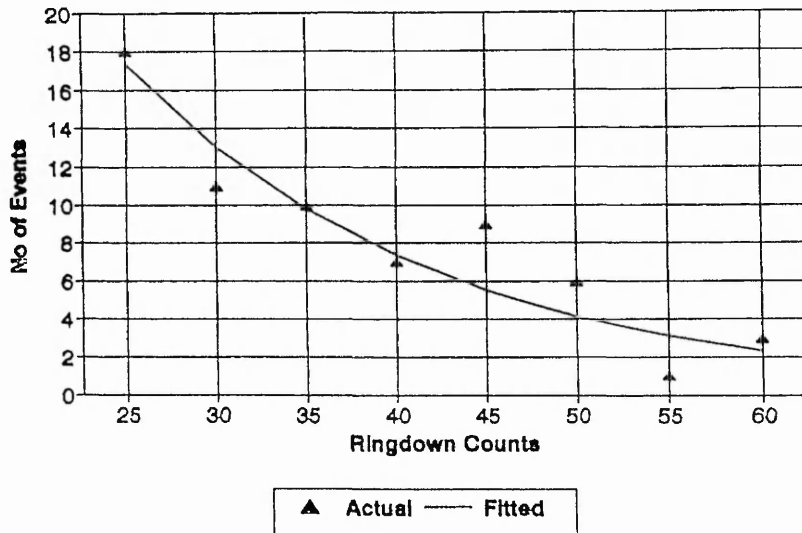


Fig. 9. Actual plot of AE data using with theoretical curve due to Weibull statistics.

51
52

7 Table 1
8 Data for room-cured (four specimens) and post-cured (seven speci-
9 mens) transverse fibre glass/polyester specimens. Average values of m
10 and RG_0

	m	RG_0
13 Room-cured specimens	1.08	17.1
24 Post-cured specimens	1.67	24.4

287 rial, the acoustic energy in a microcrack event might be
288 expected to rise, as this Weibull based measurement
289 suggests.

7. Conclusions

The quality of the transverse bonding in a composite material is significant for engineering applications of the material and a measure of the quality of interfacial bonding is important in designing composite materials. Acoustic emission has been used to monitor the growth of transverse damage in polyester resin-glass fibre 'transverse specimens' containing a single transverse fibre bundle.

The acoustic emission data have been captured as a file of single AE events associated with the generation of transverse damage in this fibre bundle. The events

302 have been characterized in terms of ringdown count per
 303 event, amplitude and duration, although only ringdown
 304 count data are discussed here.

305 Specimens cured for 7 days at room temperature show
 306 a stress–strain curve dominated by the polymer deformation.
 307 The AE events suggest a failure characteristic
 308 designated as ‘quiet–noisy’. Then the specimens were
 309 post-cured for 2 h and the samples showed a mode of
 310 failure designated as ‘noisy–quiet’. Post-curing had
 311 increased the overall strength of the fibre bundle inter-
 312 faces and increased the toughness of the bundle resin
 313 combination, resulting in a marked resistance to material
 314 failure and a relatively quiet period acoustically (towards
 315 the end of the test). Generally, these post-cured samples
 316 show enhanced AE activity immediately prior to final
 317 specimen failure.

318 Weibull statistics have been adapted to characterize
 319 the amplitude and ringdown count distributions of AE
 320 events. Weibull parameters extracted from ringdown
 321 count distributions for cured and post-cured samples
 322 suggest a tightening of the acoustic emission ringdown
 323 count distribution when the sample is post-cured coupled
 324 with a move to higher ringdown count values suggesting
 325 a more energetic AE source associated with the more
 326 brittle resin phase.

327 The use of acoustic emission and Weibull statistics to
 328 characterize the transverse composite specimens is an
 329 effective way to perceive subtle changes in material
 330 fracture characteristics and changes in material strength.

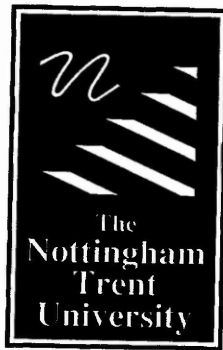
Analysis of acoustic emission data combined with
 Weibull statistics provides simple parameters relating
 acoustic emission to changing material condition.

Acknowledgement

The authors thank Scott Bader Co. Ltd for the
 provision of materials.

References

- [1] B.Z. Jang, *Advanced Polymer Composites*, ASM International, OH, 1994.
- [2] I.M. Daniel, O.Ishai, *Engineering Mechanics of Composite Materials*, Oxford University Press, Oxford, 1994.
- [3] D. Hull, T.W. Clyne, *An Introduction to Composite Materials*, Cambridge University Press, 1996.
- [4] P.J. Herrera, L.T. Drzal, *Composites* 23 (1992) 2.
- [5] E.U. Okoroafor, R. Hill, Determination of fibre–resin interface strength in fibre reinforced plastics using the acoustic emission technique, *J. Phys D. Appl. Phys.* 28 (1995) 1816–1825.
- [6] E.U. Okoroafor, R. Hill, Relating acoustic emission signal parameters to the strength of fibres used in the manufacture of polymeric composites, *Ultrasonics* 33 (2) (1995) 123–131.
- [7] E.U. Okoroafor, R. Hill, Investigation of complex failure modes in fibre bundles during dynamic mechanical testing using acoustic emission and Weibull statistics, *J. Mater. Sci.* 30 (1995) 4233–4243.
- [8] E.U. Okoroafor, R. Hill, Determination of fibre–resin interface strength in fibre reinforced plastics using the acoustic emission technique, *J. Phys D. Appl. Phys.* 28 (1995) 1816–1825.



**Libraries &
Learning
Resources**

The Boots Library: 0115 848 6343
Clifton Campus Library: 0115 848 6612
Brackenhurst Library: 01636 817049